Spark Ignition Engine Combustion Process Analysis

by

Marc William Wiseman B.Sc, AMIMechE

Thesis submitted to the University of Nottingham for the degree of Doctor of Philosophy, April 1990.

Contents

ABSTRACT

Spark Ignition Engine Combustion Process Analysis

by

Marc William Wiseman

Cylinder pressure analysis is widely used in the experimental investigation of combustion processes within gasoline engines. A pressure record can be processed to reveal detail of charge burning, which is a good indicator of combustion quality. The thesis describes the evaluation of an approximate technique for calculating the mass fraction of the charge that has burnt; a novel approach for determining heat loss to the block; the development of a powerful system for combustion analysis; and the investigation of the correlation between the crank angle location of the 50% mass burnt and minimum timing advance necessary to obtain the maximum engine torque.

A detailed examination has been carried out into the uncertainties in the determination of the mass fraction burnt as suggested by Rassweiler and Withrow. A revised procedure has been developed which does not require a priori identification of the combustion end point, and a new approach is suggested to calculate the polytropic indices necessary for the pressure processing. This particular implementation of the analysis is able to identify late burning and misfiring cycles, and then take appropriate steps to ensure their proper analysis. The problems associated with the assumption of uniform pressure; alignment of the pressure changes to the volume changes; pressure sampling rate; clearance volume estimation; and calibrating the acquired pressure to absolute are also evaluated.

A novel method is developed to ascertain, directly from the pressure history, the heat loss to the cylinder block. Both experimental and simulated data are used to support the accuracy of the suggested heat loss evaluation, and the sensitivity of the method to its inputs is examined.

The conversion of procedures for combustion analysis into a format suitable for undertaking high speed analysis is described. The analysis techniques were implemented so that the engine can be considered to be on-line to the analysis system. The system was entitled Quikburn. This system can process an unlimited number of cycles at a particular running condition, updating the screen every 1.5 seconds.

The analysis system has been used to study the potentially beneficial correlation between the location of the 50% mass burnt and MBT. The correlation is examined in detail, and found to be valid except under lean fueling conditions, which is seen to be caused by slow flame initiation. It is suggested that the optimum location of the 50% mass burnt can be used as a reference setting for the ignition timing, and as an indicator of combustion chamber performance. An engine simulation was employed to verify that changes in burn shape account for the small variation seen in the optimum 50% burn locations at different operating conditions of the engine. The burn shape changes also account for the range of optimum locations of the 50% mass burnt encountered in different engines.

Acknowledgements

The author is indebted to Professor P.J. Shayler and Dr D.G. Elliman for their good advice, encouragement and counselling throughout the research. Gratitude is also extended to: Professor G.B. Warburton for the use of the facilities of the Mechanical Engineering Department; all the technical staff for giving their generous help and time; and also Miss V. Pickard for assisting with the typing of this thesis.

Advice and equipment was generously given by members of Ford Motor Company research departments both in the UK and the USA. The author would like to thank these people, and in particular Dr T. Ma, for their kind help.

A special thanks is also given to the fellow members of the "Engines Group" for their help and advice.

Finally, the author would like to acknowledge formally his gratitude of all the support offered to him, during this project, by family and friends, and in particular Miss Dawn Hearne.

Nomenclature

A	Surface Area of the Combustion Chamber
C	Capacitance
C_p	Specific Heat at Constant Pressure
C_v	Specific Heat at Constant Volume
h	Coefficient of Heat Transfer
M	Molecular Weight
m	Mass
N_u	Nusselt Number
n	Polytropic Index
P	Cylinder Pressure
ΔP_C	An increment of pressure due only to combustion
Q	Heat Transfer
Q_f	Chemical Energy Release by the Fuel Burning
Q_{ht}	Heat Loss to Surroundings
Q_{HV}	Lower Heating Value
Q_n	Net Heat release , $Q_n = Q_f - Q_{ht}$.
R	Specific Gas Constant Resistance
R_e	Reynolds number based on mean piston speed
R_O	Molar Gas Constant
T	Temperature
t	Time Interval
U	Internal Energy
u	Specific Internal Energy
V	Volume Voltage
V_p	Mean Piston Speed

X	Mass Fraction Burnt
y	Volume Fraction Burnt
W	Work Done
γ	Specific Heat Ratio. $\gamma = C_p \ / \ C_v$.
θ	Crank Angle
θd	0-100% Burn Duration in crank angle degrees
ρ	Density
ϕ	Fuel-Air Equivalence Ratio.

Subscripts

b	Burnt Charge Region
cr	Crevice Region of the Cylinder
EOC	The point in the cycle where combustion ends
EVO	The point in the cycle where the exhaust valve opens
f	Fuel
i	A point where data is sampled
s	The point in the cycle when spark ignition occurs
u	Unburnt Charge Region
w	Cylinder Wall
θ	A Particular Crank Angle

Abbreviations

ADC	Analogue to Digital Converter
AFR	Air Fuel Ratio
ALE	Address Latch Enable
ATDC	After Top Dead Centre
BDC	Bottom Dead Centre
BIOS	Basic Input Output System
BLD	BorderLine Detonation
BMEP	Brake Mean Effective Pressure
CLK	Computer Clock Pulses
COV	Coefficient of Variance
CPAS	Cylinder Pressure Analysis System
CVH	Compound Valve Head
DEG	Degrees
EEC IV	Electronic Engine Control System
EFI	Electronic Fuel Injection
EGA	Enhanced Graphics Adapter
EOC	End of Combustion
ESC II	Electronic Spark time Controller
EVO	Exhaust Valve Open
GPIO	General Purpose Input/Output Board
HEX	Hexadecimal Number
H.P	Hewlett Packard
IBM	International Business Machines
I.C	Internal Combustion (engine)
I.C	Integrated Circuit
IMEP	Indicated Mean Effective Pressure

IO	Input/Output
IOR	Port Input/Output Read signal
IOW	Port Input/Output Write signal
ISAM	Indexed Sequential Access Method
ITAMS	Ignition Timing and Measurement System
IVC	Inlet Valve Close
MAP	Manifold Absolute Pressure
Mb	Megabyte
MBT	Minimum Spark Timing Advance for Best Torque
MEMW	Memory Write
OHC	Overhead Camshaft
PC	Personal Computer
PCTL	Peripheral Control Line signal
PFLG	Peripheral Flag Line signal
PLL	Phase Lock Loop
PMEP	Pumping Loop Mean Effective Pressure
RAM	Random Access Memory
RHS	Right Hand Side
RPM	Revolutions per Minute
SAE	Society of Automotive Engineers
S.I	Spark Ignition
TDC	Top Dead Centre
TTL	Transistor Transistor Logic
VCVS	Voltage Controlled Voltage Source filter stage
WMEP	Work Loop Mean Effective Pressure
WOT	Wide Open Throttle
WWMP	World Wide Mapping Point (2.62 BMEP at 1500 rpm)

Chapter 1

Introduction

At the present time, the combustion processes in spark ignition engines are not well understood theoretically, and experimental investigations are essential to advancing the knowledge for both fundamental and applied developments in the field. The analysis of pressure records is commonly used to investigate how the air and fuel mixture in an engine cylinder has burnt. The pressure data can be processed to reveal the cyclic and average variations of the combustion period, throughout the range of operating conditions of interest. The easiest combustion related parameters to obtain are peak pressure and indicated mean effective pressure. However, these only characterise the combustion event as a whole, and provide insufficient information to explain, for example, the cyclic variations of the combustion process. To obtain extra detail of the combustion process, analysis procedures have been developed which compute, at each crank angle, the charge mass fraction burnt. The results of these methods do not only indicate burn quality, but also suggest whether the cause of differences in the combustion rate is related to flame initiation or propagation. This information can then be used by automotive engineers, for example, to select the optimum spark timing and fueling schedules, or to improve the design of the combustion chamber.

1.1 The Objectives

This thesis is concerned with improving the techniques available to derive combustion quality information from the cylinder pressure. The aims that were behind the project can be listed sequentially:

(i) To overcome the uncertainties and develop a method of determining combustion information in a manner which is suitable for the swift processing of many cycles of pressure data.

(ii) To produce a suitable method of ascertaining the heat loss during the combustion period.

(iii) To design an advanced tool for the analysis of pressure records, which will aid research into the combustion of spark ignition engines.

(iv) To apply these analysis techniques to the study of the applications of the 50% burn location, which has recently been suggested as an indicator of combustion efficiency, Klimstra[1.1].

1.2 Layout of the Thesis

Chapter 2 contains a review of the published papers forming the background to the current work. An overview of combustion is given to describe the main mechanisms involved within gasoline engines. This is followed by a survey of the techniques used for pressure analysis, from which the most appropriate processing method, for the current work, can be selected. The last part of the chapter describes the implementation of methods used to determine the mass fraction burnt of the charge, which were carried out by other authors.

Chapter 3 details the rigs used and the technology necessary to obtain valid data signals from the engine test bed. One application of these signals was to drive the engine's ignition timing. A board, which slotted into the expansion bus of an IBM XT type computer, was designed to allow each cylinder's dwell and spark time to be set independently. This board offers more flexibility than commercially available equipment, because it is fully software programmable. Chapter 4 describes the board hardware and software design.

The pressure processing technique, which was originally suggested by Rassweiler and Withrow[1.2], was chosen for the combustion analysis,

because of it's simplicity, consistency with results from thermodynamic approaches, and fast execution time. Chapters 5 and 6 contain the evaluation and developments necessary to improve the determination of mass fraction burnt by this method. In particular, chapter 5 considers the influences of noise pickup and heat transfer, and a scheme is suggested that best calculates the values of the polytropic indices which are necessary for the processing. Chapter 6 considers the sensitivity of the pressure processing technique to the external factors of non-uniform pressure, the incorrect specification of the clearance volume, misaligned TDC and improper scaling of the acquired pressure to absolute. It was found that there was very little sensitivity to any of these factors, and a reliable analysis scheme could be established. The implementation also allowed partial burning and misfiring cycles to be identified simply, and appropriate measures to ensure proper analysis are described.

Normally, to determine the heat transfer from the cylinder, a thermodynamic analysis coupled with a heat transfer correlation needs to be employed. However, a novel approach has been devised, based on an approximate scheme that utilises the already calculated mass fraction burnt. The method is quick, simple and does not require calibrating for each particular engine testbed, as is the case with heat transfer correlations. This facilitates cycle by cycle comparisons of thermal loading. The new heat transfer method is described in chapter 7.

To investigate the described pressure processing scheme, a simple analysis system was designed for implementation on an Olivetti M24sp computer. This analysis system functioned by storing the acquired pressure records on a Winchester disk drive for subsequent analysis. The software included a database system, which facilitated quick retrieval of pertinent information from all stored data. This system was titled "CPAS" (Cylinder Pressure Analysis System) and is described in chapter 8.

Although pressure analysis was possible with CPAS, processing time was long and disk space limited data runs to seven sets of two hundred cycles. Therefore, the analysis algorithms were revised to enhance execution speed and then implemented on a Hewlett Packard 9000/320 series personal computer, operating at 16MHz. The new system, named "Quikburn" was capable of continuously acquiring ten cycles of data and displaying the processed results to the screen in under one and a half seconds. The acquired data was stored in dynamic memory, permitting an unlimited number of contiguous cycles to be analysed. The Quikburn program was designed to consist of several small modules, whose source code was easily accessible and could be interactively amended. This allowed the researcher to redirect quickly the investigation and, thereby, use the time of a test session more efficiently. In addition, the Hewlett Packard system could control the engine spark timing by using RS232 protocol to transfer information to the ignition control board, housed in the IBM XT. This allowed spark timing sweeps to be automated. Quikburn is described in chapter 9.

The penultimate chapter describes the investigation of the correlation between the location of the 50% mass burn and optimum IMEP, using the Quikburn system. The chapter starts with a short literature review of information regarding the correlation, and is followed by a detailed investigation using data obtained from a production engine. The results showed that under stoichiometric AFR conditions and richer, a 50% burn location close to 15^{o} ATDC corresponded to optimum IMEP conditions. A simple computer model is used to demonstrate that the burning pattern itself is the cause of the dependency of optimum IMEP on a certain 50% burn location. This is why there is only a slight variation in the value of the 50% burn location at optimum IMEP at different operating conditions, and on different engines. Under lean fueling conditions the correlation was no longer valid, due to the occurrence of "arrested phasing". Further investigation indicated that the arrested phasing was

related to slow combustion initiation, and was not caused by slow flame propagation. The study, also, highlighted several methods of performance assessment made possible by the behaviour of the 50% burn location in a particular engine. The possibility of a similar correlation between the location of peak pressure and optimum IMEP was also considered. Such a correlation would be beneficial because it is possible to determine the location of peak pressure onboard a production vehicle. The information could then be used to maintain engine efficiency throughout the lifetime of the power unit. However, it was discovered that although the location of peak pressure could be used satisfactorily as a performance indicator under rich fueling conditions, its application became ambiguous at lean AFRs. Therefore, the location of the 50% mass burnt appears to be the only, generally applicable indicator of engine performance.

The final chapter contains the conclusions drawn from all the foregoing work.

Chapter 2

Literature Survey

2.1 Introduction

The current understanding of the combustion processes in spark ignition engines is reviewed, to illustrate the phenomena the combustion analysist wishes to monitor. This is followed by a review of other techniques for combustion diagnostics, before going on to consider methods for pressure analysis. In this latter section, different methods of determining charge mass fraction burnt are compared and the most suitable approach for this thesis is selected. The final section looks at the implementations of analysis procedures in published papers.

2.2 The Combustion Process

Combustion processes occurring within the cylinder of a gasoline engine are a complex combination of turbulent fluid mechanic and thermodynamic processes. The charge burn period, between spark discharge and the burning of the last of the reactants, can be divided into four discrete stages; initiation of the flame kernel by the spark discharge; the growth of this flame kernel to a stable flame front; the propagation of the flame front through the main part of the charge; and, finally, the burn up of the remaining few percent of the reactants. An illustrative schematic of these four stages is given in fig 2.1.

2.2.1 Flame Initiation

A flame kernel is ignited by the temperature rise between the spark plug electrodes, due to the passing of an electron avalanche caused by the high breakdown voltage of the plug. The temperature between the electrodes reaches

an instantaneous, local value of 40,000 K during breakdown, settling to nearer 5000 K during the later glow and arc stages of spark discharge. These high temperatures not only commence the combustion, but, also, cause the kernel to swell due to the expansion of the hot gases, Kalghatgi[2.1].

Prior to 1980, investigators thought that the spark energy had no effect on the kernel growth provided it was sufficient to create a self propagating flame front, Young[2.4]. This is not the case, the early flame kernel growth has recently been shown to be enhanced by increased spark energy, because of the greater expansion of the hot spark channel gases, Baritaud[2.3]. In fact, Anderson[2.2] exploited the thermal expansion to gain a faster growing flame kernel, by increasing the power of the breakdown discharge.

The growth rate of the flame kernel tends to be consistent from cycle to cycle, Young[2.4]. One reason for this is the energy released from the spark is dependent on the charge time of the ignition coil (dwell period), and is approximately constant. In addition, during the initial period, the enflamed volume will be smaller than the microscale turbulence, and therefore, will be relatively insensitive to the randomness of mixture motion, Winsor and Patterson[2.5]. Finally, it is widely accepted that initially lamina burning occurs, Kalghatgi[2.1]. The initial ignition site will be contained within a turbulent eddy, and until this eddy is consumed, combustion remains lamina, Keck et al[2.6]. It is not until the flame reaches the eddy perimeter that turbulent spreading will occur. At this point the flame growth rate approaches the fully turbulent level, and the significance of the expansion of the hot gases diminishes, Young[2.7].

The characterisation of the early flame development involves an arbitrary specification of the kernel growth period. Yamamoto[2.12], as well as others, use the 0-1% mass burnt, whereas the Ford Motor Company recommend 0-2% mass burnt, reference[2.14]. This time for the initial burning of the charge mass is difficult to measure, because the low pressure changes involved will be

masked by noise pickup on the pressure signal and, also, a lag time occurs in sensing the pressure changes at the flame kernel. The latter point is considered in more detail in chapter 6. Therefore, pressure analysis is not well suited to studying the early growth time, and if this period is of importance then other methods should be employed; for example, ionization probes can be used to sense the arrival of the flame front at a particular location.

2.2.2 Kernel Growth to a Stabilized Flame Front

The flame kernel must reach a critical, minimum size by the time the spark discharge ceases. If it does not, the rate of heat release from the burning charge will be less than the rate of heat loss to the surroundings, causing the extinction of the combustion flame, Kalghatgi[2.1]. The prime purpose of the arc and glow discharge stages is to act as a heat source to sustain the flame kernel during this early development. The dimensions of the minimum size are dependent on the balance between the heat released and heat rejected by the flame kernel. In some cases, heat rejection rates are insufficient to extinguish the flame, but, nevertheless, restrict flame development and produce longer, less efficient burn durations. For example, Douard[2.8] found slowest flame growth when the orientation of the ground electrode of the spark plug, which acts as a heat sink, lay within the kernel's wake. Anderson[2.2] found detrimental effects to the flame progress when using large electrode tips, and, also, when the flame propagated primarily towards the quenching surface of the near cylinder wall. Consistent with the latter result, are the results of Swords[2.9] and Matekunas[2.10], which showed that the rates of flame growth were greatest when the flame propagated towards the centre of the cylinder.

During it's growth to the critical size, the dimensions of the flame kernel are of the same order as the microscales of turbulence, and the flame kernel will

be sensitive to randomness in the flow field. This stage has been attributed as the source of cyclic variation, Winsor[2.5]. Turbulence can also be beneficial because the microscales wrinkle the flame front causing an increase in surface area. This allows faster entrainment of unburnt fuel and promotes burning, Ferguson[2.15]. Evans[2.11] reports that increased microscale turbulence promoted kernel growth in his combustion chamber, which was specially designed for fast burning of the charge. However, too much turbulence can over stretch the flame front and increase the heat rejection rate, causing flame extinction. Therefore, a compromise is necessary between increased turbulence for fast flame growth, and reduced turbulence to lessen cyclic dispersion and avoid flame extinction.

A stable flame front is normally considered established by the time 10% of the charge mass has burnt, references[2.14, 2.30]. This burn point can be determined adequately by pressure processing methods, which usually treat the kernel formation and flame front stabilization as a single process, characterised by the 0-10% burn duration.

2.2.3 Propagation of the Stabilized Flame Front

The flame front propagates at the fully turbulent velocity through the remaining mixture. Ferguson[2.15] illustrated the combustion mechanics using the analogy of ink penetrating a sheet of rotating rollers. The turbulent spreading of the ignition sites was modelled by the transport of the ink through the sheet by contact of the rotating rollers, and the eddy burn up was modelled by the ink soaking into the core of each roller. This model is based around Tabacyznski's model of turbulent entrainment[2.16], where unburnt mixture is engulfed by eddies on the order of the integral scale, and consumed by lamina burning on Taylor's microscale. This concept is often referred to as a "lamina flamelet model", Moss[2.17]. Results from these models show good agreement to experimental results. The flame diameter will be greater than the turbulence

microscales, and once again it will be insensitive to the random motion of the mixture.

Like the growth of the flame kernel, the burning rate within this combustion stage is dependent upon the rate of heat rejection from the enflamed gases. The flame progress can be hindered such that burning continues throughout the power stroke, after the exhaust valve has opened. This is known as late or partial burning. Late burning is undesirable, since combustion efficiency is lowered and the hydrocarbon emissions from the exhaust increase. The degree of late burning can vary from cycle to cycle resulting in unstable engine operation. The possibility of incomplete combustion is high under lean AFR conditions because the flame propagation rate is slow and sensitive to heat rejection rates, because the heat release within the flame front is low. This combination of factors produces longer burn durations as the mixture strength is weakened, resulting in late burning occurring as the lean limit is approached. Quader[2.31] found that just beyond the lean limit, no spark timing suitable for proper engine running can be found, because advanced timings cannot initiate the combustion, and retarded timings produce late burns.

The main propagation stage is normally characterised by the 10-90% burn duration, references[2.14, 2.30]. This duration is dependent on the turbulent flame speed, which will be a strong function of AFR and a weak function of spark timing, Houpt[2.30].

2.2.4 Final Burn up of Reactants

The final reactants remaining are located close to the surface of the combustion chamber. The relatively cool metal will quench the flame front causing an increase in the time for burn up, Tabaczynski[2.16].

The final burn stage can be characterised by the 90-100% burn duration. However, this stage is not a major area of investigation and most analyses concentrate on the influences of burning the first 90% of the charge.

2.2.5 Time Taken for Combustion Stages and Relationship between Volume and Mass Burnt

In the investigations for the current work, it was found that flame initiation, 0-10% burnt, took around 20^{o} crank angle; flame propagation, 10-90% burnt, around 60^{o} crank angle; and the final burn up, 90-100% burnt, around 20^{o} crank angle. These results are similar to the durations obtained by Young[2.7]. The fact that it only takes three times longer to burn the bulk of the charge than the first 10% further indicates the importance of flame initiation.

In the visual examination of the combustion process by Gatowski and Heywood[2.13], it was found that the flame front radius was 10mm by the time the first 1% of the charge had burnt; 30mm by the 10% burnt stage;and 60mm by the 50% burnt. The distance between spark plug and head periphery was only 70mm. These authors went on to show that volume burnt, can be related to the mass burnt, by:

$$y = \frac{\frac{\rho_u}{\rho_b} X}{\left(\left(\frac{\rho_u}{\rho_b} - 1\right) X + 1\right)} \qquad 2.1$$

Furthermore, they found that the density ratio, ρ_u/ρ_b, was approximately constant and equal to 4. This is empirical proof for the relationship between mass and volume burnt, which is almost independent of engine operating conditions, and is known as the "universal burning law". The universal curve is shown in fig 2.2, which is reproduced from reference[2.32]. From equation (2.1), it can be seen that 80% of the charge volume has burnt when only 50% of it's mass has burnt. Therefore, the remaining 50% of the charge occupies

only 20% of the combustion chamber, and is situated within 10mm of the metal surfaces of the head.

2.3 Analysing the Combustion Process

Many different approaches have been applied to combustion analysis over the years. Probably the simplest method of comparing combustion rates is by the value of MBT (Minimum advance for Best Torque) timing. In chapter 10, MBT is found to correspond with a 50% mass burnt location of near 10^{o} ATDC for a number of power units, regardless of operating conditions. Therefore, the more retarded the MBT timing, the faster the combustion rate. Although this can provide a useful qualitative comparison, it's application is limited and a more quantitative approach is required.

2.3.1 Ionization Probes

Ionization probes offer a method of physically measuring when the flame front arrives at a particular position in the combustion chamber. A probe consists of an electrode gap with a high voltage applied across it. The voltage breaks down on arrival of the flame front, due to the release of free ions. Curry[2.19] placed 49 probes in a single combustion chamber to measure the burning velocities in three dimensions.

A disadvantage associated with using ionization probes is the need for machining of the head to locate the probe tip in the cylinder. Also, the probe is a physical presence in the combustion chamber and may influence the combustion process by interfering with the flow field, and by acting as a heat sink.

The advantages of the probes are cheapness and reliability. This is why, recently, both May[2.21] and Anderson[2.20] experimented with them in production engines. In these cases, the probe tips were slightly proud of the walls of the combustion chamber, and were used in an attempt to correlate the arrival time of the flame front with mixture AFR.

2.3.2 Optical Methods

High speed laser and Schlieren cinematography are non-intrusive methods of charting flame progress across the cylinder, and have been widely used in research. The physics of the adsorption, reflection and refraction of the coherent laser beam enable estimates to be made of species concentration; flow turbulence; scale and mean velocity; and, even, temperature. These methods are well reviewed by Dyer[2.22]. The major disadvantage with many laser techniques is that the measuring volume is very small. For example, Fansler[2.23], used a cylindrical measuring volume with a diameter of 0.1mm and a length of 0.5mm for flow measurements. Therefore, to build up a detailed picture of the flow field, many volume locations must be examined. As only one volume can be examined at a time, the researcher must try to reproduce identical conditions for many test runs. Therefore, detailed measurements of the combustion process are impossible because of its spatial and cyclic variational nature. This restricts the use of standard laser techniques, like Fansler's, to motored cycles only.

Schlieren photography provides a method of observing firing cycles. In this application, parallel, monochromatic light is passed through the combustion chamber and focussed through an aperture onto the lens of a camera with a fast frame speed. Variations in the refractive index of the cylinder constituents, due to density changes, cause a similar variation in image intensity. This allows easy separation of the low density burnt gases from the high density, unburnt region. To facilitate Schlieren photography of the whole combustion process the University of California, reference[2.24] and the Massachusetts Institute of Technology[2.13] have both developed engine test rigs with square pistons. Two side walls of the square cylinder are constructed from flat glass, allowing an undistorted view of the contents. Both establishments have customised their own Schlieren facility: M.I.T reflect the incident light off one of the opaque sides of the cylinder, producing two orthogonol views of the combustion

chamber, Pischinger[2.25]; the University of California replaced the standard aperture by a three-colour bullseye stop, and each of the three colours in the image represents a different density gradient, Chau[2.26]. The latter system was further enhanced with a software image improving system, Chau[2.27]. The images of the flame front obtained, although two dimensional, can be fitted by circles, and the convection of the flame centre and the increase of the flame radius investigated, in order to track the combustion process. Unfortunately, Schlieren photography necessitates machining of the cylinder head to obtain optical access. Also, the internal glass surface tends to become quickly opaque with soot deposits, limiting operation to only a few cycles.

2.3.3 Pressure Analysis

One of the best non-intrusive methods for general purpose combustion diagnosis is pressure analysis. On the modern testbed, piezo-electric pressure transducers are used, either fitted flush in a customised cylinder head, or housed in a specially designed spark plug, Amann[2.46]. Both methods produce valid pressure data, Evers[2.28].

Up to the middle of the 1960s, investigators like Patterson[2.47], were only able to calculate peak pressure, pressure rise rate and IMEP routinely. Although these parameters form a good basis to compare driveability and cyclic dispersion, they give no indication of why the combustion in one cycle differed from another. The advent of powerful digital processing made possible the routine calculation of charge mass fraction burnt, and enabled pressure analysists to examined the combustion process in detail.

2.4 Methods of Determining Mass Fraction Burnt

The variation of the mass of the burnt charge is normally presented in two forms, either depicting the mass burnt per crank angle, or the fraction of the charge mass that has burnt by a particular crank angle. The latter is an

accumulation (integration) of the former. Methods which determine the changes in the burnt mass of the mixture, from the recorded pressure history, can be grouped into two particular types. Thermodynamic approaches are based on either the conversion of heat energy to work done by the piston, or upon the variation of availability. The former methods are commonly referred to as First Law methods, and the latter Second Law methods. More approximate procedures are based on less rigorous, empirical rules, which assume that the pressure variation is some form of polytropic process.

2.4.1 First Law Thermodynamic Methods

The classic approach to analysing combustion is to apply the First Law of Thermodynamics to the closed system comprising the cylinder constituents. Most methods for the thermodynamic analysis of gasoline engines are zero-dimensional in that they offer no spatial resolution, Foster[2.29]. The combustion process can be considered to occur in either one or two zones. In a single zone procedure, no differentiation is made between burnt and unburnt gas properties; a mean temperature and pressure define the system state. A more detailed study can be accomplished by considering the burnt and unburnt gas regions separately. Common thermodynamic approaches use either the method devised by Krieger and Borman[2.32] or Benson and Whitehouse[2.36], as a basis.

The Krieger and Borman formulation eliminates the need to estimate flame front shape. From the differential forms of continuity, the equation of state and the First Law, pressure records can be processed by the following scheme:

First the rate of change of the temperature of the unburnt region was found from;

$$\frac{dT_u}{dt} = \frac{\left[\frac{T_u}{P}\frac{dP}{dt} + \left(\frac{1}{m_u R_u}\right)\left(\frac{dQ_u}{dt}\right)\right]}{\left[\frac{1}{R_u}\left(\frac{\partial u_u}{\partial T_u}\right) + 1\right]} \qquad 2.2$$

From this the rate of increase of the burnt mass can be obtained;

$$\frac{dm_b}{dt} = \frac{\left[m_u R_u \frac{dT_u}{dt} - \left[\left(\frac{P}{R_b}\right)\frac{\partial u_b}{\partial T_b} + P\right]\frac{dV}{dt} - \left[\left(\frac{V}{R_b}\right)\frac{\partial u_b}{\partial T_b} + m_b\frac{\partial u_b}{\partial P} + V_u\right]\frac{dP}{dt} + \frac{dQ_b}{dt}\right]}{\left[u_b - u_u + \left(\frac{R_u T_u}{R_b} - T_b\right)\frac{\partial u_b}{\partial T_b}\right]}$$

2.3

Finally the increase in burnt volume can be evaluated;

$$\frac{dV_b}{dt} = \left[\left(\frac{1}{m_u}\right)\left(\frac{dm_b}{dt}\right) - \left(\frac{1}{T_u}\right)\left(\frac{dT_u}{dt}\right) + \left(\frac{1}{P}\right)\left(\frac{dP}{dt}\right)\right]V_u + \frac{dV}{dt} \qquad 2.4$$

Equations (2.2) to (2.4) can be solved, at each crank interval, by iterating from an initial estimate of T_b from the adiabatic flame temperature and modifying using the differential form of the equation of state.

The heat transfer from the unburnt and burnt regions can be found using one of the correlations for the heat transfer coefficient. The most widely used correlations are by Annand and Woschni, and their merits are described by Benson and Whitehouse[2.33]. These are based on $(N_u) = a(R_e)^b$, where a and b are constants. The value usually chosen for b is 0.8, the same as used for forced convective, heat transfer in turbulent pipe flow. Annand's formula uses a Reynolds number based on mean piston speed and includes an additional

radiative term. Woschni uses a Reynolds number, adjusted for combustion induced velocities obtained from differences between the firing and motored pressure histories.

To evaluate the heat transferred from each zone, the surface temperature of the piston, valves and head must be known, as well as the gas temperature. In order to distinguish between heat transfer from the burnt and unburnt regions, Krieger and Borman suggest that V_b/V represents the proportion of the surface area of the combustion chamber that is exposed to the burnt region.

For practical engine use, the constants in the heat transfer correlations must be determined for the particular rig in question. Normally, these constants are adjusted until the combustion analysis predicts similar quantities to experimental results from an energy balance between the energy supplied by the fuel, the work done by the piston, and the heat transferred to the exhaust and cooling systems, Young[2.35].

The mass fraction burnt is determined by time marching through from spark time towards EVO, using the iteration scheme. Sample results from the Krieger and Borman method, obtained from their original paper, are presented in figs 2.3A and 2.3B. The former figure shows the cylinder pressure profile and rise rate, along with the derived rate of burning. The other figure shows the calculated mass fraction of the total mass burnt for cycles at different compression ratios.

A two zone analysis method was also suggested by Benson and Whitehouse[2.36]. This allows tracking of concentrations of particular chemical species. An initial estimate of the mass burnt during a crank angle interval is made, and the resultant burnt gas temperature calculated from combustion kinetics. The correct mass burnt can then be found by iterating the procedure until closure of the First Law occurs to within a certain accuracy. A scheme based on this approach, which takes into account dissociation and heat loss, is described by Stone[2.37].

Both the Krieger and Borman, and Benson and Whitehouse methods of analysis need extensive specification of thermodynamic data for both the unburnt and burnt gas regions. These schemes are calculation intensive and incur a significant processing time. There is also uncertainty in the heat transfer correlation, because it does not take account of the finite time required for heat transfer, nor that the heat flux varies spatially within the combustion chamber. These are difficult to appraise, and the normal compromise is to model only mean conditions with the heat transfer coefficient, Benson and Whitehouse[2.33].

In a recent attempt to simplify the thermodynamic approach, Gatowski et al[2.34] developed a single zone scheme that significantly reduced calculation time. The benefit of using a single zone was that cylinder mass loss and recovery, from crevice regions, could be easily taken into account. From fig 2.4A it can be seen that during the normal range of combustion temperatures, up to 2500K, the specific heat capacity ratio almost linearly decreases with increasing temperature. Therefore letting $\gamma = a - bT$, Gatowski et al showed that the heat release, for a perfect gas, would be given by:

$$\delta Q_f = \frac{V}{(\gamma - 1)}dP + \frac{\gamma P}{(\gamma - 1)}dV + \delta Q_{ht} - Rdm_{cr}\left[T' + \frac{T}{(\gamma - 1)} - \frac{R}{b}\log\left[\frac{(\gamma - 1)}{(\gamma' - 1)}\right]\right] \qquad 2.5$$

In this equation, if the direction of the mass flow, dm_{cr}, is into the crevices, then T' and γ' refer to the temperature and the ratio of the specific heats of the mixture within the cylinder. However, if the direction of the mass flow is from the crevices into the cylinder, then T' and γ' refer to crevice conditions.

As with the other thermodynamic approaches, the heat transfer to the surroundings, δQ_{ht}, needs to be determined from one of the standard

correlations. Sample results from this method are illustrated in fig 2.4B. The lowest curve, Q_n, is the summation of the first two terms on the right handside of equation (2.5). The higher curves show the effect of considering heat transfer and crevice interaction. The accuracy of these results is seen by the fact that Q_f differs from the available energy of the fuel by only a few percent, which is typical of normal combustion inefficiency.

The choice between the different thermodynamic methods is dependent upon the particular application. The Krieger and Borman method calculates absolute heat transfer and temperature variations, as well as the mass fraction burnt. The Benson and Whitehouse method requires a detailed knowledge of combustion kinetics, but facilitates the monitoring of the concentrations of pollutants. The Gatowski et al method derives only absolute heat release, but has the ability to allow simply for mass loss from the cylinder.

2.4.2 Second Law Thermodynamic Methods

An availability analysis, based upon the Second Law, has also been applied to the spark ignition engine. This calculates the variation of availability, which indicates the maximum possible energy that can be turned into useful work. Standard availability formulae are used, and Flynn[2.38] describes the application of these to the various processes inside the internal combustion engine. The typical variation of availability throughout the combustion period, taken from Patterson and Van Wylen[2.39], is shown in fig 2.5. The advantage of data in this form is that sources of availability destruction can be seen, and this highlights where improvements could be made to improve thermal efficiency.

Second Law analysis is of little use unless benefit can be made of any savings in availability. In a standard production engine all available energy at the end of combustion is lost to atmosphere, as is all heat rejected to the coolant. Therefore, availability analysis is most useful to power unit designers who are

able to make use of exhaust and coolant energy, for example via turbocharging. Such an analysis is best carried out during the initial design phase, rather than used for cyclic analysis, Foster[2.29].

2.4.3 Approximate Methods for Combustion Analysis

Approximate approaches are based upon less rigorous, empirical rules as opposed to thermodynamic laws. These methods, like the previously described thermodynamic analyses, are zero dimensional, but approximate schemes are simpler and much faster to evaluate. The approximate methods do not require comprehensive data of thermodynamic properties, and normally consist of only a single zone. However, recently Al-Himyary and Karim[2.18] produced a two zone method that is partly thermodynamic law and partly approximation. By examination of polytropic process within the combustion chamber, these authors showed that the temperature changes of either the unburnt or burnt zone were related in the following manner:

$$\left[\frac{T_i}{T_{(i+1)}}\right]^{(\gamma-1)} = \left[\frac{P_i}{P_{(i+1)}}\right]^{\gamma} \qquad 2.6$$

$$\frac{(T_i - T_W)}{(T_{(i+1)} - T_W)} = \frac{C_{ni}}{C_{n(i+1)}} \qquad 2.7$$

Where the polytropic specific heat, $C_n = \frac{(\gamma - n)}{(1 - n)} C_v$

Each zone is analysed separately, starting from known initial conditions. A value of specific heat ratio is assumed and equation (2.6) is used to predict the temperature at the end of a particular crank interval. Then equation (2.7) is used to re-estimate γ. The iteration continues until the modification to the temperature is insignificant. The process is then repeated for the next crank interval.

The known conditions for the unburnt region are at spark time, and analysis proceeds towards the end of combustion. In the case of the burnt

region, the known conditions are at the end of combustion and analysis proceeds backwards towards spark time. An added complication is that the initial temperature of the burnt zone must be estimated from the combustion chemistry and should take dissociation into account. Once the temperatures of both zones are calculated at each crank interval, the burnt charge mass may be obtained from the equation of state:

$$PV = m R_u T_u + m_b (R_b T_b - R_u T_u) \qquad 2.8$$

This iterative, dual zone model is not as economic in computer time as other approximate approaches, and is unable to derive as much information as a true thermodynamic method. Furthermore, the authors did not substantiate their results. For these reasons it is better to concentrate on the other approximate models.

There are three similar approximate approaches described by Marvin[2.40], McCuiston, Lavoie and Kauffman[2.41] and Rassweiler and Withrow[2.42]:

Marvin assumed that under isochoric conditions, combustion liberating a particular amount of heat energy would produce a proportional increase in pressure. In the real engine, combustion occurs at varying volumes. Marvin allowed for this by a polytropic expansion to reference conditions. The scheme can be obtained entirely from the logarithmic indicator diagram, an illustrative example is seen in fig 2.6. In the figure, X, Y and Z lie on a reference line at constant volume, and the pressure at X is the referenced pressure for conditions in the cylinder at X'. The pressure at X is obtained by interception, at the reference conditions, of a polytropic process line through X'. This line should be parallel to the compression line at the start of combustion and parallel to the expansion line at the end of combustion. The mass fraction burnt from this is given by;

$$X = \frac{(P_X - P_Z)}{(P_Y - P_Z)} \qquad 2.9$$

The approximate method within the EDPAC system developed by Young and Lienesch[2.35], is an implementation of Marvin's approach. In this implementation a linear switch over between compression and expansion lines was used.

McCuiston et al[2.41] deduced their approach from the adiabatic, isochoric form of the First Law:

$$X = \frac{\left(P\,V^{\gamma} - P_s\,V_s^{\gamma}\right)}{\left(P_{EOC}\,V_{EOC}^{\gamma} - P_s\,V_s^{\gamma}\right)} \qquad 2.10$$

There is a strong similarity between the approaches of McCuiston et al and Marvin. In fact, if the specific heat ratio is kept constant throughout combustion, it can be shown that Marvin's method is identical to the other. Therefore any differences between the results of these methods must be due to the selected variation of γ.

Rassweiler and Withrow's technique[2.42] is much more widely used than the other approximate approaches. These authors based their method on two empirical rules from experiments with constant volume bombs. The final calculation of mass fraction burnt is similar in form to Marvin's, except that the pressure changes due to combustion are separated from the effects of piston motion, as well as being referenced to isochoric conditions. A full derivation of the Rassweiler and Withrow method is covered in chapter 5.

All three approximate models are only able to determine mass fraction burning, however they do so in a very time efficient fashion. Of the three methods, the Rassweiler and Withrow version is the most established, and has a strong fundamental basis, because it uses a direct analogy to proven results

from combustion bombs. For these reasons the Rassweiler and Withrow method is preferred by the current author.

Very good agreement has been observed between results from approximate methods and thermodynamic analysis. Published evidence is presented in fig 2.7. In the upper part of this figure, a comparison is shown between the ignition delay and main combustion durations determined by thermodynamic and approximate techniques. Ideally the points should fall on the 1:1 line, which is plotted for reference. Although there is deviation, the effect is not marked. The lower part of Fig 2.7 shows all the approximate methods compared to the analysis procedure used by Young and Lienesch[2.35], which was based on the Krieger and Borman method. This consistency is surprising because the approximate methods appear to ignore heat transfer and dissociation affects. However, Stone[2.37] found that although the absolute magnitudes of the heat release were affected by heat transfer and dissociation, the mass fraction burnt was not. This was due to the dissociation being constant for the main burn period, and that most of the heat transfer occurs towards the very end of combustion. The latter point is commented upon in chapter 5.

Table 2.1 is a summary of comparisons between thermodynamic and approximate methods of analysis. As the objective of the current work is to develop a system which quickly determines combustion diagnostics on a cycle by cycle basis, the technique suggested by Rassweiler and Withrow will be the most suitable.

2.5 Implementation of the Procedures for Combustion Analysis

The software implementation of the above methods has changed with the development of the computer technology. In the middle 1970s dedicated units for pressure acquisition appeared which saved the data on to tape. The data was analysed off-line on a mainframe at a later date, Young and

Lienesch[2.35]. These "post analysis" systems were enhanced by the development of high speed data acquisition systems, Evans[2.43]. With the advent of larger computer memory and faster processing speeds, personal computers have allowed investigators to have dedicated machines for data acquisition and combustion analysis, Hayes and Savage[2.44]. Today most testbed facilities incorporate a personal computer.

Until recently the analysis sequence was unchanged; pressure data was acquired, stored onto a permanent medium and later analysed. However, in the last year there has been a move to produce real time burn information. Knowing burn times whilst the rig is running is advantageous because the effect of changes to operating conditions can be observed at once. This allows the investigator to direct his experiment in the most beneficial direction. Beck, Hahn and Miller[2.45] have developed an instrument that calculates IMEP and RPM data in real time. The very latest example along these lines has been the development of an on-line, PC based, combustion analyser, Bain et al[2.48]. The latter package records the cylinder pressure history, and displays the results within minutes. The concept behind this system is very similar to the Quikburn system developed during this work. However, the end products are complementary, fulfilling slightly different needs. The above package is based on simplified assumptions and is aimed at undergraduate and postgraduate courses. It is a versatile combustion data logger. Whereas, Quikburn is based on an accepted technique for combustion analysis, and is intended to be a flexible research tool. The main conclusion about analysis implementation is that there is a demand for fast, on-line processing packages, and Quikburn is one system that can make a valuable contribution as a research tool.

Chapter 3

Test Facilities and Signal Preparation

3.1 Introduction

The data presented in this thesis was acquired from four different engine testbeds. The variety of engine configurations produced a wide range of operating environments. This ensured that the developed system for pressure analysis would be applicable to any typical rig. All of the engine testbeds used were previously commissioned by investigators engaged in other projects. A resume of the facilities made available to the author is given in table 3.1, and further details may be found in the references given.

This chapter describes the technology necessary to obtain valid data signals from an engine testbed. Figure, 3.1, is a schematic of a typical rig, and illustrates the integration of the components described below. For high speed data acquisition of cylinder pressure at intervals of one crank angle degree, three signals are required from the engine:

(i) The cylinder pressure, represented as an analogue voltage.

(ii) A digital TTL pulse train at a frequency of 1 crank angle degree, to sample the pressure data.

(iii) A pulse once per engine revolution, which provides a reference to crank location.

In addition, it is convenient to have a TTL pulse at spark time. The methods necessary to obtain these required signals are described below.

3.2 Analogue Pressure Signal

It is common place in the engine research to use piezo-electric transducers for sensing pressure. With these instruments, a change in the pressure acting on the sensor diaphragm alters the spacing of two capacitance plates, creating a measurable shift in stored charge. This is converted to a calibrated voltage by a charge amplifier. Throughout this investigation, pairs of Kistler transducers, type 601A, and charge amplifiers, type 5007, were used.

The preferred location for a pressure transducer is flush to the wall of the combustion chamber, where it is directly exposed to the combustion gases. However, the disadvantage of flush fitting is the difficulty in machining an access to the combustion chamber, between the cooling channels of the engine block. For this reason, spark plugs that house pressure transducers have become commercially available. When using the adapted spark plugs, resonance effects within the tube between transducer and spark plug cause a slight distortion to the measured pressure, Evers[3.5]. The distortion will be common to all readings taken with the spark plug transducers. Provided no direct comparisons are made between results derived from flush fitted and spark plug transducers, either type of sensor installation is satisfactory for most applications.

The output from the charge amplifier is a continuous, periodically varying voltage of mixed frequencies. Shannon's sampling theorem [3.6] states that the highest fully determinable frequency in the signal will be at half the sampling frequency. Should frequencies above this threshold be present, aliasing errors will occur. Filtering is the best method of removing the undesirable, higher frequencies.

Fig 3.2 shows a 6 pole Bessel filter for anti-aliasing, which was designed following the guide lines of Horrowitz and Hill[3.7]. This particular filter consists of three voltage controlled, voltage source filter stages. Each stage has a cutoff frequency around 2 kHz, which was considered to be sufficiently

below half the minimum sampling frequency, which is 4.8 kHz when sampling every degree at 800 rpm.

Unfortunately, the production tolerances of the passive components can impair the filter performance, resulting in slight differences in the cutoff frequency and gain of each VCVS stages. This can affect the filter's response around the -3dB point, but the function of the filter is satisfactory at frequencies removed from this point, Horrowitz and Hill[3.7].

An alternative approach is possible with the Kistler 5007 series charge amplifiers These instruments allow a low pass filter to be fitted, which limits the upper sampling frequency. Kistler supply a 2.2 kHz filter, and this can be used in place of the above Bessel filter, if desired.

As a precaution against noise pickup, a screened BNC cable was used between charge amplifier and computer interface. The cable between the transducer and charge amp was also enclosed in an earthed ferrous tube to suppress the pickup of spark noise onto the charge signal, from the high tension leads.

No other measures for noise suppression were used to condition the data signals. The reasons for, and the effects of, this decision are described in chapter 5, where noise effects are considered in more detail.

3.3 Digital Signals

Digital signals from the engine are used to signal the occurrence of a particular event, for example spark timing, and to provide a sample trigger for the pressure acquisition system. The following methods were used to ensure best quality signals at the computer interface.

A signal pulse, once per crank angle degree, acts both as a sample trigger, and an indicator of crank location. On the testbeds available to the author, the pulse train was generated by a Hall Effect sensor, mounted through the flywheel bell housing, to sense the passing of teeth on the ring gear of the

starter motor. This approach was used in the development of ITAMS, which measures and controls the spark timing of an engine, Collings[3.8]. A phase lock loop circuit multiplied the 135 flywheel teeth pulses by 8/3 to give 360 pulses a revolution. However, two problems were encountered. The first was the speed dependence of the required air gap between sensor and flywheel teeth. The optimum gap increases as engine speed increases. The consequence of having the wrong air gap can be either the breaking up of some pulses, producing 1 or two extra pulses per revolution in an intermittent fashion, or teeth pulses being missed altogether. The second problem is the behaviour of the PLL output is uncertain when irregularities occur in the flywheel teeth signal. The distortions can be due to missed, or extra pulses, or even engine transients. The result being the common observation of fluctuations, by 1 or two pulses, either side of the nominal 360.

These effects are present but not immediately evident in the operation of ITAMS, because ITAMS measures and sets spark timing by using a single signal from its own PLL. The system appears to drive at a perfectly constant spark timing, whereas one or two degrees spark jitter are occurring. Although such fluctuation could be accepted for ignition purposes, as this will have only a very small effect on engine performance, the fluctuation will be detrimental to pressure analysis. To overcome the problem, the rigs have been updated recently to use optical shaft encoders. These incorporate a glass disc, etched with 360 markings, which rotates, triggering an optical sensor. The encoders appear to give a clean output signal at all engine speeds.

A marker pulse, occurring once every engine revolution, is used to align the captured pressure data with an absolute crank location. A common reference point is TDC, and alignment to the position of the marker pulse of the shaft encoder can be made in software. The pulse itself does not have to occur at TDC, because, by use of a strobe light and a timing disc located on the front pulley, the angular offset of the marker from TDC can be measured. Originally,

a single grubscrew, inserted into the front pulley and sensed by a magnetic pickup, was used to produce a marker pulse. This suffered from the same air gap problems encountered with the flywheel pickup, previously mentioned. The situation was rectified by employing a shaft encoder with a second channel that generates a marker pulse each revolution.

Spark timing is the combustion initiation point of each cycle, and it is useful to be able to identify this point in any acquired set of data. This can be facilitated by having a digital signal go high when a spark is discharged at the plug gap. To produce the signal, a small section of steel tube, split in two and held in plastic for ease of use, is placed around the relevant high tension lead forming a capacitive pick-up. The pick-up is connected to the circuit of fig 3.3 by a BNC cable. The circuit has been developed over the last couple years by researchers at Nottingham, and the version shown includes the final modifications made by the author. The spark detection circuit operates as follows:

(i) Between pick-up and A-A, shown in fig 3.3.

With no spark being discharged, the left handside of the 2700pf capacitor is held at ground. The right handside and, therefore, the input to the Schmitt trigger inverter charges to 5V. When a discharge takes place, a negative voltage is induced in the pick-up, the magnitude of which depends on the magnitudes of the resistors. The negative spike causes a temporary drop in voltage on the right handside of the capacitor and causes an inversion in the output voltage from the schmitt trigger.

The diode just upstream of the inverter clamps the applied voltage to below 5V. This protects the chip from being overloaded when the negative spike returns to zero, which causes a positive voltage transient. The variable resistors are used to ensure that TTL voltage thresholds are crossed, producing a pulse from the inverter.

(ii) From A-A to B-B.

This is a standard digital filter circuit, consisting of a high frequency removing, low pass filter, -3dB point at 100 kHz, and two schmitt trigger inverters to reshape the pulse. The action of this part of the circuit is explained in more detail, when digital signal conditioning is discussed later.

At the beginning of spark time, a falling edge will be present at B-B.

(iii) From B-B onwards.

The rest of the circuit consists of two retriggerable monostables. The first is simply triggered by the falling edge, at spark time, to give a non-inverted pulse, of around 1/10 ms duration. The second, on the output of the new pulse lights a L.E.D for almost 1/2 second. This L.E.D should be permanently on, when the engine is running, indicating the circuit is functioning correctly.

3.3.1 Digital Signal Conditioning.

Signal conditioning is usually required to provide valid voltage levels at the computer. Normally, the rig is remote from the computer by wire length of at least 5 metres. To drive the pulses along this distance, digital circuits with open collector outputs are required at the rig end of the connecting cable, and load resistances at the computer end.

Noise spikes on digital lines can cause false triggering of the logic circuits. The spike can be reduced to below the TTL switching threshold by using the digital filter circuit previously used in the spark detection circuit, between A-A and B-B of fig 3.3 . This consists of two Schmitt trigger inverters either side of a simple RC low pass filter. The first inverter restricts the noise spike amplitude to the max TTL voltage of 5V. The filter then removes the high frequency signal components, associated with the spike, and the second inverter reshapes the pulse.

The performance of the *RC* filter is important. The textbook analysis, Horrowitz and Hill[3.9], of this is based on the filter's response to an input sinusoidal voltage. For digital signals it is more relevant to consider the response to a step input voltage, as illustrated in fig 3.4. The current through the resistor equals that through the capacitor:

$$\frac{(V_{in} - V_{out})}{R} = C\frac{dV_{out}}{dt} \qquad 3.1$$

This has the solution:

$$V_{out} = V_{in}\left(1 - e^{\left[\frac{-t}{RC}\right]}\right) \qquad 3.2$$

For a given value of *RC*, there is a certain delay time before the pulse reaches the TTL threshold (about 2.4V). A noise pulse of less duration will be eliminated. These effects are also shown in fig 3.4. Care must be taken to ensure that the delay has no effect on the data acquisition. As a guide, assuming the time taken for the pulse to rise from ground to 5V is instantaneous, table 3.2 shows the delay times for different values of *RC* , and as this time is half the period of the eliminated noise, the corresponding filter cutoff frequency. In solving noise problems, the duration of noise spikes is unknown. A trial and error procedure has been used to select the best values of *RC* for noise elimination and minimum delay. If the required *RC* value for noise suppression introduces a significant transmission delay, this must be allowed for within the software analysis.

Another interfacing problem occurs when some electronic elements are triggered by the leading edges of pulses and some by the logic level of a pulse. For example, when a digital pulse occurs when the 1 degree pulse train is low. There will be a time difference between a circuit triggered by the digital pulse's

rising edge, compared to a circuit where the digital pulse is clocked in by the rising edge of the 1 degree pulse. Similarly, errors in synchronising particular events with absolute crank position can occur with level triggering if pulsewidths are greater than 1 crank angle degree.

Both these problems can be overcome by the use of two 'D' type flipflops. The first synchronizes the rising edge of the signal to coincide with the rising edge of the 1 degree pulse train. The second flipflop causes a similar synchronization of the falling edge, which reduces the signal pulsewidth to that of the 1 degree pulse train. The connections for the flipflops are shown in fig 3.5. This figure is a complete solution to all the afore mentioned factors, and has been reliably used in this work. The transformations to an applied digital pulse are shown in fig 3.6.

Chapter 4

A Slot-in PC Board for Engine Spark and Dwell Timing

4.1 Introduction

Accurate spark timing control and measurement are often essential for engine research. Several systems have been developed to provide this facility, such as ITAMS[4.1], but none can provide the flexibility which was desired for the work reported in this thesis. This particular need was to be able to treat each cylinder individually and run it through a particular sequence of ignition timings. By running three cylinders at similar, normal operating conditions whilst investigating the effect of changes on the fourth, a wide range of conditions could be investigated. The technology was readily available to build this style of ignition control system, and the design of a software programmable board for setting and measuring the spark time and dwell period of any cylinder of the power unit is described here.

4.2 The Timing Control System

The open architecture and abundance of commercial software support of the IBM PC computer family makes it attractive for hosting an adaptable ignition control system. A hardwired board can be slotted into the expansion bus, and the required timing schedule achieved in software. The timing settings could be contained within a data file, entered via the keyboard or, even, supplied through RS232 communication from another computer. The last case was used with the Quikburn system, where spark timings are downloaded to the PC, during an MBT sweep (see chapters 9 and 10).

The conventional layout for an engine ignition system is shown in the top part of fig 4.1. The points close and remain closed for the dwell period, which charges the coil. When the points re-open, the breakdown of the electric

field causes a voltage to be induced in the high tension side of the coil creating a spark at the plug electrodes. The voltage variation downstream of the points is shown in the middle of fig 4.1. This is essentially an inverted digital pulse of dwell period width, with a rising edge at spark time. Although this signal is easily computer generated, large currents occur during switching, and the computer should be protected by using the power transistor stage of an electronic ignition system, varieties of which are commercially available. Lumenition was found to be a reliable make. The bottom part of fig 4.1 shows a relay actuated switch between the computer driven timings and the conventional engine points. The relay is configured with safety in mind so that should an accidental break occur in the switch circuit, the ignition system reverts back to normal points operation.

4.3 The Board Hardware

To replace the ignition system points, a hardware and software solution was required. An Olivetti M24sp was selected to host the board, and the required signal lines, available in the expansion slot, are the 20 line address bus; port read and write; and 7 interrupts. Commercially available prototyping boards usually have facilities to buffer these lines and also decode the upper 17 address lines to map the board into port memory addresses between locations 300 - 30f hex. This area of memory is set aside for board use by IBM. Only 8 consecutive memory locations were required for the ignition control board, and the relevant chip can be selected by the output of a 3 to 8 line de-multiplexer, driven by the three lowest address lines. The addresses of the various chips lie from 300 hex through to 308 hex. The action at each address is tabulated in table 4.1.

Data is transferred into or out of the computer under control of the IOW and IOR lines. The timing diagrams for these are shown in fig 4.2. These are taken from Royer[4.2], which was used as the primary source for interfacing

information. The conclusions from the timing diagrams are that during a read cycle the data should be placed on the bus on the falling edge of the IOR, and, with a write cycle, data from the computer should be latched on the rising edge of the IOW. Whether data should be transferred is of course dependent on the state of the address bus, and correct operation for both cycles can normally be performed by ORing the chip select and the I/O control line.

The functions of the board can be split into two, the controlling circuits and the measuring. To execute these function four signals from the engine are required, these are:

1^{o} Pulses	From a shaft encoder
TDC	Also from the shaft encoder.
Coil spark present	A TTL pulse each time a cylinder is fired.
Cylinder 1 spark	A TTL pulse when cylinder 1 fires.

The last two signals are generated by the spark detection circuitry described in chapter 3. In addition each signal was filtered and the pulsewidth modified to be the same length as the 1^{o} pulse. The necessary methods are also given in chapter 3.

The board was designed to be programmed for either polling or interrupt techniques. With the former, the program continually reads a status register waiting for certain events to happen and then acts. It is important that the computer does not miss an event whilst polling, because this could result in a delay in the desired timing. As a warning, not only does an event occurrence set a bit in the status register, but if the register is not read within the pulsewidth of the event, an overflow bit is set. The circuitry for the occur and overflow bit setting is shown in fig 4.3, and its timing diagram in fig 4.4. On the rising edge of the signal, the first flipflop is set indicating the event has occurred. If the register is read before the falling edge of the signal, the flipflops are cleared.

Otherwise, the falling edge clocks the second flipflop setting the overflow bit. Note that the register is latched using the MEMW line. This ensures that data is latched into the register at a high frequency.

Interrupting allows the processor to perform other tasks, but undertake a service routine when an event occurs. The processor is interrupted by pulsing one of the 7 interrupt lines high, and program flow is directed to the code pointed to by the address vector for the particular interrupt. Computer performance may be severely limited if the processor is interrupted every degree of crank angle. As a remedy, ten 1^{o} pulses are counted before interruption occurs, causing minimal strain on the computer.

4.3.1 The Control Circuitry

The board alerts the computer via the status register, or by interrupting, when the following events happen: ten 1^{o} pulses have arrived; TDC marker pulse occurred; or when cylinder 1 has fired. To trigger the dwell start and spark time, the software must count the number of ten degree blocks until within one block of the desired timing. Then the number of degrees between this block and the required timing is written to the board, which creates the desired variation in coil voltage. The TDC pulse is used to synchronize the counting to absolute crank angle space, and the cylinder 1 spark pulse is used to establish the correct firing order in software. If this latter pulse is omitted then the computer will not know which cylinder it is firing in any one revolution.

The function of the hardware is to help perform the above operations. The circuit is shown in fig 4.5. The top of the diagram shows the resetable, decade counter used to inform the computer when ten degrees have been rotated through. Below this are the two down counters used to initiate the voltage transitions. Starting at the dwell counter, the necessary value is written to the counter on the simultaneous occurrence of the address being valid and a port write cycle starting. Similarly, the counter commences counting on any write to

the flipflop below it. This dummy write operation sends the flipflop output high, which allows the 1 degree pulses to pass through the AND gate. When the down counter value goes past zero, the borrow clears and presets the flipflop controlling the output voltage of the board. At the same time the borrow clears the count enable flipflop, inhibiting the 1 degree pulses to the counter. The down counter controlling the spark time works in a similar fashion, but this time clearing the final flipflop. The output voltage of the board is then buffered, and driven along the line to the engine. After traveling the line, the pulse is reshaped using a Schmitt inverter and triggers the Lumenition through a transistor. The passive components just up stream of the transistor, raise the threshold base bias to four diode drops, approximately 2.8V, and smooth out high frequency noise. The transistor acts as an inverter and the signal at the Lumenition corresponds to the voltage variation downstream of the points, as shown in fig 4.1.

4.3.2 The Measure Circuitry

The circuit for the measurement of spark timing retains the number of 1 degree pulses between TDC and each spark presence on the king lead, which is between the coil and distributor. The maximum possible count on a one cylinder engine would be 360, and therefore, a 12 bit counter is sufficient for the task. This counter is comprised of three 4 bit counters connected to two tristate buffers, one for the low byte, one for the high. This arrangement is shown in fig 4.6. The counter is reset every TDC, and then counts continuously upwards, in one degree steps. At every spark presence the value in the counter is latched into the tristate buffers. Simultaneously, the computer is interrupted, or the relevant bit in the status register is set. The tristate buffers are enabled during an addressed read cycle and deposit the data onto the data bus. To ensure correct logic levels are present on the data bus, pull up resistors are used. The software is then be able to interpret the read value as a spark advance.

4.4 The Ignition Software

The best way of programming the board is to use the routines of a high level language, for example the C language, to carry out screen and file handling, but to control the board using 8086 assembler. This combination allows good control over the main functioning of the board by writing the drive procedures in machine code, whilst the C subroutines carry out the labour intensive operations.

The measurement of spark timing is easily accomplished by just forming the data word from the low and high bytes which store the crank degrees between TDC and the spark presence. This can be converted to timing advance by subtraction from 360 or 180, depending on when the cylinder fires compared to the TDC marker. Allowances can be made within the software if there is an offset between the marker pulse and engine TDC.

The spark and dwell time control software is slightly more complicated, and a Warnier-Orr diagram (described in chapter 8) charting the program structure is shown in fig 4.7. To operate, the software has to use two counters. One holds the number of ten cycle blocks counted, and the other the number of the next cylinder to fire. This latter counter is usually sequential, the firing order is then determined from a look up table. Irrespective of whether the board is polled or interrupts, a set series of functions must be undertaken. The required changes to ignition timing must be specified. The information includes which cylinders' settings are to be altered, whether dwell or spark period is to be changed, and the new values must be given. If the data is to come from a file, it should be loaded into memory when the program first commences. This eliminates possible system crashes due to file handling problems, whilst the board is operating. Instead data could be typed in from the keyboard. Some high level language functions capture keypresses by using the MSDOS interrupt functions. This tends to hang the computer when the board is interrupting. The

problem can be overcome by writing the routines for reading of keyboard characters in assembler, which accesses the keyboard through the low level BIOS functions. RS232 communication is supported by C library functions, and the necessary subroutine can be written entirely in C and called from the program in assembler. Again to avoid the possibility of causing a fatal error to the system, the RS232 port was polled to obtain information instead of letting it interrupt.

Once the program has the timing information, it needs to determine the number of ten cycle blocks before the down counters need to be loaded and enabled, and, also, the values that need to be written to these counters. As is seen in fig 4.7, this can be accomplished from integer division. It should be noted that if the spark time is changed, the dwell start must also be reset to maintain the same length dwell period.

The rest of the program covers the necessary service routines to incoming events. Every ten degrees the block counter is incremented. Depending on the individual timing requirements for each cylinder, it may be necessary to load and enable one of the down counters. If a fire occurs then the record, indicating which of the cylinders was the last to fire, needs to be updated.

When a TDC pulse arrives, the number of received blocks of ten degree pulses is reset to zero. This enables the block counter to correspond to absolute crank angle space.

Finally, when a spark presence is detected on cylinder 1, the cylinder firing record can be checked to ensure that it is synchronized with the firing order of the engine.

The above is the general program structure, and this may be customised to suit particular applications.

4.5 The Board in Operation

The board and software can be configured, by the user, to generate the desired ignition timings. For the current work, a MBT sweep was performed. On command from the Quikburn system, the board sets the required ignition timings for the sweep. Before the tests were carried out, a check was made on the combustion response to a step change in spark timing. The engine was run at the main conditions used throughout this thesis, namely 1500 rpm part load (WWMP) and 2000 rpm WOT attained under the management system of the production engine. At the former condition the timing was advanced thirty degrees, but at the latter step, a change of only twenty degrees was possible if knock was to be avoided. When timing are retarded, the cylinder pressure will be lower than at advanced conditions, and the block walls will be cooler. The first few cycles after the sudden timing step change may well produce a lower cylinder pressure than would normally be seen at the advanced timing, because of the increased heat loss to the cooler wall conditions. The higher heat loss will quickly raise the wall temperature, and some oscillation can be expected whilst conditions settle. Fig 4.8 shows the variation of peak pressure before and after the step change in ignition timing. Although the effects are masked by cyclic dispersion, both plots appear to exhibit minor transient oscillation for nearly a hundred cycles after the change. As a hundred cycles is only a few seconds of engine running time, it is prudent to delay analysis for this period when taking results. The Quikburn system waits for ten seconds, before acquiring data, even though the MBT sweep only advanced the ignition timing in 1 degree steps.

Chapter 5

Development of the Rassweiler and Withrow Technique for Determining Mass Fraction Burnt

5.1 Introduction

This chapter and the next deal with the appraisal and development of a method to calculate the variation of the burnt mass fraction of the cylinder contents with crank angle. This approach is based on Rassweiler and Withrow's pioneering work [5.1]. An appraisal of the original formulation necessary to produce a reliable and readily applied form of the method is given in this chapter. This is followed by an examination of the sensitivities and inaccuracies inherent within the analysis method in chapter 6.

The evaluation of the approximate method is based upon the detail analysis of pressure data recorded on the test rigs described in chapter 3. The range of the data was chosen to ensure that the method was applicable to any configuration of gasoline engines. Typically, one hundred cycles of data were examined at each operating condition. The cycles, presented here, are those that illustrate the pertinent information from all the data taken.

5.2 Formulation of the Method for Combustion Analysis

The main disadvantage of the thermodynamic analysis of engine combustion is the processing time required. These techniques are impractical for much needed cycle by cycle calculations of the burn period, and therefore fast methods of analyis are desired. The Rassweiler and Withrow approach is based on observations from experiments with combustion bombs of constant volume. Namely at any instant in the combustion bomb, the fraction of the charge mass that has burnt is directly proportional to the fractional pressure rise. The latter is defined as the pressure at the particular instant divided by the final pressure

attained from all the mixture burning. In addition, this final pressure attained from the combustion of a unit mass of mixture is inversely proportional to the volume of the bomb. To make use of these experimental observations, Rassweiler and Withrow devised a procedure whereby the combustion within the spark ignition engine could be considered analogous to that within a combustion bomb, and hence, the burnt fraction of the charge deduced. The main difference between the combustion in bombs and engines is that part of the pressure attained in the engine is attributable to the motion of piston, which compresses or expands the mixture. Rassweiler and Withrow hypothesised that the measured pressure in the engine cylinder was produced by the independent effects of combustion and the movement of the piston. Therefore, the pressure increments, due only to combustion, can be found by subtracting the pressure induced by the piston motion from the actual cylinder pressure. Now, if all these increments of combustion pressure, each calculated at a different crank location and, hence, different volume, are referenced to a common volume, then analogous conditions between combustion within the engine and combustion within a single bomb will have been attained. Having determined the changes in combustion pressure, the fractional pressure rise at any crank location is known, and, therefore so is the mass fraction burnt.

Rassweiler and Withrow suggested that the effects of piston motion could be separated from the effects of combustion by assuming that, in a short interval of crank angle, the measured pressure in the cylinder is obtained by the piston movement alone during the interval, followed by the instantaneous combustion of fuel at the end of the interval. Consider the processes occurring between discrete pressure readings (i-1) and i. The pressure changes due to piston motion are modelled by a polytropic process. At the start of the interval the measured pressure in the cylinder will be $P_{(i-1)}$ and, at the end of the interval, the pressure due only to the motion of the piston P_{pi}, will be given by:

$$P_{pi} = P_{(i-1)}\left[\frac{V_{(i-1)}}{V_i}\right]^n \qquad 5.1$$

To use equation(5.1), the value of the index, n, must be specified, which needs to model correctly the changes in pressure due to piston motion in the absence of combustion. The only periods in the engine cycle, when the correct values of n are known, are prior to spark timing and after the end of combustion. The correct value is not known during combustion, where it is actual needed. In the original paper, Rassweiler and Withrow assumed that the average of the indices before spark timing and after combustion would be representative of the required index for the combustion period.

Equation(5.1) decouples the effects of piston motion from the measured pressure, and the difference between the cylinder pressure, P_i, and P_{pi} is assumed to be entirely due to the combustion occurring at volume, V_i . These increments in the combustion pressure can be determined throughout the burning period. However, to complete the analogy to combustion within a single bomb, these increments need to be referenced to a common volume, V_{ref}. This can be achieved from the knowledge that, for a given mass of mixture, the pressure attained in a bomb is inversely proportional to its volume. Therefore, the increment in the combustion pressure at any reading, i, and referenced to the common volume is given by:

$$\Delta P_{ci} = (P_i - P_{pi})\left(\frac{V_i}{V_{ref}}\right) \qquad 5.2$$

These increments in the combustion pressure can be summed from spark time (i=0) to a particular crank angle (i=θ) to determine the combustion pressure attained up to that crank angle. Similarly, the summation of increments up to the end of combustion (i=EOC) yields the final pressure that would have been obtained if all the mixture had been burnt within a bomb. As was stated

earlier, the mass fraction burnt is directly proportional to the fractional rise in combustion pressure, which is given by the division of these two summations:

$$X_\theta = \frac{\sum_{i=0}^{\theta} \Delta P_{Ci}}{\sum_{i=0}^{EOC} \Delta P_{Ci}} \qquad 5.3$$

In the original work, EOC was assumed to be reached once equation(5.2) calculated negative increments of combustion pressure. With the above information, equations(5.1) to (5.3) can be solved to determine the mass fraction burnt from just the pressure-volume relationship for a cycle.

5.3 Summary and Significant Features of the Burn Information Calculation

The procedure is illustrated in fig 5.1. Starting at point *A*, first the pressure induced by piston motion is calculated using equation (5.1) to give point *B*. The increment in combustion pressure is then given by *BC*, which is referenced to the common volume. This "saw-toothing" continues to determine the remaining increments of combustion pressure. These combustion pressure increments are then summed to give the mass fraction burnt from equation (5.3).

An idealised example of the variation of the increments of combustion pressure and the associated mass fraction burnt is represented schematically in fig 5.2. There are several points worth noting about the approximate method suggested by Rassweiler and Withrow:

(i) The isolation of the effects of the piston motion from the cylinder pressure is undertaken afresh during each interval, and the initial pressure for the polytropic process is the actual cylinder pressure that was measured at the end of the previous interval. This measured pressure contains the previous

movement of the piston are not related to the pressure that would be attained if the engine had been motored.

(ii) Before spark time and after the end of combustion, the increments of combustion pressure must ideally be zero. A deviation from this ideal pinpoints an inaccuracy in the calculation of the polytropic process. The most likely cause is an error in the polytropic index, and this is considered in more detail later.

(iii) The mass fraction burnt is the ratio of the burnt mass at a particular crank angle divided by the mass of all the mixture which burns during the cycle. Therefore the denominator of equation(5.3) must be proportional to the final burnt mass of the mixture. Cyclic variations in the summation of all the increments of combustion pressure will directly reflect the variations in the ability of each cycle to combust its induced charge.

(iv) The reference volume acts as a scaling factor on the combustion pressure, as ΔP_C is inversely proportional to V_{ref}. However, there is no effect on the calculated mass fraction burnt, as V_{ref} will appear in both numerator and denominator of equation (5.3). In their paper Rassweiler and Withrow suggest using the cylinder volume at spark time as the reference. If this practice is followed, the final combustion pressure obtained will be a function of spark timing as well as burn efficiency. The consequence is that the afore mentioned measure of the amount of fuel burnt will be lost. The volume at TDC was used as the reference volume in the work presented here.

(v) One application of the methods of thermodynamic analysis is the calculation of heat energy liberation, as a route to determining the fuel burning rate. The equivalent mass fraction burnt, from a heat release calculation is expressed by:

$$X_\theta = \frac{\sum_{i=0}^{\theta} \Delta m_{bi} Q_{HV}}{\sum_{i=0}^{EOC} \Delta m_{bi} Q_{HV}} \qquad 5.4$$

The mass fraction burnt calculated by approximate and thermodynamic approaches will differ if the lower heating value of the fuel changes significantly with crank angle. In the literature survey of chapter 2, it was seen that the calculations by several investigators showed that approximate methods yield burn histories that are almost identical to the results from thermodynamic analyses. Stone [5.2] attributed this good consistency to the constant dissociation rates during the main burn period.

(vi) Due to the normalising of the summed pressure increments, by dividing by the summation of all the increments in combustion pressure, the RHS of equation(5.3) *always* attains the value of 1.0. Therefore, even if only a few percent of the charge mass burns by EVO, the calculated percentage of the mass fraction burnt will always reach 100%. Under the majority of operating conditions this has no significance on the combustion analysis, since a very high proportion of the induced charge is burnt. The two main exceptional cases are late (partial) burning and misfiring cycles, which are considered in detail later in this chapter.

5.4 Detailed Examination of the Approximate Method

There are several uncertainties in the approximate method. The index, n, and EOC both need to be specified, but Rassweiler and Withrow did not offer any firm guidelines on how these might be evaluated. In particular, the specification of the polytropic index must have a strong influence on the method, because it dictates the rate of heat transfer implicit to the calculations. The necessary procedures are further complicated by the imperfections of data acquisition from real engines, because noise oscillations are present in the measured pressure. These oscillations are caused by unavoidable pickup of electromagnetic radiation on the signal lines, and are also quite possibly due to resonance effects near the pressure transducers. In this thesis, the oscillations due to the unknown sources are collectively referred to as 'noise'.

To have confidence in the method all these uncertainties must be addressed. The rest of this chapter examines each in turn, starting with the determination of the end of combustion.

5.5 Determining the End of Combustion

In their original method, Rassweiler and Withrow terminated the calculations once the combustion pressures became negative, and EOC was assumed to have been reached. This method of determining the end of combustion is not ideal. It relies on either the index being wrong, else the increments of combustion pressure would be zero after EOC, or a degree of noise pickup on the pressure record such that the increments of combustion pressure oscillate between positive and negative values about a zero mean. A search was initiated for a more physically representative method of determining the termination of combustion. One approach tried was based on the convergence of the combustion pressure to zero after the charge had finished burning. When calculating the expansion index, a regression line was fitted to the logarithmic variations of pressure and volume, at a point just before the instant where the exhaust valve opened (EVO). It was assumed that the standard error of the fit, itself associated with oscillations in the pressure trace, was an adequate measure of the noise fluctuations of the increments of combustion pressure. EOC was assumed to be reached when these increments had settled to within one standard error of zero. The advantage of this method is that the limits for the convergence would be self compensating to the noise amplitude, through the standard error value.

Three different methods of locating combustion termination are compared in fig 5.3. The "first-negative" method assumed combustion had ended as soon as a negative increment of combustion pressure was calculated. The "sum-negative" waited for the total of three consecutive increments to be negative. This was less sensitive to noise spikes than the "first-negative"

method. The final curve shown has been obtained using the method based upon the standard error. As can be seen, each method indicates a significantly different EOC and marked differences are exhibited in the burn history. Unfortunately, each method of predicting EOC is sensitive to the criterion used, and this casts a doubt on whether any of these methods could be used with confidence. Although the standard error method appears the most appropriate to use, on some occasions it seemed to predict excessively late EOC.

With these uncertainties in mind, an alternative approach appeared necessary. In the original paper, EOC was required so that the calculations were stopped to avoid the, physically impossible, negative increments of combustion pressure. If the correct polytropic index can be found, then the increments of combustion pressure will be zero after the end of combustion, and the calculation procedure can continue right up to the end of the power stroke, i.e EVO. This would eliminate the need to locate EOC. Two potential problems associated with this are: the possibility of problems created by noise fluctuations; and the difficulty of identifying the correct value of polytropic index.

5.6 Noise Pickup

The surroundings of testbeds are regions of high level, electromagnetic noise and the ignition system is a major source of the radiation. As a result all pressure records suffer from noise pickup. Calculations of mass fraction burnt amplify the problem, because pressure differences are utilised as opposed to absolute pressures. This effectively increases the noise to signal ratio. Therefore, although only slight ripples may be observed in the pressure trace itself, strong oscilations appear in the calculated increments of combustion pressure, Shie and Sheng[5.3].

A common approach to eliminating the noise is by hardware or software filtering. Shie and Sheng[5.3] devised a digital filter that was capable of

removing noise effects, including passage resonance around the pressure transducer. However, such filters are time consuming to configure and need tuning to each particular rig. In order to preserve the general applicability of the current method of analysis, other forms of noise handling were considered.

Acute noise pickup was observed in the data from the rig with the 1.6L CVH engine, despite attempts to suppress it. A typical variation of the increments of combustion pressure from this rig is shown in fig 5.4. To suppress the high frequency fluctuations in the data, the Savitzy-Golay[5.4] method of least square smoothing was employed. This method adjusts a set number of points to best fit a parabola. The smoothed curve produced is very similar to the curve that would be produced if the points were smoothed by eye. The greater the number of points involved the greater the smoothing effect. However, too large a number can obliterate detail. Trials using a range of values indicated that the most appropriate number of data points used in the smoothing was 9, and this smoothed curve is compared with the original in fig 5.5.

An interesting feature can be seen when the curves of mass fraction burnt from the smoothed and unsmoothed variations of the increments of combustion pressure are compared as in fig 5.6. There is only a very slight difference, except for minor fluctuations, despite the high level of noise present. There are two reasons for this:

(i) The noise pickup is of high frequency and almost constant amplitude over each period. Therefore, because the burn history is calculated by the summation of increments of combustion pressure, the value of the noise elements summed over each whole period will be zero.

(ii) The effect of any noise elements, not cancelled, will be small compared to the total of the summation of the increments.

Therefore, noise oscillations have a very small effect on the calculated mass fraction burnt and can be ignored. This means there will be no problems encountered by continuing the analysis calculations up to EVO. To adopt the

new approach, all that is now required is to estimate correctly the polytropic index.

5.7 Calculating the Polytropic Index

5.7.1 Heat Transfer Considerations

In the published data of Alkidas[5.5] it can be seen that the heat lost from the cylinder during combustion is approximately twenty percent of the fuel input energy. This must play a significant role in the rate at which the fuel burns, and the heat transfer implicit within the calculation scheme needs to be examined in detail.

Rassweiler and Withrow assume that, during a short interval, the combustion process can be divided into the piston motion followed by the instantaneous combustion of the fuel at the end of the interval. The latter event essentially will be adiabatic, and the former is described as a polytropic process. The magnitude of the polytropic index defines the implicit heat transfer during the interval. For the analogy of the combustion occurring at a common volume, the heat transfer that would occur within a bomb must be catered for. This is not strictly related to the actual heat transfer within the cylinder of the engine, because the temperature differences across each interval of the analysis are reduced. The actual cylinder heat transfer is a consequence of the cylinder pressure and temperature, whereas the heat transfer of the Rassweiler and Withrow method is related to the pressures generated by the movement of the piston. This can be illustrated by reference back to fig 5.1. The cylinder heat transfer, for each interval, will be between conditions AC, CE, and EG. The corresponding conditions for the approximate analysis are AB, CD and EF. Therefore, the heat transfer within the cylinder will be greater than that implicit to the calculations of mass fraction burnt.

The consequence of the above is a difficulty in assessing the correct magnitude of the polytropic index that should be used during each interval.

However, the qualitative effect of variations in the value of the polytropic index can be studied by considering the heat transferred during a polytropic process. From the First Law;

$$\Delta Q = \Delta U + \Delta W \qquad 5.5$$

and for a perfect gas:

$$\Delta U = mC_v\Delta T = \frac{mR\Delta T}{(\gamma - 1)}$$

and;

$$\Delta W = \frac{\Delta(PV)}{(1 - n)} \qquad 5.6$$

Combining these three equations, the heat transferred is given by;

$$\Delta Q = \frac{(\gamma - n)mR\Delta T}{(\gamma - 1)(1 - n)} \qquad 5.7$$

By convention Q is positive when heat is transferred to the cylinder gases. During the compression stroke of the spark ignition engine the induced fuel and air mixture will be of similar temperature to the surrounding block walls. Hence, the heat flow between gases and surroundings will be low and can occur in either direction. Therefore the compression index will not be far removed from the adiabatic value.

In contrast, during the expansion, the product gases are considerably hotter than the cylinder, and heat flow will normally be towards the surroundings. Table 5.1 shows a breakdown of the sign of ΔQ in equation (5.7) for a range of index values in both the compression and expansion stages.

A positive heat flow, i.e heat addition, during the expansion stroke will only occur when combustion is taking place.

To illustrate the effect of the index on the calculation of mass fraction burnt, fig 5.7 shows the results of the analysis using a range of values for the index, which are kept constant throughout the combustion period. The marked differences in the curves are caused by the use of an incorrect value for the index during expansion. The value of 1.3 is greater than the adiabatic, which is approximately 1.26, and during expansion the heat is modelled as being lost to the surroundings as expected. This value is very close to the correct index, because the mass fraction burnt drops slightly from 100% by EVO (the use of the correct index would maintain the mass fraction burnt at 100% through to EVO).

The isothermal value of 1.0 models a process where heat is added to the cylinder gases from the surroundings. This reduces the calculated change in pressure due to the movement of the piston during the expansion. Eventually this change becomes less than the actual change in the measured cylinder pressure, and results in *negative* increments of combustion pressure. The effect on the calculation of the mass fraction burnt is a burn history which prematurely reaches 100% then falls rapidly. Surprisingly, this dropping off of mass fraction burnt is not uncommon in published papers, for example Dye[5.6].

The index value of 1.6 is both greater than the correct index and the adiabatic, therefore, excessive heat loss is implied. In this case the change in pressure due to the piston motion is increased and diverges from the measured pressure of the cylinder. The calculated increments of combustion pressure will be positive throughout the combustion period, and the curve of mass fraction burnt wrongly suggests that burning continued right up to EVO. The index value of 2.6 is a more severe case than the value of 1.6. Although fig 5.7 was exaggerated, it can be seen from the smaller range of index in fig 5.8, that a deviation of 0.05 from the correct value has a marked effect.

Fig 5.9 shows the effects on the calculated pressure due to the movement of the piston when the value of the polytropic index is varied between two extreme values, 1.0 and 1.4. The curves are almost identical until near peak cylinder pressure. The calculation of the mass fraction burnt up to this point will be less sensitive to the value of the index because any differences between calculated pressures of the piston motion will be small compared to the resultant increment of combustion pressure. In the period after peak pressure, which occurs towards the very end of combustion, a more marked deviation in the calculated pressures induced by the piston motion is seen. As this deviation is now large compared with the resultant increment of combustion pressure, the effect on the calculated mass fraction burnt can be severe. This highlights the importance of the values of polytropic index when combustion rates are low, especially at the end of combustion. The main combustion phase is not sensitive to the value of the index due to the dominating effect of the combustion over the piston motion. Provided the correct value for the index is used at the initial and final stages of combustion, there should be little error in the calculated burn history.

5.7.2 Identifying the Correct Index

A commonly used method of calculating the polytropic index is by fitting a regression line to the logarithmic variation of pressure and volume. The slope of this line is equal to the index. However, the author has found the regression method to be unsatisfactory, because, when used in the analysis, most cycles tend to show mass fraction burnt reaching 100% and then dropping off. This will be due to the slight inaccuracies within the calculated indices, caused by noise oscillation in the pressure trace. In searching for a more appropriate method, it was found possible to adjust a given polytropic index to a value which produced little or no drop off. This adjusted value will be the correct index for the analysis.

5.7.3 Adjustment of the Polytropic Index

The adjustment technique was found by considering the relationship between the index, n, and the calculated increment of combustion pressure, ΔP_C . A value of n needs to be chosen that gives ΔP_C equal to zero before combustion commences, in order to set the compression index; and zero after the combustion period in order to set the expansion index value. Now, from equation (5.2);

$$\Delta P_{Ci} = \left(P_i - P_{(i-1)} \left[\frac{V_{(i-1)}}{V_i} \right]^n \right) \left(\frac{V_i}{V_{ref}} \right) \qquad 5.8$$

Taking logs and manipulating;

$$n = \frac{\log \left[\frac{P_i}{P_{(i-1)}} \right] + \log \left[1 - \frac{\Delta P_{Ci}}{P_i \left(\frac{V_i}{V_{ref}} \right)} \right]}{\log \left[\frac{V_{(i-1)}}{V_i} \right]} \qquad 5.9$$

Normally, $[\Delta P_{Ci} / (P_i (V_i / V_{ref})] << 1$, therefore, by expanding out the second log term in the numerator as far as the first power gives:

$$n = \left(\frac{1}{\log \left[\frac{V_{(i-1)}}{V_i} \right]} \right) \left(\log \left[\frac{P_i}{P_{(i-1)}} \right] - \left(\frac{\Delta P_{Ci}}{P_i \left(\frac{V_i}{V_{ref}} \right)} \right) \right) \qquad 5.10$$

For a particular interval in the pressure history, the pressure and volume values will be constant and, therefore, n is linearly related to the increment of combustion pressure, ΔP_{Ci}, with the value decreasing for the compression process and increasing with the expansion due to the sign of $(V_i / V_{(i-1)})$.

When dealing with real data, noise will cause ΔP_{Ci} to fluctuate with crank location. Therefore, it is advisable to use a value of ΔP_{Ci} averaged over a

small crank angle period. The relationship between n and mean ΔP_{ci} from actual data is shown in fig 5.10, for the compression stroke, and fig 5.11 for the expansion. The experimental data of fig 5.10 shows a slight curvature of the n vs ΔPc_i, curve, which is a consequence of $[\Delta P_{ci}/(P_i\ (V_i/V_{ref})]^2$ being ignored.

The linear relationship is advantageous because the correct index value can be interpolated by calculating ΔPc_i, from two initial estimates of n. This is further helped by knowing that the correct index will be near the adiabatic value. For example, the correct index can be found from trial values of 1.2 and 1.35:

$$\frac{n - 1.2}{1.35 - 1.2} = \frac{-\left(\Delta P_{ci}\ @n = 1.2\right)}{\left(\Delta P_{ci}\ @n = 1.35\right) - \left(\Delta P_{ci}\ @n = 1.2\right)} \qquad 5.11$$

To ensure good accuracy in determining the index, the interpolation of equation(5.13) can be repeated, using refined estimates of n, until satisfactory convergence occurs.

The effect of correctly adjusting the index is clearly shown in figs 5.12 and 5.13. The former figure shows a derived curve of the increments of combustion pressure where the expansion index obtained from the log indicator diagram is too large. The increments of combustion pressure converge to a positive value. When the index is adjusted, fig 5.13, these increments converge to an oscillation around zero as expected. The curves of mass fraction burnt from these two conditions can be seen in fig 5.14. The burn history, where the indices are unadjusted, continues to EVO, whereas the case for the adjusted indices finishes combusting at just after 60^o crank angle.

As further evidence that the adjustment of indices produces a valid burn history, a check was made on the combustion endpoint. Because of the uncertainty of the earlier methods of computing EOC, a more physically

representative method was searched out. Karim, Al-Aloisi and Anson[5.7] recommend the use of the variation of the polytropic index calculated at one degree intervals. These investigators noted that EOC could be predicted by the convergence of these polytropic indices to a constant value during expansion The variation of the polytropic index for the previously mentioned cycle is shown in fig 5.15, and, although noise oscillations are present, the values settle to a constant, mean value around 60^{o} crank angle.

The adjustment method is preferred to the regression method because the adjustment acts directly on the calculated increments of combustion pressure, and ensures that after combustion the increments of combustion pressure are zero. Under ideal conditions, the polytropic indices calculated by both the adjustment method and regression would be identical. However, with noise fluctuations and possible small aberrations from the ideal polytropic process, adjustment is the superior method.

Having decided to adjust the indices in this fashion, two questions arise: how many points should the increments of combustion pressure be averaged over, and at what point in the cycle should the adjustment process take place? The former question is answered by examination of fig 5.16. Although fluctuations are apparent, idle data is most susceptible to noise due to the low combustion level, the index appears settled after 10 points (1 point every 1^{o}). Before and after the combustion period, the pressure changes can be calculated by a single index for each process. Therefore, in answer to the latter question, the optimum time to adjust the indices would be at points where combustion is most unlikely to be occurring. Accordingly, the most appropriate location to adjust the compression index is just before spark time, and, for the expansion index, immediately prior to EVO.

Recapping; it is possible to quickly and accurately adjust both the expansion and compression indices to their correct values. And, from the earlier heat transfer study, it was concluded that the accuracy of these values was

essential at the start and end of combustion. The variation of the index value during the main combustion stage is not important, because combustion effects dominate over the piston motion effects. In the work presented here, the index used was the compression value until combustion was underway, and from then on the expansion value was used.

Adjustment of the polytropic index provides a reliable method of calculating the best values to be used in the combustion analysis. This, combined with the earlier observation that noise oscillations have no detrimental effect on the calculated burn trend, means that accurate analysis can be achieved by starting the calculations at spark time and continuing to EVO. This removes the earlier necessity to determine EOC.

5.8 Late Burning Cycles

Under most normal conditions the adjustment method should give accurate results for the mass fraction burnt, but there are two common conditions which are problematic; when the charge is still burning after EVO, and when there is a complete misfire.

A late (partial) burning cycle will have positive increments of combustion pressures up to EVO, and attain 100% mass burnt at this point as a consequence of the normalising of the summed combustion pressure increments. However, when the adjustment to the index value is undertaken on a late burning cycle, the polytropic index is given a value that produces a zero mean over a number of summed points. This results in a low index value that makes the last few increments of combustion pressure negative in order to compensate for the otherwise positive increments. An example of this is shown in fig 5.17, where the averaging of the increments is carried out over 30^{o} to exaggerate the effect. The best remedy is to reset the obtained value of the polytropic index to a higher, more typical magnitude. Resetting should not effect the accuracy of the analysis, because, as described earlier, the calculation

of the mass fraction burnt is insensitive to the index value during the main burn stage. The index has been reset to 1.25 in fig 5.18, and the unadjusted and adjusted index versions of the burn history are given in fig 5.19. Evidence, to confirm that this is indeed a late burning cycle, is given by the non-convergence and low value of the instantaneous polytropic index, fig 5.20.

It is necessary to set an arbitrary condition which will tell when it is appropriate to reset the index in this manner. For the adjustment to produce the negative increments of combustion pressure, the calculated drop in pressure due to the movement of the piston must be less than the drop in the measured pressure. From the earlier considerations of heat transfer, this would require an increase in the heat addition to be implied by the index value. If combustion rates are still moderately high at EVO, the cylinder temperature will still be increasing. By reference to table 5.1, the index value for late burning cycles will be near or less than 1, and unity is a possible threshold value that could distinguish between late and normal burning cycles. Fig 5.21 shows the variation of the index value, for a non-late burning cycle, as the interval during, which the adjustment is made, moves further and further away from EVO, until it crosses into the combustion period. The value of the index drops sharply when the adjustment is undertaken in the combustion zone. The effect is noticeable but less marked for no load due to the much reduced rate of combustion. The sharp drop of the index through the isothermal value suggests that unity is indeed suitable for distinguishing between late and normal burning cycles.

To conclude, if the index drops below the isothermal value, then a late burn has occurred and it is necessary to reset the index to a higher value, for example 1.25.

5.9 Misfires

A complete misfire creates an analysis problem if not identified, because the analysis procedures will still try to determine a mass fraction burnt for the cycle. The calculation scheme will succeed in this because noise and deviations from ideal polytropic behaviour will produce small, false burn increments. As, by definition, there is no burning associated with a misfire, any calculated combustion will be incorrect. This can invalidate the whole analysis, especially if the erroneous data is averaged with the data from normal burning cycles. This can all be avoided if misfires can be identified. Fortunately, the noise oscillations on the pressure records and the non-polytropic behaviour are both minor effects, and misfiring cycles are easy to detect because the summations of all the increments of combustion pressures are close to zero. Fig 5.22 shows the increments of combustion pressure for idle, the operating condition with the smallest value for the summation of all increments. In the hundred cycles analysed at this condition, the final combustion pressure attained, at idle, was always above 5.5 bar. Misfiring cycles have much smaller increments of combustion pressures as can be seen in fig 5.23. The summation of all increments for a misfire was never seen to exceed 2 bar. Therefore, by setting an arbitrary level for a minimum value for the summation that would constitute a valid fuel burning cycle, for example 4 bar, misfires can be eliminated from the analysis.

The approximate method for determining mass fraction burnt has been developed to overcome the uncertainties surrounding the determination of both EOC and the correct values of polytropic index. Also, the method of analysis is able to diagnose, and correct for, late burning and misfiring cycles, which may otherwise confuse the analysis. The next chapter examines the weaknesses and sensitivities in its application.

Chapter 6

Examination of the Inaccuracy Sources in the Determination of the Mass Fraction Burn

6.1 Introduction

There are several sources of experimental uncertainty that are common to all schemes for combustion analysis. These stem from the difficulty in acquiring precise pressure data: the pressure will not be uniform throughout the combustion chamber; the pressure sensed by the piezo-electric transducer is converted to a voltage relative to the datum of the charge amplifier, and therefore needs relating to absolute pressure; the pressure data from the transducer is not aligned to the volume changes, and requires synchronisation; the clearance volume of the cylinder can only be estimated, unless the cylinder head is removed; and finally, accuracy may be lost through the pressure sampling rate being too slow. These uncertainties, although small, may seriously influence the derived burn trend, and, therefore, each effect has been examined in more detail.

6.2 Irreversibility and the Non-Uniformity of Pressure

Combustion analysis schemes, whether approximate or based on the Laws of Thermodynamics, assume pressure to be uniform throughout the cylinder. However, in reality the processes of the internal combustion engine are irreversible, and the properties of the reacting mixture will vary spatially within the cylinder. In the particular case of the approximate method of analysis, described in chapter 5, changes in state are assumed to be polytropic. For polytropic processes, these changes are expressed in terms of pressure and volume, and, therefore, will still apply to the system if it is irreversible. However, the spatial variation of the properties cannot be accounted for, and the

assumption is made that the pressure local to the transducer is representative of the pressure throughout the cylinder. The changes in pressure are distributed by wave action, and normally the flame speed in spark ignition engines is well below the sonic speed. Therefore the pressure gradients within the cylinder will be slight, and the assumption of uniform pressure is reasonable. Furthermore, these analysis methods are not used to determine absolute rates of burning, but are used as a basis for comparing the combustion of one engine cycle, or one engine condition, relative to another. Therefore it is acceptable to ignore the non-uniformity of pressure. The same concept is applied when calculating the work done by the system. The actual work done by the system is given by the integral of the pressure variation over the area of the piston face, A_p, as the piston moves in the x direction:

$$W = \int \int P \, dA_p \, dx \qquad 6.1$$

The variation of pressure is again ignored and equation(6.1) is integrated, between two crank locations, by the trapezium rule:

$$W = \sum_{i=\theta_1}^{\theta_2} \frac{(P_i + P_{i-1})(V_i - V_{i-1})}{2} \qquad 6.2$$

Equation (6.2) will be equivalent to equation (6.1) provided the pressure is uniform, and there are an infinite number of readings between θ_1 and θ_2. Neither of these two criteria are realised in the actual engine, but both can be ignored because, again, the approximation is close to reality, and the work done is normally used as a basis for comparison. Good correlation is achieved between the indicated work, calculated from equation(6.2), and the actual work that is measured at the brake dynamometer.

Although in general the pressure is assumed uniform throughout the cylinder, it is important, during the early stages of combustion, to consider the finite time required for the pressure waves to propagate across the cylinder from the burning zone. A delay time will be incurred before the transducer is able to register the small rises in pressure in the flame kernel. In this early combustion stage, the kernel is confined to the small region near the spark plug electrodes and is surrounded by the compressed fresh charge. Normally the transducer is situated away from the spark plug by nearly the radius of the bore, which is almost 5cm for the engines used in this thesis. At spark time the temperature of the unburnt charge is around 500K and the delay, before the pressure changes in the kernel reach the transducer, will be 115 μs. This is equivalent to over two crank degrees at 3000 rpm. Therefore, pressure analysis is not the best method of investigating the early growth of the flame kernel, especially at high speeds. As the current work investigated operating conditions at similar, low engine speeds, 1500rpm and 2000rpm, the delay time was not of significance.

6.3 Relating the Measured Pressure to Absolute

The pressure measuring system of a piezo-electric transducer and a charge amplifier generates a voltage representing the difference between the sensed pressure and the charge amplifier datum. To obtain absolute pressure the relative pressure should be referenced to a known absolute pressure within the engine cycle. For example average MAP, which can be measured using a mercury manometer. The importance of proper referencing can be evaluated by an examination of the sensitivity of the polytropic indices to changes in the reference MAP value. For the polytropic process:

$$PV^n = \text{constant} \qquad 6.3$$

taking logs and differentiating:

$$\frac{dP}{P} = n\frac{dV}{V} \qquad 6.4$$

therefore,

$$n = - \frac{V\,dP}{P\,dV} \qquad 6.5$$

Changing the reference pressure, will alter *only* the value of P, because the pressure differences and the volumes will be unchanged. Therefore, n is inversely proportional to pressure, and by taking logs and differentiating, equation (6.5) can be expressed in terms of the reference pressure, P_{ref}

$$\frac{dn}{n} = - \frac{dP_{ref}}{P_{ref}} \qquad 6.6$$

Therefore, changes in polytropic index are linearly related to the changes in reference pressure. The experimental variation of the polytropic indices with reference pressure is shown in fig 6.1. Not only do the results show good linearity, but table 6.1 shows that the magnitude of change in index value when the value of the reference pressure (MAP) is altered, is close to the prediction from equation (6.6). In this table, the compression index was determined 20^{o} crank angle before spark time, corresponding to 50^{o} BTDC, and the expansion index was evaluated just before EVO. The behaviour of the indices with changes in the reference pressure explains the large range of index values that can be observed in pressure analysis results.

In contrast, the value of the reference pressure has only a small effect on the calculated burn history, fig 6.2. This is because the previously described method to determine the polytropic indices produces values which are best suited to describe the pressure history, regardless of the reference pressure. The

resultant, slight variation in burn trend will be due to the non-absolute pressure no longer displaying true polytropic behaviour. In fig 6.2, although the compression index is worse effected, if negative burning is ignored, the difference would not be so marked. In any case fig 6.2 is an exaggeration and normally by referring the raw pressure data to average MAP, the calibrated value should be within 200 mbar of absolute. This will have negligible affect on calculated mass fraction burnt.

Although the use of average MAP as a reference pressure is well established in research, there are different schools of thought about which part of the cycle to reference. Lecouna and Rodriguez[6.1] recommend that referencing takes place during valve overlap (-20^{o} to 20^{o} crank angle), whereas Hayes and Savage[6.2] prefer induction stroke BDC (180^{o} crank angle), because the inlet valve is nearly fully open and the effects of piston motion are minimal. Fig 6.3 shows the part of an unreferenced pressure history during the induction period. The high rate of pressure change, from exhaust pressure to intake pressure during valve overlap, effectively rules out this period for accurate referencing. Alternatively, at BDC, pressure variation is comparatively small, indicating a good reference point. To eliminate any effect of pressure ripples, the raw pressure was averaged between BDC $\pm$ 10^{o} and then referenced to MAP. The result, shown in fig 6.4, is close to absolute, because the exhaust pressure at the far left of this figure is just below atmospheric.

6.4 Aligning the Crank Angle Marker

The pressure and crank angle data is acquired using a continuous pulse stream from the shaft encoder. This data must be related to absolute crank location before volume calculations can be made. The standard procedure for alignment is to use the once per revolution marker pulse to relate the crank angle data to engine TDC. This is accomplished by first locating engine TDC as accurately as possible. Lancaster et al[6.3] suggest that by taking dial gauge

readings either side of TDC and interpolating, TDC can be found to within 0.1^{o}. Next, a timing disc is fitted to the crankshaft pulley, and aligned to TDC. Finally, the once per revolution marker pulse is used to trigger a stroboscope and the offset of the marker pulse from TDC can be read off the timing disc. The offset is then used to relate the pressure variation to the volume changes in the analysis software.

Errors in fitting the timing disc, and reading difficulties when using the stroboscopic light on a vibrating engine, suggest that the pressure variation could be offset by up to 0.5^{o} crank angle from the true volume changes. The calculated mass fraction burnt is not affected by this, as can be seen in fig 6.5. It is not until the pressure is out of synchronous with the volume by 4^{o} crank angle that distortions become noticeable. Results taken from the same rig will have common small alignment offsets and this will not affect cycle comparisons. More accuracy is necessary when comparing cycles from different testbeds, because the calculated mass fraction burnt will reflect the alignment errors of the the particular rig. This can be the cause of discrepancies between results from different rigs.

6.5 Estimating the Clearance Volume

The clearance volume can be determined in two ways. One is to remove the cylinder head and measure the quantity of white spirit necessary to fill the combustion space. The other is to calculate the clearance volume from the compression ratio. The first method is not always practical, and the second can be inaccurate due to production tolerances in the compression ratio. Fig 6.6 shows the effect of changing the specified clearance volume on the calculated mass fraction burnt. Although the burn shape does not appear to be distorted, for the 20% change in clearance volume from 51cc to 63cc, a shift of nearly 4^{o} crank angle is seen at the 70% burnt point. Again fig 6.6 is an exaggerated illustration, and normally production tolerances result in only about 5%

variation in clearance volume. Therefore, the calculated burn history can be expected to be within 1^{o} crank angle, if the clearance volume is determined from the compression ratio.

6.6 Resolution of the Sampling Rate

The sampling rate must be sufficient to record the pressure changes. Clark and Challen[6.4] suggest reading every 1^{o} for petrol engines. The uncertainty with the approximate analysis is that erroneous increments of combustion pressures may arise if the sampling interval is too large, because the piston motion will not be totally independent of the combustion process. The sensitivity of the calculated mass fraction burnt to the sampling rate was examined and the results shown in fig 6.7. As can be seen, there is no substantial difference in burn history between sampling intervals of 1/3 and 3 degrees. Therefore, the sampling rate is not critical in determining the mass fraction burnt. The convenient sampling interval to use is 1^{o}, as burn durations and locations are normally expressed in whole degrees.

6.7 Conclusions from the Appraisal of the Technique

The assumption of uniform pressure within the combustion chamber is untrue, but the pressure gradients normally encountered in petrol engines are slight and can be ignored. A potential problem, associated with the non-uniformity of pressure, is the time delay for the early combustion pressure to be registered by the transducer. Allowances should be made for the delay when comparing early combustion data of cycles at high engine speeds.

Inaccuracies in calibrating the raw measured pressure to absolute have a pronounced effect on the polytropic index. This explains the wide range of values encountered in pressure analysis. However, because index values are calculated that are appropriate to the ill referenced pressure, there is no marked effect on the calculated durations of mass fraction burnt.

Alignment errors of pressure to volume are negligible up to being 2^{o} crank angle adrift in as far as the effect on the analysis calculations. However, the offset must be taken into account when comparing burn locations in data acquired from different testbeds.

Incorrect calculation of the clearance volume can also be a source of error. Normal production tolerances in compression ratio can cause an error of 1^{o} crank angle in the burn duration. If a greater accuracy is necessary, the cylinder head should be removed and the combustion space measured using white spirit.

The mass fraction burnt appears insensitive to sampling rate, and a reading every crank angle degree is sufficient and also convenient.

The above points indicate that the implemented method of analysis is not engine specific and can be readily applied to any test facility. If the above points are carefully followed to ensure proper data acquisition, then the errors in burn duration will be limited to around 1^{o} crank angle, which is acceptable for comparisons of combustion performance.

As an example of the portability between rigs of the analysis system, and as a check on the calculation of mass fraction burnt, the method was used to analyse data from an engine operating in the cold cell at $-20^{o}C$. Four cycles of data that showed peculiar characteristics in their combustion, are presented here. Fig 6.8 shows the pressure histories acquired from the testbed in the cold cell. The results from applying the described version of the combustion analysis technique are identified in fig 6.9.

The pressure history of cycle 1, resembles a motoring trace up to 30^{o} ATDC. From then on, the pressure only drops slightly to EVO. This would suggest a long time for the development of the flame kernel; the flame front not beginning to propagate until near 30^{o} ATDC. Once propagation starts, it proceeds slowly up to EVO. The calculated burn trend for cycle 1, in fig 6.9, corresponds exactly with this hypothesis.

A similar statement can be applied to cycle 2, except that the kernel development is slightly shorter, and the subsequent combustion rate is faster, producing a second higher peak pressure. After this second peak the pressure history begins to follow the normal expansion shape, suggesting that combustion finishes before EVO. Again these statements are seen to be calculated by the method.

The flame kernel development is faster again in cycle 3. The main combustion phase appears similar to cycle 2 except there is a noticeable slowing in the rate of pressure rise at about 30^{o} ATDC. The calculated burn history for cycle 3 agrees with the speculations made from the pressure trace, and the calculated main combustion phase has a longer duration than cycle 2.

Cycle 4 is, by far, the best burning cycle. The main burn stage starts slightly after TDC and proceeds quickly to produce a much greater peak pressure than the other three cycles. Once again these points are revealed in the burn patterns shown in fig 6.9.

Figs 6.8 and 6.9 prove that inferences about combustion behaviour are correctly calculated by the analysis procedure. Obviously the burn histories shown in fig 6.9 contain more information than can be qualitatively obtained from fig 6.8. This analysis example highlights the general applicability of the analysis method and its ability to calculate combustion trends.

Chapter 7

Determination of Heat Lost During Combustion

7.1 Introduction

The evaluation of the heat exchange between the cylinder contents and their surroundings plays an important part in determining engine performance. The heat flow through the cylinder head and piston influences such quantities as block temperature, coolant load and engine warm up time. Current methods of calculating the gas to wall heat flux are complicated. Direct measurement has been attempted using a surface thermocouple, Alkidas and Myers[7.1]. This consists of two thermocouples, one situated on the surface of the device, and the other a known distance behind it. The heat flux can then be calculated from the two temperature readings by assuming one dimensional heat transfer occurs between the thermocouples. However, this technique is difficult to exploit for several reasons: the spatial variation of the heat flux requires the placing of several surface thermocouples; the presence of the thermocouple may distort the true flux field; and the complexity of machining the cylinder head or block to allow location of the thermocouple in the correct orientation.

An alternative approach is to perform a complete thermodynamic analysis, in which the heat lost to the cylinder walls is assumed to be given by:

$$\frac{dQ_{ht}}{dt} = h A (T - T_w) \qquad 7.1$$

Woschni[7.2] and Annand[7.3] have both derived correlations commonly used for h. These take the form, $h = aR_e^{\,b}$, which is typical of turbulent and convective heat transfer. The constant, a, in the correlation needs to be set to a value which predicts the same quantity of heat rejected to the surroundings as

determined by a heat balance on the test engine. This requires several iterations of the thermodynamic analysis before satisfactory results can be obtained, and the procedure must be repeated for each engine under test.

If the instantaneous heat transfer could be calculated simply, in the same fashion that it is possible to use an approximate method to calculate the charge burn history, some of the disadvantages associated with current methods of determining the heat flow could be avoided. The following describes a novel method of achieving this by using First Law analysis to extend the interpretation of cylinder pressure data. The work on the heat loss scheme is on going, but the outline of the method, and a qualitative examination of its accuracy, is included in this thesis.

7.2 The Heat Transfer Analysis

By expressing the First Law of Thermodynamics in terms of a polytropic process, the net heat transferred during a particular interval can be found:

$$\Delta Q_n = \left(\frac{\gamma - n}{(\gamma - 1)(1 - n)}\right) \Delta(PV) \qquad 7.2$$

It was seen in chapter 5 that inserting the polytropic indices, used for the calculation of mass fraction burnt, into equation(7.2) will only determine the actual cylinder heat transfer at points before and after the combustion event.

A completely new approach is now suggested that can determine the heat exchange, during the whole combustion period, by using equation(7.2). Consider fig 7.1, this shows the measured pressure history and the "saw-toothing" of the computations used to determine the mass fraction burnt. In this figure *AB* is the polytropic compression of the cylinder gases by the piston motion, and *BC* would be the increment of combustion pressure from the

approximate analysis scheme. As explained in chapter 5, the heat transfer implicit to the combustion analysis is derived from the process A to B. The actual heat transfer within the cylinder is dependent on the process A to C. However, if only the measured pressure variation is considered, the process A to C can itself be assumed to be a polytrope, and the associated index can be calculated from the pressures and volumes at A and C. When this local index value, as opposed to the combustion analysis value, is inserted in equation (7.2), the actual cylinder heat exchange between A and C will be determined.

The heat transfer determined by equation (7.2) in this manner will be the combination of the heat released by the fuel burning and that lost to the surroundings. Therefore, in principle, the heat lost (positive for transfer to the surroundings) can be evaluated by:

$$\Delta Q_{ht} = \Delta Q_f - \Delta Q_n \qquad 7.3$$

The heat released by combustion during each crank angle interval can be obtained from knowledge of the mass fraction burnt:

$$\Delta Q_f = m_f Q_{HV} \Delta X \qquad 7.4$$

Equations(7.2) to (7.4) can be applied in a step-wise procedure to determine the instantaneous heat transfer throughout the combustion period, by using local values of polytropic index, obtained directly from the cylinder pressure variation.

One of the necessary inputs for the heat loss analysis is the ratio of the specific heats, γ. For a preliminary evaluation of the model, approximate data published in Heywood[7.4] was used to obtain γ for combustion reactants and products at various equivalence ratios and temperatures. For simplicity the temperature variation was ignored and two values of γ were determined at

particular equivalence ratios, one for the reactants and the other for the products. The values used are shown in table 7.1. Linear interpolation was used to determine γ at the non-specified equivalence ratios. These γ values are for the initial, unburnt mixture, and final, completely burnt mixture. The magnitude during combustion would be given by:

$$\gamma = \frac{X\,Cp_b + (1 - X)\,Cp_u}{X\,Cv_b + (1 - X)\,Cv_u} \qquad 7.5$$

Equation(7.5) can be inconvenient, and close approximation is possible using a simplified variation for γ:

$$\gamma = (1-X)\,\gamma_u + X\,\gamma_b \qquad 7.6$$

Another quantity that needs to be specified is the induced mass of fuel. This may be calculated from the rate of fuel consumption, F_C, of the engine. If allowances are made for mal AFR distribution by assuming the mass flow of air is the same to each cylinder, the fuel mass can be determined: b_7 :

$$m_f = \left(\frac{1}{N_C}\right)\left(\frac{F_C}{N_S}\right)\left(\frac{AFR_{common}}{AFR_{cylinder}}\right) \qquad 7.7$$

In this case, N_C is the number of cylinders in the engine, N_S is the number of engine cycles per second, AFR_{common} is the average air-fuel ratio of all cylinders, and $AFR_{cylinder}$ is the air-fuel ratio of the cylinder under investigation.

Fig 7.2 shows the typical accumulative heat transfers calculated by the new method. The heat released by the fuel is represented by the top curve and underneath is the calculated net heat transfer from the summation of equation

(7.2) over the combustion period. The net heat flow is positive up to about 40^{o} ATDC, due to the dominance of the fuel heat release. After this point, heat loss dominates and the accumulation of the net heat addition begins to fall. The lowest curve is the accumulated heat rejection from the combustion gases, and is accompanied by fig 7.3, which is the rate of heat loss per crank angle degree. The heat loss curve goes slightly negative for the first few crank angles after spark time, then increases slowly until just after TDC. After this point, the gas temperature will be rapidly increasing and produces a corresponding increase in the rate of heat loss. Once combustion has terminated, heat transfer from the combustion chamber continues due to the temperature difference between gas and surrounding walls, but the rate of heat loss begins to diminish as the combustion products expand and cool.

7.3 Discussion

It is difficult to verify the accuracy of this scheme to determine the heat lost. However, a qualitative examination of the method's results were made using experimental data and by alternative methods of theoretical analysis. Engine pressure data was obtained at two load-speed conditions: a low speed, part load condition (constant throttle position set at 1500 rpm, 2.62 bar BMEP under the control of the production system for engine management); and a full load condition (2000 rpm WOT). The part load condition corresponded to WWMP, an American standard for test conditions, which typifies the average of the world's running conditions.

The first evidence showing that the calculations for the heat flow are consistent with expectation is seen in the total heat lost seen in fig 7.2. The total represents approximately 30% of the fuel input energy, which is in agreement with the anticipated value, Taylor[7.5]. In addition, consistency with published data can be obtained by scaling fig 7.3 into MW/m^2 and comparing it to the heat flux values measured by Alkidas and Myers[7.1] at similar operating

conditions. The pattern of heat loss appears to be virtually identical, and the two sets of data are shown in fig 7.4.

A further source of information to assess the analysis technique is from the qualitative examination of changes in heat loss that is determined when operating conditions are altered. From equation(7.1), if the heat transfer coefficient is assumed constant, the amount of heat rejected to the surroundings can be varied by altering either the temperature of the combustion gases, or the block wall temperature. The former can be effected by altering the AFR from lean combustion to a setting near best power, and the latter by comparing data taken just after engine start up, and when the engine is fully warmed up. Duplicate tests, to show repeatability, were carried out at four suitable conditions. In each case the pressure was averaged over 100 cycles and then the heat analysis applied.

Fig 7.5 indicates the amount of fuel input energy and heat loss at each condition. In changing from 12:1 to 16:1 at 2000 rpm WOT, the mass of fuel induced will decrease, because the mass flow of air will remain constant; and the fuel input energy decreases. However, the decrease seen in the predicted heat loss far outweighs the reduction in heat liberation, and will be attributable to the reduction in the gas temperature, as anticipated. Similarly as expected, at part load, the cold engine has increased heat loss due to the lower wall temperature. In this case, as the engine is running at the same speed-load in both cold and hot states, more fuel input energy is required for the former condition to overcome the increased heat and frictional losses.

Fig 7.6 shows the heat lost as a percentage of the fuel input energy. This is a better illustration of the variation in heat loss as operating conditions are changed. At full load, the heat loss drops from near 35% to around 20% when the AFR is made leaner; and at part load the heat loss increases from 32% to nearly 40% by running the engine cold.

The final figure in this set, fig 7.7, shows for each of the above cases, the distribution of fuel input energy to the processes of work done, loss to coolant and loss through the exhaust. These results are also consistent with anticipated trends, Taylor[7.5].

As a method of checking the absolute accuracy of the calculated magnitudes of the heat loss, the First Law was again applied between spark time and EVO. However, this time, equilibrium conditions were assumed at these two cycle points, and a "textbook" analysis performed using thermodynamic data obtained from Heywood[7.4]. The data used is shown in fig 7.8, and the following set of equations were applied to derive the heat lost to surroundings:

$$R_u = \frac{R_O}{M_u} \qquad \text{and} \qquad R_b = \frac{R_O}{M_b} \tag{7.8}$$

$$C_v = \frac{C_p}{\gamma} \tag{7.9}$$

$$T_s = \frac{(PV)_s}{m\,R_u} \tag{7.10}$$

$$T_{EVO} = \frac{(PV)_{EVO}}{m\,R_b} \tag{7.11}$$

$$Q_f = m_f\,Q_{HV} \tag{7.12}$$

$$W = \int_s^{EVO} P\,dV \tag{7.13}$$

Equations (7.8) to (7.13) allow the heat lost during the combustion period to be determined from the First Law:

$$Q_{ht} = Q_f - W - m\,(C_{vb}\,T_b - C_{vu}\,T_u) \qquad 7.14$$

Table 7.2 tabulates the above analysis at the four conditions shown in figs 7.4-7.6. At the part load condition there is good agreement between the above analysis and the new method's results. Agreement is not as good at 2000rpm WOT, for no obvious reason. A major difficulty in drawing conclusions from such comparisons is the uncertainty in the accuracy of experimental data. Consequently, studies have been carried out to examine the accuracy of calculations of the heat transfer made from theoretically generated test data.

7.4 Comparisons to an Engine Pressure Simulation Model

The best method of examining the uncertainties within the above scheme for determining heat loss is to analyse a pressure trace generated by a simulation procedure. A known heat loss variation can be prescribed, and the ability of the calculation scheme to recover this information examined. The simulation procedure was formed by deriving the pressure rise during a discrete interval using the First Law applied to a perfect gas.

$$\Delta P = \frac{(\gamma - 1)\,\Delta Q_n - \gamma P \Delta V}{V} \qquad 7.15$$

and the pressure after each interval is obtained from:

$$P_i = P_{(i-1)} + \Delta P \qquad 7.16$$

To obtain the pressure history the net heat transfer during each interval is required:

$$\Delta Q_n = \Delta Q_f - \Delta Q_{ht} \qquad 7.17$$

The cosine burning law was assumed for heat release , Ferguson[7.6];

$$\Delta Q_f = \left(\frac{m_f Q_{HV}}{2}\right)\left(\cos\pi\left(\frac{\theta_i - \theta_s}{\theta_d}\right) - \cos\pi\left(\frac{\theta_{(i-1)} - \theta_s}{\theta_d}\right)\right) \qquad 7.18$$

And the Eichelberg heat loss correlation, from Benson and Whitehouse[7.7] was used for heat loss, because of its simplicity compared to other correlations;

$$\frac{dQ_{ht}}{dt} = K A V_p^{\left(\frac{1}{3}\right)} \sqrt{(PT)}\,(T - T_w) \qquad 7.19$$

The dimensional parameter, K, in the heat loss correlation was adjusted to produce the desired level of heat rejection, namely about 30% of the fuel input energy.

Intrinsic within the simulation code is the data describing the 2.0L OHC engine dimensions, spark timing and the burn period to be used. The simulation required input of fuel mass and the pressure at IVC, and then stepped through to EVO generating the corresponding pressure history. The parameters used to govern the simulation are presented in table 7.3.

One requirement for running the simulation is the specification of the crank angle interval across which each pressure rise is calculated. When there is no combustion or heat loss taking place, the calculation method for the heat loss, described earlier, becomes a simple First Law formulation, and is sensitive to the polytropic indices derived from the pressure history. Therefore when a suitable interval size is used in the simulation, the heat loss calculated by this method will be zero. Motored, adiabatic conditions were described within the simulation and the step size was varied. The heat loss calculated by the new method was recorded, and the results are presented in fig 7.9. As the step size was decreased the polytropic indices derived from the simulated pressure

became closer to the value of the specific heat ratio specified in the simulation, and the calculated heat loss approached zero. A step size of 0.01 of a crank angle was considered to offer satisfactory accuracy.

By introducing combustion and heat loss into the simulation, the performance of the method for determining heat loss was assessed. Two simulated conditions for firing cycles were used: an adiabatic combustion case; and a case where heat loss was modelled by the Eichelberg correlation. The comparisons are presented in table 7.4. Good agreement between the heat loss determined by the new method and the simulation heat loss was seen for both baseline conditions. For the case of the Eichelberg heat loss, the variations of the calculated and simulated results virtually overlay each other, fig 7.10. This illustrates that the calculation scheme accurately calculates the heat lost during combustion.

The next step was to examine the sensitivity of the calculation method to changes in the ratio of the specific heats and the fuel mass. The results are shown in Table 7.5. The calculated total heat loss is strongly influenced by γ, and this is compounded by the data in fig 7.11, which shows that the pattern of heat loss also becomes skewed. An under-estimation of γ produces the worse distortion. Negative heat loss, corresponding to heat addition from the surroundings, is calculated in the earlier part of the combustion period. After this, the instantaneous rate of heat loss rises steadily until 410^{o} crank angle, which corresponds to EOC. A slight discontinuity in the heat loss is seen in both deviant curves at this point. With the over-estimate in the specific heat ratio, an earlier and greater peak rate of heat loss is attained. The effect on the predicted total heat loss is reduced because in either case, an over-estimated rate of heat loss on one side of the peak is counterbalanced by an underestimation on the other side of the peak. The conclusion from fig 7.11 is that, for credable calculations, it is important to determine the specific heat ratio to within 0.025 (2%), and a slight over-estimation is preferable. Referring back to table 7.1, it

can be seen that the temperature variation of the product γ is slight and should not be a source of large error. However, the reactant γ does exhibit a strong temperature variation, which was not allowed for in the above analysis of the experimental data. This is the most probable cause for the earlier discrepancy between the calculated and the theoretical heat loss at 2000 rpm WOT. The loaded condition is more sensitive to inaccuracies in γ because the heat rejection rates are greater. This variation of the reactant specific heats with temperature is difficult to allow for, because the fresh charge becomes heated as combustion proceeds. One possible solution is to find the unburnt and burnt mixture temperatures from the equation of state:

$$T_u = \frac{PV_u}{m_u R_u} \qquad 7.20$$

$$T_b = \frac{PV_b}{m_b R_b} \qquad 7.21$$

The mass fraction burnt will be known from the combustion analysis, and a relationship between mass burnt and volume burnt is described in equation (2.1) of the literature survey (chapter 2). As the gas constant is a function of temperature, the actual zone temperatures can be found by a simple iteration between temperature and R. Unfortunately, there is no obvious method of verifying this calculation technique, as there is no definitive heat flux measurement or calculation method. Work is on going to validate these proposals.

The heat loss calculated by the new method is also sensitive to the fuel mass. This is a direct reflection of the change in fuel input energy, and produces an almost one to one change in the percentage of the heat lost, as seen in table 7.5. Incorrect fuel mass can also skew the heat loss trend, fig 7.12, but the

effect is not as severe as seen with the specific heat ratio. Again over estimation produces an earlier and greater peak heat loss, and an under estimation a later and lower peak. The method stated for calculating the induced fuel mass, equation (7.7), should be accurate to within a couple of percent, and is of sufficient accuracy for comparison of heat loss calculated at different operating conditions.

7.5 Conclusions

The proposed method of determining the instantaneous heat lost during combustion does not require the time overhead of adjustment to each particular engine configuration as is the case with heat transfer correlations. Nor does this method require the wall temperatures of the combustion chamber to be defined. Instead the heat flows are calculated in a much simpler scheme, based on a polytropic version of the First Law.

One problem is that the calculations are sensitive to the specific heat ratio, and γ needs to be found to within an over estimate of 2%. If the specific heat ratio is correctly specified, the method will accurately determine the heat loss to the block.

Previously, approximate methods for combustion analysis have not been able to calculate heat transfer rates. The development described above indicates it is possible to overcome this deficiency and provides an alternative to the more complex methods which are normally required.

Chapter 8

The Cylinder Pressure Analysis System (C.P.A.S)

8.1 Introduction

The calculations for the mass fraction burnt, described earlier, have been developed for applications using a personal computer. This is possible because of the recent technical advances in computer architecture, which provide increased resources of dynamic memory, fast processor speeds, and expansion slots for data acquisition boards. In addition, software packages are available, which give flexibility of programming language, data storage and retrieval, and data presentation. The whole analysis system can be supported on a single PC, in this case an Olivetti M24sp, and the resources used are given in table 8.1. The processing system was named CPAS (Cylinder Pressure Analysis System).

The interactions of each program stage are presented as a data flow diagram in fig 8.1. Pressure data is captured directly from the engine at the far left of fig 8.1. Then, through a variety of processes, the data is analysed and stored in a database system for retrieval at the far right of the same figure. C.P.A.S is a post analysis system, in that the pressure cycles are stored on disk and analysed subsequently. All the figures of pressure analysis presented in previous chapters, except chapter 7, were generated using C.P.A.S.

An important part of any complex system, is the user interface. This is the only contact the investigator has with the data. If the interface is difficult to use, then human errors may influence the analysis or even crash the system losing all the acquired data. With this is in mind, considerable time has been spent on providing a "user-friendly" front end for CPAS.

The rest of this chapter describes the three components of acquisition, analysis and databasing that form CPAS.

8.2 Data Acquisition

Data is acquired into the personal computer via a Labmaster, 12 bit, 100kHz, ADC board. Pressure is referenced to crank location on each engine cycle, as opposed to on each engine revolution. The reference point chosen was induction TDC, and was obtained by halving the occurrence of the normal TDC marker pulse, by use of a 'D' type flipflop. The marker pulse at induction TDC can be maintained in hardware by clearing the flipflop with an inverted pulse occurring at spark time. This produces a marker pulse with a long pulsewidth, which is passed through a monostable to shorten the duration to 25μs. This pulsewidth was chosen because the digital port is TTL level sensitive, and a pulse duration of less than 1 degree crank angle at 6000rpm avoids any potential errors in alignment. These steps are shown in fig 8.2, along with the engine signals required to drive the ADC. The logic behind producing the marker pulse at induction TDC is given in fig 8.3.

8.2.1 Acquisition Software

Once the hardware is installed, the acquisition process can be driven by software. The algorithms for data capture are straightforward. The most complicated example includes a check on the alignment of the pressure to absolute crank angle, and is flow charted in fig 8.4. The routines can be coded in any programming language. Assembler, although the fastest executing, is not convenient for either writing file handling operations or for the design of a suitable user interface. The choice fell between Turbo Pascal and 'C'. Turbo Pascal appeared superior because when benchtested it had a higher rate of data transfer and, also, it permitted the use of in-line machine code. Embedded machine code was necessary to detect the presence of the short marker pulse at induction TDC pulse. The software uses a polling technique to read the data into the computer, and the application of Turbo Pascal and the Labmaster ADC

enabled a data capture rate of 30Khz. This permitted acquisition up to a maximum engine speed of 6000rpm.

With the MS-DOS operating system and the acquisition software being memory resident, there are about 600 kbytes of RAM available for data storage. Analogue pressure comprises two bytes per reading and spark data one. Therefore it is possible to capture 277 contiguous cycles of data before it is necessary to transfer the data to hard disk.

8.2.2 User Interface

The acquisition system is menu driven. One set of options allow the update of ADC calibration, readings per cycle and the number of cycles to be captured. Another main menu controls the data capture. It either enables the user to obtain pressure data with or without spark data, saving the information to file, or as another alternative to continuously present samples of pressure histories on the screen.

The menus are user-friendly in use permitting only the menu selection characters to be entered from the keyboard, and not allowing the termination of the acquisition routines by mistake.

8.3 Analysis Program

The analysis stage of C.P.A.S reads the acquired data from disk and proceeds to calculate the cyclic values of the combustion diagnostics given below:

Peak Pressure value and crank angle location

Peak Rate of Pressure Rise and it's location

Work loop Mean Effective Pressure, WMEP

Intake loop Mean Effective Pressure, PMEP

Indicated Mean Effective Pressure, IMEP = WMEP + PMEP

Spark Advance

2%, 10%, 50%, 90% and 10 to 90% Burn Durations

Final Combustion Pressure Attained

Peak Rate of Combustion Pressure Rise and its Location

Percentage of Partial Burns and Misfires

The mean and coefficient of variance, defined as the standard deviation divided by the mean, of these parameters are computed to characterise the combustion of the particular data set.

C.P.A.S itself does not display any results. Instead ASCII files are written which can be sent to the printer or imported into data plotting packages, for example GEM Graph. A hardcopy can then be obtained from a laser printer. Four files in all are created by CPAS. The first contains the analysis report, an example of which is presented in fig 8.5. The second file contains the frequency of IMEP values within the data sample. This can be used to generate a bar chart within GEM Graph, an example is shown in fig 8.6. The third contains the increments of combustion pressure and is used to construct the curves of mass fraction burnt previously seen. The last file contains a diagnosis of unusual cycles; if a cycle was a partial burn, misfire or never had a TTL spark presence pulse, this information is reported in the diagnosis file.

8.3.1 Analysis Software

The program for the analysis is too large to explain in detail in this thesis. Instead a general overview is given. The program is a straight forward interpretation of the previously described calculation scheme for mass fraction burnt. The function interactions, and steps to evaluate the parameters, are expressed in Warnier-Orr diagrams in Fig 8.8 and 8.9. Fig 8.7 is given to illustrate how best to interpret Warnier-Orr diagram.

The programming language 'C' was chosen to develop the analysis software. 'C' has the advantage of allowing small, easily readable and maintainable function modules to be linked together to form the otherwise extensive analysis program. 'C' is well supported, with libraries for graphics, screen handling and data communications, making it a flexible, environment for developing programs.

8.3.2 User Interface

For user guidance, the number of the cycle being analysed plus the part of the calculation currently being executed are displayed on the screen. The analysis software is self contained and the user access is through a special software interface. This isolates the pressure data from accidental corruption by the user. The inputs required from the operator are details of engine geometry, valve timing, MAP, the number of cycles read and the sampling rate. The user interface presents to the screen a list of the required data titles and input fields. The field values default to the most recently used data set. The user can transfer randomly between the data fields by use of the cursor keys. As a further precaution, the software does not permit letters to be written in a numerical field and vice versa. Only when the user is satisfied that all values are correct, will the interface write them to file for use by the analysis software.

8.4 Database Program

An electronic database was designed to facilitate a quick retrieval of relevant combustion data. The primary objective of the database was to allow immediate recall of all data sets conforming to one or more target parameters. For example, a listing of all data sets having a 10-90% burn duration of 30^{o} crank angle at an engine speed of 1500 rpm.

Although various database programs are commercially available, for the flexibility that was required for C.P.A.S it was decided to create a specialised

database from the C-TREE routines. This is a library of ISAM functions with the index keys stored within a B-TREE. Such databases have powerful recall ability, being able to search through one million keys in 5 disk accesses.

8.4.1 Database Software and User Interface

The software was split into two programs. The first simply stores and indexes the analysis report and information concerning the running conditions of the rig. For this, user interface is employed that is similar to the one used for the input of the data for combustion analysis. The second program allows the database to be searched by up to five target keys. The software locates all conforming records, and the information within each record extends to three pages. These records are displayed on the screen one page at a time. The user may then select whether to update a particular value, go on or back a page, or receive a hard copy of all the records via the printer. An example screen output of the search routine is presented in fig 8.10.

Chapter 9

The Quikburn Analysis System - An On-line Combustion Analysis Facility

9.1 Introduction

The utility of CPAS was restricted by the 640kb of memory available, which allowed a maximum of 277 cycles to be acquired. The raw data was transferred to hard disk, which in turn could accommodate only 7 data runs in any one session. This acquire, then analyse approach has a large processing time overhead, and limited the amount of useful work that could be achieved in a single test session. Although this is a common processing arrangement, these systems do not conform to the researcher's wishes. The need is for a fast analysis system so that the researcher can adjust the running conditions of the engine and immediately observe the effect on the combustion. Operating conditions that produce desired combustion behaviour can be quickly obtained, and a volume of relevant data collected. This is a great benefit, because in the past the data would be taken at a point approximately where the phenomena occur, and only a small part, if any, of the data would be directly of use. The latest innovations in computer technology allow these goals to be approached.

Even if the burn histories could be calculated and displayed in real time, the human eye would not be able to register the constantly changing screen. Instead it would be preferable to acquire and analyse a few cycles and display their average properties every couple of seconds. The researcher would then be able to observe the combustion process at a comfortable rate. This was the objective of the analysis system, named Quikburn, where the engine can be considered to be on-line to the processing system.

The literature survey showed the latest developments to combustion analysis systems was to incorporated some form of processing in real time. A

system with fast analysis has been developed by other researchers, Bain et al[9.1], but it did not concentrate solely on calculating burn histories, and the resulting processing time was approximately 40 seconds per cycle. This system appeared to be aimed at university undergraduate and postgraduate teaching and was dedicated to the analysis of particular quantities. The aim of the system developed during the current work was to go much further than this. Its specification was that cycles were to be updated to the screen within a couple of seconds, and also, the system was to be as flexible in its operation as possible. The flexibility required that the program was written in a highly structured format, so that the investigator could easily modify any section to achieve different analysis strategies during the same engine test session. An additional feature, used in this thesis, was a facility for automating the sweep to locate MBT timing. For this, Quikburn calculated WMEP, burn durations and peak pressure, whilst setting the spark timing on the engine via an RS232 link with an Olivetti computer. The spark timing control was explained in chapter 4. Although the user has direct access to the analysis procedures, a professional working environment was maintained by communicating with the system via user-friendly menus and data input screens. These communication aids control operations such as the input of the engine geometry data, diagnostics of the incoming signals, and the on-line analysis itself. It is felt that the Quikburn system has great potential for combustion research, far exceeding the two applications of monitoring and MBT sweeping described here. The detailed description of the system is presented in this chapter.

9.2 Hardware Resources and Interfacing

Details of the computer system used to develop and implement Quikburn are given in table 9.1. Although the necessary data signals from the engine are the same as used with CPAS, the interfacing is slightly different. The Infotech AD200 board has no enable line to start the acquisition, nor any digital ports.

The consequence of the former is that referencing the acquired pressure to induction TDC must be done within software, and the latter requires a GPIO board to be used for digital input. Referencing the pressure changes to TDC can be accomplished in software by acquiring the analogue and digital data simultaneously into two arrays, and then locating the array element in which TDC occurred. Induction TDC, as opposed to firing TDC, then can be found by using a version of the algorithm used to check the alignment of the pressure changes previously described in chapter 8. Simultaneous acquisition of digital and analogue signals can be attained by sampling the GPIO and ADC at the same instant. This synchronization can be attained by triggering the ADC board from the shaft encoder, and the GPIO board from the ADC SYNCH OUT line, which is an echo of every trigger seen by the ADC board. In this manner, the acquisiton of the data at the GPIO can be enabled each time the ADC board is triggered. The GPIO trigger needs to conform to the protocol for full mode handshaking, shown in fig 9.1A. The data acquisition requires a slower response time from the computer system than the normal peripherals used. Therefore, as the computer will always be ready and waiting for the next trigger, there is no need to check PCTL is set. Data can be latched into the GPIO by the rising edge of the ADC SYNCH OUT, which corresponds to a ready to busy transaction on the PFLG line. Both ADC and GPIO can now be successfully triggered by the shaft encoder 1^{o} pulses output. The ADC trigger is very sensitive to noise ripples, and a worthwhile precaution is to use the digital filter circuit, described in chapter 3, on the trigger line. The propagation delay through the filter is advantageous in that it allows time for the digital data to settle, before sampling occurs. The circuitry for the above is shown in fig 9.1B.

9.3 The Quikburn Software

The complete analysis package was designed to be simple to use. The engine data is acquired, stored in dynamic memory, analysed, and displayed in one operation without disk access. The user interacts with the system via menus and the user-friendly input screens to obtain the results required. The user also has easy access to the program source code, and may tailor the analysis to an alternative specification. The data flow diagram for the Quikburn system used in this thesis is shown in figure 9.2A. When the program is running, the user communicates with the software via a menu which controls the operating environment. This then passes control to the part of the program responsible for the desired action. A task usually requires the three stages of acquisition, analysis and display, and in the case of an MBT sweep, RS232 communication with the dedicated microcomputer. By comparing this data flow diagram with the CPAS equivalent, fig 8.1, the simplicity of the Quikburn approach can be seen.

To support easy alteration of the program, by the researcher, the program was coded as separate modules. Each module encapsulates a number of procedures necessary to accomplish a set function, for example calculate mass fraction burnt. The investigator may then customise the system to his requirements by simply changing or inserting a module. The main module hierarchy is shown in fig 9.2B. As can be seen, each module is highly cohesive in not relying on the action of other modules, and communication with the Quikburn system is through dedicated data variables which are globally accessible to all modules. Example user interactions are the rewriting of the display module to show only the variation of certain parameters, or the insertion of a module to calculate the engine heat balance from averaged pressure histories, using the method described in chapter 7. In fact the data shown in chapter 7 was obtained using Quikburn in this manner. The modular code does not just save the operator time in investigating particular combustion

phenomena, but also eases the maintenance of the program by allowing small parts of the code to be amended, instead of a complete rewrite of the whole program.

9.3.1 The Present System

On running Quikburn, the user is asked to confirm the engine geometry and configuration data, and then the main menu, shown in fig 9.3, appears. A particular option is selected by moving the tick, using the cursor keys, and pressing RETURN. Any other key presses are ignored. The system alerts the operator audibly, via a sequence of high or low pitched bleeps, whether or not a suitable key has been pressed. If the system diagnostics topic is chosen, then another menu appears enabling the user several more options. The first of these is a repeating plot of averaged pressure of which an example is shown in fig 9.4. This is used to confirm visually that the pressure is aligned to induction TDC and that the correct scaling factor of volts to bar is being used. The second choice is a check on the incoming digital signals, and a sample display is given in fig 9.5. The engine speed, number of revolutions and the number of degrees for which each data signal was high are displayed in the top table. The engine speed is calculated from the time to acquire a set number of cycles and gives an approximate check that the sampling rate is correct. A further check on the sampling rate is given in the lower table, which shows the distribution of TDC occurrences. The final applications, under topic of system diagnostics, are two special screens for the input of data, which alter the parameters for the engine geometry and system configuration. The engine geometry screen is shown in fig 9.6. The user moves the box, around the values, up and down with the cursors, and may type over the current value. Once return is pressed the typed value is checked to fall within the range shown, and if successful the value is accepted. Otherwise, the old value is re-displayed. A separate, lower menu, not

shown in the figure, allows the user to reload the original values, save the new values or abort the data input altogether.

9.3.2 On-line Combustion Analysis

The on-line analysis is the central theme of the Quikburn system. The module is comprised of the three smaller modules of acquisition, analysis and display. The main structure of the code is an optimised version of the algorithms used for CPAS, described in chapter 8. However, some novel approaches were used to reduce the calculation time, and it is appropriate to mention these in more detail. The time consuming aspect of the calculation of mass fraction burnt is the derivation of the increments of combustion pressure, which are referenced to the clearance (TDC) volume. This is because the n^{th} power of a volume ratio is required. However, for a fixed interval of crank angle, the ratio is constant. Therefore, this quantity could be obtained from a table of volume ratios raised to a range of n powers. Similarly, time can be saved in all volume calculations by having the values in look up tables. Fig 9.7 shows how by incorporating three look up tables, the calculation of the increments of combustion pressure can be reduced into two multiplications and one subtraction.

Once the combustion pressures have been calculated, the location of the relevant burn times still needs to be found. As mass fraction burnt increases monotonically, a binary search can be used to locate the crank angle where the mass fraction burnt reached a given target value. The theory behind this is shown in fig 9.8. This search is a powerful tool in that it can locate a given target among N values in $\log_2 N + 1$ attempts. Therefore, a particular burn location, in an array of 128 crank angle degrees can be found in 8 attempts.

In the same fashion the time for the IMEP calculation can be reduced by having a look up table of the instantaneous changes volume, divided by swept volume. In addition the calculation time can be halved by ignoring the effects of

the pumping loop. The PMEP is approximately constant from cycle to cycle, and the combustion effects are contained within the power loop. To distinguish the power loop, mean effective pressure from the IMEP and PMEP, it has been termed WMEP, standing for Work loop Mean Effective Pressure. The three quantities are related by;

$$WMEP = IMEP - PMEP \qquad 9.1$$

Also, increased savings in the processing time can be made by ensuring that calculations and loop operations are optimised to reduce the number of repetitions.

The programming environment of the Basic language, supplied with the computer, was benchtested to discover the lead time required to analyse one cycle. The benchtest code was a series of array manipulations simulating the calculation of the combustion parameters. The time taken to execute this code will give the cycle analysis time. However, the accuracy of the computer clock is only 0.01s, therefore many repetitions of the code is necessary to obtain an accurate analysis time. Also, there is a slight processing overhead, due to the timing and repetition statements of the benchtest. Therefore, the benchtest was repeated 1000 and then 2000 times, and the difference between the two execution times, divided by 1000, used to predict the cycle analysis time. Table 9.2 shows the benchtest times for several implementations of the combustion analysis. It was decided that the third option of evaluating burn durations; referencing to manifold pressure; determining peak pressure and its location; and WMEP instead of IMEP was the best compromise for cycle throughput. The Quikburn system is able to acquire, analyse and display the results from ten cycles of data within 1.5 seconds.

9.3.3 On-line Display and Operating Modes

The screen update must not only be quick, but also the results must be easy to read. The graphics abilities of the H.P system were exploited, and the parameters shown in the form of analogue meters, see fig 9.9. The lines and text defining the screen are drawn once, when the analysis starts, and only the short lines indicating the parameter values are re-plotted.

The bottom of the screen gives the current mode of the Quikburn analysis and also the menu to change the system operation. In the monitoring mode, the researcher sets the total number of cycles to be averaged, and the number of cycles to be acquired before the screen is updated. In fig 9.9, 1000 cycles are averaged in total, these being collected and the results displayed in 10 cycle blocks. After the 1000 cycles are analysed, or if the operator selects the restart option, the whole process is repeated.

The alternative option, mentioned earlier, is the MBT sweep. In this case, the operator supplies the number of cycles to be averaged at each spark timing plus the starting and ending spark advance, and the step size of the advance. Quikburn then repeats the stages of setting the timing and analysing the required number of cycles, until the sweep is complete. Afterwards, data may be transferred to disk or printer depending upon how the user tailors the program.

9.4 Summary

Quikburn is a highly flexible, combustion analysis system. It is capable of analysing and displaying the combustion trends of 10 cycles within 1.5 seconds. The program code is well structured and has highly cohesive modules that permit the operator to simply maintain and customise the system to his own objectives.

The main form of Quikburn used for this thesis consists of a monitoring mode, where a set number of cycles are acquired and averaged in blocks; and a MBT sweep mode. In the latter mode, Quikburn takes the engine spark timing through a set range of advances and calculates the combustion parameters.

Combustion analysis systems of this style are at the fore front of engine research, and Quikburn provides a professional and powerful tool for fast and user-orientatable processing; and is applicable to all areas of combustion research.

Chapter 10

Investigation of Optimum 50% Fuel Mass Burnt Location

10.1 Introduction

Spark timing has a strong influence on the performance characteristics of a gasoline engine. The target settings for the ignition timing of a production engine are usually those which are identified by carrying out a spark timing sweep and measuring torque, or IMEP in the case of single cylinder investigations. The aim of the sweep is to locate the spark timing that gives peak torque at a fixed AFR and speed. Under some conditions when advancing the spark timing, knock occurs before the optimum timing can be reached, and the onset of knock is referred to as BLD (BorderLine Detonation). Knock must be avoided else severe damage will occur to the combustion chamber. A safety limit in the ignition timing is normally imposed, where the greatest timing advance permittable is a few degrees in retard of BLD. The dependency of the engine torque on the spark timing is normally weak in the vicinity of peak torque, and therefore as an added anti-knock precaution, the ignition setting chosen is slightly retarded of the optimum timing, Ferguson[10.14]. The amount of retard is subjective, normally maintaining -1% of peak torque, and is dependent upon the flatness of the torque-timing curve near peak torque and the degree of data scatter. This ignition setting is referred to as MBT (Minimum advance of spark timing for Best Torque) and is widely used as a calibration target for engine operation, and as a reference setting for performance comparisons. A particularly unattractive feature of using the MBT approach for setting the reference conditions is the absence of a priori indications of its location, and, hence, the time required to locate it.

A better solution would be to replace MBT with a combustion parameter which is more fundamental and easier to define. Encouragingly, as will be

presented later in this chapter, there is published evidence that a correlation exists between the crank angle location of the 50% mass burnt time and MBT. The variation of the location of the 50% mass burnt with spark timing is almost linear, as opposed to the parabolic trend of torque and spark timing. Therefore, If the correlation exists, MBT can be located directly by interpolations from calculations of the 50% mass burnt location. The MBT search could then be simply incorporated within a computer analysis and control system, providing swift, automated calibration of the data maps used in the management systems of production engines.

The significance of the correlation warranted a detailed study to reveal its applicability to engine research and testing, and the Quikburn system was used for this task because it was well suited to this type of investigation.

10.2 The Literature Evidence for a Correlation between MBT and the Location of the 50% Mass Burnt

Indications that a particular location of the 50% mass burnt corresponded to conditions of optimum power output can be found in several papers: Matekunas[10.1] commented that MBT timing occurred for a 50% mass burnt location of 10^{o} ATDC; Douard et al[10.6] found that MBT timing on their rig corresponded to a 50% mass burnt location of between 5 - 10^{o} ATDC; and Clark and Challen[10.5] stated that MBT occurs for a 50% mass burnt location of between 6-8^{o} ATDC. All of these results appear to hold regardless of operating conditions.

Although other researchers do not comment on the occurrence, further evidence can still be found: Muranaka et al[10.10] used a 50% mass burnt location of 10^{o} ATDC to imply MBT timing in their engine simulation. By extracting the pertinent information from published curves of mass fraction burnt, the location of the 50% mass burnt for MBT timing of a number of test

facilities can be found. These and the results of the above papers have been summarised in table 10.1.

Of all these authors, only Klimstra[10.12] makes any comment on the potential use of the 50% mass burnt as a target to obtain the best engine performance. Klimstra's paper implies that the relationship between 50% mass burnt and MBT is universal and an easily used parameter.

Hoppie[10.11] and Klimstra[10.12] produce similar arguments to explain why the optimum burn shape is centred after TDC. In the ideal Otto cycle, isochoric combustion at TDC is the most efficient. However, in a real engine cycle, combustion occurs in a finite time, and the burning that occurs before TDC will produce negative work. Therefore, the optimum burn shape must be centred about a point after TDC. Although this explains why the optimum position of 50% mass burnt occurs after TDC, it does not explain why this should be independent of engine operating conditions nor why only slight differences are observed between the optimum locations, of the 50% mass burnt, from different rigs. Douard[10.6] proposed that the small changes in the optimum location of the 50% mass burnt were due to changes in gas to wall heat exchange, but he offered no proof.

All the above evidence suggests strongly, but not equivocally, that there is a good correlation between 50% mass burnt and MBT. In addition, from table 10.1, the correlation appears to be almost independent of operating condition, but can vary between different engines.

10.3 Experimental Investigation of the Behaviour of the 50% Mass Burnt Location

10.3.1 The Operating Conditions

The 2.0L OHC (EFI) engine was used for this investigation, to examine the two operating conditions used earlier in the thesis, namely 2000 rpm, WOT at non knocking AFRs, and 1500 rpm part load. The part load condition was

obtained by running the engine at 1500rpm, under the control of the management system of the production engine, and closing the throttle until the torque corresponded to the WWMP. The throttle was then kept constant at this position throughout the subsequent tests.

The data was taken from cylinder four, counting from crankshaft pulley towards the bellhousing of the flywheel. Table 10.2 presents the AFR and spark timing spreads at MBT for the part load conditions. In all cases, the AFR was set for cylinder four, and, this cylinder is always leaner than the other three. However, as the investigation was limited to the effects on the single cylinder, the AFR spread was not a cause of concern.

10.3.2 Characterising the Running Condition

The combustion analysis at a particular test condition generates several hundred sets of cyclic data, but the researcher usually only wishes to record the information that pertains to the operating condition in general. The cycles of data acquired are composed of a mixture of slow and fast burns, which can produce several modes of combustion, Martin[10:4]. The calculated parameters could be distributed around these distinct modes, and the averaging of the quantities would not be an appropriate method of characterising the operating condition. As well as investigating this uncertainty, the number of cycles that are sufficient to create a true sample also needs to be determined. The parameters under investigation are WMEP and the location of the 50% mass burnt. Fig 10.1 is a plot of these two parameters for of each of the cycles in a sample of one hundred cycles. There is a wide distribution of both parameters, but cyclic dispersion obscures any trends. As no practical information can be obtained from this figure, the distribution of the two parameters was examined independently. For this, data was taken at four conditions, 12:1 and 16:1 AFRs

at part and full load. Table 10.3 summaries the variation of the parameters at these conditions.

Dealing first with the 50% mass burnt location, the standard deviation is large at all conditions, being about 3 degrees crank angle. However, the distribution plots shown in fig 10.2 indicate that the burn locations are distributed approximately evenly around a single mode. Therefore, the sample average will be representative of the 50% mass burnt location for each running condition. In Fig 10.3 it can be seen that the average location of the 50% mass burnt is settled after one hundred cycles at 15.26^{o} ATDC, and that considering more cycles has little effect, because after three hundred cycles the average is 15.39^{o} ATDC. This suggests that the 50% mass burnt location can be averaged after one hundred cycles to characterise the operating condition.

The mean effective pressure distributions, fig 10.4, are not as well defined as the 50% mass burnt location. However, the level of variation is significantly smaller, being only about 5% of the mean. The distribution appears to be single moded and, because the variation is low, the average after a hundred cycles will also be sufficient to characterise the mean effective pressure at each operating condition.

10.3.3 Part Load Results

At each AFR, the spark timing was advanced in steps of one degree, and at each timing a hundred cycles of pressure data were acquired and processed. Fig 10.5 shows the results for the richer mixture AFRs at part load. There is slight data scatter on these plots, but WMEP can clearly be seen to pass through a maximum. In all cases, the optimum 50% mass burnt location occurs about 15^{o} ATDC. The flatness of the WMEP curve near its peak allows a shift of two or more degrees from the optimum location before there is a noticeable drop in torque. Retarded spark advances produce late 50% mass burnt locations, and an equivalent MBT timing would be associated with a location of

50% mass burnt about 16^{o}-17^{o} ATDC. However at this juncture, the main consideration is the strength of the correlation, and further modifications, for example a knock safety limit, can be added at a later date. These results appear to confirm that a particular 50% mass burnt location does correspond to MBT, and the value is independent of AFR.

The results at the leaner AFRs, fig 10.6 show an interesting trend. The trend at an AFR of 14:1 appears similar to that of the richer AFRs in fig 10.5, but at 15:1, the WMEP just passes through its maximum value. This restricted range of 50% mass burnt locations becomes smaller at 16:1, where the maximum point is just reached, and at 17:1 maximum WMEP is not reached at all. In the 17:1 case, spark advances up to 45^{o} BTDC could not produce a 50% mass burnt location earlier than 20^{o} ATDC. In fact these locations of mass burnt seem to be clustered around 21^{o} ATDC for a range of spark timings. This instance where an increase in the spark advance does not produce an earlier 50% mass burnt location was first noticed by Matekunas[10.1], who called this phenomenon "arrested phasing".

Matekunas[10.1] found that arrested phasing could be averted if the swirl in the cylinder was increased. This suggests that arrested phasing is related to the engine's capability of combusting lean mixtures, and that it could be used as a measure of lean burning efficiency; arrested phasing will occur at the leanest AFR in the combustion chamber which is best designed for burning weak mixtures. Also at 17:1 AFR in fig 10.6, the mean effective pressure is greatest at the earlier burn locations, and suggests that an even greater mean effective pressure would have been attained if the optimum location, 15^{o} ATDC, could have been reached. This also could be used as a measure of lean combustion performance, because the design with the location of 50% mass burnt closest to optimum (under arrested phasing conditions) would be the most efficient.

Arrested phasing is a consequence of the inefficiency of the combustion process, and it would be useful to know whether it occurs because of slow flame initiation, slow flame propagation or a combination of the two. Now, the change in the location of the 50% mass fraction burnt, $\Delta\theta_{50\%}$, is the result of the difference between the change in spark advance, $\Delta\theta_s$, and the increase in 0-50% burn duration, $\Delta\theta_{0\text{-}50\%}$:

$$\Delta\theta_{50\%} = \Delta\theta_s - \Delta\theta_{0\text{-}50\%} \qquad 10.1$$

In equation(10.1) a positive $\Delta\theta_{50\%}$ means an earlier 50% burn location; a positive $\Delta\theta_s$ is an increase in timing advance; and an increase in $\Delta\theta_{0\text{-}50\%}$ is an increase in burn duration. Therefore, the burn phasing will be arrested if $\Delta\theta_{50\%}$ is less than or equal to zero, which implies that with arrested phasing:

$$\Delta\theta_s <= \Delta\theta_{0\text{-}50\%} \qquad 10.2$$

The 0-50% burn duration can be split into the two periods of flame initiation, 0-10% mass burnt, and flame propagation, 10-50% mass burnt. Hence equation(10.2) can be written:

$$\Delta\theta_s <= \Delta\theta_{0\text{-}10\%} + \Delta\theta_{10\text{-}50\%} \qquad 10.3$$

Now, the flame propagation period, 10-90% burn duration, is known to be a weak function of spark timing, and a strong function of AFR, Houpt and Andreadakis[10.3]. The variation of flame propagation with spark timing is seen in fig 10.7. Although there is some data dispersion, at 12:1 the burn duration is virtually independent of spark timing up to 35^{o} ATDC, after which the duration and the dispersion increase. At 17:1, there is a decrease in duration up to to 35^{o} advance, and then levels off. This is consistent with Blizzard and

up to to 35^{o} advance, and then levels off. This is consistent with Blizzard and Keck[10.13], who reported that 10-90% burn duration is a minimum near MBT and increases with either retarded or advanced timings. Local to MBT the duration is approximately independent of timing changes. The duration of the flame propagation with AFR, for MBT timings, is shown in fig 10.8. Although up to 15:1 AFR the duration has only altered by 4^{o}, the variation has a minimum near 11:1 AFR, and is again consistent with Blizzard and Keck's work [10.13]. Now, Arrested phasing occurs at conditions unable to reach their optimum spark timing, and as flame propagation does not increase until MBT is exceeded, flame propagation cannot be the cause of arrested phasing. Therefore slow flame initiation must be the cause of arrested phasing, and from equation(10.3) when arrested phasing occurs:

$$\Delta\theta_s <= \Delta\theta_{0\text{-}10\%} \qquad 10.4$$

or;

$$\frac{\Delta\theta_{0\text{-}10\%}}{\Delta\theta_s} \geq 1 \qquad 10.5$$

For more evidence to prove that arrested phasing results from slow flame initiation, equation(10.5) was applied to the data recorded at the non-arrested phasing AFR of 12:1, and the arrested phasing conditions at 17:1. Fig 10.9 shows a plot of burn initiation period against spark advance, with the lines of unity slope super-imposed to illustrate the criterion necessary for arrested phasing to be caused by slow flame initiation. These lines are for illustration, and their intersection with the data points is not of relevance. The burn duration at 12:1 has a slope of less than 1 for the majority of spark timings, and as was seen in fig 10.5, arrested phasing did not occur. The exception is towards the

furthest advanced timings, well in excess of MBT, where the initiation period increases at a greater rate. Noting back to fig 10.8. the 10-90% period is also increasing in this region, and implies that with advances exceeding MBT, the 50% mass burnt locations will stop becoming earlier in the cycle.

At 17:1 the rate of growth of the initiation period is near or greater than unity for the majority of timings. Again referring back to fig 10.8, retarded timings produce a reduction in the propagation period, and this accounts for the initial advance in 50% mass burnt location seen in fig 10.6. However, at about 32^{o} spark advance, arrested phasing occurs because the propagation period becomes independent of spark timing, and the initiation period is still increasing at a rate exceeding the above criterion in equation 10.5. This indicates that arrested phasing is a flame initiation problem. If the rate of growth of the flame kernel could be enhanced at 17:1, then the arrested phasing would not occur. This is consistent with Matekunas finding that increased swirl, which shortens flame initiation, eliminated the arrested phasing in his test engine.

The spark advances and the corresponding 50% mass burnt locations for all the part load conditions are shown in fig 10.10, and illustrates the near linear variation of 50% mass burnt location with spark advance. This makes the 50% mass burnt location preferable to MBT as a reference condition, because the optimum condition can be located by interpolating between values as opposed to searching for peak torque. Reading along the 16^{o} ATDC line for the location of 50% mass burnt gives the equivalent MBT spark timings.

10.3.4 Full Load Results

The results from the tests at 2000 rpm WOT, are presented in fig 10.11. Arrested phasing occurs at 17:1, as with the part load condition, and indicates that this particular rig is not efficient at any lean operating condition. In addition a noticeable difference in results did occur at the richer AFRs, because the optimum location of the 50% mass burnt has shifted to be nearer 11^{o} ATDC. At

12:1, the WMEP has a relatively flat response at all the burn locations, but the peak can be subjectively placed around 12^{o} ATDC. Unfortunately knock restricts testing at the other AFRs at this speed-load condition, but the results suggest that the optimum location of 50% mass burnt is a couple of degrees earlier at the full load condition, than at part load.

The literature review also showed that small differences occurred between the optimum 50% mass burnt at different operating conditions. No explanations have been put forward to explain why there is only a slight variation of the optimum 50% mass burnt location at different engine operating conditions, nor why a greater variation is then seen between different power units. As described earlier, the reason for the optimum location occurring after TDC is because the burn history needs to be centred in the expansion stroke in order to overcome the negative compression work. This suggests that the optimum location of the 50% burnt is a result of best phasing between the heat release of the fuel to the changes in cylinder volume. This being the case, then the actual optimum location of the 50% mass burnt is dependent solely on the burn pattern. Therefore, the variations of the optimum location of 50% mass burnt, observed above, is due to the different burn patterns that occur at different operating conditions.

10.4 Investigation of the Optimum Location of 50% Mass Burnt by Computer Simulation

In an attempt to clarify the foregoing statements, the engine simulation, described in chapter 7, was developed to undertake MBT sweeps using various burn patterns. The simulation was run with nominal settings to represent the 1500 rpm, part load condition. Then the main influences of burn duration, heat loss, magnitude of heat released, manifold pressure and engine dimensions were varied in turn. Sample WMEP vs 50% mass burnt location plots are shown in fig 10.12, for variations in the ratio of heat loss to fuel input energy,

and for changes in burn duration. The results for all the influences are given in table 10.4 and their effect summarised in table 10.5.

The change in engine geometry from the 2.0L OHC to the 1.1L Valencia engine had no effect on the optimum 50% mass burnt location. This indicates that the rate of fuel burning is dominant over the volume changes in deciding the optimum location of the 50% mass fraction burnt.

Increasing either the fuel input energy or the manifold pressure has only a small effect. Again this is not surprising because the burn shape is essentially unaltered by these effects.

The heat rejection is more significant because it directly influences the heat energy available to produce work. The amount of heat lost at any instant is dependent on the gas temperature, and this temperature will be greatest when the combustion is centred at TDC. Therefore, the magnitude of the heat loss distorts the pattern of the effective heat release, and, hence, affects the optimum location of the 50% mass burnt.

Burn duration also has a marked influence on the optimum burn location, because it directly effects the burn shape. A fast burn can release more energy near TDC without incurring large compression losses. The increase in energy release at TDC will produce a higher cylinder pressure, due to the smaller volume, and will produce more work done. Therefore, a fast burning charge will have an optimum 50% mass burnt location nearer to TDC than a mixture whose combustion is slow. This result is clearly shown by the model. In addition a fast burning mixture releases more energy per crank angle than a slow burning mixture, and therefore generates greater work output. This means that fast combustion is most efficient. The fact that the optimum location of the 50% mass burnt becomes closer to TDC as the combustion rate increases,. means that it is possible to use the actual value of the optimum 50% mass burnt location to compare the combustion efficiency of different engines; the more efficient engine having the optimum 50% burn location closest to TDC.

The simulation results support the suggestion that the variation of the optimum location of the 50% mass burnt is due to changes in the burn pattern. The large range of the optimum locations of the 50% mass burnt seen in published papers will then be attributable to the burn shape of the particular engine under test. The value of 10^{o} ATDC, quoted by some researchers, would indicate a fast burning, efficient combustion unit. Conversely, an optimum location of 17^{o} ATDC occurred for the rig with the square piston, where the combustion is slow in comparison. The optimum location will appear insensitive to AFR, because although the amount of heat lost drops with increased AFR, the burn duration will increase, and these two effects will partially self cancel. Differences between operating conditions can only be expected if the burn shape changes significantly. In the case of the 2.0L OHC engine the main effect in changing from 1500 rpm, part load to 2000 rpm WOT is the decrease in burn length from 85^{o} to 60^{o} crank angle. The above model was run with conditions approximately equal to the 2000 rpm WOT case. The result, shown at the bottom of table 10.4, indicates an optimum 50% mass burnt location of 12^{o} ATDC as opposed to the 15.5^{o} ATDC for the 1500 rpm part load. The predictions made using the simulation show good consistent with the experimental results taken at the part and full load conditions.

The 50% mass burnt location has been seen to be a good indicator of combustion efficiency. It can be used to set the reference conditions for engine operation, or to compare the combustion performance of different power units. The simplicity in determining the optimum 50% mass burnt location and therefore the best ignition settings, makes it easy to implement in a system for the automated calibration of the data maps of electronic engine controllers. This would save automobile manufacturers considerable time in establishing the settings for their production engines. Another desirable application would be an ignition controller mounted onboard the vehicle, which would maintain the

ignition process at its optimum settings throughout the lifetime of the power unit.

10.5 An Alternative Method of Determining MBT

A disadvantage of using burn durations to optimise the ignition timing is that the processing required can be inhibitive. For example, at present it is difficult to provide the necessary processing power onboard a production automobile. A faster approach could be to use the peak pressure and its location. Fig 10.13 shows the variation of these two parameters at part load. The curves fall into the two regions of linear and hookback, as named by Matekunas[10.1]. At AFRs of 14:1 and 15:1, the points reside mostly in the linear region. Advanced spark timings just move the 16:1 AFR curve into the linear region, but not so the 17:1. Although arrested phasing is known to occur at 17:1, there is nothing in figure 10.13 to predict it.

Consider instead the relationship between location of the peak pressure and the location of the 50% mass burnt, fig 10.14. For richer AFRS, a good correlation is seen, and the location of the peak pressure could be used to optimise the ignition timing under these conditions. However, problems occur at leaner AFRS. The correlation still holds at 14:1, but retarded spark timings at 15:1 and 16:1, also produce peak pressure at locations designated as optimum, due to their parabolic shape. It is possible to overcome this set back by careful analysis, but the problem becomes more severe at 17:1. At this AFR, the optimum 50% mass burnt location is never reached, but the curve does go into the region of peak pressure locations that normally represents optimum conditions. For these reasons, peak pressure location is not suitable for use in general procedures to optimise the ignition timing, and combustion analysis offers the only alternative which is universally applicable.

10.6 Conclusions

The location of the 50% mass burnt is an indicator of combustion performance. It can be used easily to optimise the ignition settings, because it benefits from having a linear relationship with spark timing. It can be used in automated routines for the calibration of an engine management system.

At stoichiometric and richer AFRs, the 50% mass burnt location is dependent on the burn history, where the faster the burn period, the greater the efficiency, and the closer the 50% mass burnt locations becomes to TDC. This suggests that the value of the optimum 50% mass burnt location is indicative of the combustion efficiency, and may be used to compare the designs of combustion chambers.

Under lean conditions, arrested phasing occurs due to slow flame initiation. Both the onset of arrested phasing and the behaviour of the 50% mass burnt location under these conditions can be used to assess lean mixture burning capabilities.

An alternative indicator of combustion performance is the location of peak cylinder pressure. This has a good correlation with the 50% mass burnt location under rich running conditions. However, the relationship becomes ambiguous at lean AFRs, and undermines its general applicability to the optimise the ignition settings.

Chapter 11

Conclusions

The literature survey indicated that there is a requirement for undertaking combustion processing in real time. Pressure analysis is the best non-intrusive approach for obtaining information concerning burn quality, and there is consistency between the results calculated by approximate methods and those based upon the Laws of Thermodynamics. Approximate procedures are more suited to high speed data analysis due to their simplicity and non-iterative calculations.

The most popularly used approximate method for determining mass fraction burnt was originally suggested by Rassweiler and Withrow. This method was found to be insensitive to noise fluctuations on the pressure signals, and cycle processing can commence at spark time and continue until EVO without the possibility of noise corruption. This removes the necessity for a priori location of EOC.

A new approach to determine the polytropic indices was developed, where an estimate is adjusted to the true value. This method is quicker in computer time than using logarithms, and it is suggested that as the adjustment procedure acts directly upon the calculated inrements of combustion pressure it will be more appropriate for the analysis than other methods of evaluating the polytropic index.

The new implementation of the processing scheme is able to identify late burning cycles from the low value of index associated with them. By using a more typical value, a representative burn history can be evaluated. Misfires can be detected from the low total of the summed increments of combustion pressure, and these cycles should be excluded from cycle averaging procedures.

One uncertainty in combustion analysis, to which there is no realistic alternative, is the assumption of uniform pressure within the cylinder. Pressure gradients can be problematic when studying the growth of the flame kernel, and pressure processing techniques are not well suited to investigations of this period.

Provided the marker pulse for alignment of the acquired pressure to crank angle is within two degrees of TDC, and the clearance volume is known to within $\pm 5\%$, the calculated mass fraction burnt will be undistorted. The derived burn history is also insensitive to the calibrating of the pressure, acquired from the charge amplifier, to absolute. However, the reference pressure does have a marked influence on the calculated values of the polytropic index, which accounts for the wide range of index values encountered in combustion research.

One normal deficiency with approximate methods of combustion analysis is the inability to obtain information concerning the heat loss. However, a novel method has been devised where the heat transfer can be derived directly from the pressure trace. This method is rig independent and considerably less complex than heat transfer correlations. The method can swiftly calculate the thermal loading of the production engine. The predicted heat loss is sensitive to the specific heat ratio. For accurate results, the reactant γ needs to be determined to between 0 and +2%. Although the variation of γ with temperature and equivalence ratio is known, it is difficult to estimate the temperature of the fresh charge once combustion has commenced. Work is on going to verify the most suitable method of calculating the appropriate specific heat ratio. The heat loss calculations can still be employed in its current form to compare the relative differences in the heat lost at different operating conditions.

The mass fraction burnt and the computations of heat loss were implemented as an on-line system of flexible techniques for the processing of engine pressure data. The system was named Quikburn, which was able to acquire ten cycles and display their combustion parameters to the screen within 1.5s. Control of the engine spark timing was possible via RS232 communication to another dedicated microcomputer. The Quikburn system code is user orientatable in order to perform an engine test session more efficiently. The system was developed to be transportable between different test facilities, and to be a powerful tool for combustion process analysis.

The final part of the thesis examined the correlation between 50% burn location and MBT. At the richer AFRs, a particular value of 50% burn location was found to correspond to optimum efficiency. This value was almost constant between AFRs, and only varied slightly between loads. The optimum 50% burn location was found to be dependent on burn pattern, and the more efficient the combustion process the closer the optimum became to TDC. Therefore, the 50% burn location can be used be used to compare the efficiency of different designs of combustion chamber.

The location of the 50% mass burnt has an almost linear variation with spark advance, and the optimum timing conditions can be found quickly by interpolation. This indicates that the optimum location of the 50% mass burnt could be used as a calibration setting for production ignition timing, instead of MBT. The calibration procedure can be automated and great time savings made in the producing the necessary data for the electronic engine control systems. In the future, an onboard vehicle system could be implemented that maintains optimum combustion efficiency throughout the engine's lifetime.

The optimum 50% burn location is not attainable at lean conditions. This is due to arrested phasing, caused by poor flame initiation. If the early kernel growth could be enhanced then arrested phasing will be adverted.

References

1.1 Klimstra J — "The Optimum Combustion Phasing Angle - A Convenient Engine Tuning Criterion". SAE Paper 852090. 1985.

1.2 Rassweiler G M, Withrow L — "Motion Pictures of Engine Flame Correlated with Pressure Cards". Reprinted SAE 800131, 1980.

2.1 Kalghatgi G T — "Spark Ignition, Early Flame Development and Cyclic Variation in I.C. Engines". SAE Paper 870163, 1987.

2.2 Anderson R — "The Effect of Ignition System Power on Fast Burn Engine Combustion". SAE Paper 870549, 1987.

2.3 Baritaud T A — "High Speed Schlieren Visualisation of Flame Initiation in a Lean Operating S.I. Engine". SAE Paper 872152, 1987.

2.4 Young M B — "Cyclic Dispersion in the Homogenous Charge S.I. Engine - A Literature Survey". SAE Paper 810020, 1981.

2.5 Winsor R E, Patterson D J — "Mixture Turbulence - A Key to Cyclic Combustion Variation". SAE Paper 730086, 1973.

2.6 Keck, J C, Heywood J B, Noske G — "Early Flame Development and Burning Rates in S.I. Engines and their Cyclic Variability". SAE Paper 870164, 1987.

2.7 Young M B — "Cyclic Dispersion - Some Quantitive Cause and Effect Relationships". SAE Paper 800459, 1980.

2.8 Douard A, de Soete G, Henault C — "Experimental Analysis of the Initiation and Development of the Part Load Combustion in a S.I. Engine". SAE Paper 830338, 1983.

2.9 Swords M D, Kalghatgi G T, Watts A — "An Experimental Study of Ignition and Flame Propogation in a S.I. Engine". SAE Paper 821220, 1982.

2.10 Matekunas F A — "Modes and Measures of Cyclic Combustion Variability". SAE Paper 830337, 1983.

2.11 Evans R L, Cameron C — "A New Combustion Chamber for Fast Burn Applications". SAE Paper 860319, 1986.

2.12 Yamamoto H, Misumi M — "Analysis of Cyclic Combustion Variation in a Lean Operating S.I. Engine". SAE Paper 870547, 1987.

2.13 Gatowski J A, Heywood J B — "Effects of Valve Shrouding and Squish in a S.I. Engine". SAE paper 852093, 1985.

2.14 Shayler P J — "Ford Burnrate Program". Personal Communication.

2.15 Ferguson C R — "Internal Combustion Engines - Applied Thermoscience". John Wiley and Sons Ltd, 1986

2.16 Tabaczynski R — "A Turbulent Entrainment Model for S.I. Engine Combustion". SAE 770647, 1977.

2.17 Moss J B — "Modelling Combustion Chemistry for Practical Fuels in Engine Flowfield Computations". IMechE CO2/87, 1987.

2.18 Himyary A L, Karim G A — "A Diagnostic Two Zone Combustion Model for S.I. Engines based on Pressure-Time Data". SAE Paper 880199, 1988.

2.19 Curry S — "A Three Dimensional Study of Flame Propogation in a S.I. Engine". SAE Trans Vol 71, pp 628 - 650, 1963.

2.20 Anderson R — "In Cylinder Measurement of Combustion Characteristics using Ionization Sensors". SAE Paper 860485, 1986.

2.21 May M G — "Flame Arrival Sensing Fast Response Double Closed Loop Engine Management". SAE Paper 840441, 1984.

2.22 Dyer T M — "New Experimental Techniques for In Cylinder Engine Studies". SAE Paper 850396, 1985.

2.23 Fansler T D — "Laser Velocimetry Measurement of Swirl and Squish Flows in an Engine with a Cylindrical Piston Bowl". SAE Paper 850124, 1985.

2.24 Bonini J et al — "Visualisation of Flow and Combustion Processes in a Square Piston Engine Simulator". SAE Paper 870452, 1987.

2.25 Pischinger S, Heywood J — "A Study of Flame Development and Engine Performance with Breakdown Ignition Systems in a Visualisation Engine". SAE Paper 880518, 1988.

2.26 Chau E et al — "Experimental and Numerical Modelling Study of Engine Combustion". SAE Paper 872103, 1987.

2.27 Chau E et al — "Effect of Intake Valve Configuration on Lean Combustion". SAE Paper 880202, 1988.

2.28 Evers L W — "Spark Plug Pressure Transducers for Measuring Indicated Work". SAE Paper 780148, 1978.

2.29 Foster D E — "An Overview of Zero-Dimensional Thermodynamic Models for I.C. Engine Data Analysis". SAE Paper 852070, 1985.

2.30 Houpt P K, Andreadakis S — "Estimation of Fuel Air Ratio from Cylinder Pressure in S.I. Engines". SAE Paper 830418, 1983.

2.31 Quader A A — "What Limits Lean Operation in S.I. Engines - Flame Initiation or Propogation". SAE Paper 760760, 1976.

2.32 Krieger R B
Borman G L
"The Computation of Apparent Heat Release for I.C. Engines". ASME 66, WA/DGP-4, 1966.

2.33 Benson R S
Whitehouse N
"Internal Combustion Engines". Vol 1, pp 158 - 161, Pergamon Press.

2.34 Gatowski J A
Balles E N
Chun K M
Nelson F E
Ekchian J A
Heywood J B
"Heat Release Analysis of Engine Pressure Data". SAE Paper 841359, 1984.

2.35 Young M B
Lienesch J H
"An Engine Diagnostic Package (EDPAC) - Software for Analysing Cylinder Pressure-Time Data". SAE Paper 780967, 1978.

2.36 Benson R S
Whitehouse N
"Internal Combustion Engines". Vol. 2 Pergamon Press.

2.37 Stone C R
Green-
Armytage D I
"Comparison of Methods for the Calculation of Mass Fraction Burnt from Engine Pressure-Time Diagrams". Proc. IMechE, Vol. 201, No. D1, 1987.

2.38 Flynn F P
et al
"A New Perspective on Diesel Engine Evaluation Based on Second Law Analysis". SAE Paper 840032, 1984.

2.39 Patterson D J
Van Wylen G
"A Digital Computer Simulation for Spark Ignition Engine Cycles". SAE Paper No. 633F, 1963.

2.40 Marvin
"Combustion Time on the Engine Cylinder and its Effect on Engine Performance". NACA Tech Report 276, 1927.

2.41 McCuiston F
Lavoie G A
Kauffman C W
"Validation of a Turbulent Flame Propagation Model for S.I. Engine". SAE Trans. Vol. 86, pp 200 - 221, 1977.

2.42 Rassweiler G M
Withrow L
"Motion Pictures of Engine Flame Correlated with Pressure Cards". Reprinted SAE 800131, 1980.

2.43 Evans P G
"Fast Data Acquisition System for Investigating Combustion Phenomena in S.I. Engines". SAE Paper 840057, 1984.

2.44 Hayes T H
Savage L D
"Cylinder Pressure Data Acquisition and Heat Analysis on a PC". SAE Paper 860029, 1986.

2.45 Beck E
Hahn K
Miller M
"A Real Time Combustion Analysis Instrument". SAE Paper 880689, 1988.

2.46 Amann P A
"Cylinder Pressure Measurement and its Use in Engine Research". SAE Paper 852067, 1985.

2.47 Patterson D J — "Cylinder Pressure Variations, A Fundamental Combustion Problem". SAE Paper 661029, 1966.

2.48 Bain R, Chen S K, Chang T Z, Cheng S U — "On-line PC Based Engine Analyzer and Simulator". SAE Paper 881256, 1988.

3.1 Bradshaw B J — "Fuel Injection with Multipoint Distribution for Spark Ignition Engines". PhD Thesis, University of Nottingham, 1988.

3.2 Marshall W D — "Fuel Injection Factors Affecting Spark Ignition Engine Performance". PhD Thesis, University of Nottingham, 1989.

3.3 White D — "Diagnosis of Spark Ignition Engine Faults". Thesis, to be submitted for PhD, University of Nottingham, 1989.

3.4 Isaacs R M — "Cold Starting of Fuel Injected Spark Ignition Engines". PhD Thesis, University of Nottingham, 1988.

3.5 Evers L W — "Spark Plug Pressure Transducers for Measuring Indicated Work". SAE Paper 780148, 1978.

3.6 Shannon C E — "Comminications in the Presence of Noise". Proc. I.R.E., Vol. 37, pp 10 - 21, 1949.

3.7 Horrowitz P, Hill W — "The Art of Electronics". pp 157 - 160. Cambridge University Press, 1985.

3.8 Collings N — "A Multipurpose Ignition System (ITAMS) for Production Development and Research". I.S.A.T.A. Cologne, pp 671 - 687, September 1983.

3.9 Horrowitz P, Hill W — "The Art of Electronics". pp 29 - 32. Cambridge University Press, 1985.

4.1 Collings N — "A Multipurpose Ignition System (ITAMS) for Production Development and Research". I.S.A.T.A. Cologne, pp 671 - 687, September 1983.

4.2 Royer J P — "Handbook of Software and Hardware Interfacing for IBM PC". Prestice-Hall Inc., 1987.

5.1 Rassweiler G M, Withrow L — "Motion Pictures of Engine Flame Correlated with Pressure Cards". Reprinted SAE 800131, 1980.

5.2 Stone C R, Green-Armytage D I — "Comparison of Methods for the Calculation of Mass Fraction Burnt from Engine Pressure-Time Diagrams". Proc IMechE, Vol 201, No DI, 1987.

5.3 Shie S X
Sheng H Z
"Numerical Simulation and Digital Signal Processing in Cylinder Pressure of I.C. Engines". Proc IMechE CO/87, 1987.

5.4 Savitzy A
Golay M
"Smoothing Differentiation of Data by Simplified Least Squares Procedures". Analytical Chemistry 36:8, pp 1627 - 1639, 1964.

5.5 Alkidas A C
"Heat Transfer Characteristics of a S.I. Engine". Journal of Heat Transfer, Vol. 102, May 1980.

5.6 Dye A
"A New Approach to Combustion Analysis". Automotive Engineer, 11(i) pp 32 - 35, 1985.

5.7 Karim G A
Al-Aloisi Y
Anson W
"Consideration of Ignition Lag and Combustion Time in a S.I. Engine using a Data Acquisition System". SAE Paper 820758, 1982.

6.1 Lecuona A
Rodriguez P A
"Evaluation of Pressure and Crank Angle Errors from Recriprocating Engine Indicator Diagrams". SAE Paper 860027, 1986.

6.2 Hayes T H
Savage L D
"Cylinder Pressure Data Acquisition and Heat Release Analysis on a Personal Computer". SAE Paper 860029, 1986.

6.3 Lancaster D R
Krieger R B
Lienesch J H
"Measurement and Analysis of Engine Pressure Data". SAE Paper 750026, 1975.

6.4 Clark E A
Challen B J
"Examining High Speed Data during Engine Transients". SAE Paper 850402, 1985.

7.1 Alkidas A C
Myers J P
"Transient Heat Flux Measurements in the Combustion Chamber of a S I Engine". J. Heat Transfer, ASME Trans, Vol 104, pp 62 - 67, 1982.

7.2 Woschni G
"A Universally Applicable Instantaneous Heat Transfer Coefficient in the IC Engine". SAE Paper 670931, 1967.

7.3 Annand W J D
"Heat Transfer in the Cylinder of a Reciprocating IC Engine". Proc IMechE, Vol 177, No 36, pp 973 - 990, 1963.

7.4 Heywood J B
"IC Engine Fundamentals" McGraw Hill Inc, 1988.

7.5 Taylor C F
"The IC Engine in Theory and Practice". MIT Press, 1982.

7.6 Ferguson C R
"Internal Combustion Engines - Applied Thermoscience",John Wiley & Sons, pp 80-81, 1986.

7.7 Benson R S
Whitehouse N
"Internal Combustion Engines". Pergamon International Library, Vol 1, pp 155 - 161, 1979.

9.1 Bain R
Chen S K
Chang T Z
Cheng S U
"On-line PC Based Engine Analyzer and Simulator". SAE Paper 881256, 1988.

10.1 Matekunas F A
"Modes and Measures of Cyclic Variability". SAE Paper 830337, 1983.

10.2 Latsch R
"The Swirl Chamber Spark Plug: A Means of Faster, More Uniform Energy Conversion in the S.I. Engine". SAE Paper 840455, 1984.

10.3 Houpt P K
Andreadakis S K
"Estimation of Fuel-Air Ratio from Cylinder Pressure in S.I. Engines". SAE Paper 830418, 1983.

10.4 Martin J K
"Burn Modes and Prior Cycle Effects on Cyclic Variation in Lean Burn Engine Combustion". SAE Paper 880201, 1988.

10.5 Clark C A
Challen B J
"Examining High Speed Data during Engine Transients". SAE Paper 850402, 1985.

10.6 Douard A
de Soete G
Henault C
"Experimental Analysis of the Initiation and Development of Part Load Combustion in a S.I. Engines". SAE Paper 830338, 1983.

10.7 Gatowski J A
et al
"Heat Release Analysis of Engine Pressure Data". SAE Paper 841359, 1984.

10.8 Chau E
et al
"Effect of Intake Valve Configuration on Lean Combustion". SAE Paper 880202, 1988.

10.9 Pischinger S
Heywood J B
"A Study of Flame Development and Engine Performance with Breakdown Ignition Systems in a Visualisation Engine". SAE Paper 880518, 1988.

10.10 Muranaka S
et al
"Factors Limiting the Improvement in Thermal Efficiency at Higher Compression Ratios". SAE Paper 870548, 1987.

10.11 Hoppie L O
et al
"Optimum Heat Release for a Reciprocating I.C. Engine". SAE Paper 870572, 1987.

10.12 Klimstra J
"The Optimum Combustion Phasing Angle - A Convenient Engine Tuning Criterion". SAE Paper 852090. 1985.

10.13 Blizard N C
Keck J C
"Experimental and Theoretical Investigation of Turbulent Burning Model for I.C. Engines". SAE Paper 740191, 1974.

10.14 Ferguson C R
"Internal Combustion Engines - Applied Thermoscience". John Wiley & Sons, pp 472 - 477, 1986.

Tables

Contributory Factor	Thermodynamic Analysis	Approximate Analysis
Data Input	Extensive: Pressure-Volume Data. Thermodynamic Tables. Heat Transfer Correlation.	Only Pressure-Volume Data.
Analysis Time	Long. Runge-Kutta Method. Iteration required at each step.	Very Short. No Iterations.
Heat Transfer	Heat transfer correlation used. Uncertainty as heat flux varies spartially within cylinder, and coefficient requires adjusting to each test rig. Effects absolute heat release, but not mass fraction burnt.	Implicit in selection of polytropic index. Not problematic as mass fraction burnt is not sensitive to heat transfer.
Output	Mass Fraction Burnt. Absolute Heat Release. Temperature Profiles. Emissions calculations.	Mass Fraction Burnt only.
Applicability	Analysis of averaged pressure histories. Not very useful for cycle by cycle analysis.	Good for comparing the combustion at one operating condition to another. Ideal for cycle by cycle analysis.

Table 2.1 Comparison Between Thermodynamic and Approximate Methods of Combustion Analysis

Reference	Bradshaw [3.1]	Marshall [3.2]	White [3.3]	Isaacs [3.4]
Engine Details	Ford 2.0L OHC EFI Standard Power Unit EEC IV Management System	Ford 1.6L CVH EFI Modified to a Single Cylinder In-house Management System	Ford 2.0L OHC Carbutetted Standard Power Unit ESCII Electronic Ignition	Ford 2.0L OHC EFI Standard Power Unit EEC IV Management System
Testbed	Eddy Current Dynamometer Lambdascan AFR sensing ITAMS Oil and Water Temperature Control Controlled by DEC PDP 11/23	Water Brake Dynamometer Lambdascan AFR sensing CO, CO_2 and NO Detection	Eddy Current Dynamometer Lambdascan AFR sensing ITAMS Controlled by DEC PDP 11/23	Regenerative Dynamometer Refrigerated Test Cell(-30^{o}C) Specialised Emissions Equipment

Table 3.1 Description of Engine Facilities

RC ΩF	Delay μs	Cutoff Frequency kHz
10^{-7}	0.0654	7645.00
10^{-6}	0.654	764.50
10^{-5}	6.54	76.45

Table 3.2 Delay Time and Cutoff Frequency of a *RC* Filter

Address (hex)	Read or Write	Function
300	Write	Resets 1^{o} decade counter
301	Write	Loads Dwell value into a down counter
302	Write	Enables the count down to dwell start
303	Write	Loads Spark value into a down counter
304	Write	Enables count down to spark time
305	Read	Event status register
306	Read	High byte of measured spark time
307	Read	Low byte of measured spark time

Table 4.1 Memory Addresses of the Ignition Control Board

COMPRESSION				EXPANSION			
Heat addition for n > γ. Heat rejection if n < γ. The smaller n, the greater the heat rejection.				Heat addition for n < γ. Heat rejection if n > γ The larger n, the greater the heat rejection.			
Sign of the terms in equation (5.9).				Sign of the terms in equation (5.9).			
Index Value	$\frac{(\gamma - n)mR}{(\gamma - 1)(1 - n)}$	ΔT	Comments	$\frac{(\gamma - n)mR}{(\gamma - 1)(1 - n)}$	ΔT	Comments
n> γ	+ve	+ve	Heat addition to gases	+ve	-ve	Heat rejection
n=γ	0	+ve	Adiabatic	0	-ve	Adiabatic
1<n<γ	-ve	+ve	Heat rejection	-ve	-ve	Heat addition
n=1	∞	0	Isothermal: Heat rejection	∞	0	Isothermal: Heat addition
n<1	+ve	-ve	Strong heat rejection	+ve	+ve	Strong heat addition

Table 5.1 Variation of Mode of Heat Transfer with Selected Value of Polytropic Index

Stroke	$\frac{P}{(\text{bar})}$	Poltropic Index MAP = 0.4 bar	$\frac{\Delta P}{(\text{bar})}$	Δn from equation(6.6)	Predicted Index Value MAP = 0.9 bar
Compression	2.42	1.60	0.5	- 0.33	1.27
Expansion	10.50	1.35	0.5	- 0.06	1.29

Table 6.1 Theoretical Calculation of Index Value due to Change in Reference Pressure of 500mbar. Ford 2.0L OHC Carburetted Engine. Production Settings for 2000rpm, WOT.

	Reactants			Products		
ϕ	γ_u @ 300K	γ_u @ 800K	Mean γ_u	γ_b @ 1750K	γ_b @ 2500K	Mean γ_b
0.4	-	-	-	1.272	1.246	1.259
0.5	1.374	1.316	1.345	-	-	-
0.8	1.362	1.297	1.329	1.262	1.234	1.248
1.0	1.356	1.283	1.319	1.255	1.216	1.236
1.2	1.347	1.257	1.302	1.265	1.252	1.259
1.4	-	-	-	1.268	1.257	1.263
1.5	1.338	1.243	1.291	-	-	-

Table 7.1 Specific Heat Ratio for Fresh and Burnt Mixtures, from Heywood[7.4]

Operating Conditions	Conditions at Spark Time					Conditions at EVO					First Law Analysis				Heat Loss Method Result
	P bar	V m^3	M_u	T_u K	Cv_u kJ/kgK	P bar	V m^3	M_b	T_b K	Cv_b kJ/kgK	Qf J	W J	U J	Q_{ht} J	Q_{ht} J
1500rpm WWMP Coolant 80°C AFR 14.9:1 m_f 1.293e^{-5} kg	3.62	9.99e-5	30.25	640	0.815	2.22	3.87e-4	29.0	1504	0.95	569	198	186	185	189
1500rpm WWMP Engine Cold AFR 13.1:1 m_f 1.53e^{-5} kg	3.63	9.99e-5	30.50	618	0.807	2.36	3.87e-4	29.0	1481	0.95	673	221	195	257	266
2000rpm WOT Coolant 80°C AFR 12.2:1 m_f 3.54e^{-5} kg	8.20	8.71e-5	30.75	565	0.81	5.85	3.87e-4	27.6	1609	0.926	1560	596	482	482	561
2000rpm WOT Coolant 80°C AFR 16.4:1 m_f 2.76e^{-5} kg	8.15	8.71e-5	30.0	533	0.795	5.97	3.87e-4	28.8	1667	0.925	1214	507	537	170	259

Table 7.2 First Law Analysis Applied to Cylinder Contents, Compared to Results from Heat Loss Method of Chapter 7

Fuel Mass, mf	1.53e-5 kg
Lower Heating Value, Q_{HV}	44 MJ/kg
Fuel Input Energy, $m_f Q_{HV}$	673 J
AFR	14:1
Mixture Mass, (AFR+1)m_f	2.30e-4 kg
Specific Gas Constant	287 J/kgK
Specific Heat Ratio, γ	1.3
Spark Timing, θ_s	30^o BTDC
0-100% Burn Duration, θ_d	80^o
Piston Speed, Vp	3.84 m/s
Block Temperature, T_w	600 K

Table 7.3 Parameters for Engine Simulation

Heat Transfer Conditions	Heat Loss by Simulation $\frac{Q_{ht}}{J}$	Heat Loss by Model $\frac{Q_{ht}}{J}$
Adiabatic Combustion	0	0.342
Combustion with Heat loss by Eichelberg Correlation	217.63	217.96

Table 7.4 Comparison between Simulated Heat Transfer Conditions and those Determined by the Analysis Method of Chapter 7

Case Study	γ	$\frac{m_f}{kg}$	$\frac{Q_{ht}}{J}$	$\frac{Q_{ht}}{m_f Q_{HV}}$	Error in heat loss expressed as a percentage of Q_{ht}	Error in heat loss expressed as a percentage of $\frac{Q_{ht}}{m_f Q_{HV}}$
Baseline	1.3	1.53e-5	217.96	32.4%	-	-
Sensitivity to the specified ratio of specific heats	1.2	1.53e-5	124.6	18.5%	-42.8%	-13.9%
	1.25	1.53e-5	180.6	26.8%	-17.1%	-5.6%
	1.35	1.53e-5	244.6	36.3%	12.2%	3.9%
	1.4	1.53e-5	264.6	39.3%	21.4%	6.9%
Changes to specified fuel mass	1.3	1.38e-5	151.96	22.6%	-30.3%	-9.8%
	1.3	1.45e-5	182.76	27.2%	-16.2%	-5.2%
	1.3	1.60e-5	248.76	37.0%	14.13%	4.6%
	1.3	1.68e-5	293.96	43.7%	34.9%	11.3%

Table 7.5 Sensitivity of the Calculated Heat Loss to the Inputs Necessary for the Analysis Method

C.P.A.S Computer System Specifications	
Hardware	Software
Olivetti M24sp (IBM XT clone) 8086 processor running at 8 MHz EGA graphics card 20 Mbytes Winchester Disk drive 360 Kbytes Floppy disk drive 640 Kbytes RAM Labmaster 100KHz ADC Board	Languages: Microsoft C version 4.0 Borland Turbo Pascal version 4.0 Microsoft MASM macro-assembler version 3.0 Packages: C-TREE Database Library Routines C-Utilities Library Routines EDIT ASCII editor Microsoft WORD text processor GEM Operating Environment GEM GRAPH curve plotter GEM DRAW sketching utility Ventura Desk Top Publisher.

Table 8.1 Personal Computer Resources for C.P.A.S

Hewlett Packard 9000/320 Series Desktop Computer and Expansion Box
68020 processor running at 16MHz
68821 maths co-processor

4 Mb RAM

20Mb Winchester disk drive

1.44Mb 3.5 in Flexible disk drive

HP GPIO board

HP RS232 Communication board

Infotech AD2000 200kHz ADC board

Infotech Compiled Basic Operating System version 5.0

Table 9.1 Quikburn System Hardware

	Analysis Time for 1 Cycle	
	Uncompiled (sec)	Compiled (sec)
1 Spark time WMEP 10%, 50%, 90% Burn Locations	0.3796	0.067
2 Spark time WMEP Pressure referenced to MAP 10%, 50%, 90% Burn Locations	0.4194	0.0731
3 Spark time WMEP Pressure referenced to MAP 10%, 50%, 90% Burn Locations Peak pressure and Location	0.477	0.0849
4 Spark time IMEP Pressure referenced to MAP 10%, 50%, 90% Burn Locations Peak pressure and Location	0.978	0.1301

Table 9.2 Basic Language Execution Times for the Combustion Analysis

Reference	50% Mass Burnt Location	Operating Conditions
10.1	10° ATDC	3 Intake Configurations All AFRs
10.2	10° ATDC	2 Ignition Systems All AFRS
10.3	8° - 15° ATDC	2 Engine Speeds 2 AFRs
10.5	6° - 10° ATDC	All Operating Conditions
10.6	5° - 10° ATDC	All Operating Conditions
10.7	14° ATDC	$\phi = 0.9$
10.8	13° - 18° ATDC	3 Intake Configurations Lean and rich AFRs
10.9	11° - 18° ATDC	2 Intake Configurations 3 Ignition Systems All lean AFRs
10.12	10° ATDC	All Operating Conditions

Table 10.1 Published Occurrences of the Optimum Location of 50% Mass Burnt

2.0L OHC (EFI) 1500 rpm WWMP MBT timing									
AFR					Spark time (deg BTDC)				
Base	Cyl 1	Cyl 2	Cyl 3	Cyl 4	Base	Cyl 1	Cyl 2	Cyl 3	Cyl 4
10	9.41	9.36	9.64	10.07	35	35.34	34.90	35.80	35.40
11	10.41	10.16	10.7	10.86	32	31.88	32.00	33.12	32.15
12	11.48	11.16	11.30	11.93	26	25.60	25.75	26.02	26.00
13	11.90	12.19	12.24	12.90	30	30.37	30.65	31.12	30.40
14	13.32	12.88	13.07	14.03	30	29.29	29.27	30.14	29.80
15	14.23	13.72	13.95	14.95	36	35.42	35.63	36.49	35.89
16	15.49	14.85	15.07	16.09	35	34.51	34.62	35.22	34.80
17	16.13	15.56	15.79	17.08	38	37.76	37.86	37.55	38.77

Table 10.2 Measured AFR and Timing Spreads at WWMP under Control of Production EEC IV Management System.

Operating Conditions	WMEP (bar)				Location of 50% Mass Burnt (deg ATDC)			
	Min	Mean	Max	COV (%)	Min	Mean	Max	COV (%)
1500 rpm WWMP 12:1 AFR	3.53	3.78	4.05	3.18	1	9.12	15	34.3
1500 rpm WWMP 16:1 AFR	3.49	3.91	4.36	5.85	8	15.82	24	22.3
2000 rpm WOT 12:1 AFR	9.32	10.30	11.33	5.06	8	14.91	22	20.5
2000 rpm WOT 16:1 AFR	8.00	8.88	10.85	5.14	13	21.44	30	15.9

Table 10.3 Distributions ofWMEP and Location of 50% Mass Burnt Within a 100 Cycle Sample

Condition		Optimum Location of 50% Mass Burnt Degrees ATDC
Nominal: 1500 rpm, Part Load 2.0L OHC engine.geometry $\theta_d = 85^o$; $m_f = 1.3$ e-5 kg MAP = 0.5 bar; $Q_{ht}/Q_f = 0.3$		15.5
As Nominal Except	$Q_{ht}/Q_f = 0.4$	18.5
	$Q_{ht}/Q_f = 0.24$	13.5
	$\theta_d = 55^o$	13.5
	$\theta_d = 110^o$	18.0
	MAP = 1 bar	14.5
	$m_f = 2.0$ e-5 kg	14.5
	Valencia 1.0L engine geometry	15.5
Settings for 2000rpm WOT 2.0L OHC engine geometry $\theta_d = 60^o$; $m_f = 3.54$ e-5 kg MAP = 1 bar; $Q_{ht}/Q_f = 0.3$		12.0

Table 10.4 Predicted Optimum Locations of 50% Mass Burnt

Variable	Heat Loss	Burn Duration	MAP	Fuel Mass	Engine Size
Effect on Optimum Location of 50% Mass Burnt	Increased heat loss causes the optimum location to be earlier in the cycle. Q_{ht}/Q_f change from 0.2 to 0.4 retards by 5^o.	The shorter the burn the earlier the optimum location. θ_d change from 55^o to 110^o retards the location 4.5^o.	A slight effect. WOT advanced the optimum location by 1^o from nominal.	A slight effect Increased fuelling from 1.3 to 2.0 e-5 kg advanced the location by 1^o.	No effect

Table 10.5 Summary of Variables' Effect on the Optimum Location of the 50% Mass Burnt

Figures

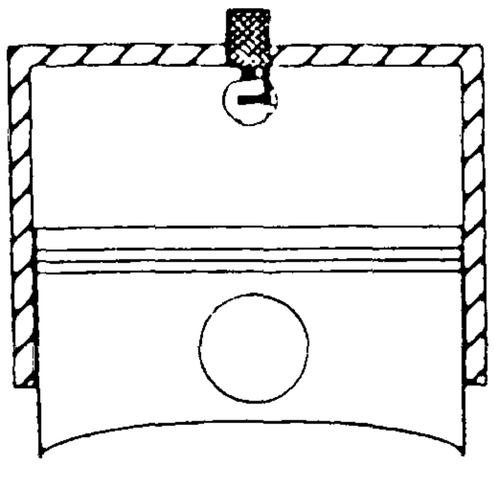

Formation of Flame Kernel

Combustion initiated by spark. Early expansion due to temperature rise between electrodes. Dependent on spark ignition system energy.

Characterised by 0-2% mass burnt. However, pressure changes of this order are too small to detect accurately.

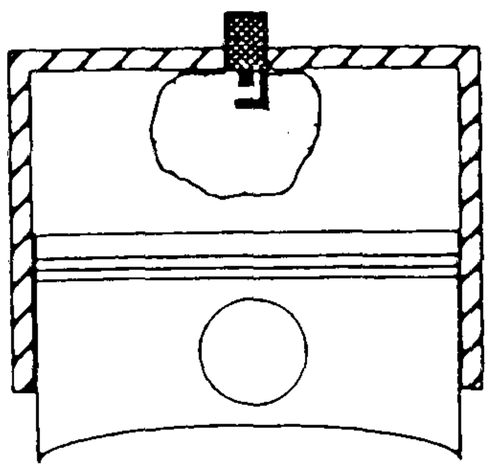

Development to Fully Stabilized Flame Front

Flame kernel grows and becomes subjected to heat loss and turbulence. Must reach a critical size before the spark discharge ceases else flame will be extinguished

Characterised by 0-10% mass burnt

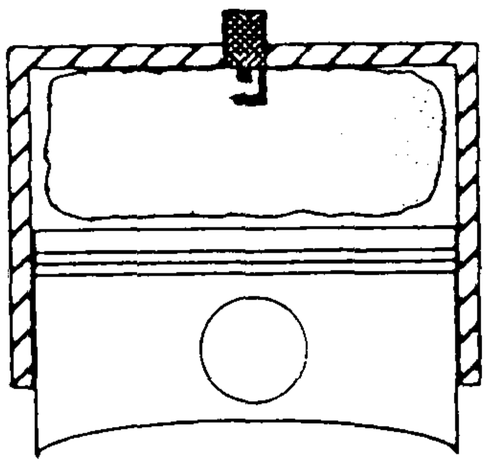

Main Fuel Burning Stage

Turbulent propagation of flame front. Lamina burning occurs within eddies. Majority of charge mass consumed in this stage.

Characterised by 10-90% mass burnt.

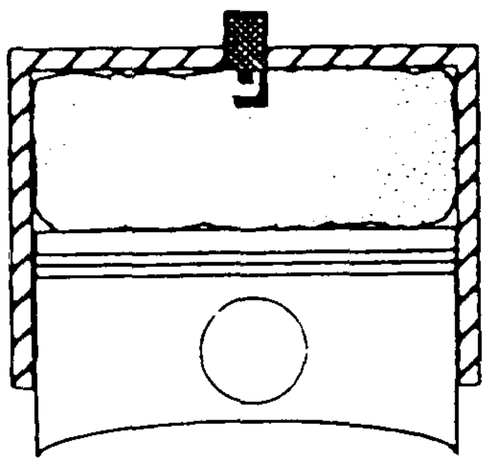

Burn up of Remaining Charge

The burning of the last few percent of the charge is slow. This is due to the unburnt region being close to the cylinder walls, which quench the flame front.

Characterised by 90-100% mass burnt.

Fig 2.1 The Different Stages of Combustion

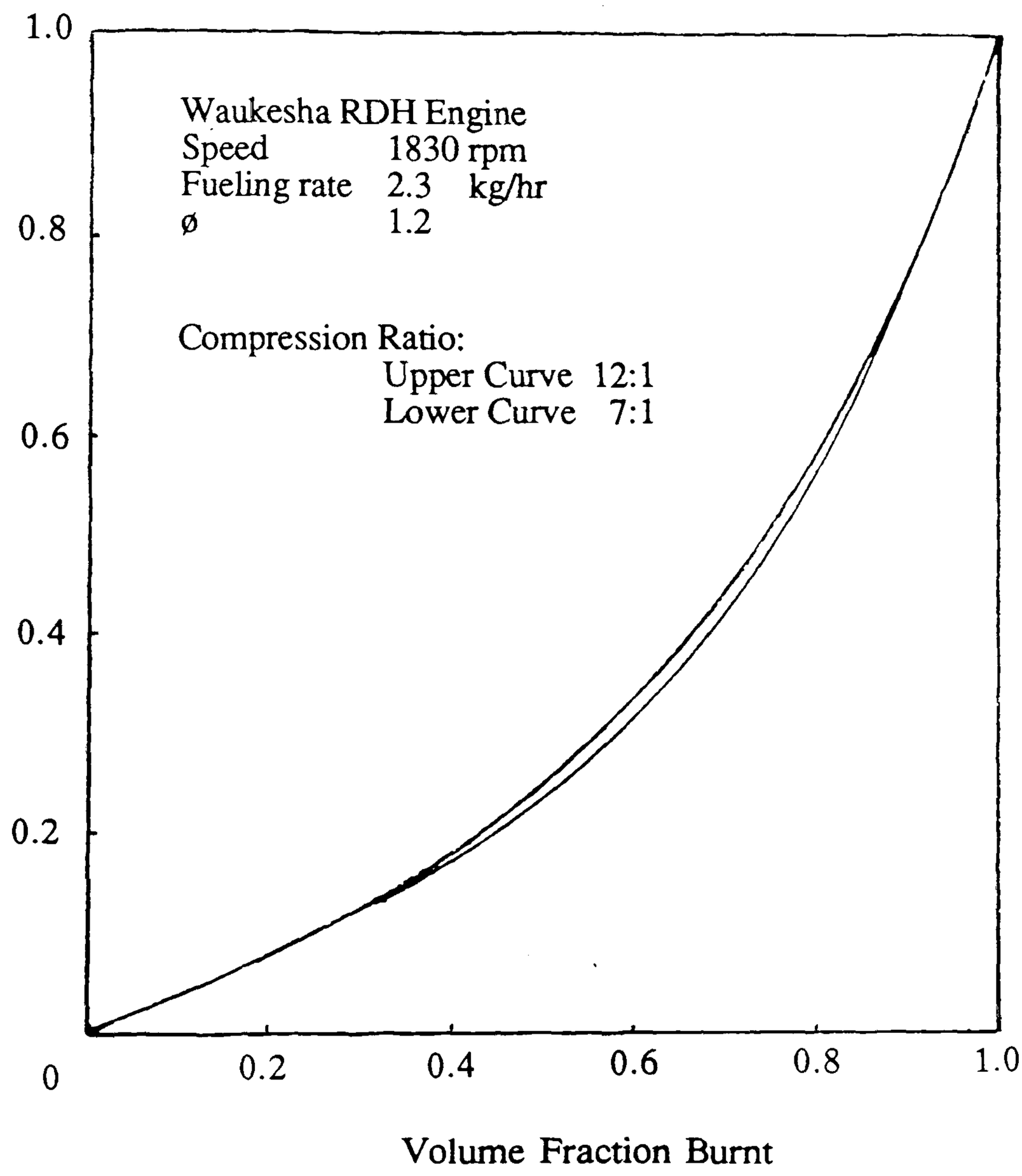

Fig 2.2 Universal Burning Curve taken from Krieger and Borman[2.32].

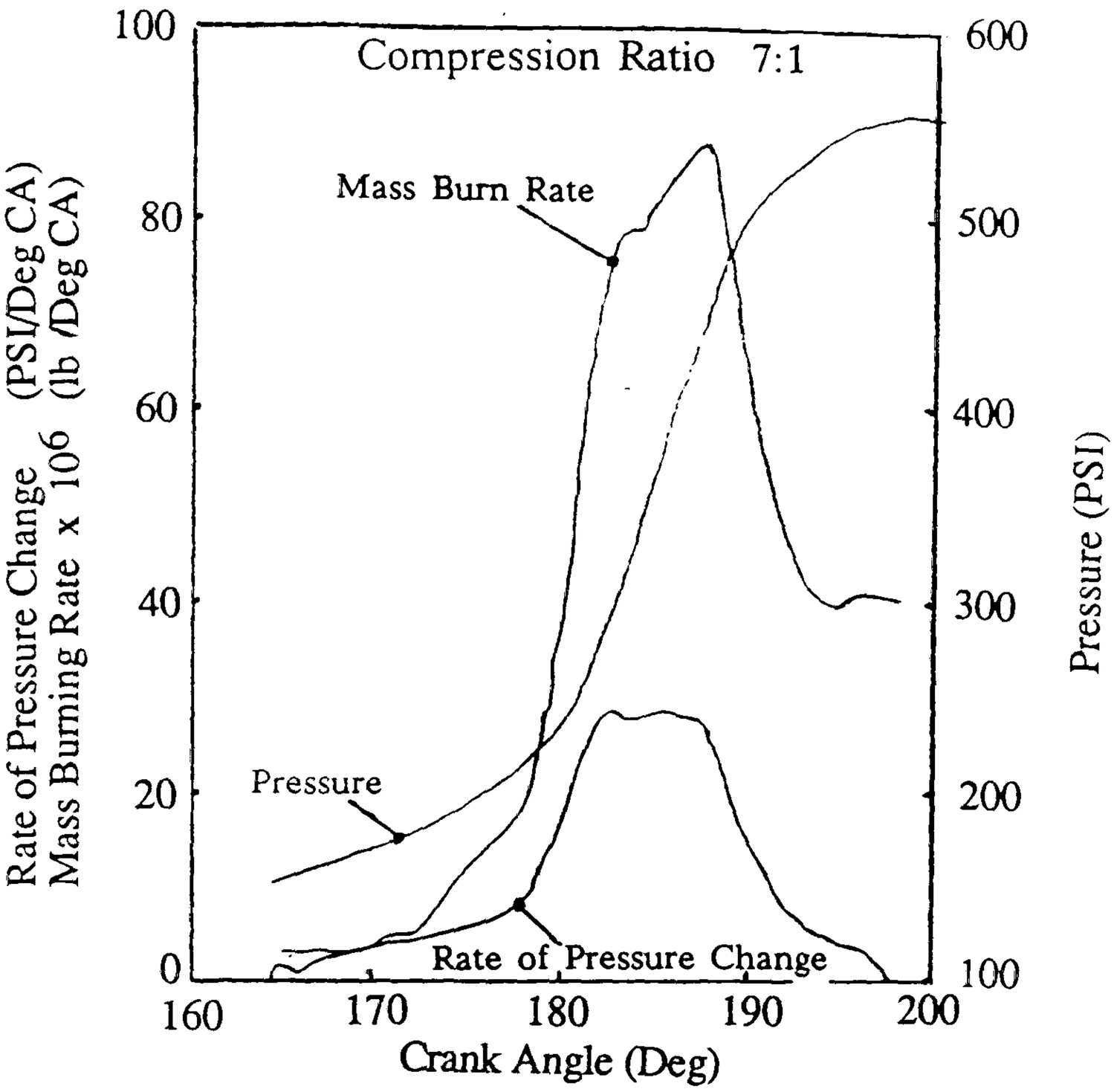

Fig 2.3A Example Output from Analysis by Krieger and Borman [2.32]. Waukesha RDH engine operating at 1830 rpm, fueling rate of 2.4 kg/hr, and equivalence ratio 1.2.

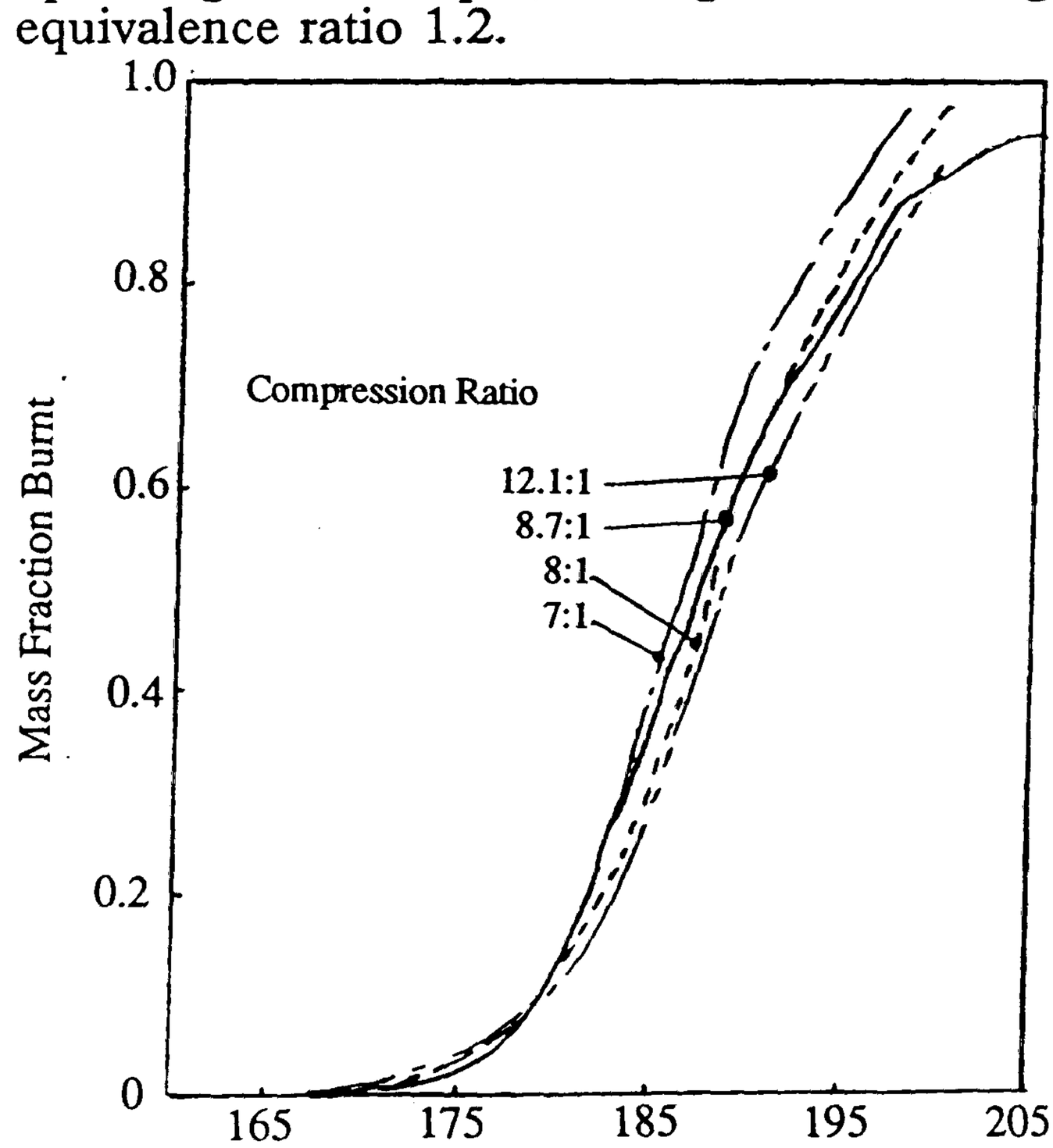

Fig 2.3B Curves of Mass Fraction Burnt obtained by Krieger and Borman[2.32]. Same engine operating conditions as above.

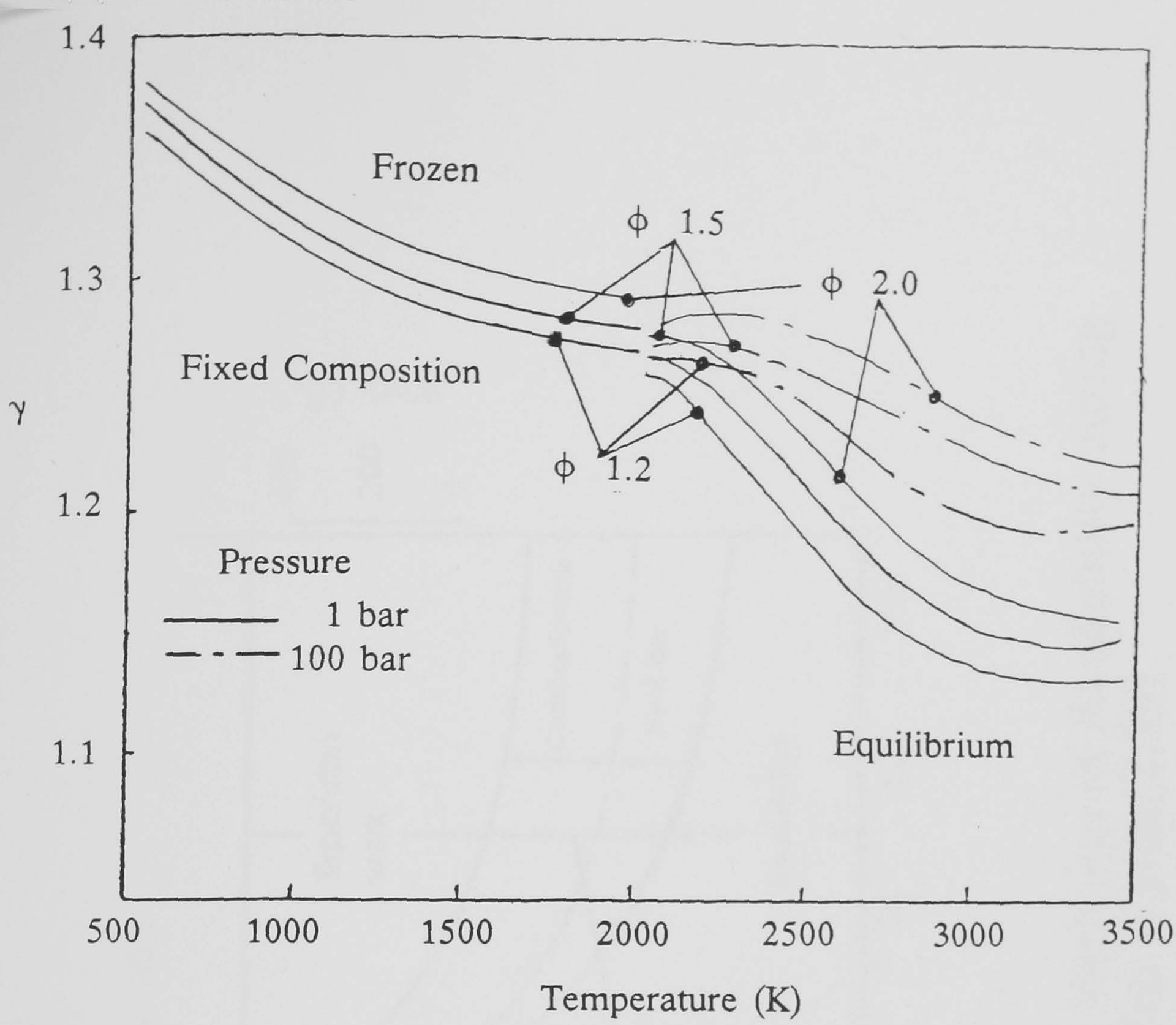

Fig 2.4A Variation of Specific Heat Ratio for the Combustion Products of a Hydrocarbon fuel, C_nH_{2n}, from [2.34].

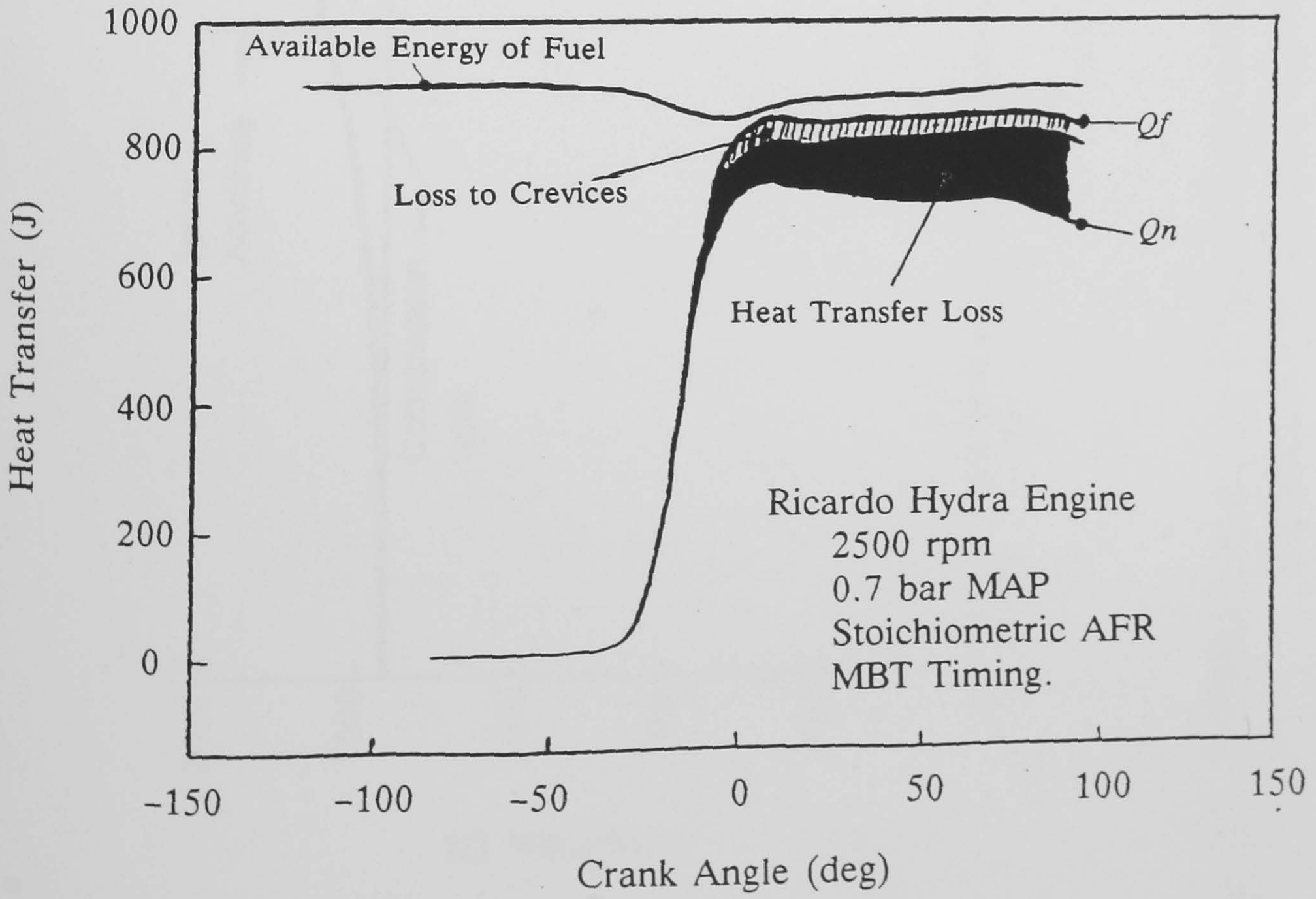

Fig 2.4B Sample Heat Release from the Single Zone Analysis[2.34].

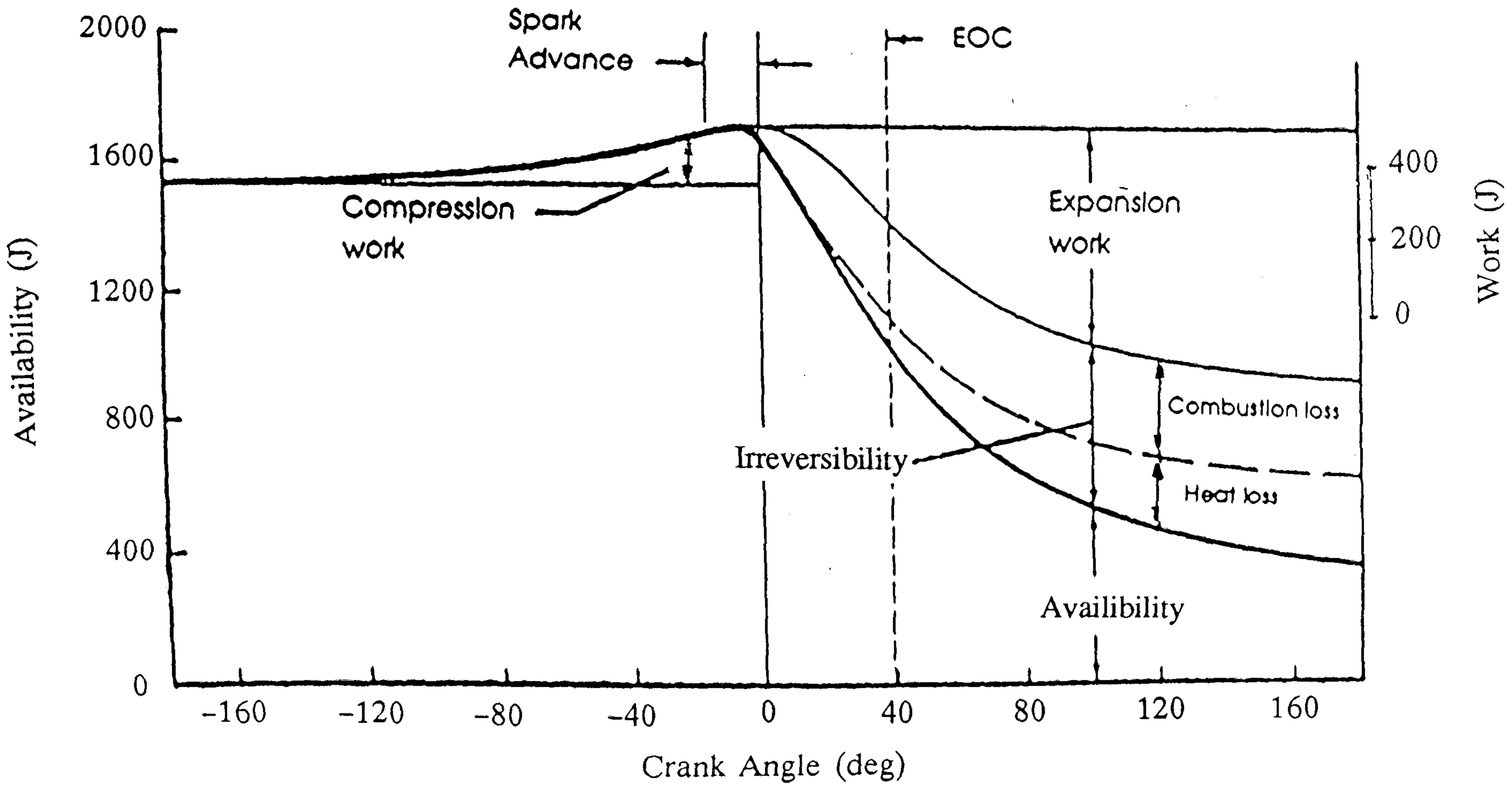

Fig 2.5 A Prediction, by Engine Simulation, of the Variation of Availability during Combustion, from Patterson and Van Wylen[2.39]

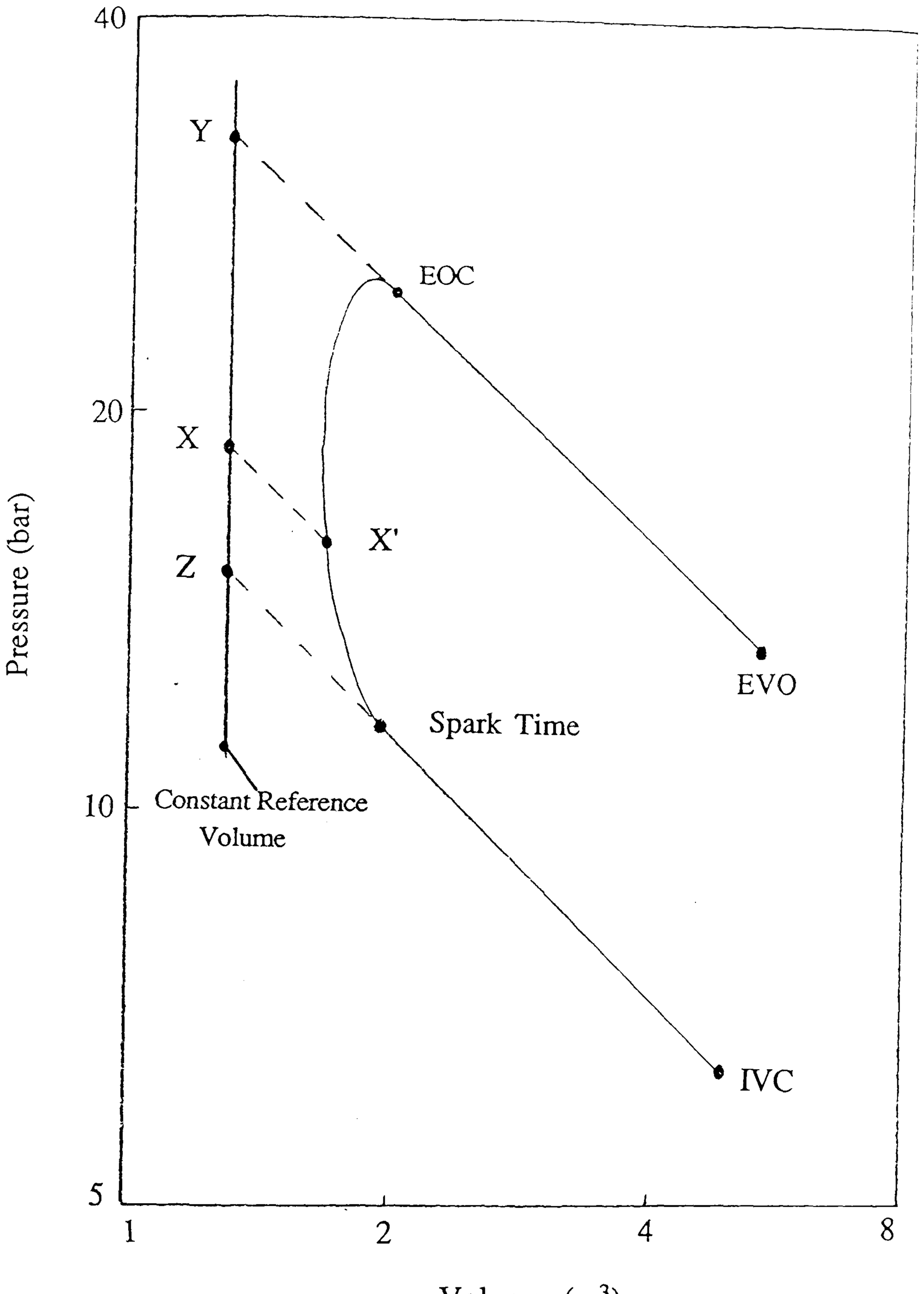

Fig 2.6 A Logarithmic Indicator Diagram Illustrating Marvin's Analysis Method[2.40]

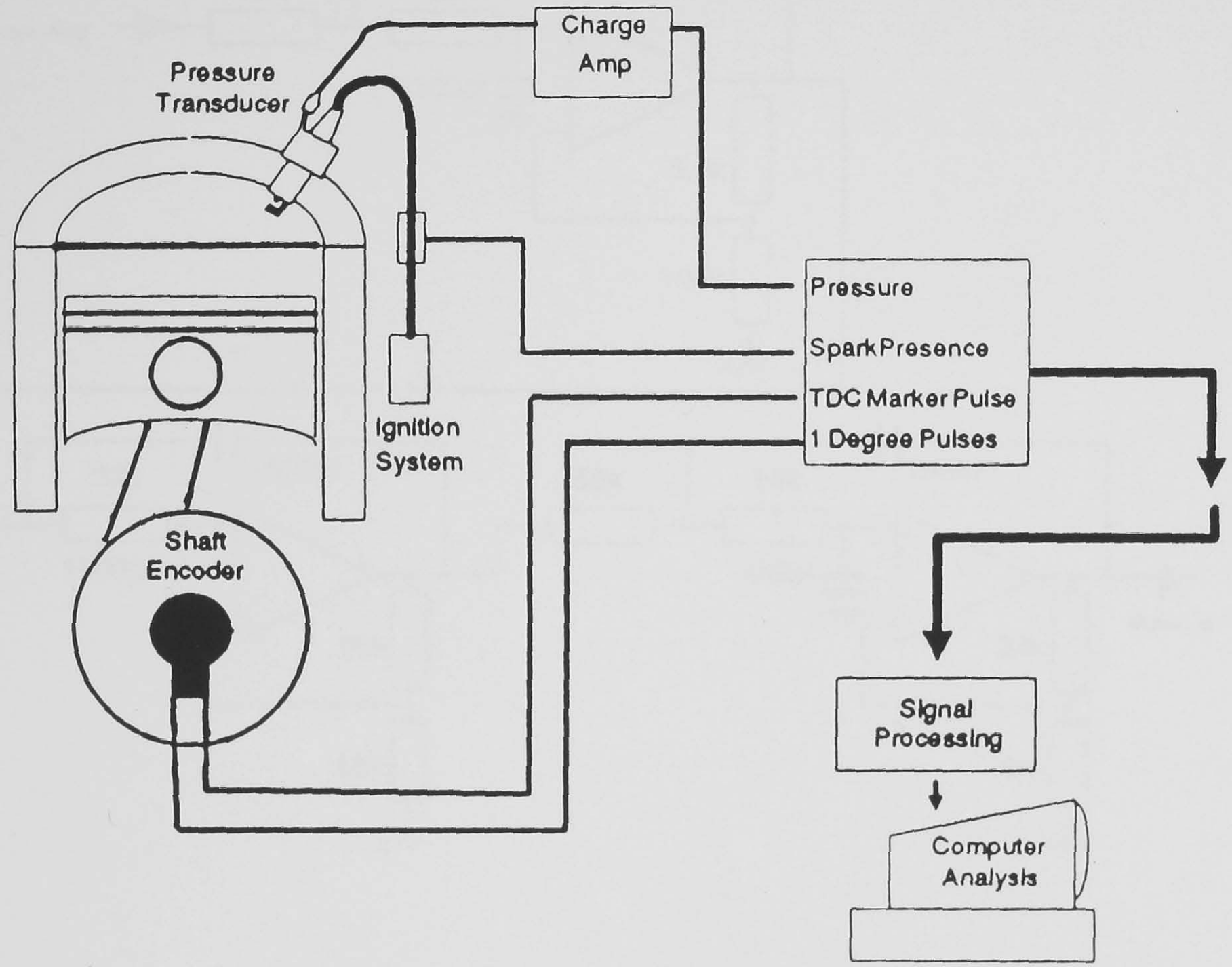

Fig 3.1 Schematic of Testbed Sensors and Remote Computer Analysis

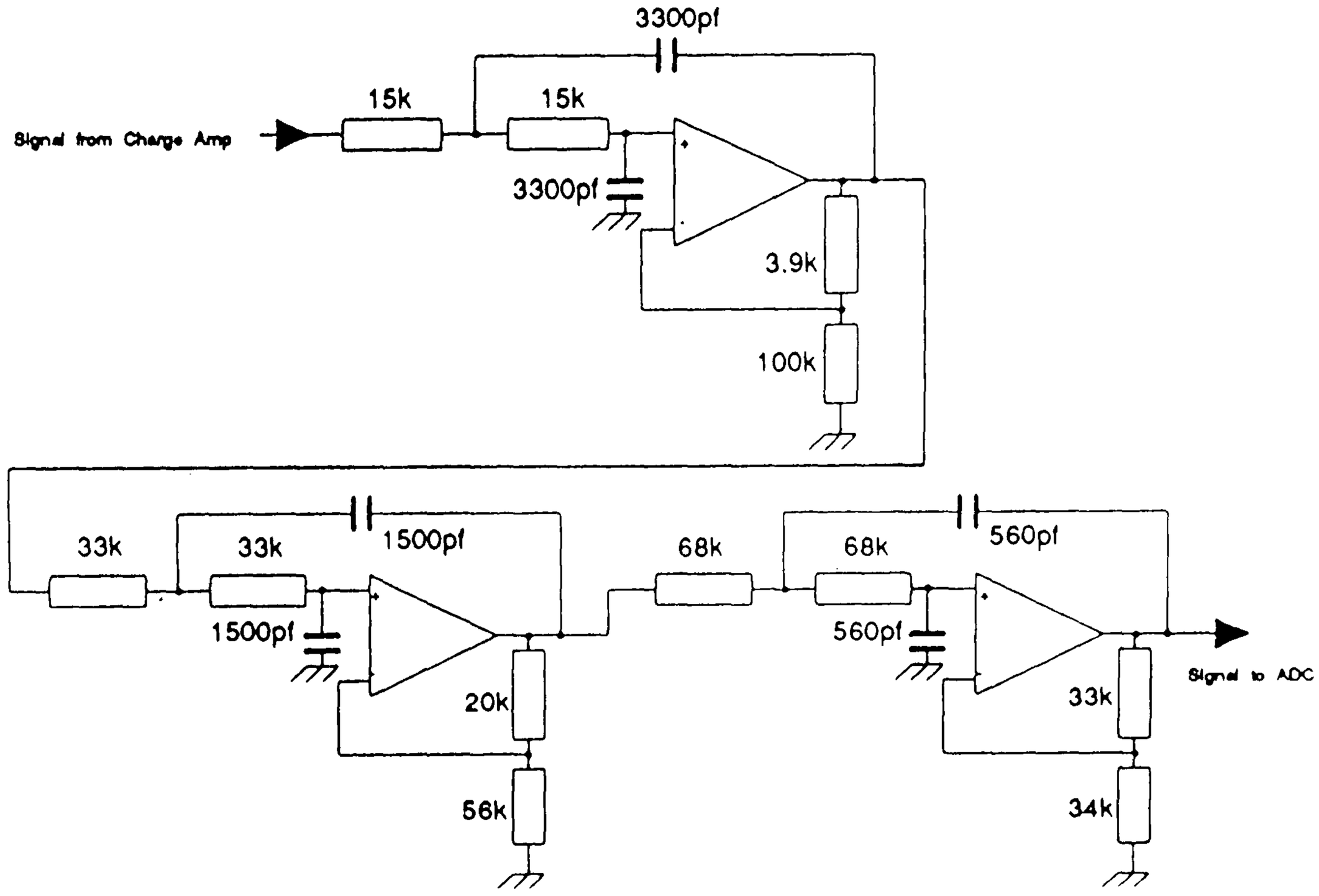

Fig 3.2 6 Pole Bessel Anti-Aliasing Filter - Cutoff Frequency 2kHz

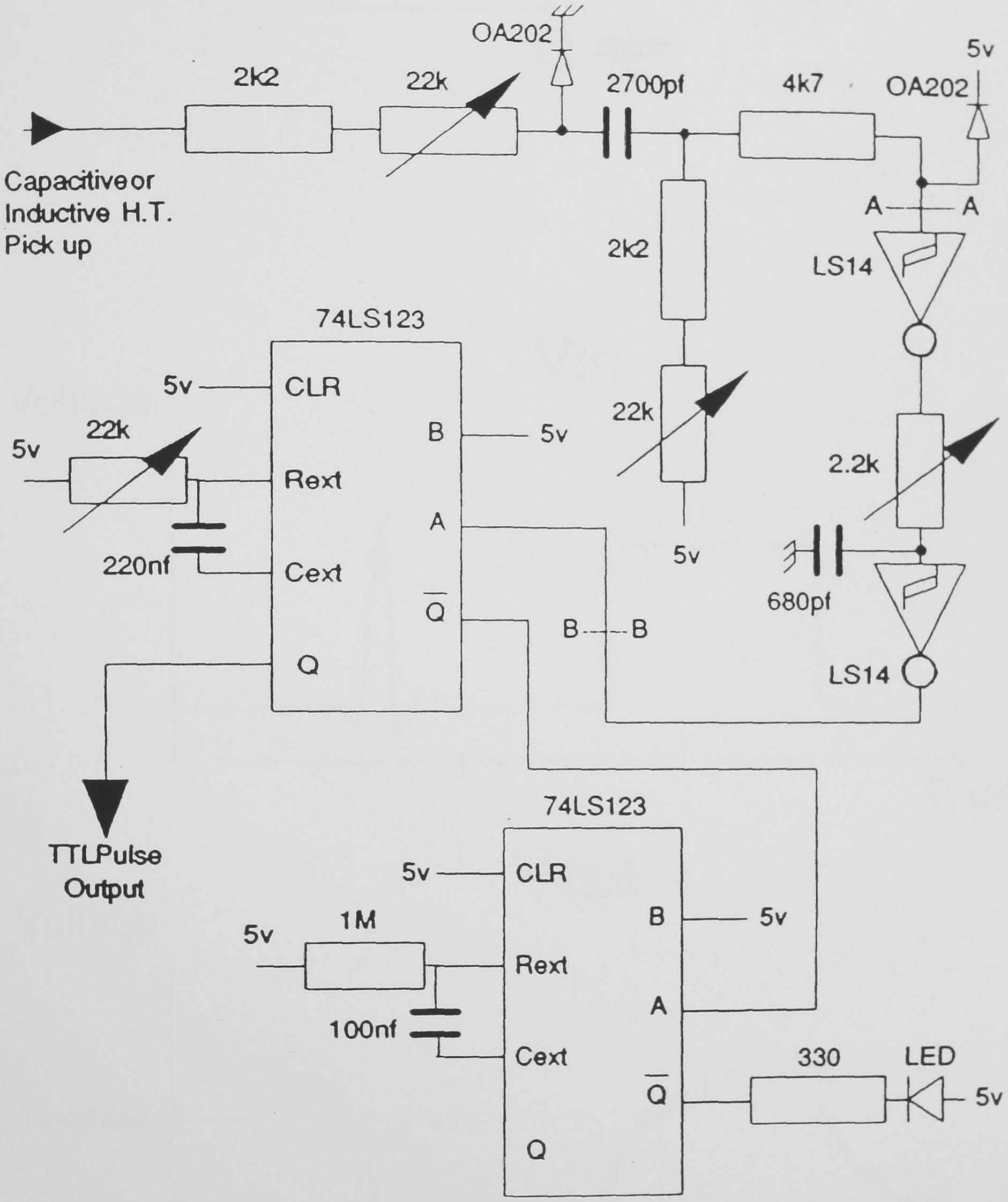

Fig 3.3 Spark Detection Circuitry

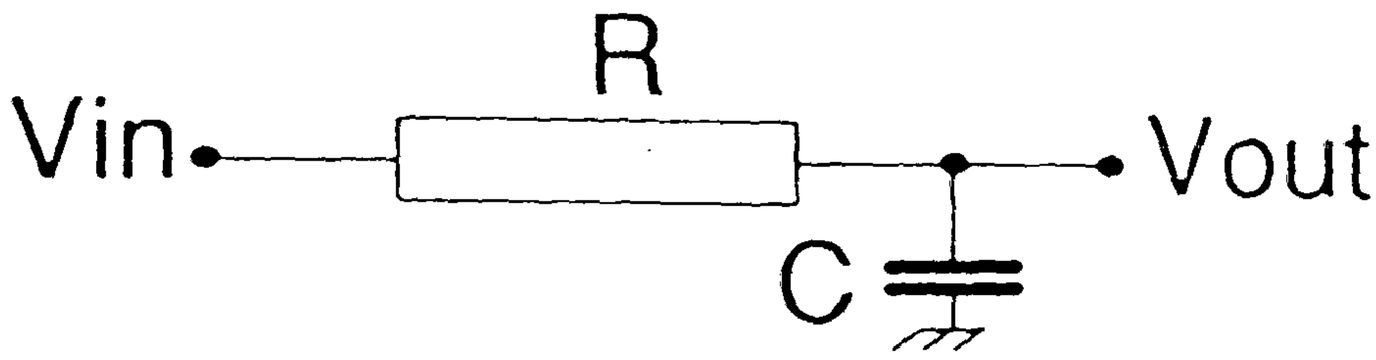

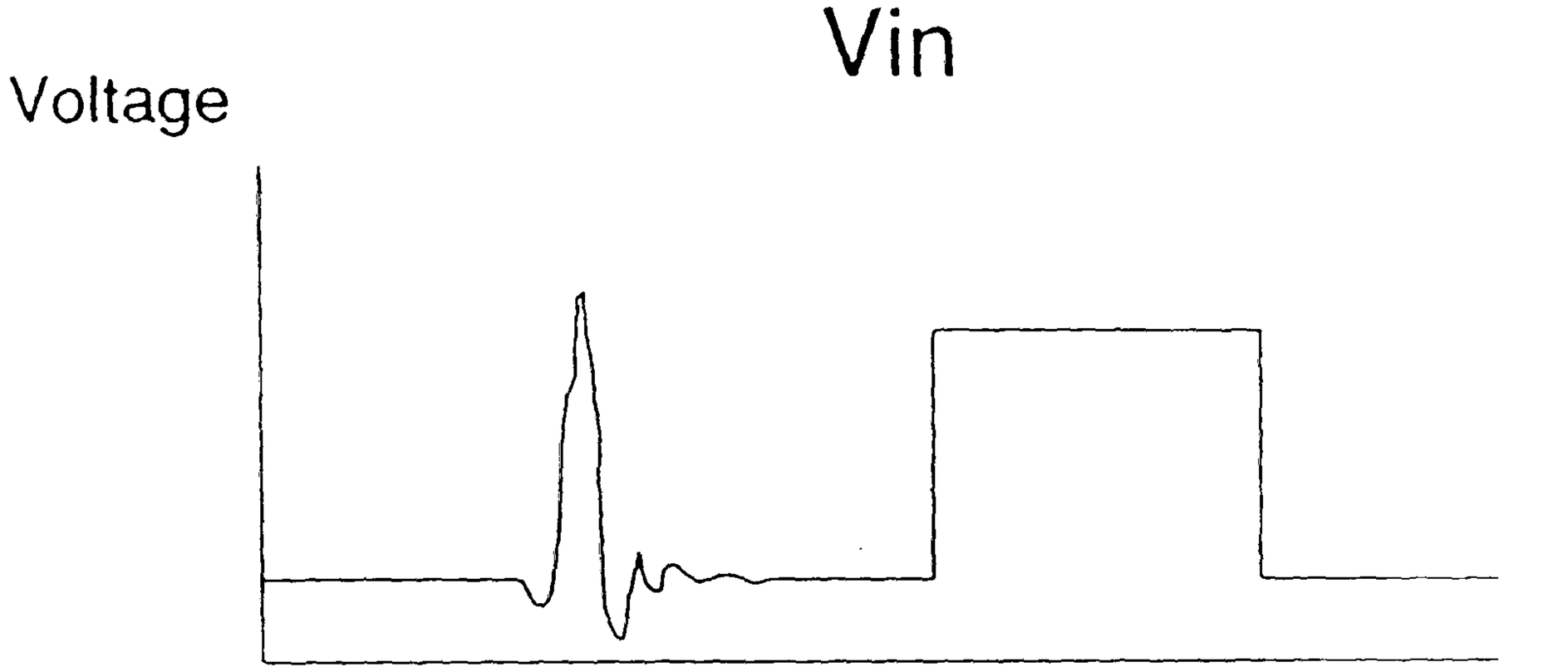

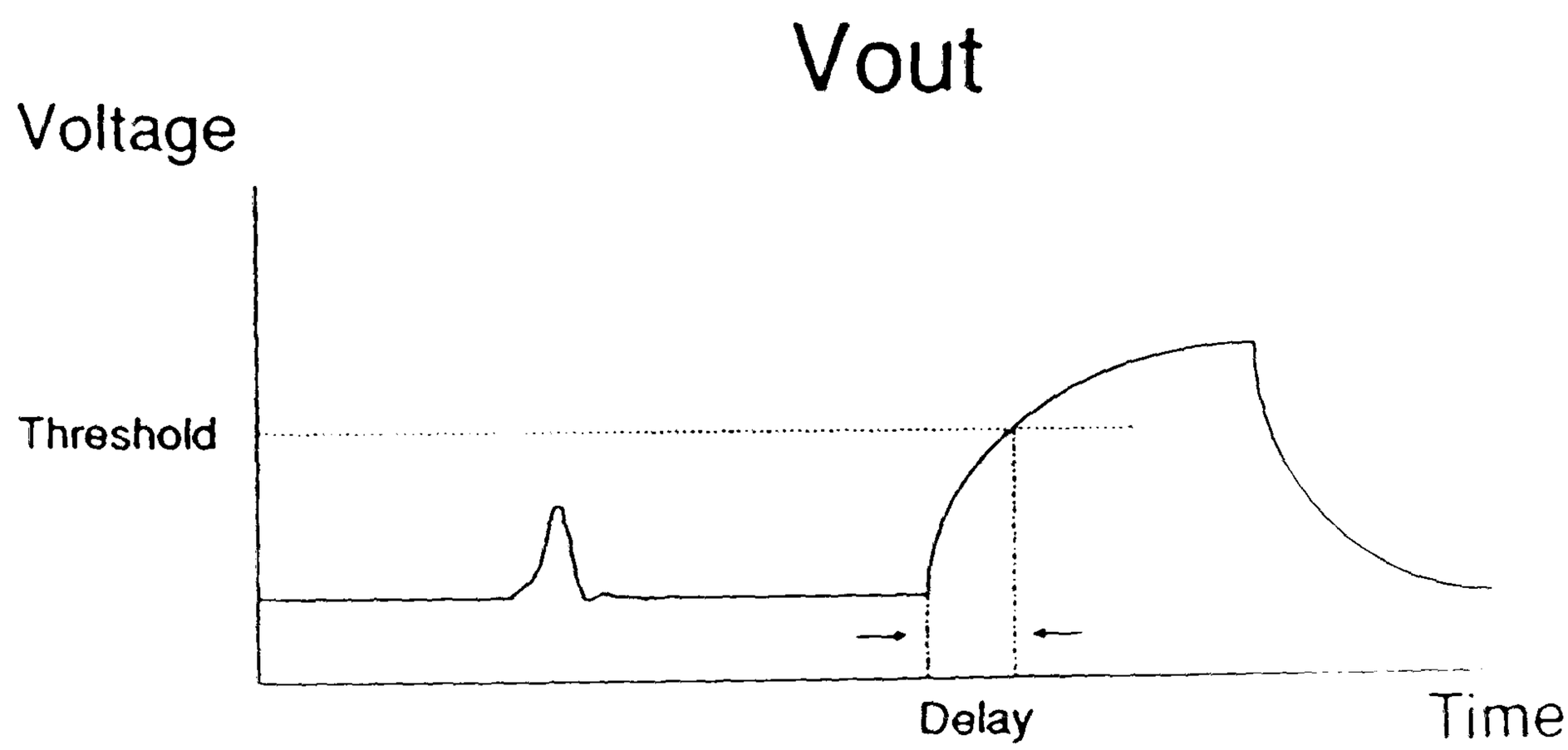

Fig 3.4 Effect of Filtering Digital Signals

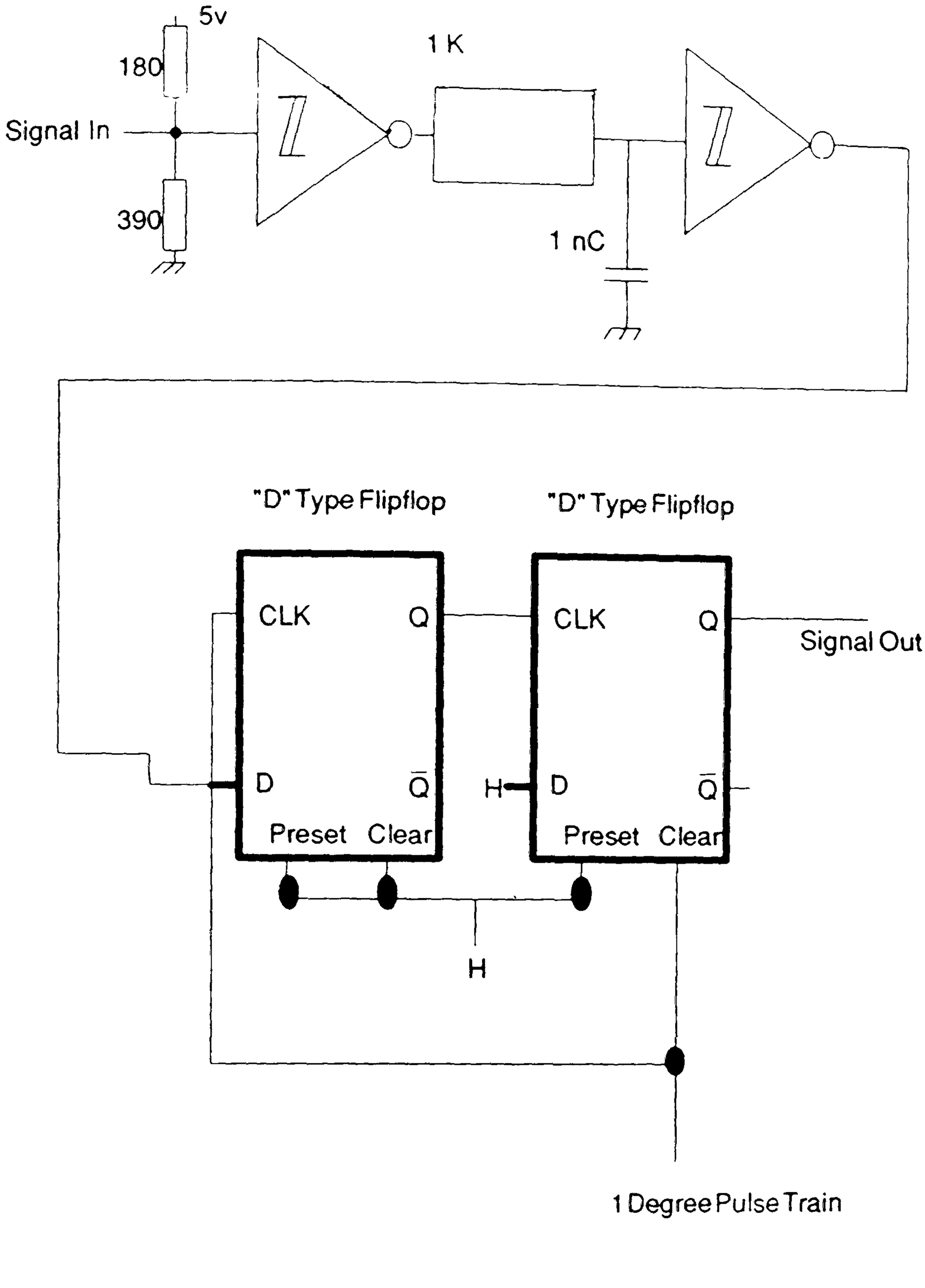

Fig 3.5 Input Signal Processing Circuitry for Noise Rejection and Synchronisation, with Pulsewidth Sizing, to 1 Degree Pulses

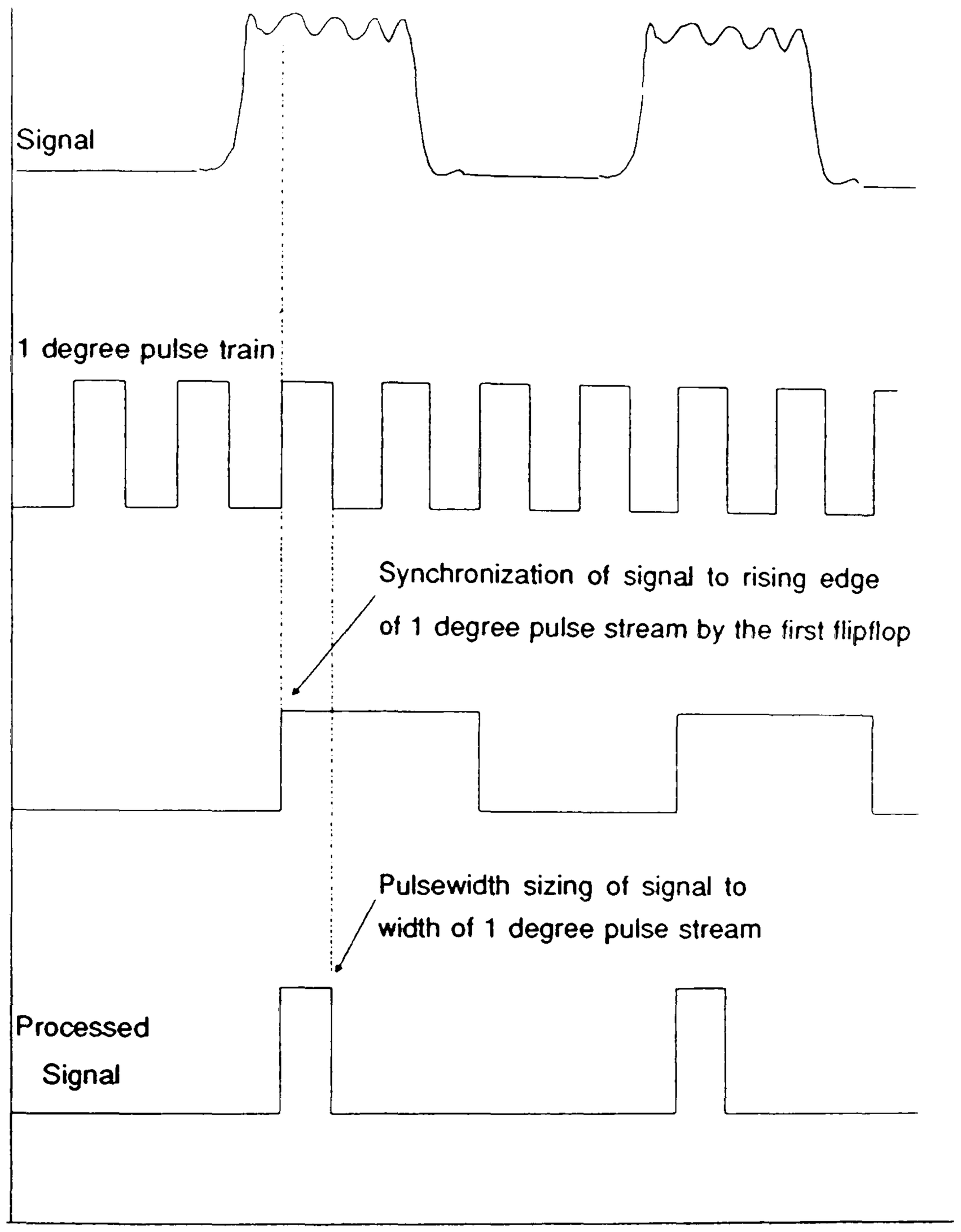

Fig 3.6 Timing Diagram for Signal Processing

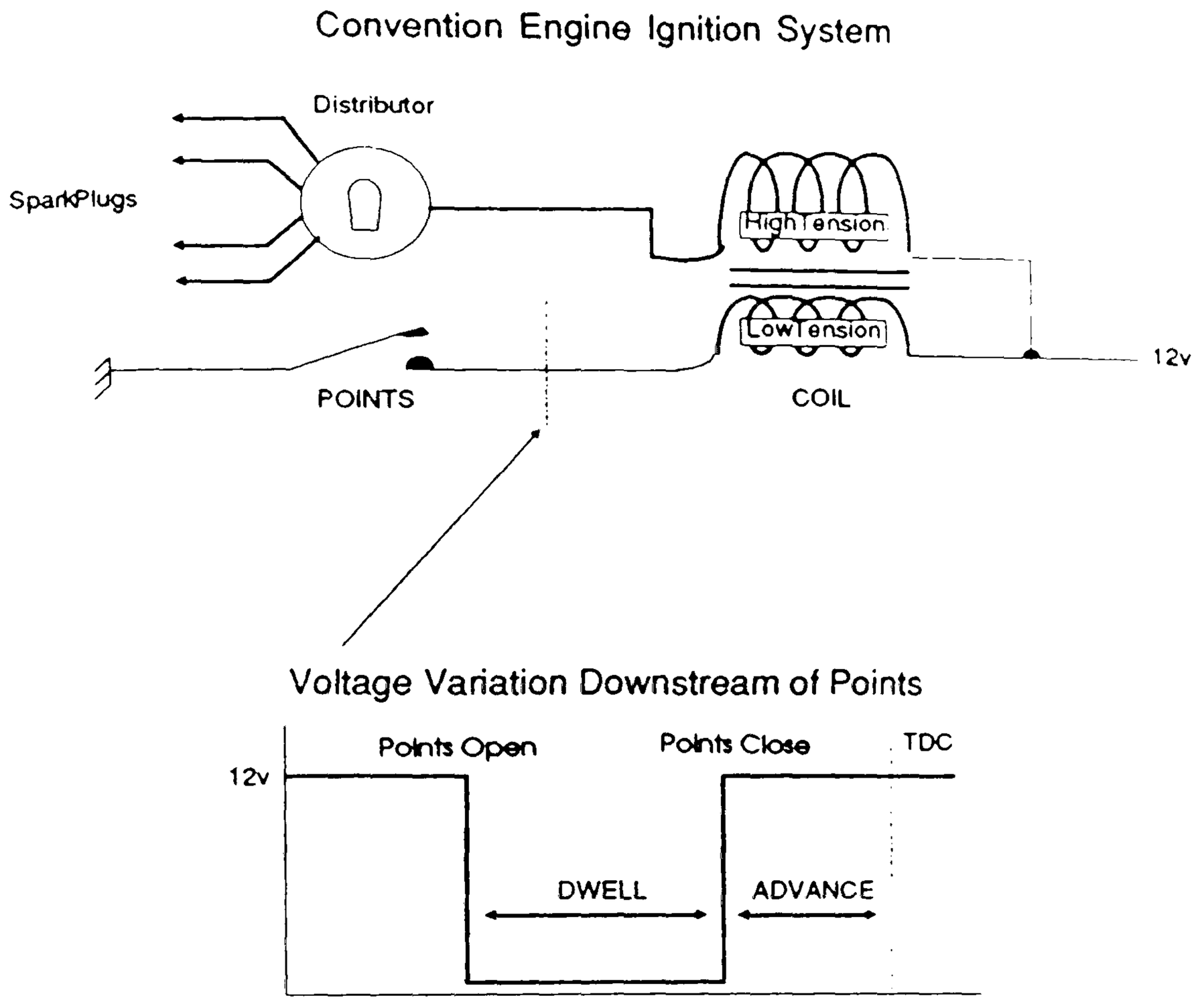

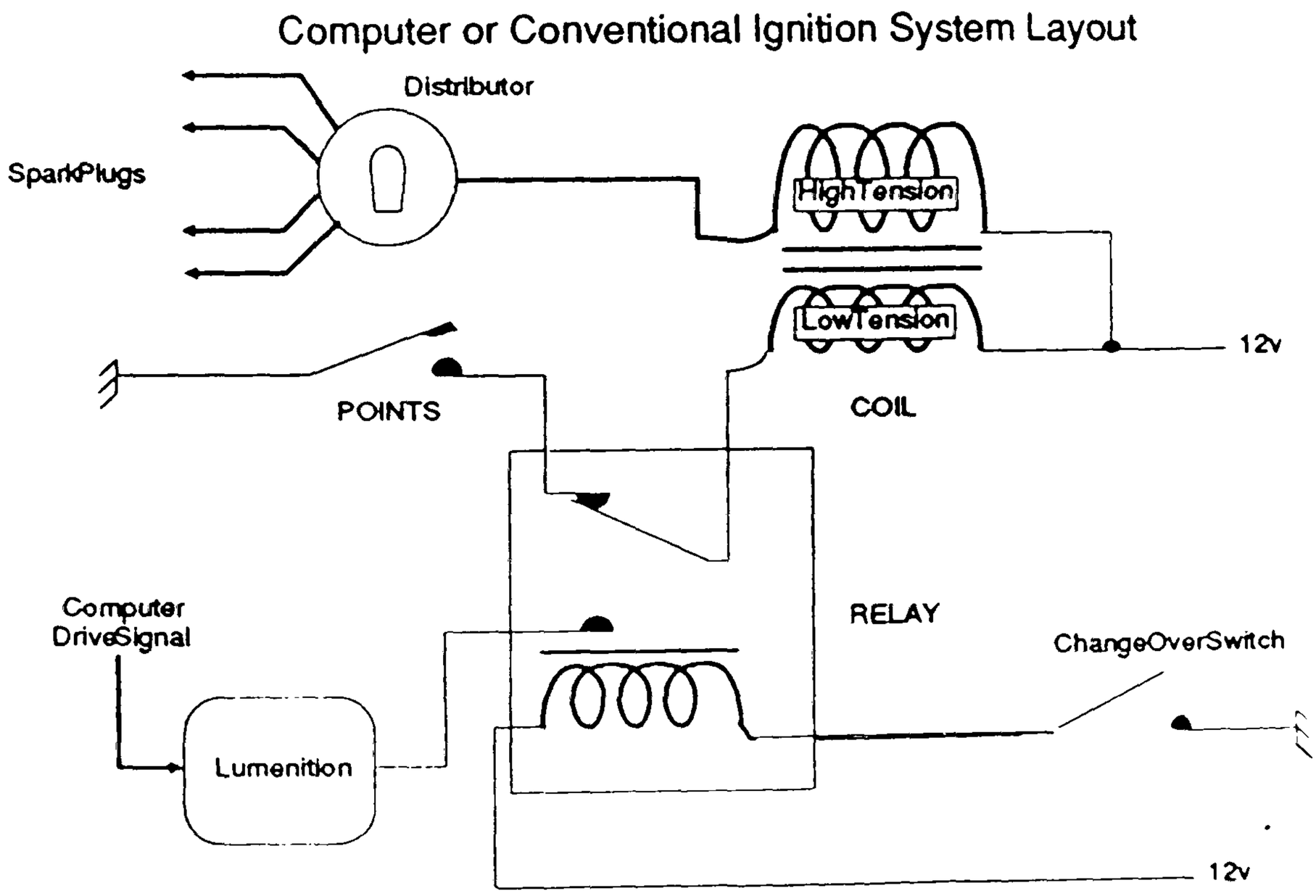

Fig 4.1 Conventional and Computer Driven Ignition Layouts

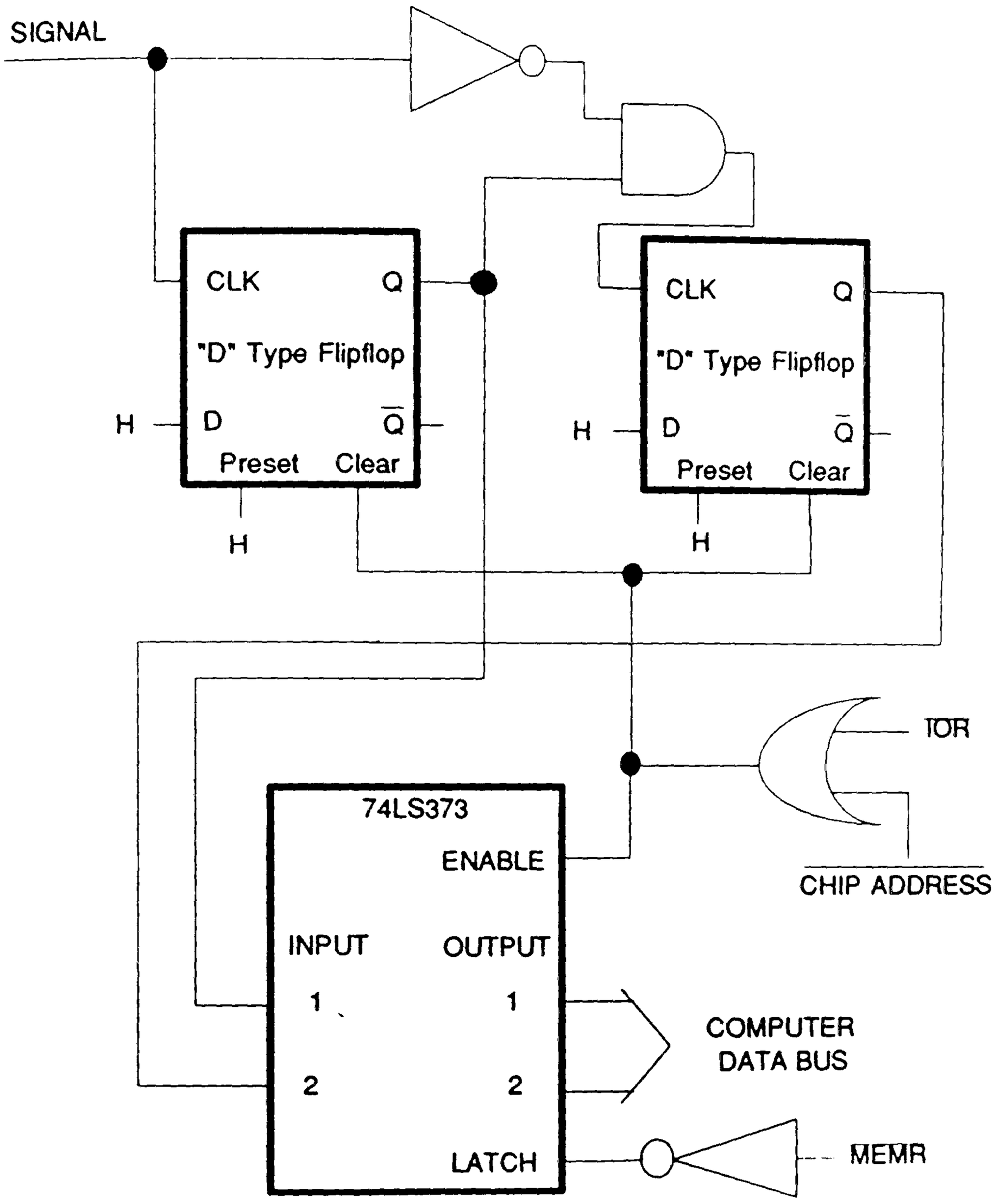

Fig 4.3 Event Occur and Overflow Circuit to Form the Status Register

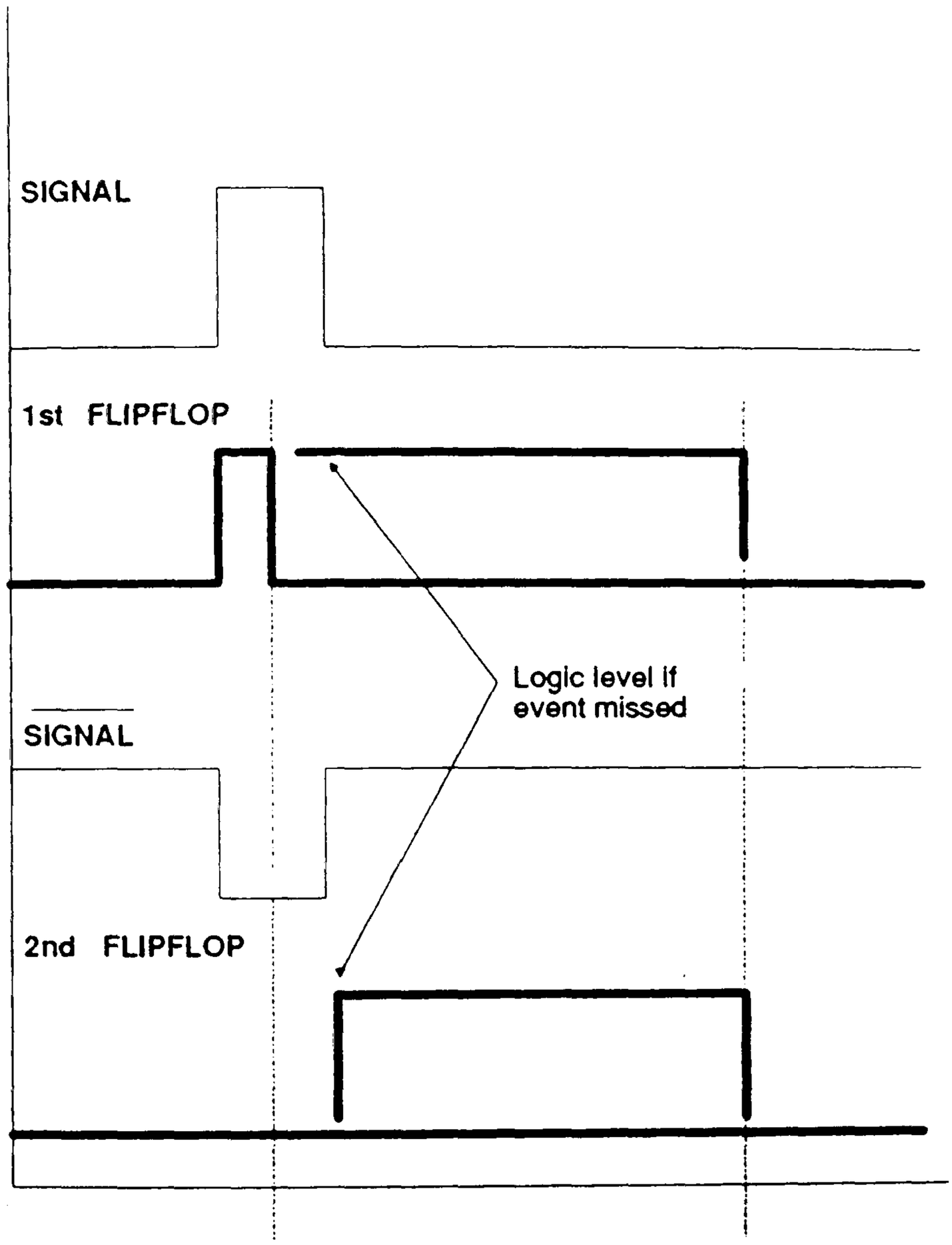

Fig 4.4 Timing Diagram for Event Occur/Overflow Circuitry

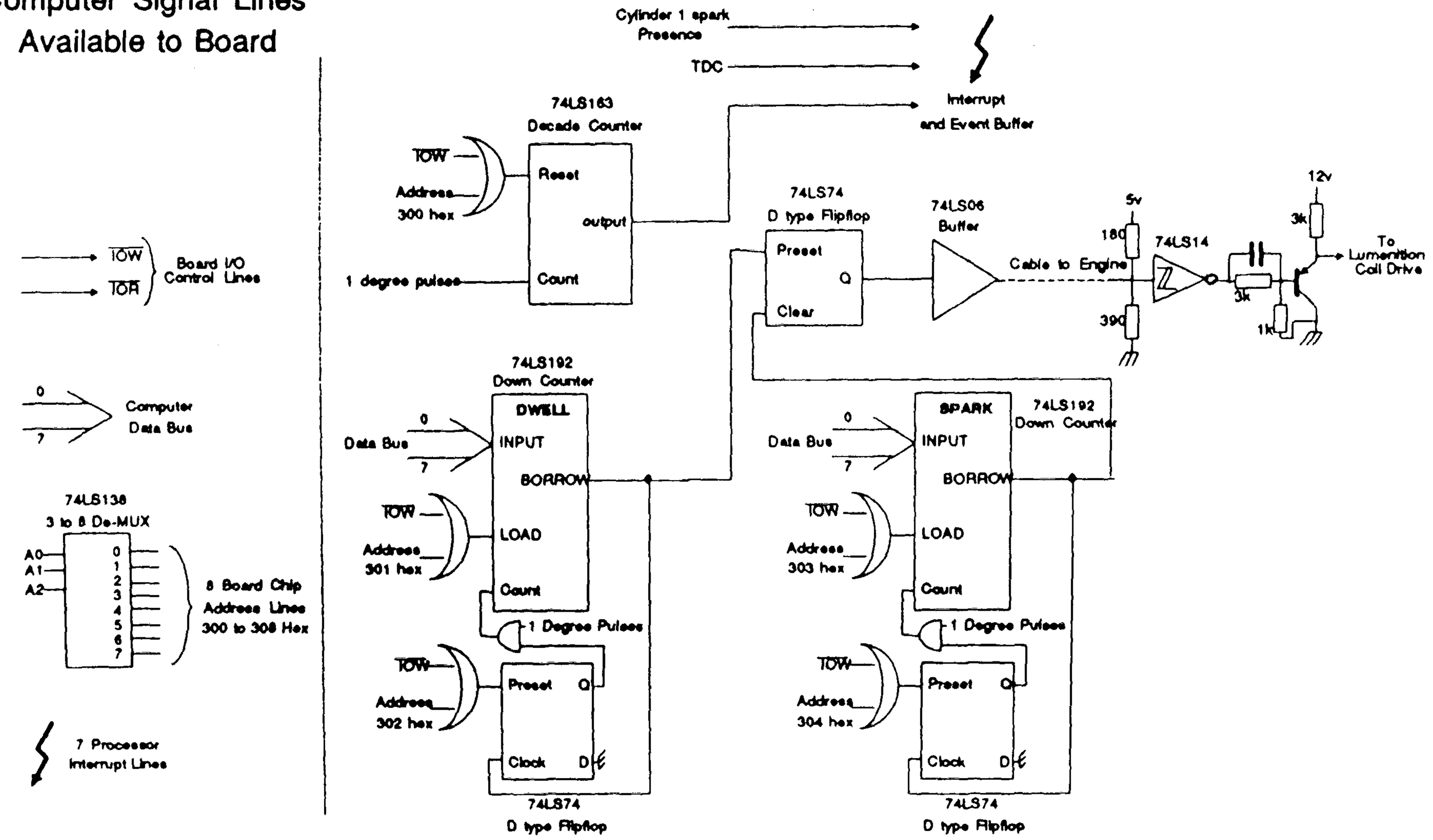

Fig 4.5 Ignition Timing Control Circuitry

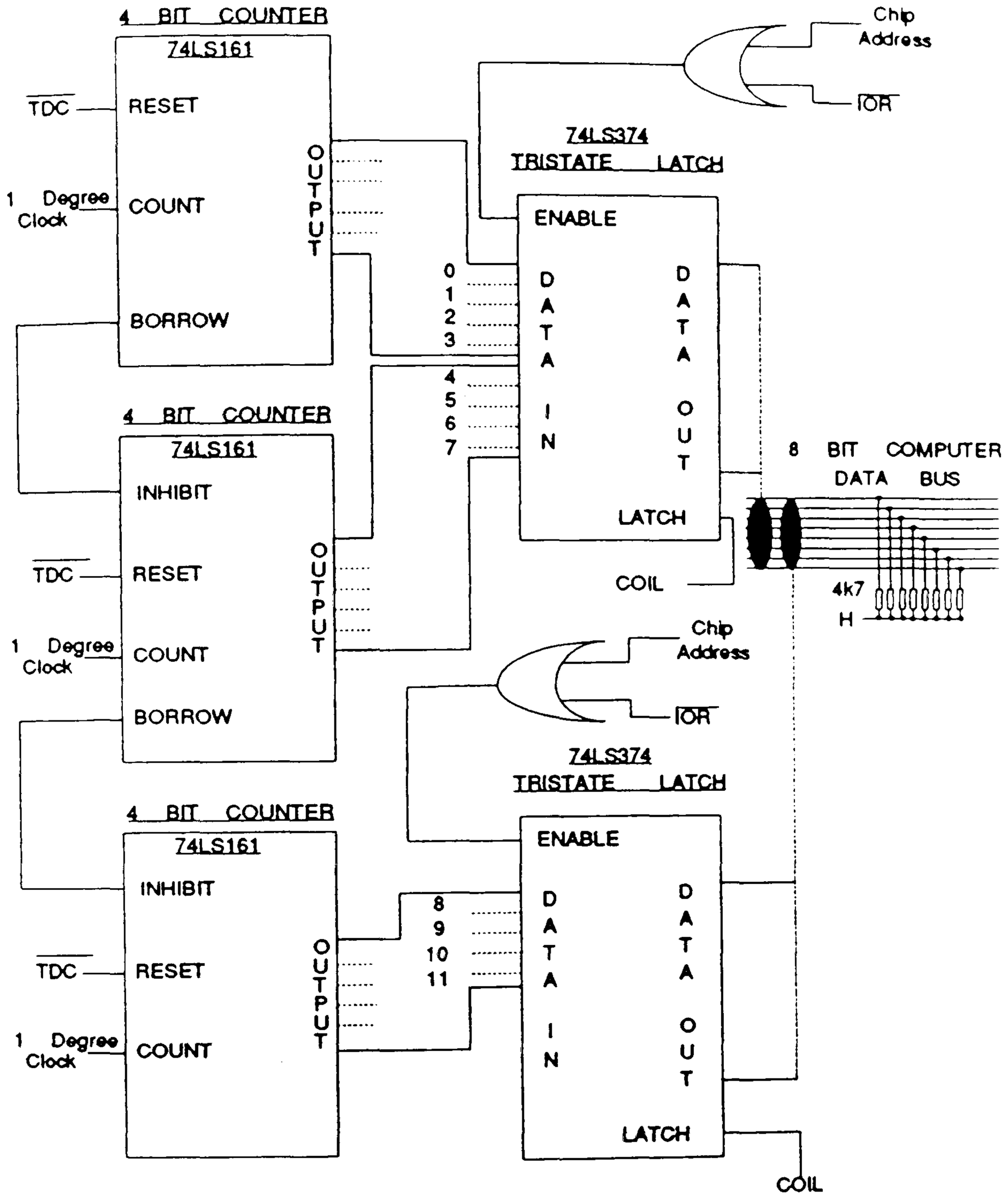

Fig 4.6 Spark Timing Measuring Circuitry

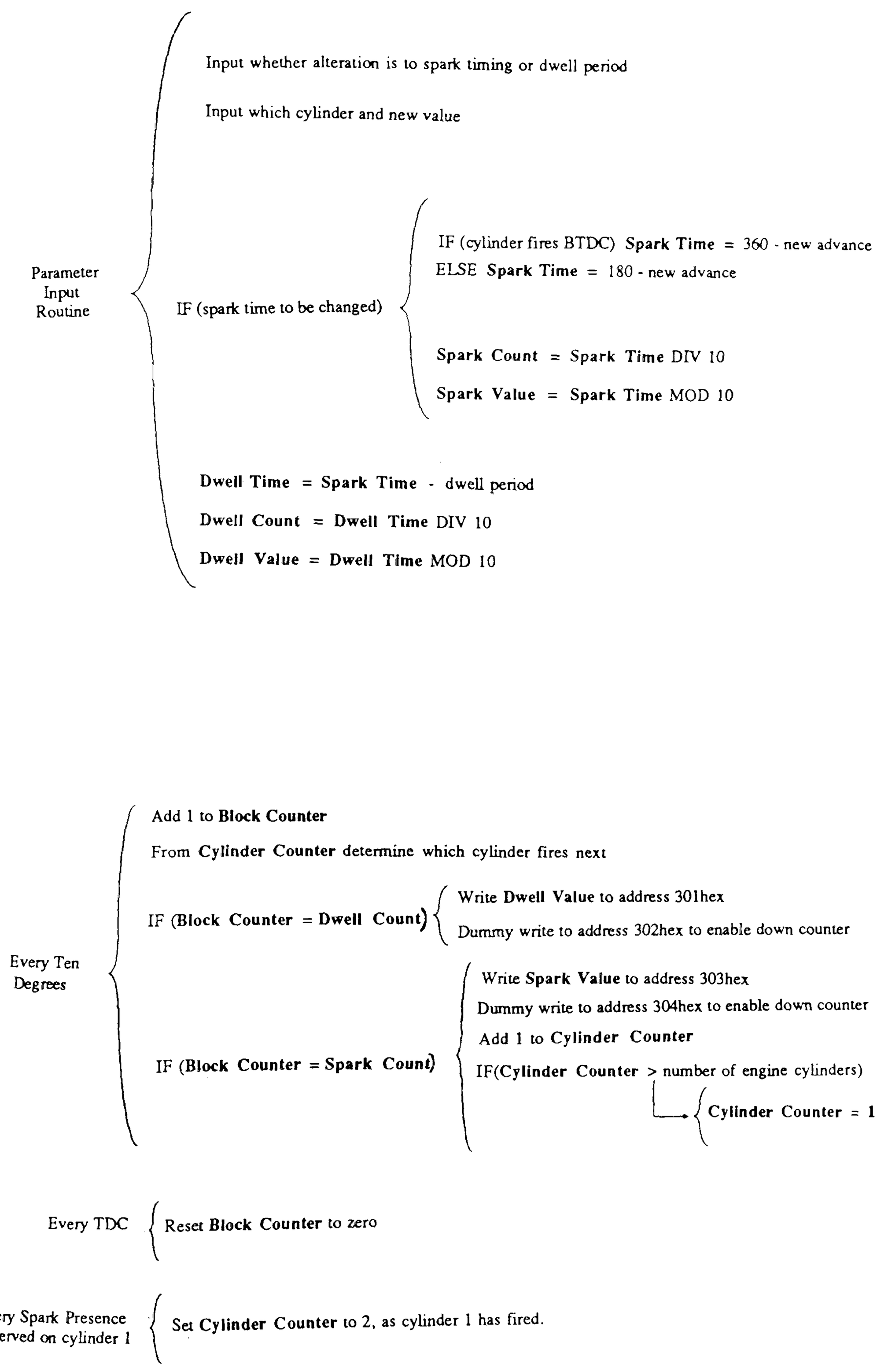

Fig 4.7 Warnier-Orr Diagrams to Enable Software Ignition Timing Control

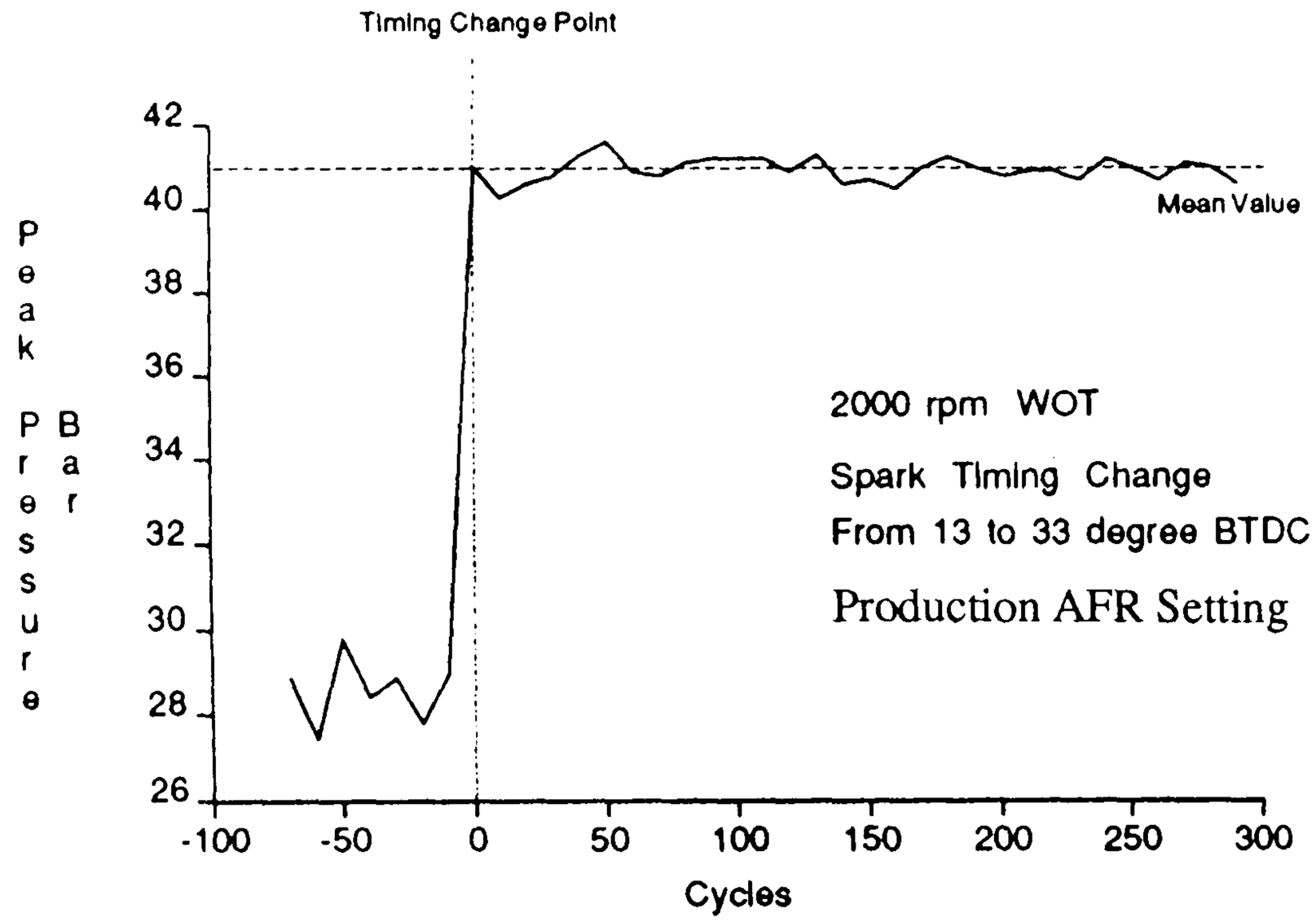

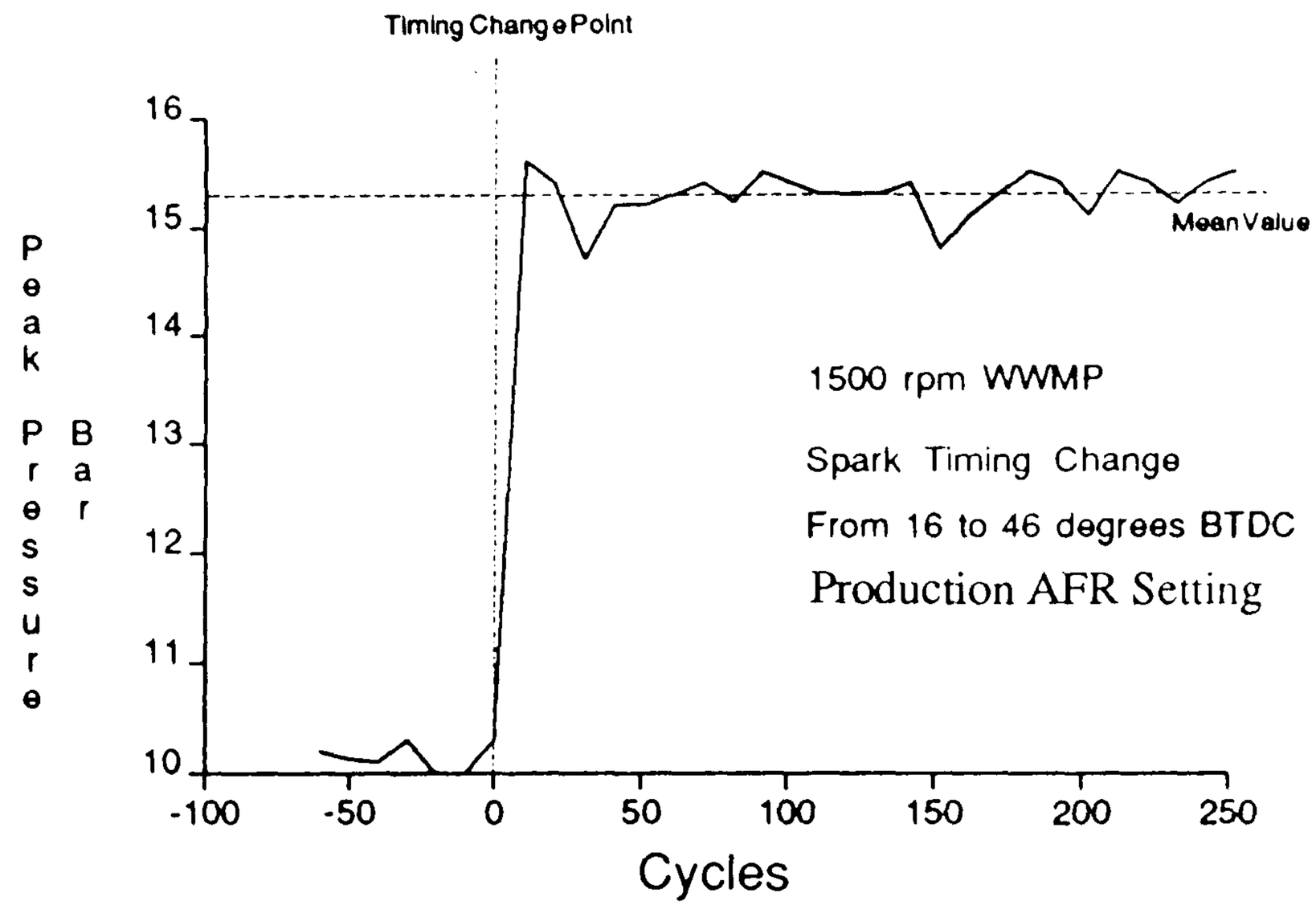

Fig 4.8 Variation of Peak Pressure, Averaged over Ten Cycles,
During a Step Change in Spark Timing

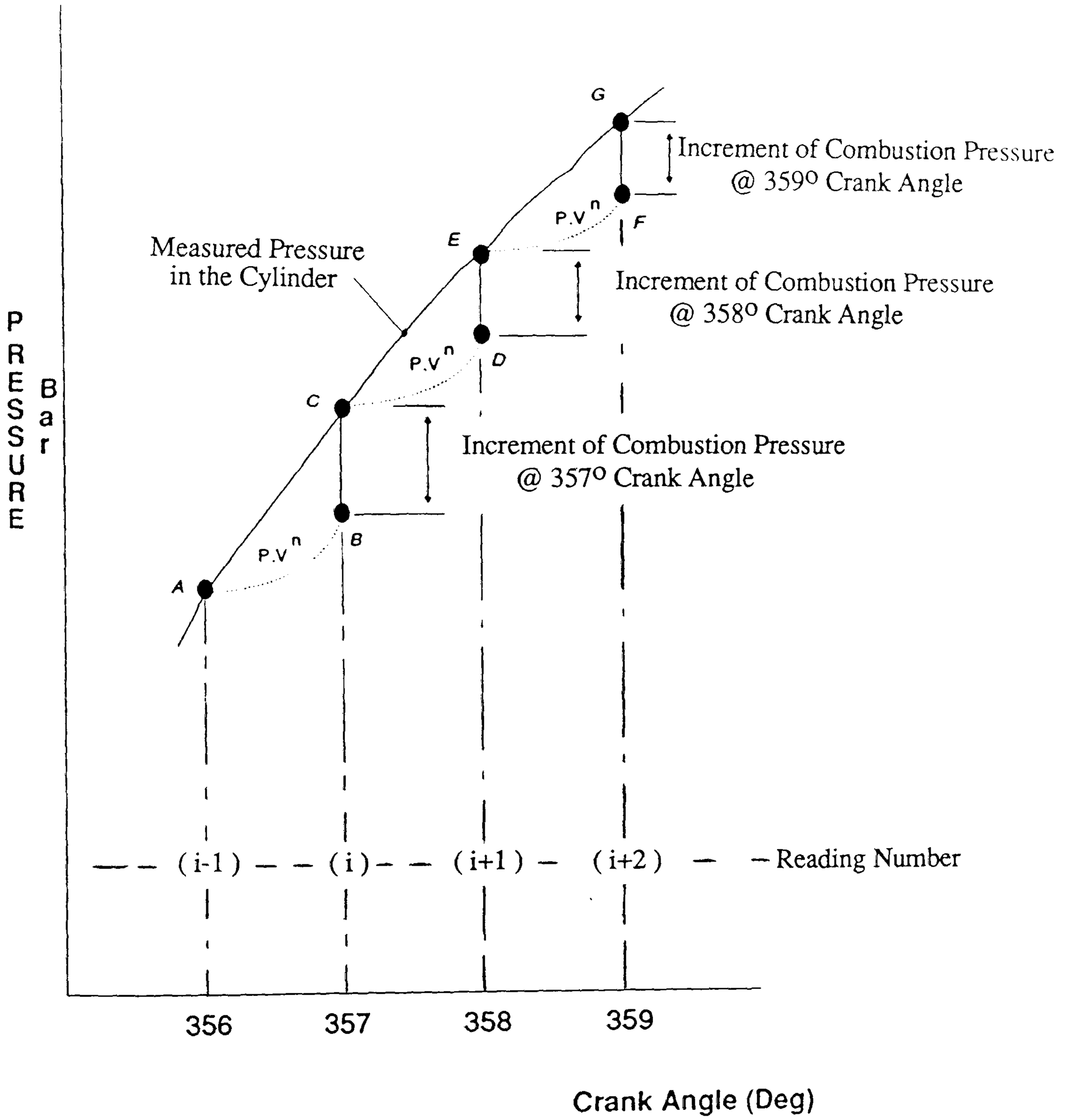

Fig 5.1 Determination of the Increments of Combustion Pressure From the Measured Pressure in the Cylinder

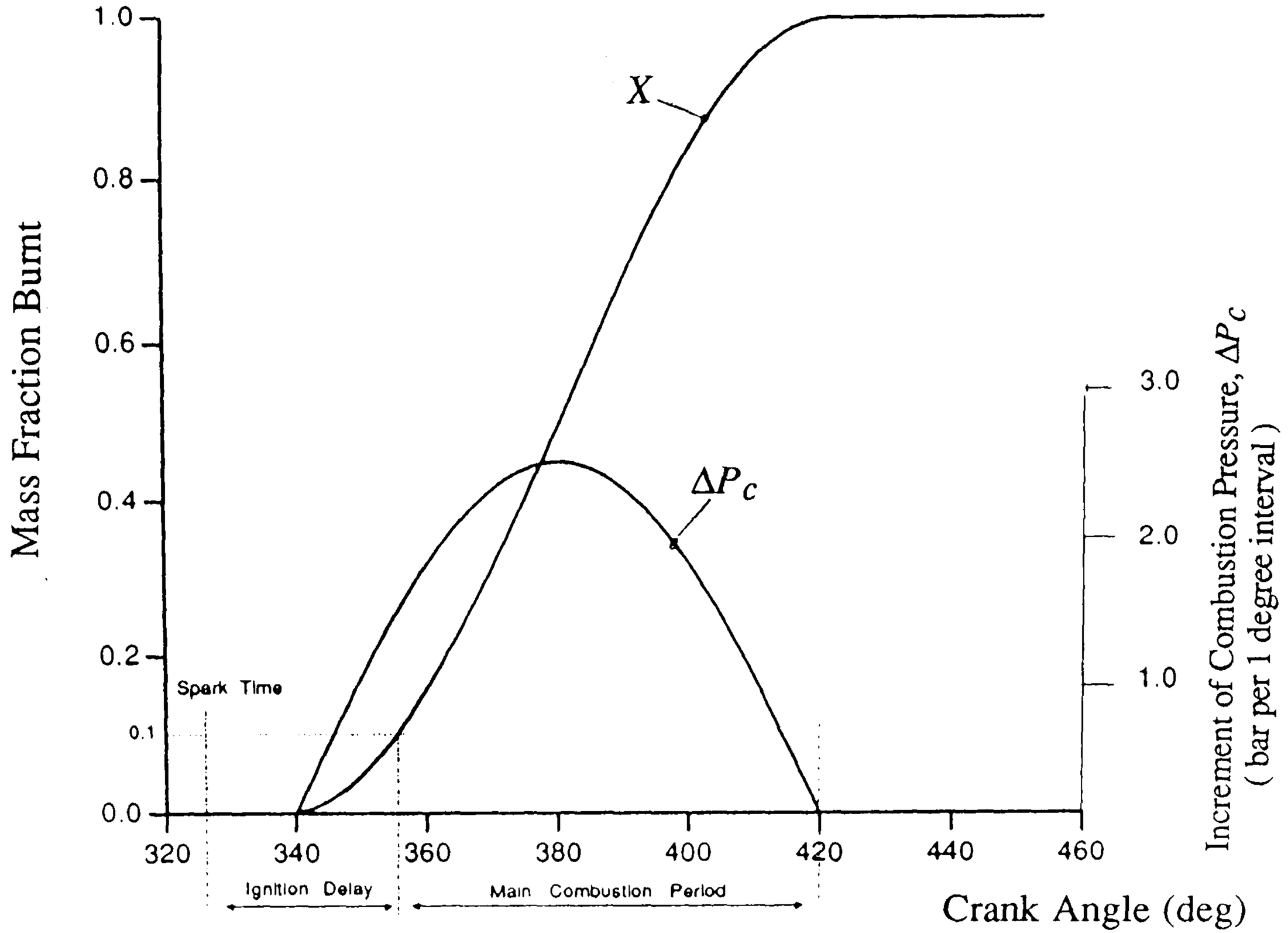

Fig 5.2 Idealised, Sinusoidal Variation of Combustion Pressure Increments and Derived Mass Fraction Burnt

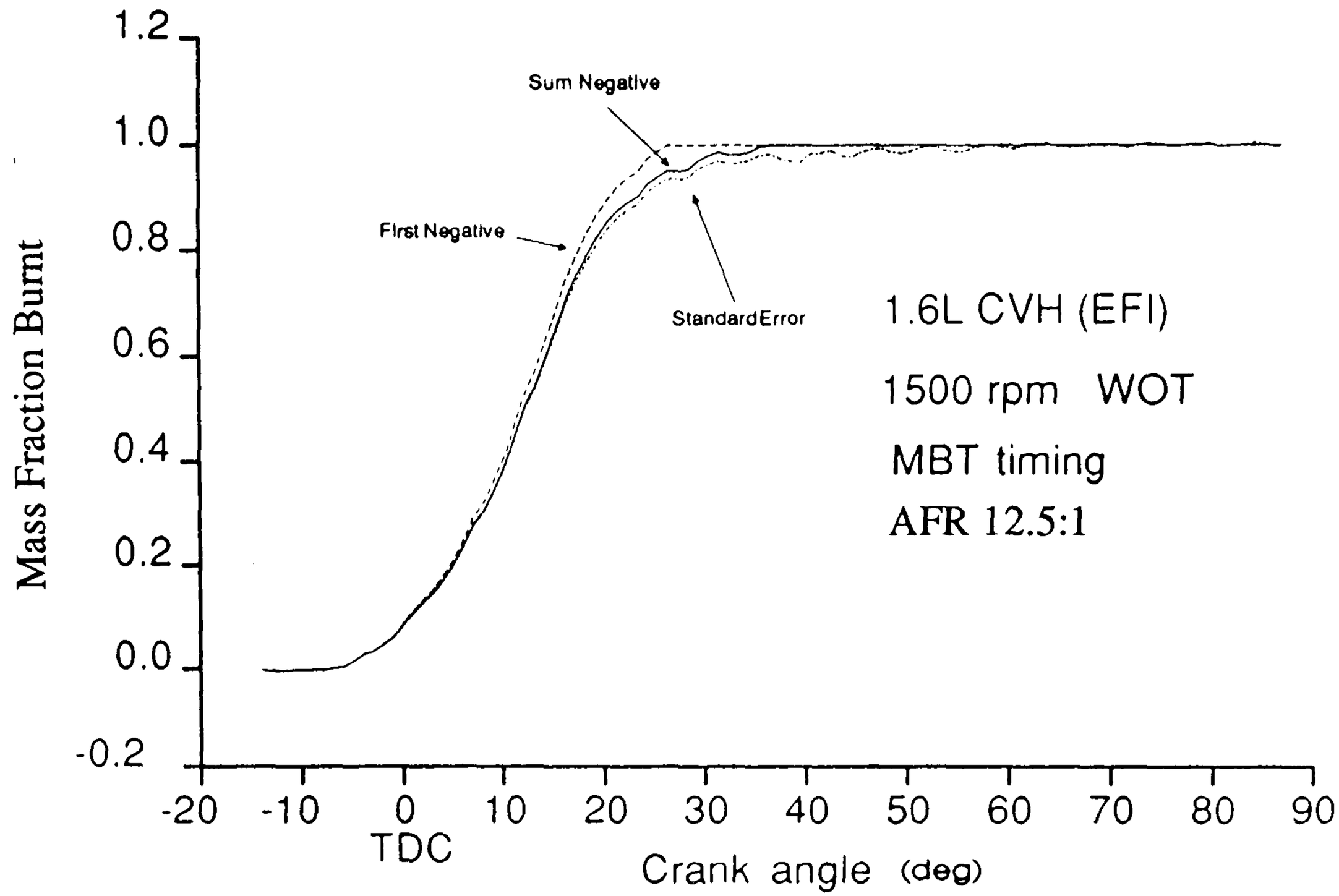

Fig 5.3 Mass Fraction Burnt Calculated from Same Cycle using Different Methods of Determining EOC

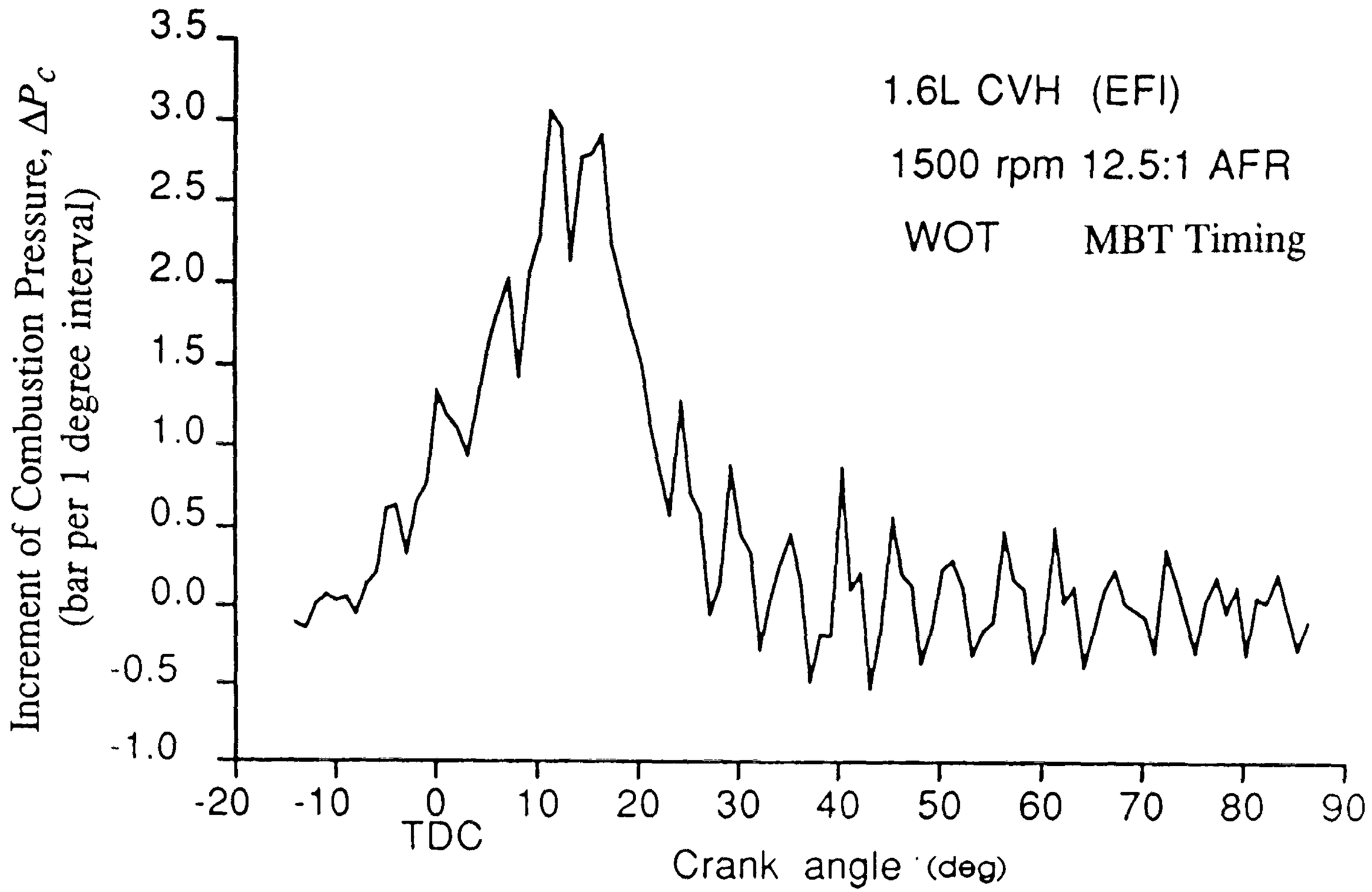

Fig 5.4 Marked Noise Pickup on the Increments of Combustion Pressure Calculated from Readings 1 Crank Angle Degree Apart

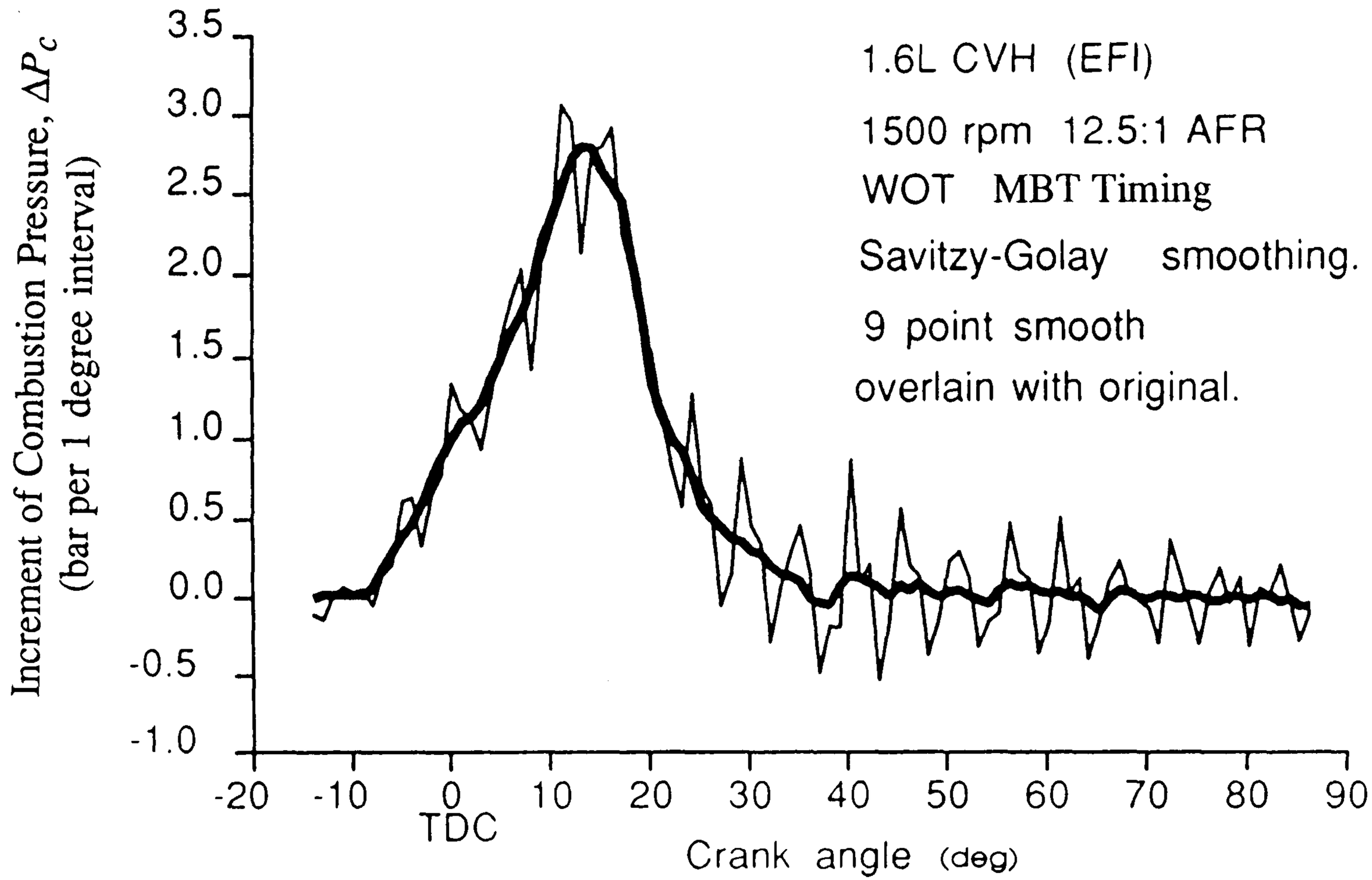

Fig 5.5 Effect of Smoothing on the Combustion Pressure Increments

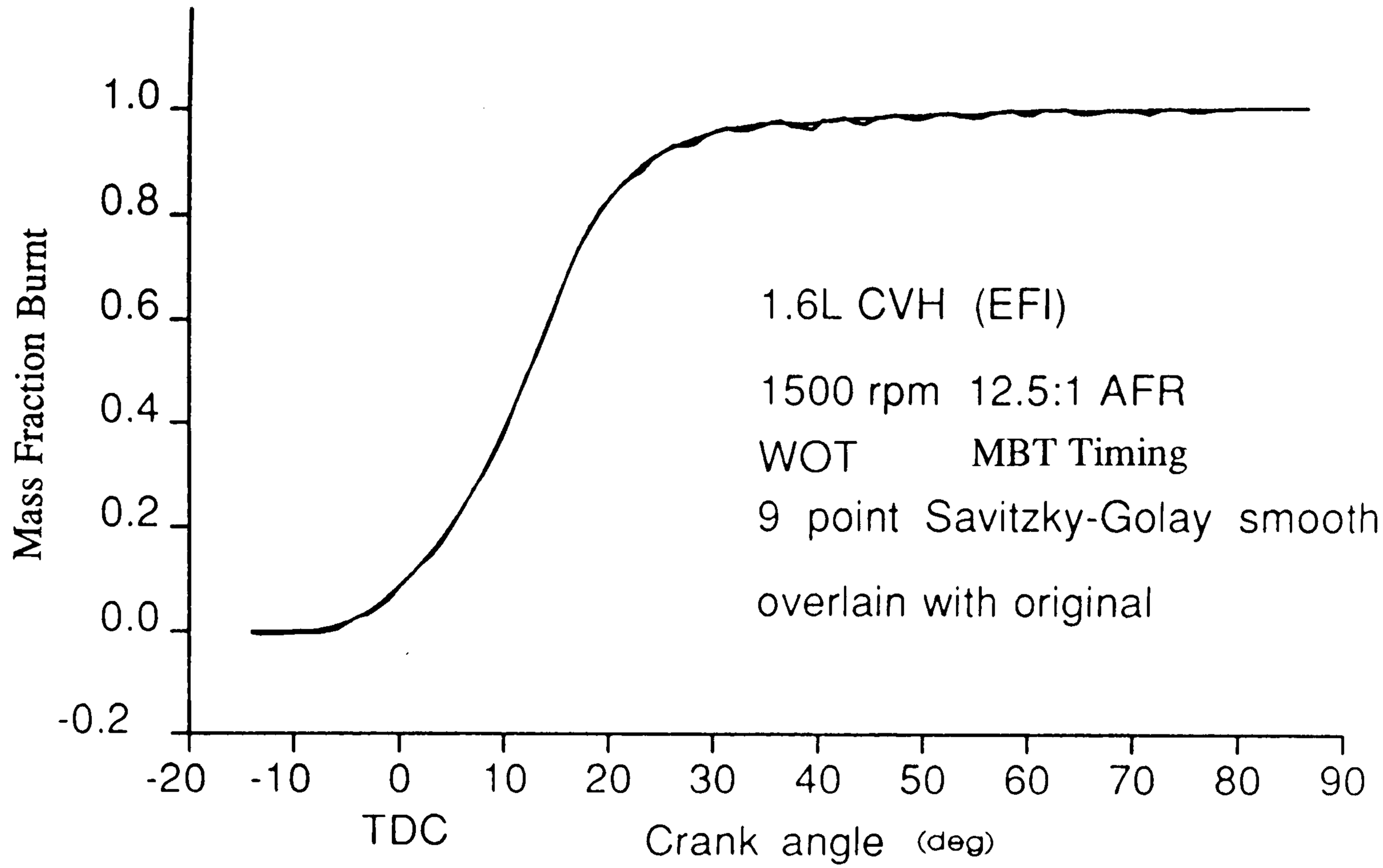

Fig 5.6 Comparison of Mass Fraction Burnt Predictions from Raw and Smoothed Combustion Pressures

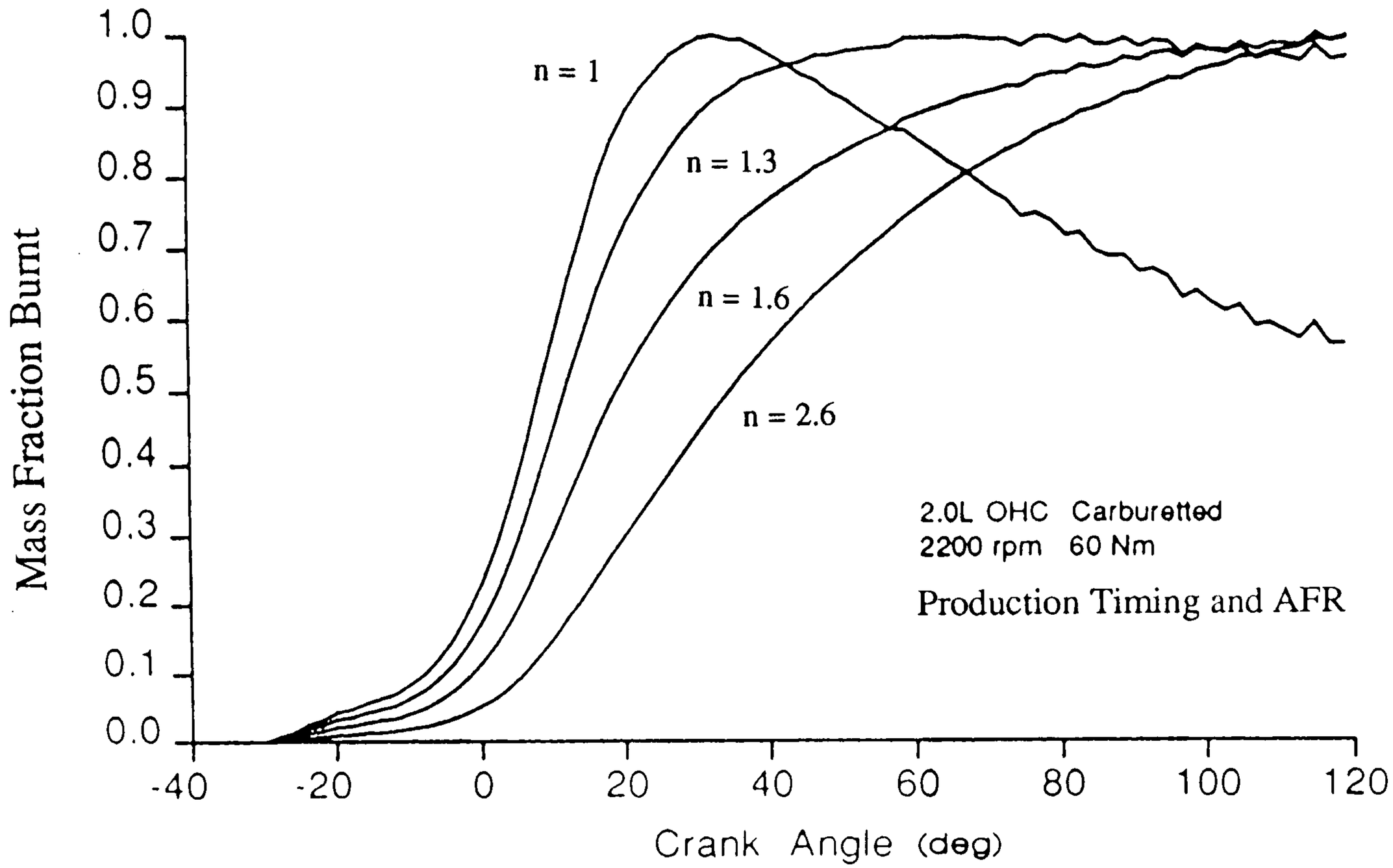

Fig 5.7 Mass Fraction Burnt Dependency on Polytropic Index

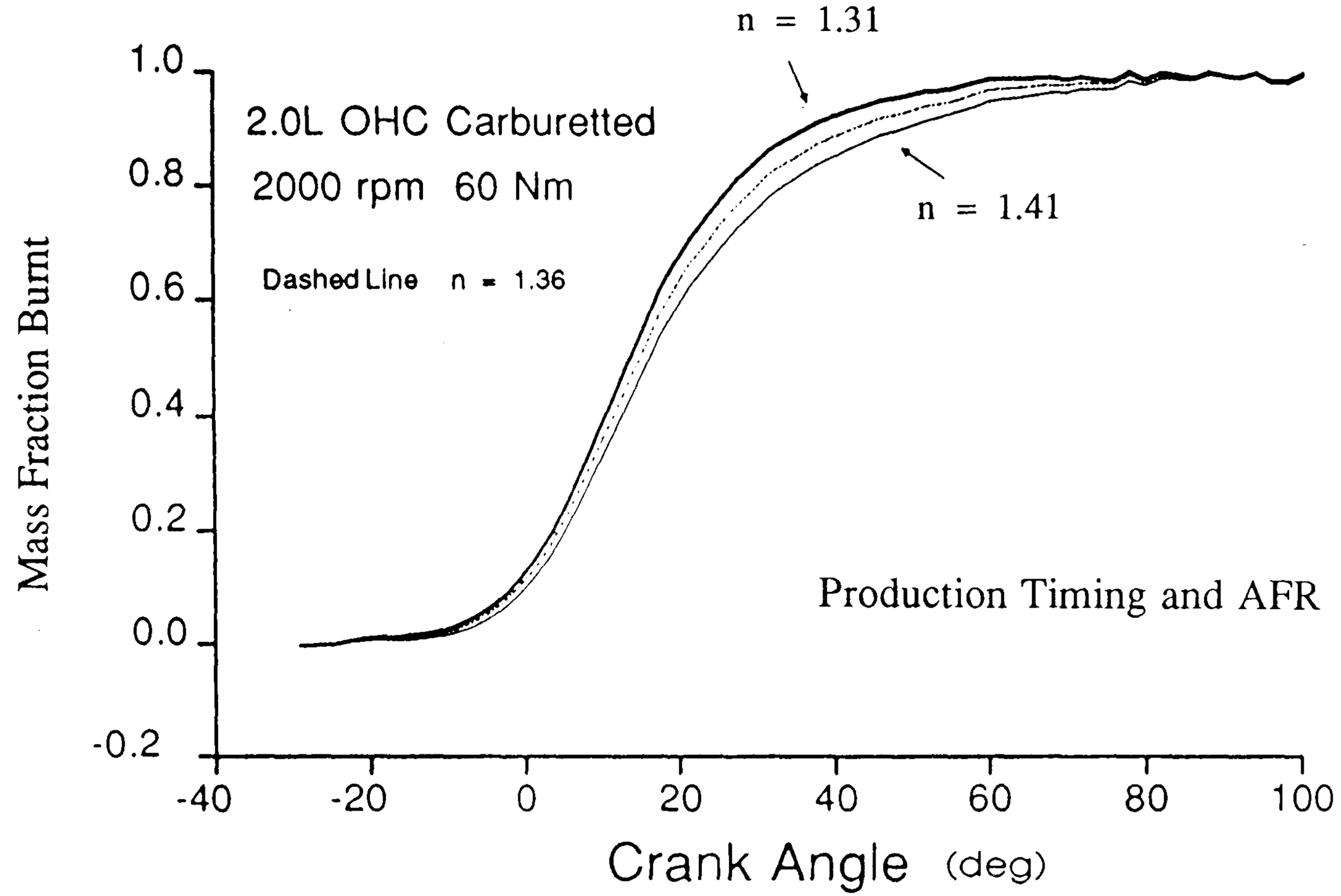

Fig 5.8 Mass Fraction Burnt Dependency on Polytropic Index - Smaller Range of Values

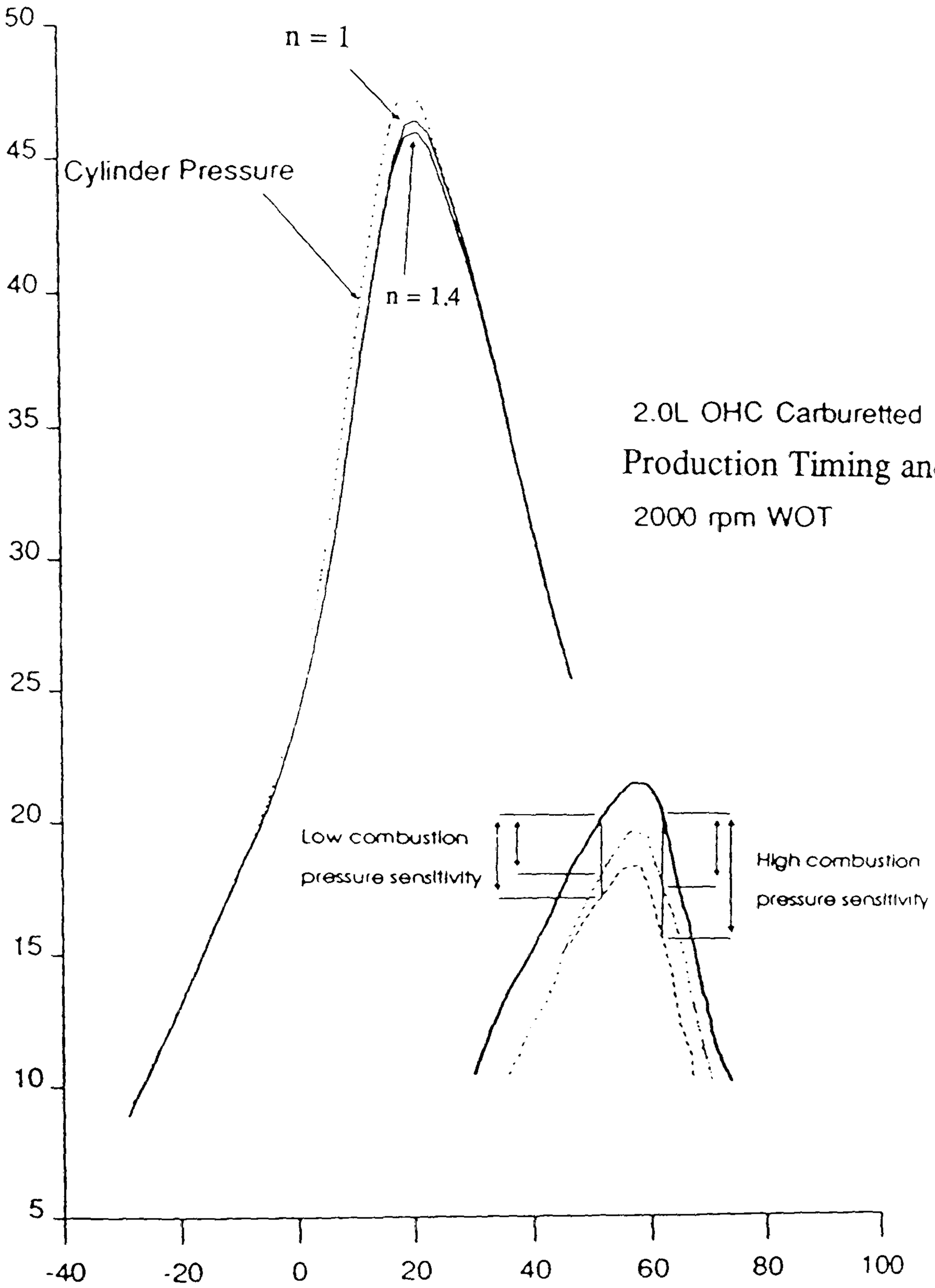

Fig 5.9 Effect of Expansion Index on the Computed Pressure due to Piston Motion

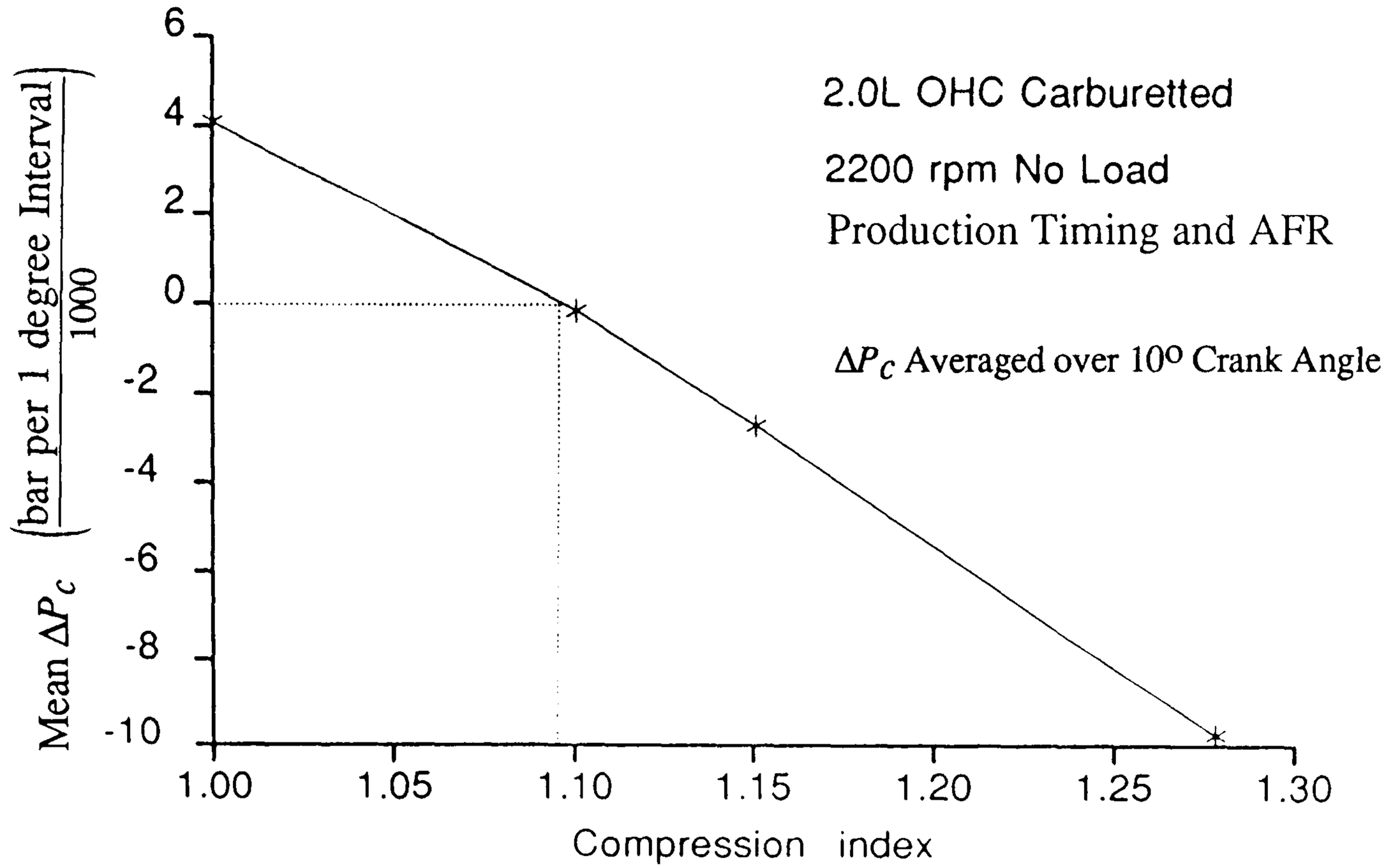

Fig 5.10 Relationship Between Compression Index and Mean Increment of Combustion Pressure before Spark Time

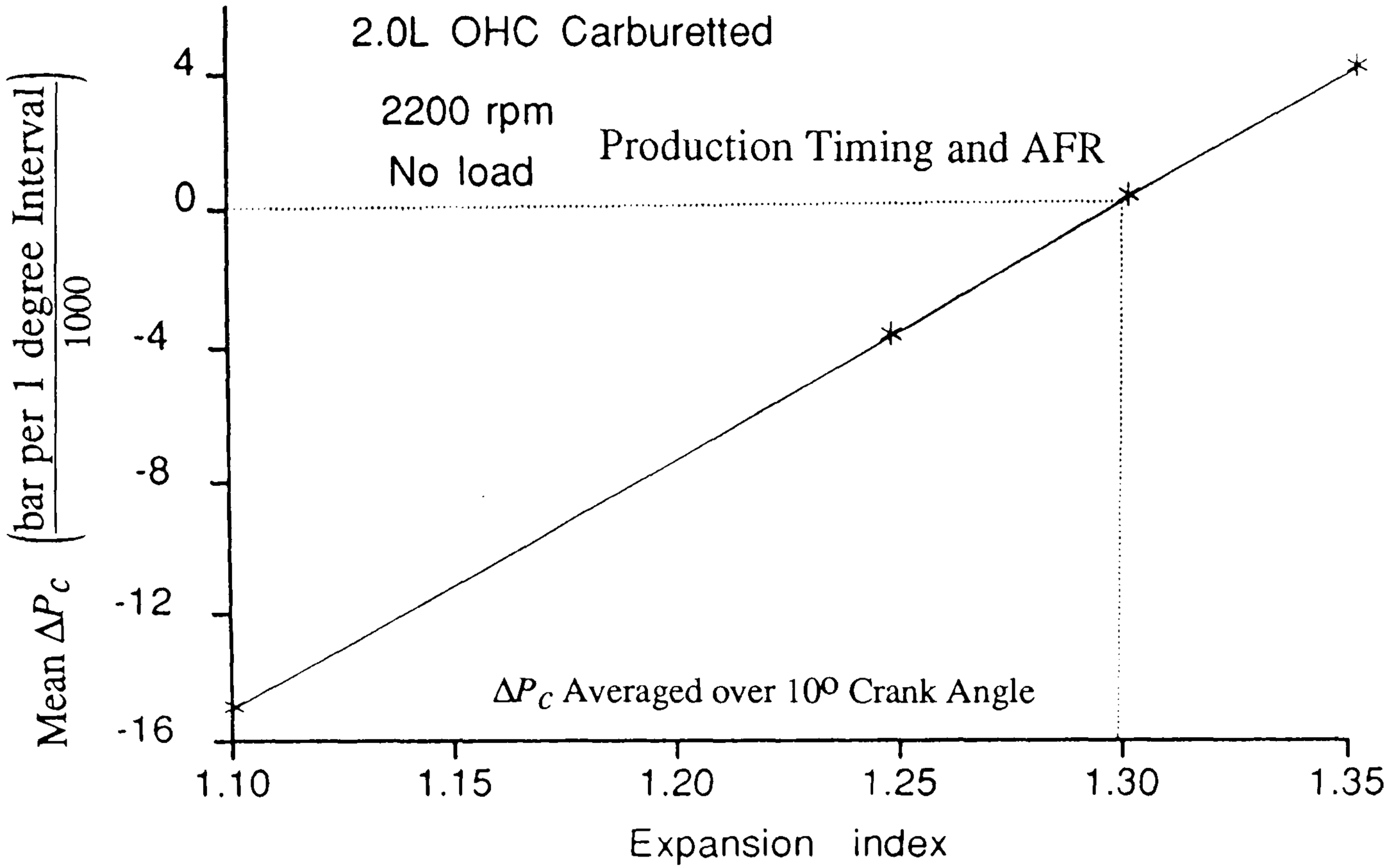

Fig 5.11 Relationship Between Expansion Index and Mean Increment of Combustion Pressure after EOC

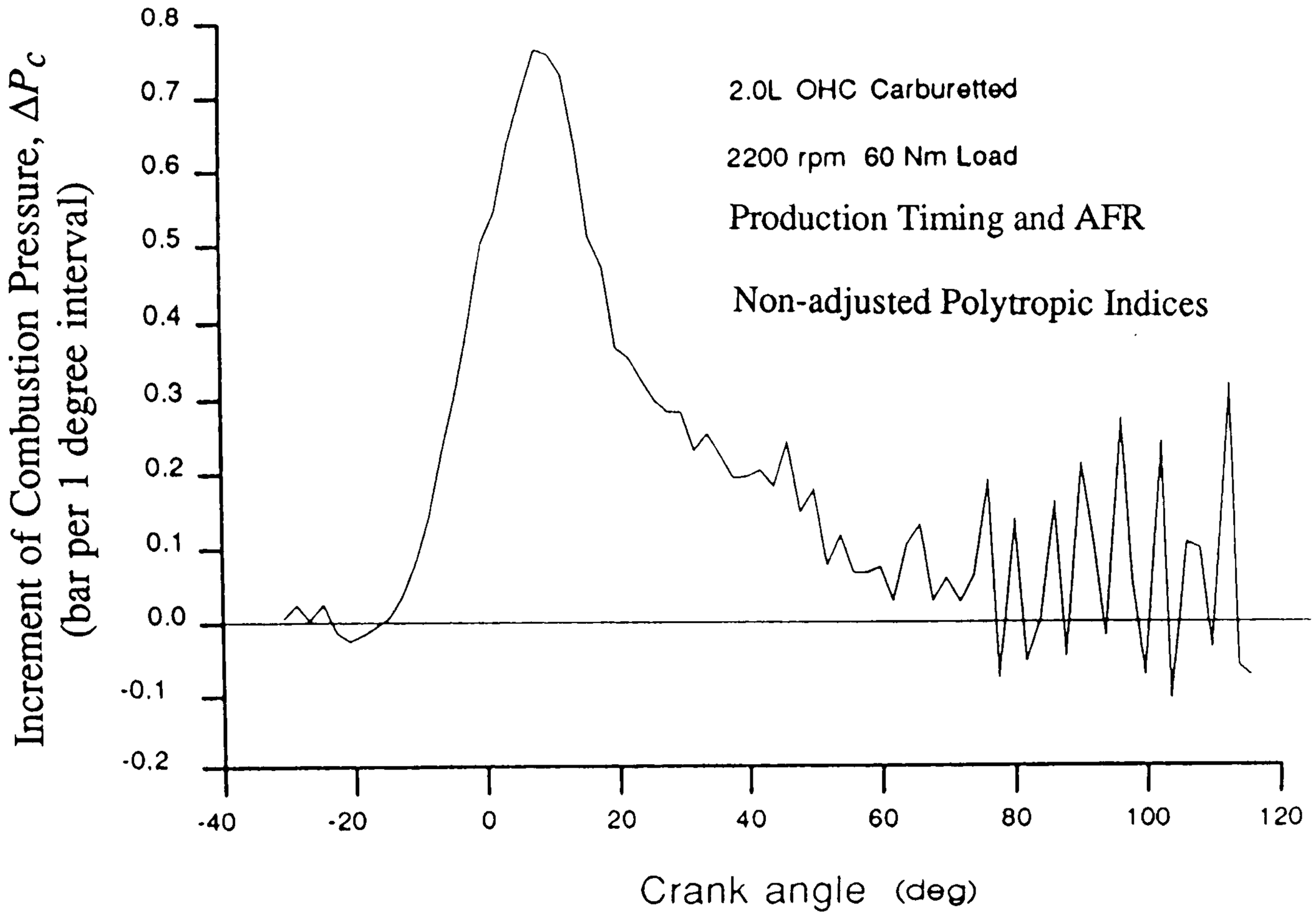

Fig 5.12 Increments of Combustion Pressure Calculated by Non-Adjusted Indices

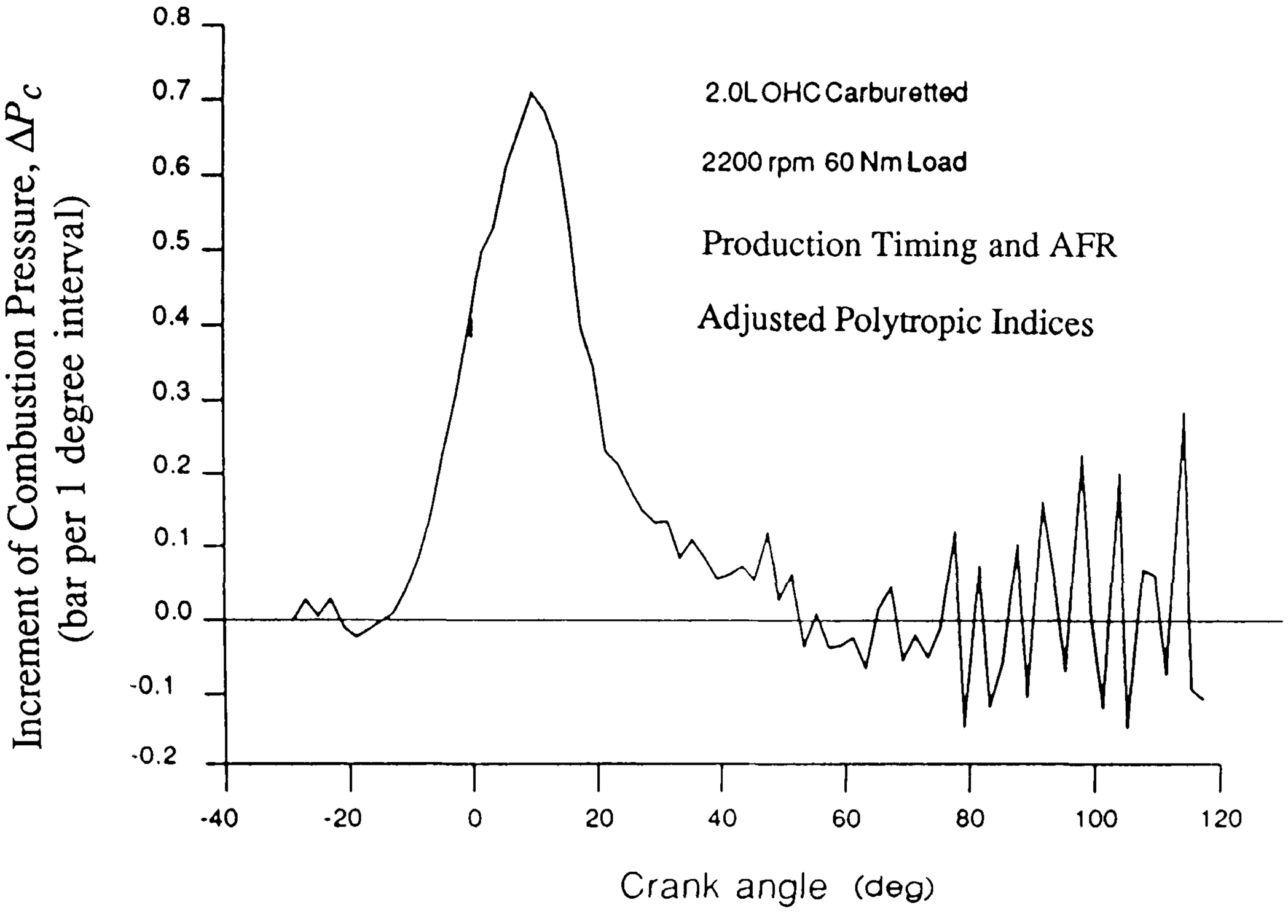

Fig 5.13 Increments of Combustion Pressure Calculated by Adjusted Indices

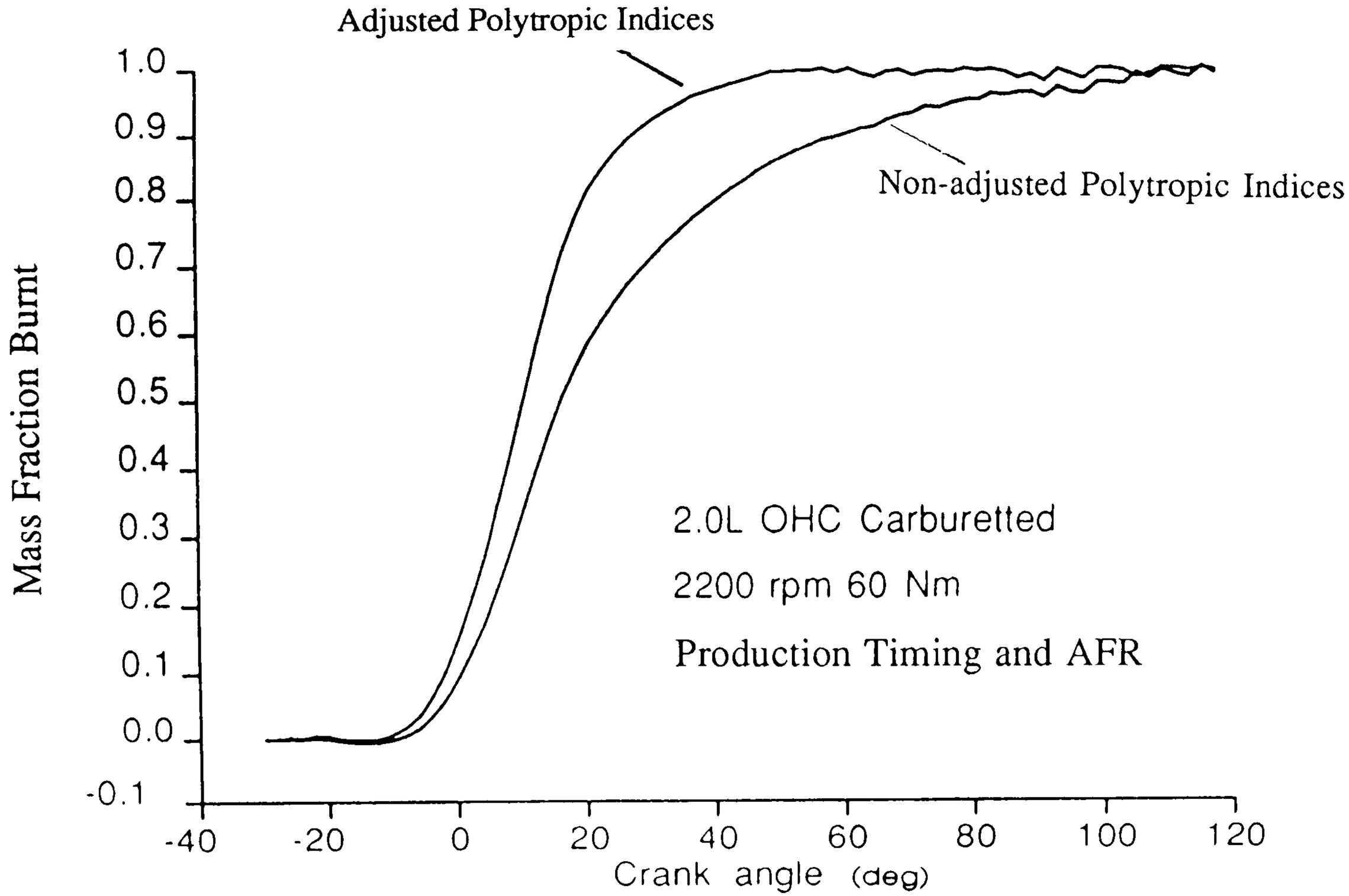

Fig 5.14 Comparison of Mass Fraction Burnt Derived from Adjusted and Non-Adjusted Indices

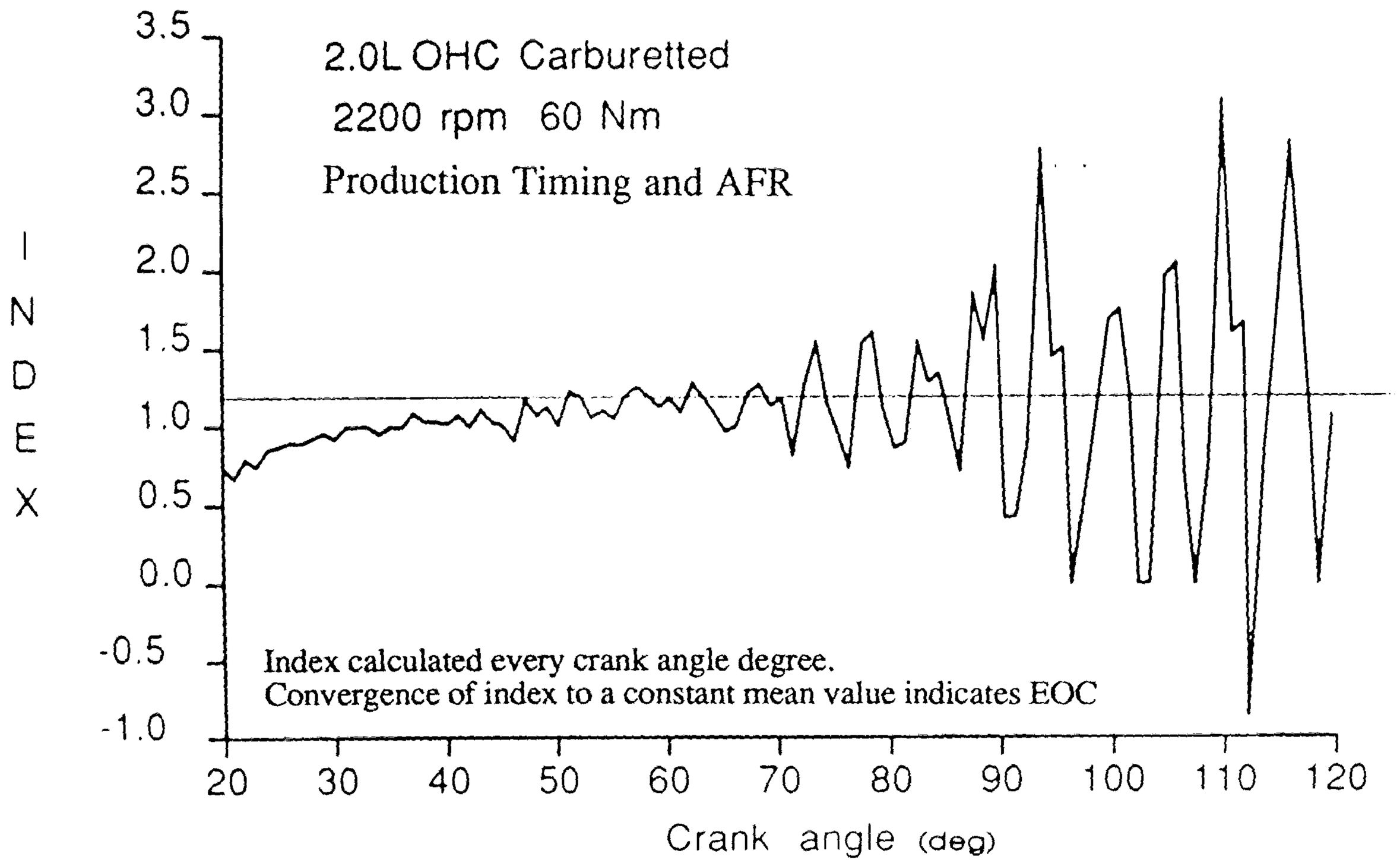

Fig 5.15 Variation of the Instantaneous Polytropic Index Corresponding to the Engine Cycle of Figures 5.12-5.14

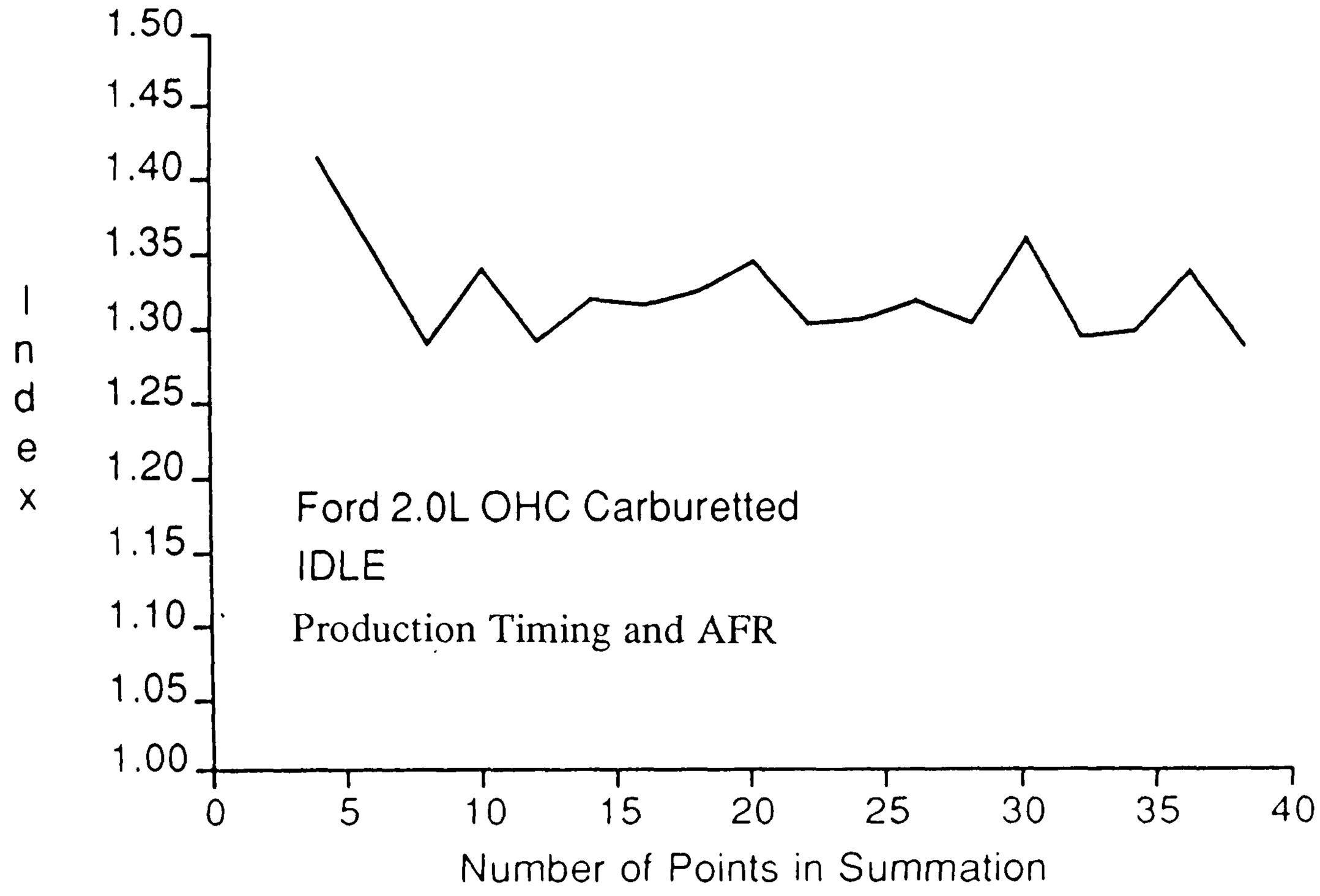

Fig 5.16 Variation of Adjusted Polytropic Index As the Number of Points in the Averaging Process are Increased

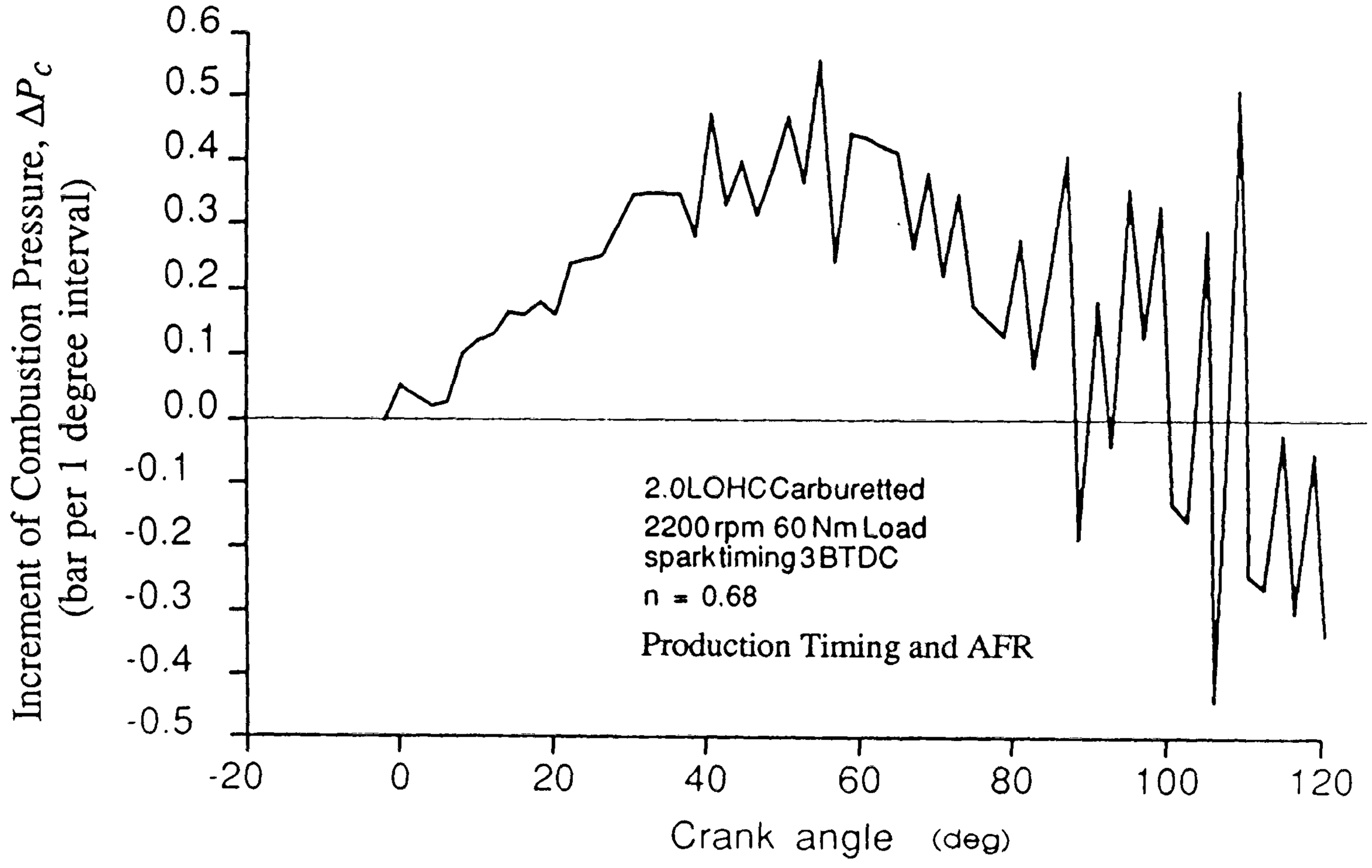

Fig 5.17 Increments of Combustion Pressure for a Late Burn using Adjusted Polytropic Indices

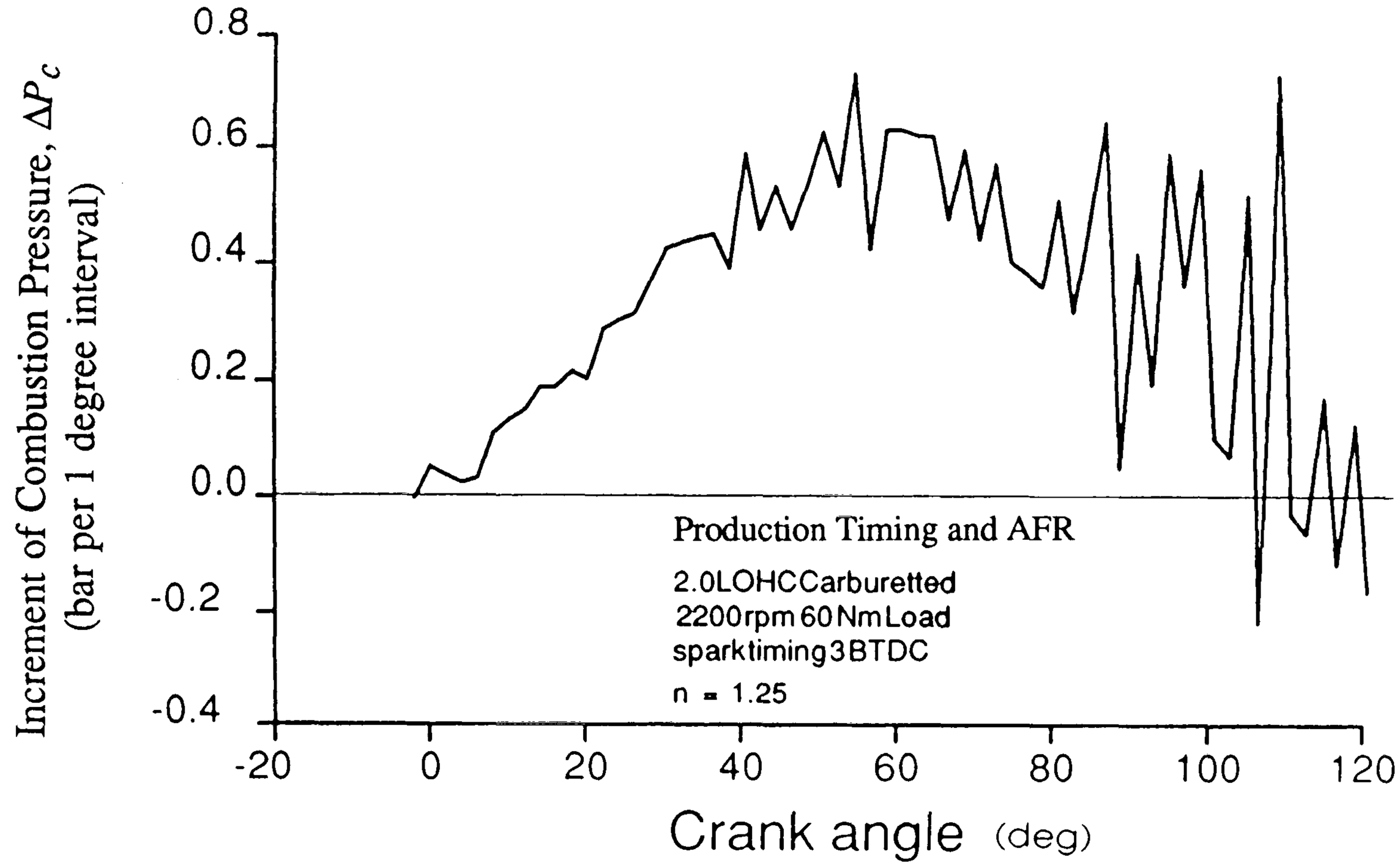

Fig 5.18 Increments of Combustion Pressure for a Late Burn using an Expansion Index of 1.25

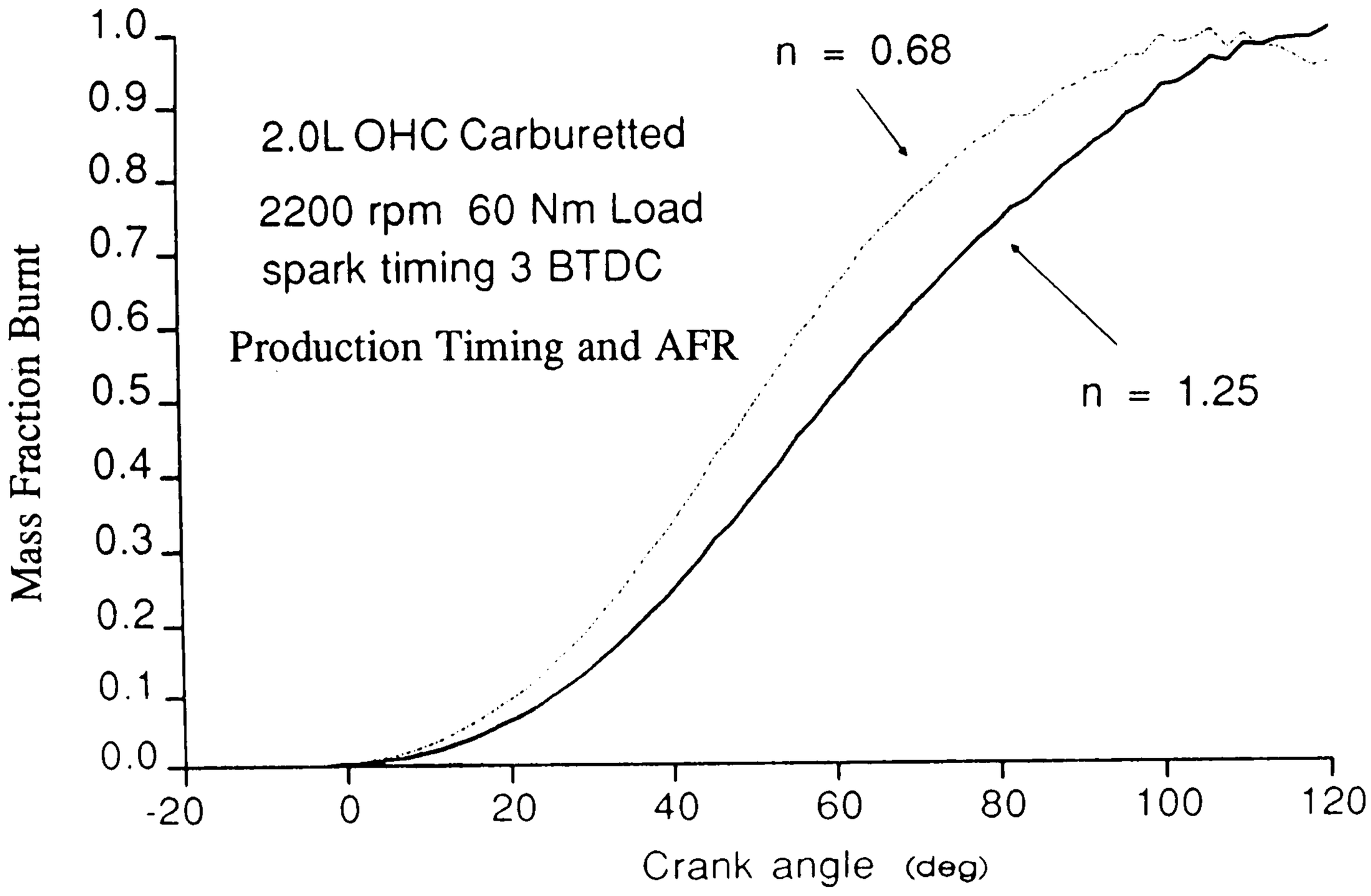

Fig 5.19 Mass Fraction Burnt for a Late Burn with Adjusted (n=0.68) and Reset (n=1.25) Indices

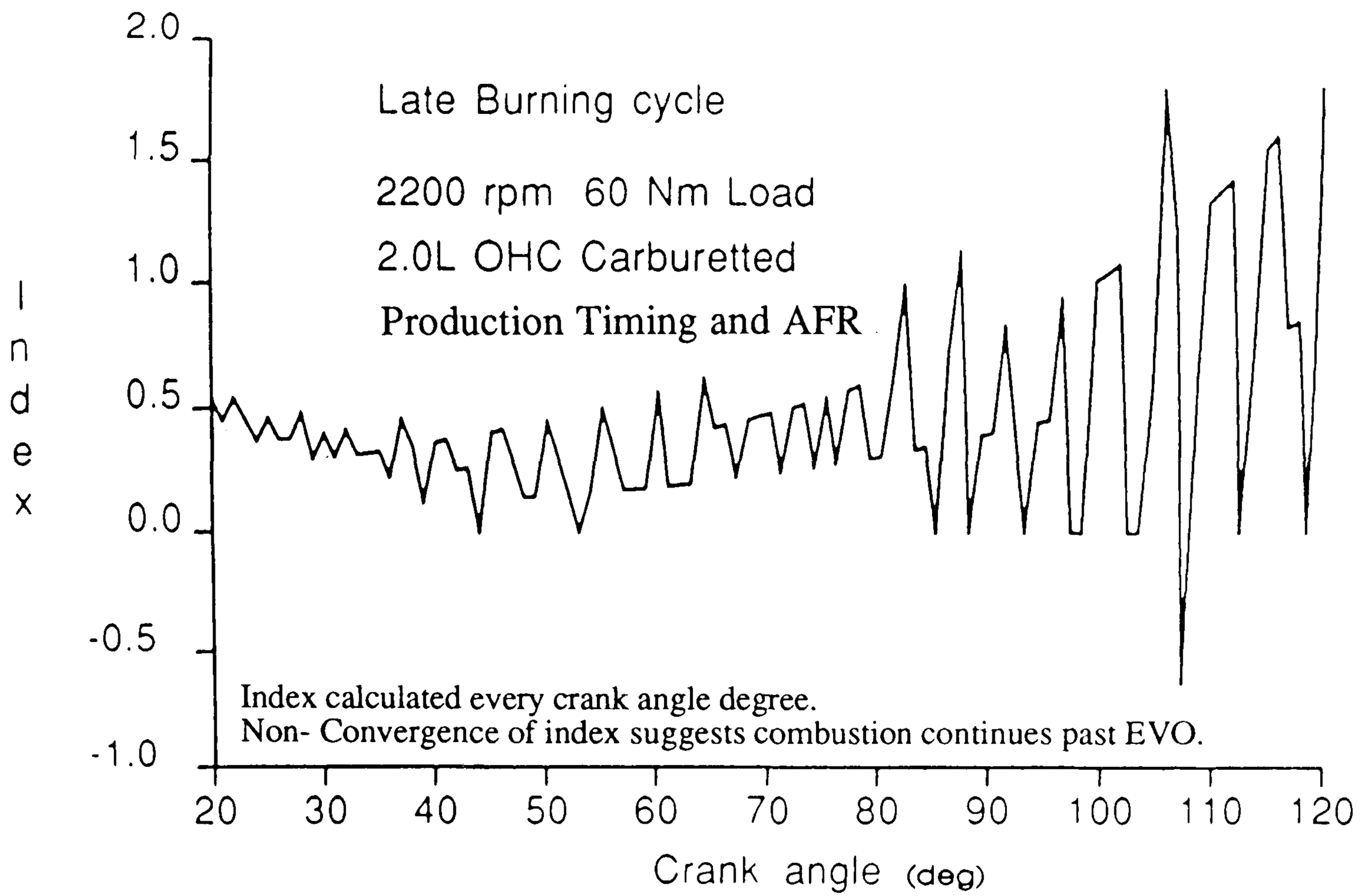

Fig 5.20 Instantaneous Polytropic Index for Late Burning Cycle

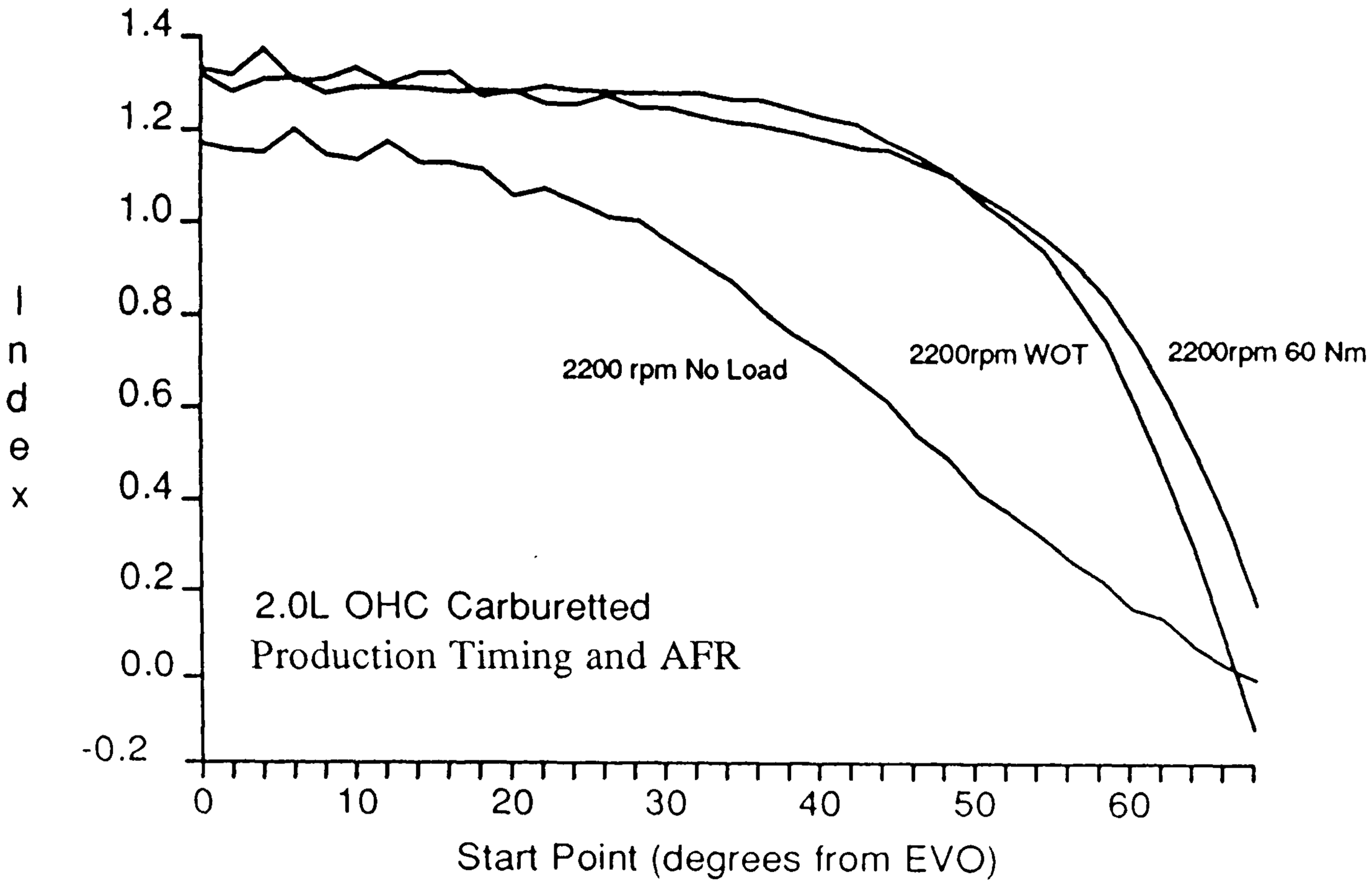

Fig 5.21 Variation of Adjusted Index As the Evaluation Point Moves Closer to TDC

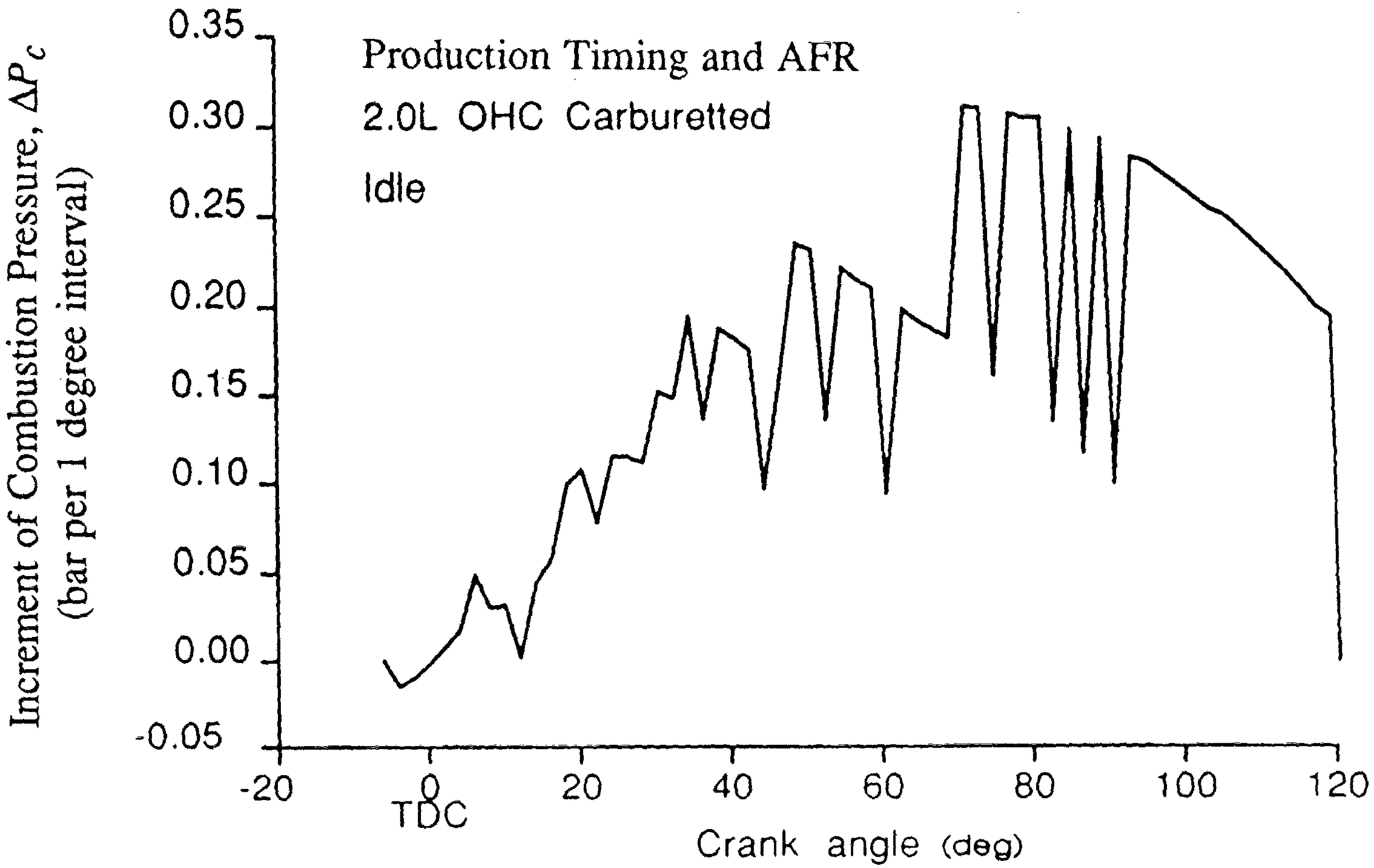

Fig 5.22 Typical Increments of Combustion Pressure at IDLE

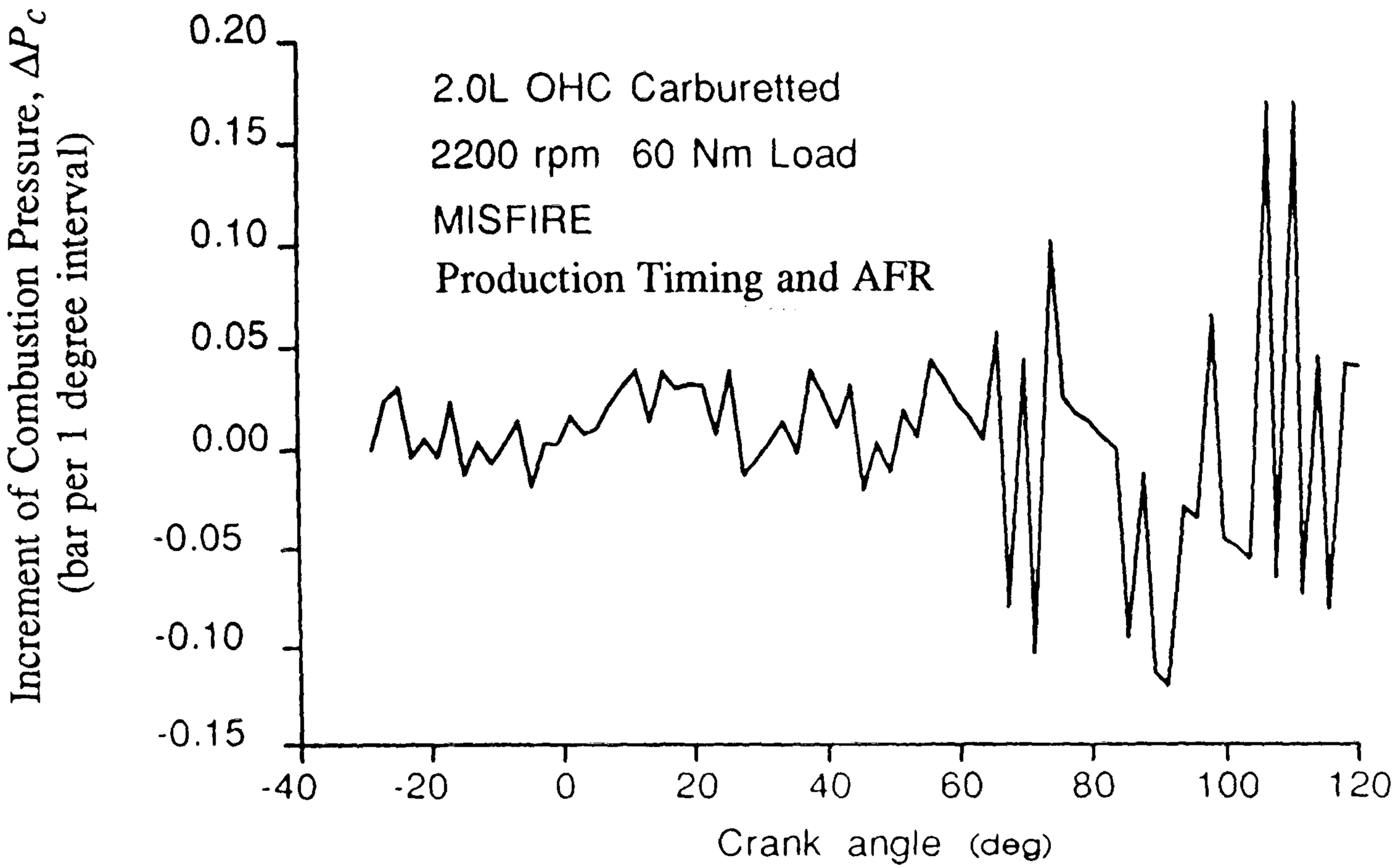

Fig 5.23 Typical Increments of Combustion Pressure for a Misfire

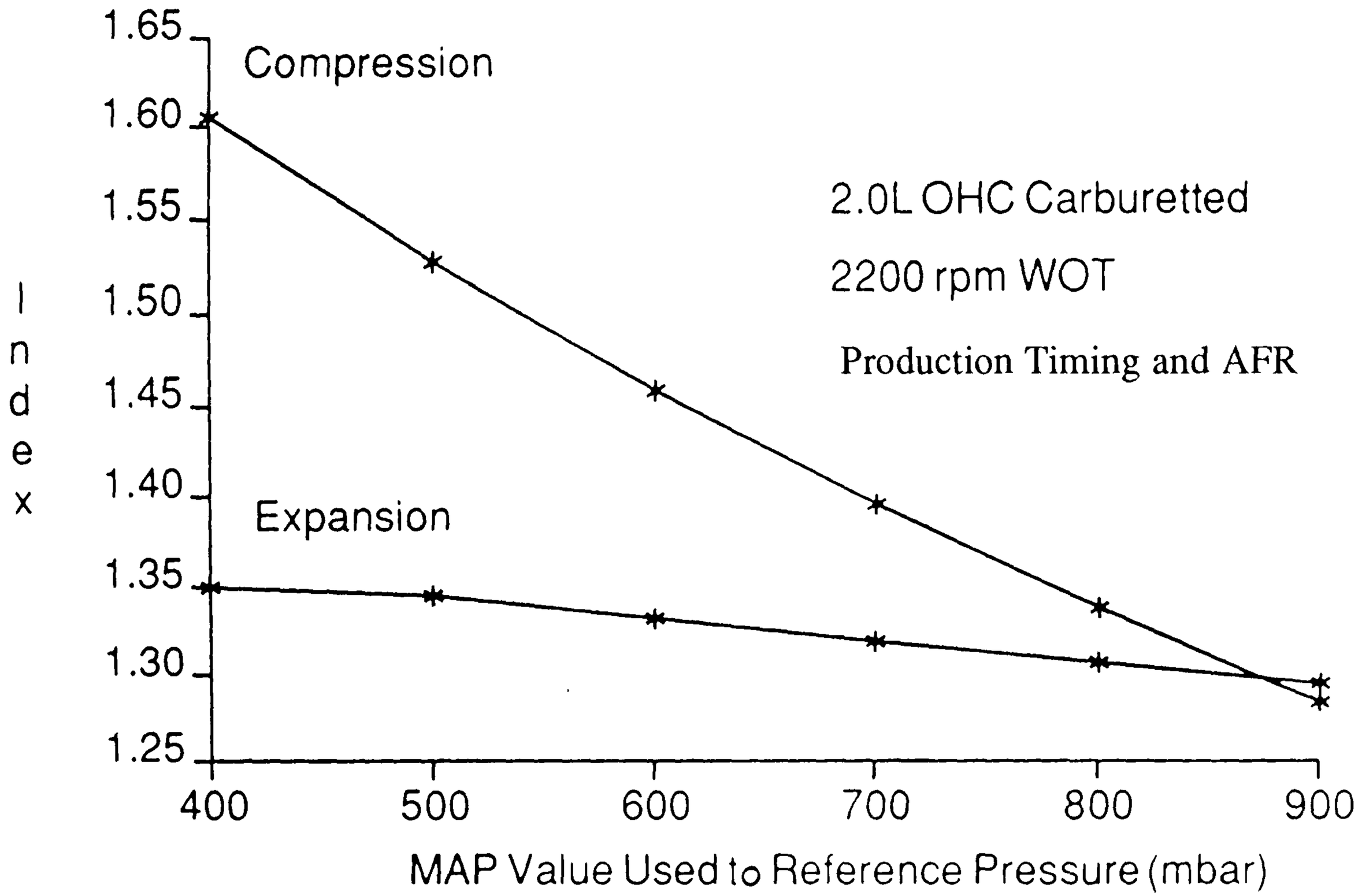

Fig 6.1 Polytropic Index Dependency on Reference Pressure

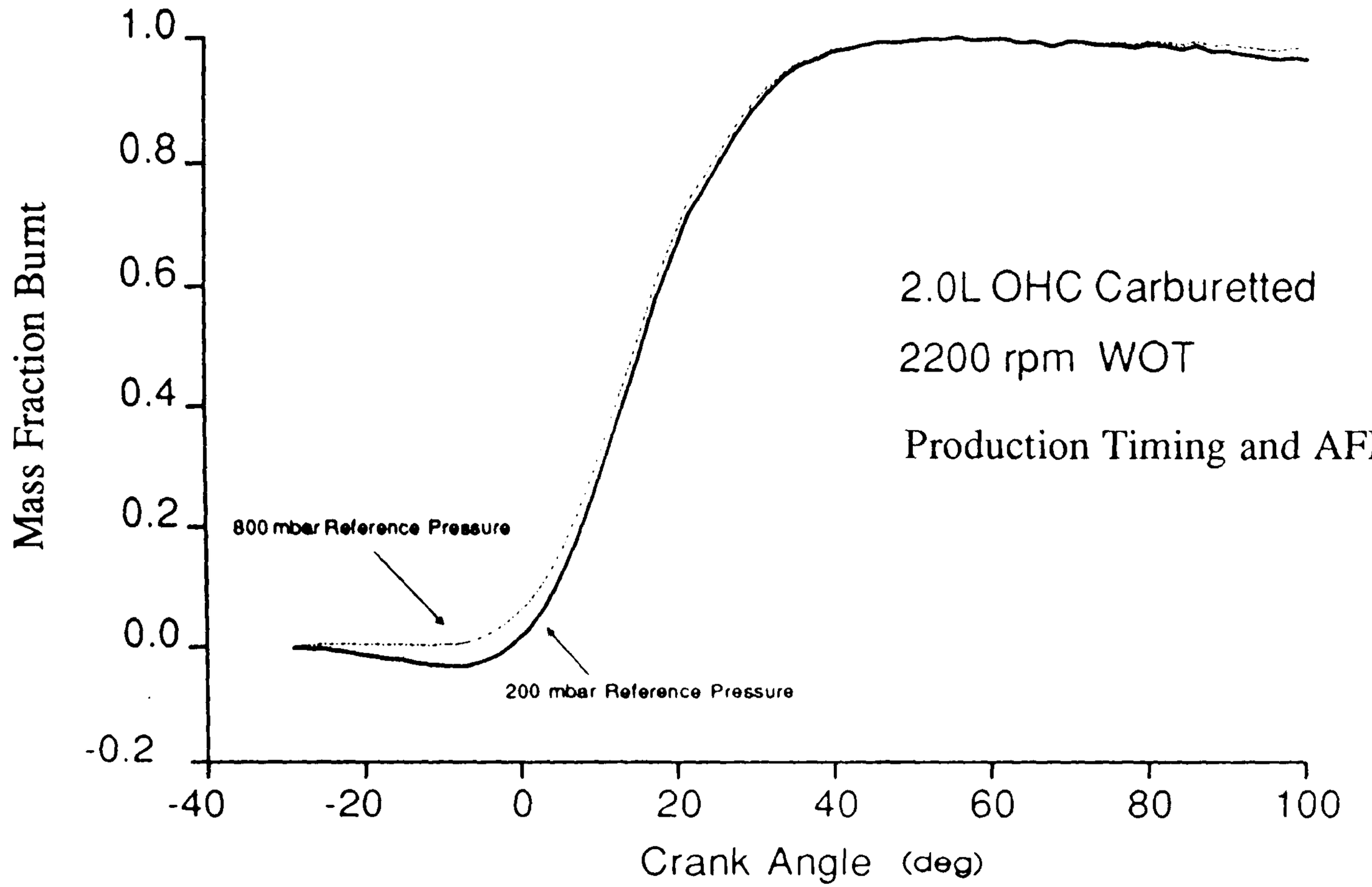

Fig 6.2 Mass Fraction Burnt Dependency on Reference Pressure

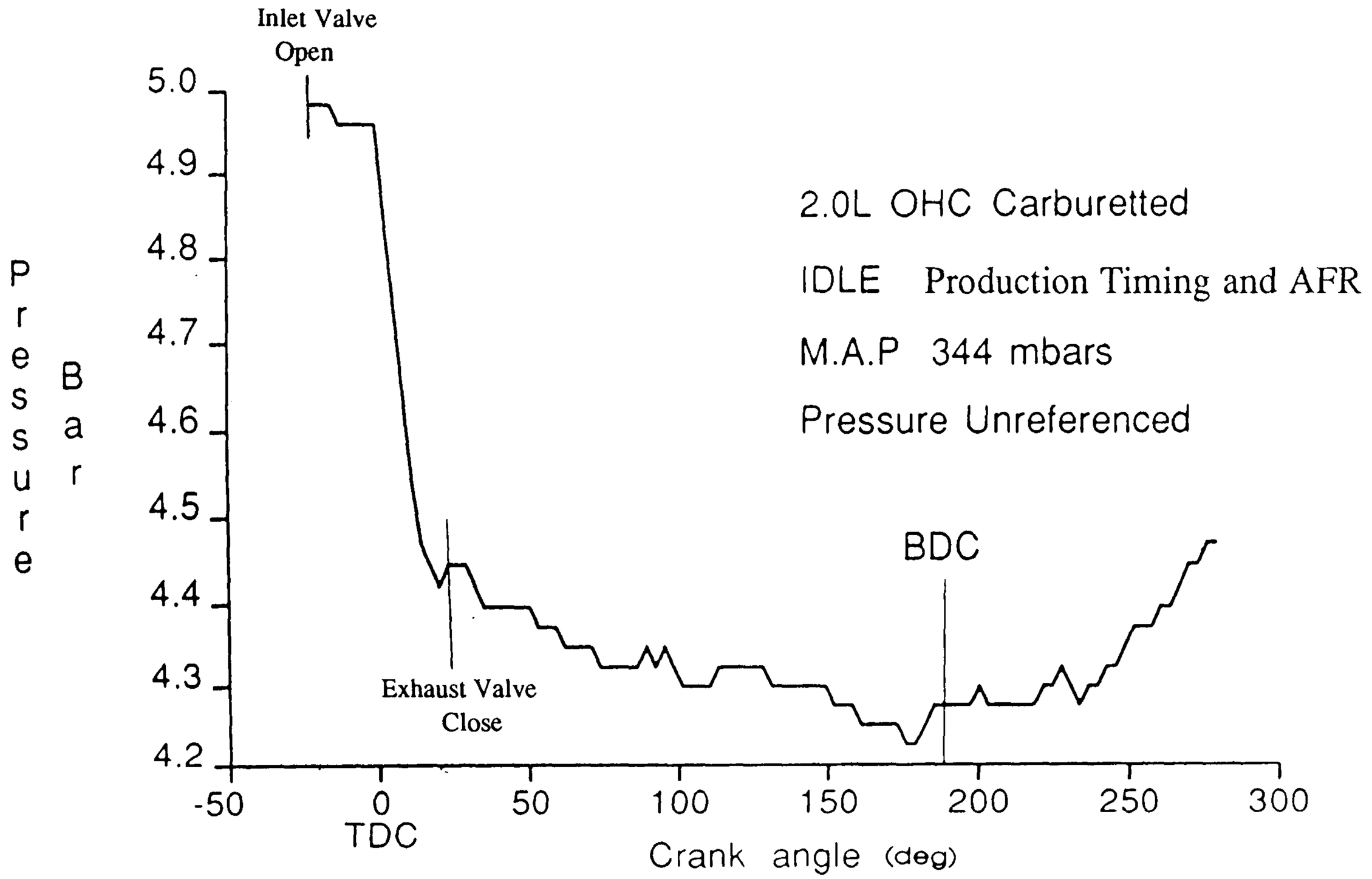

Fig 6.3 Raw Measured Pressure Variation during Intake Stroke

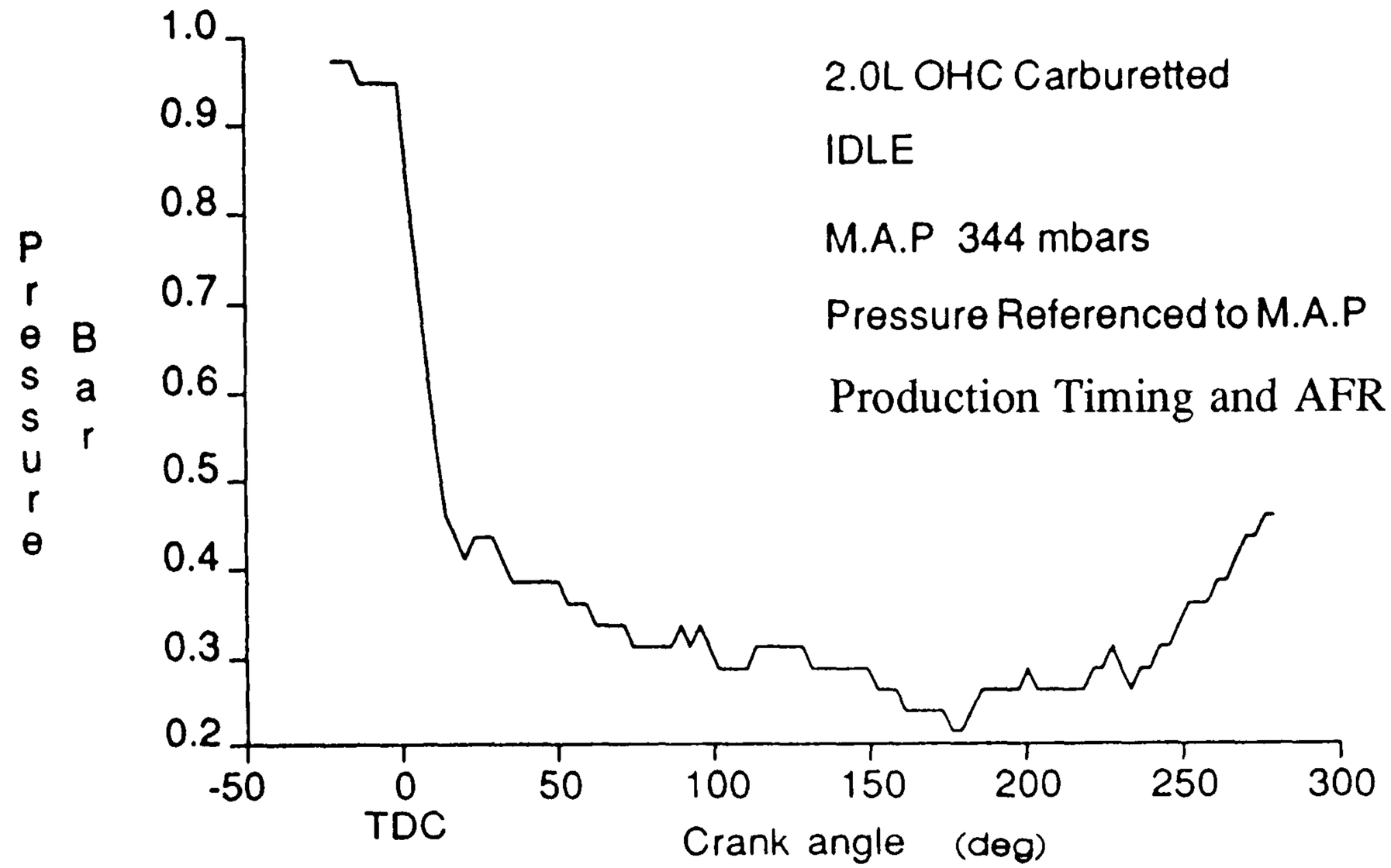

Fig 6.4 Referenced Pressure Variation during Intake Stroke

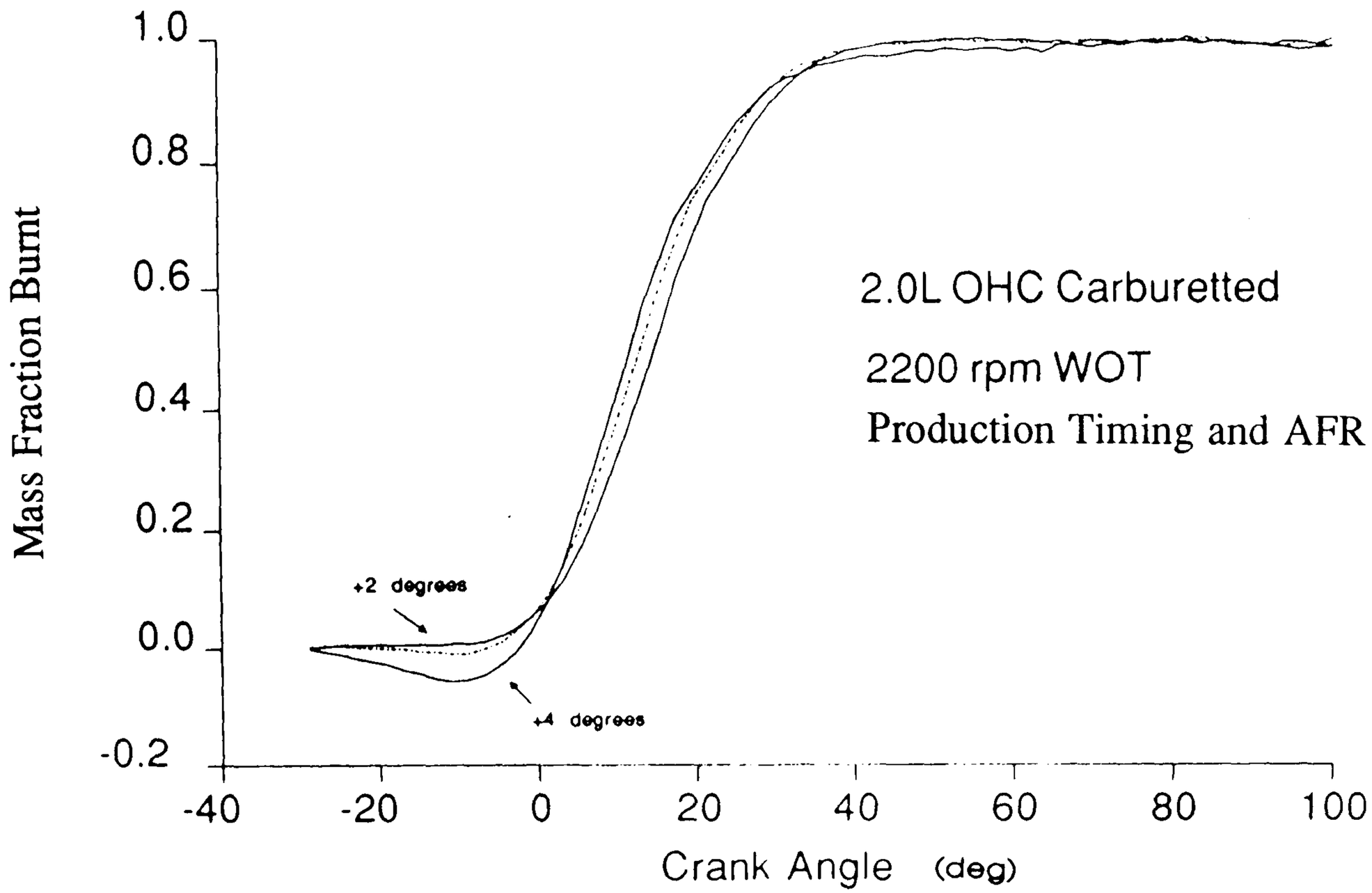

Fig 6.5 The Effect of Pressure-Volume Alignment Errors on Mass Fraction Burnt. Central Curve is Correctly Aligned

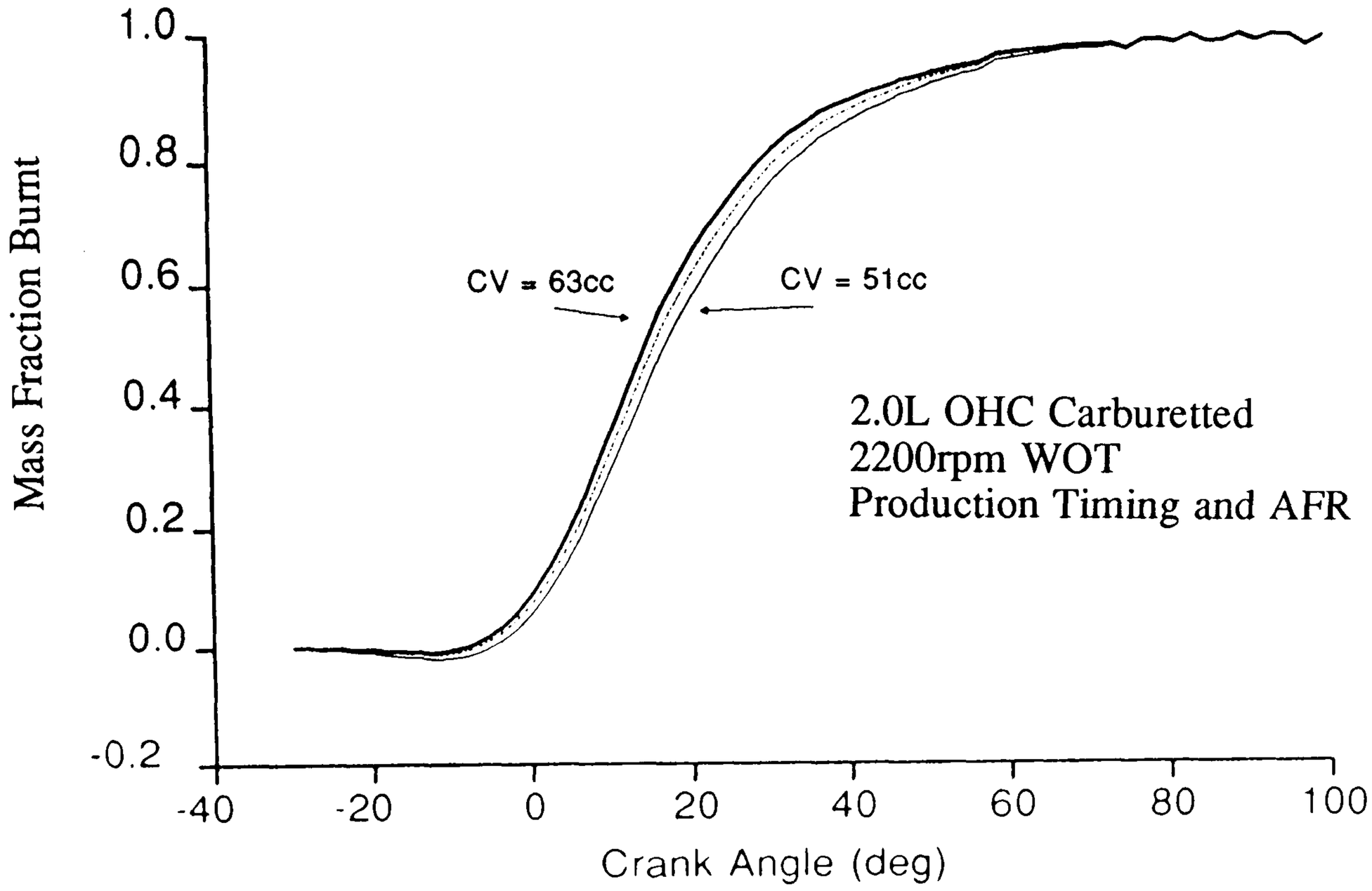

Fig 6.6 Mass Fraction Burnt Dependency on Clearance Volume Value
Central Curve is Correct Value - 57cc

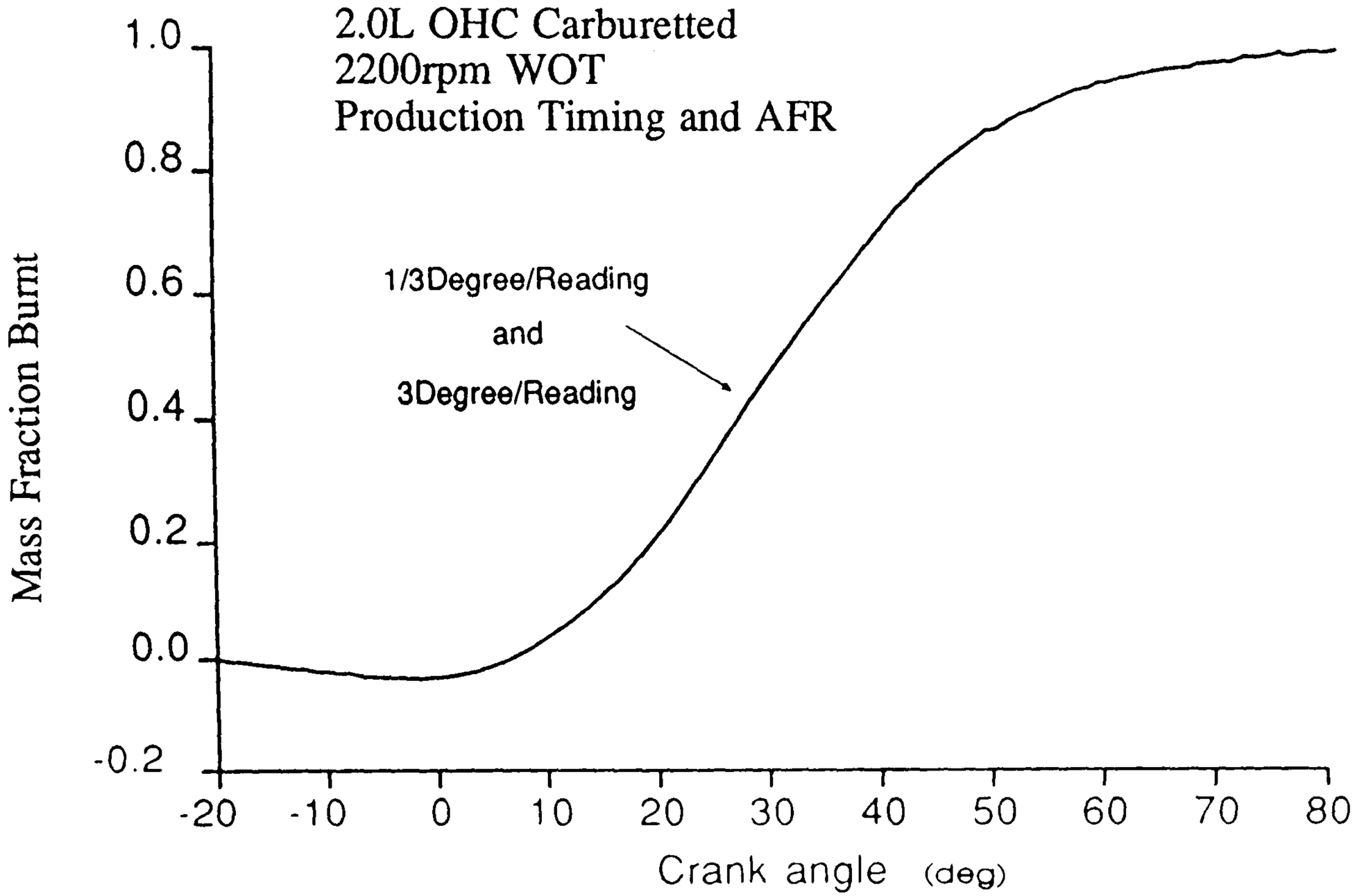

Fig 6.7 Mass Fraction Burnt Sensitivity to Sampling Rate

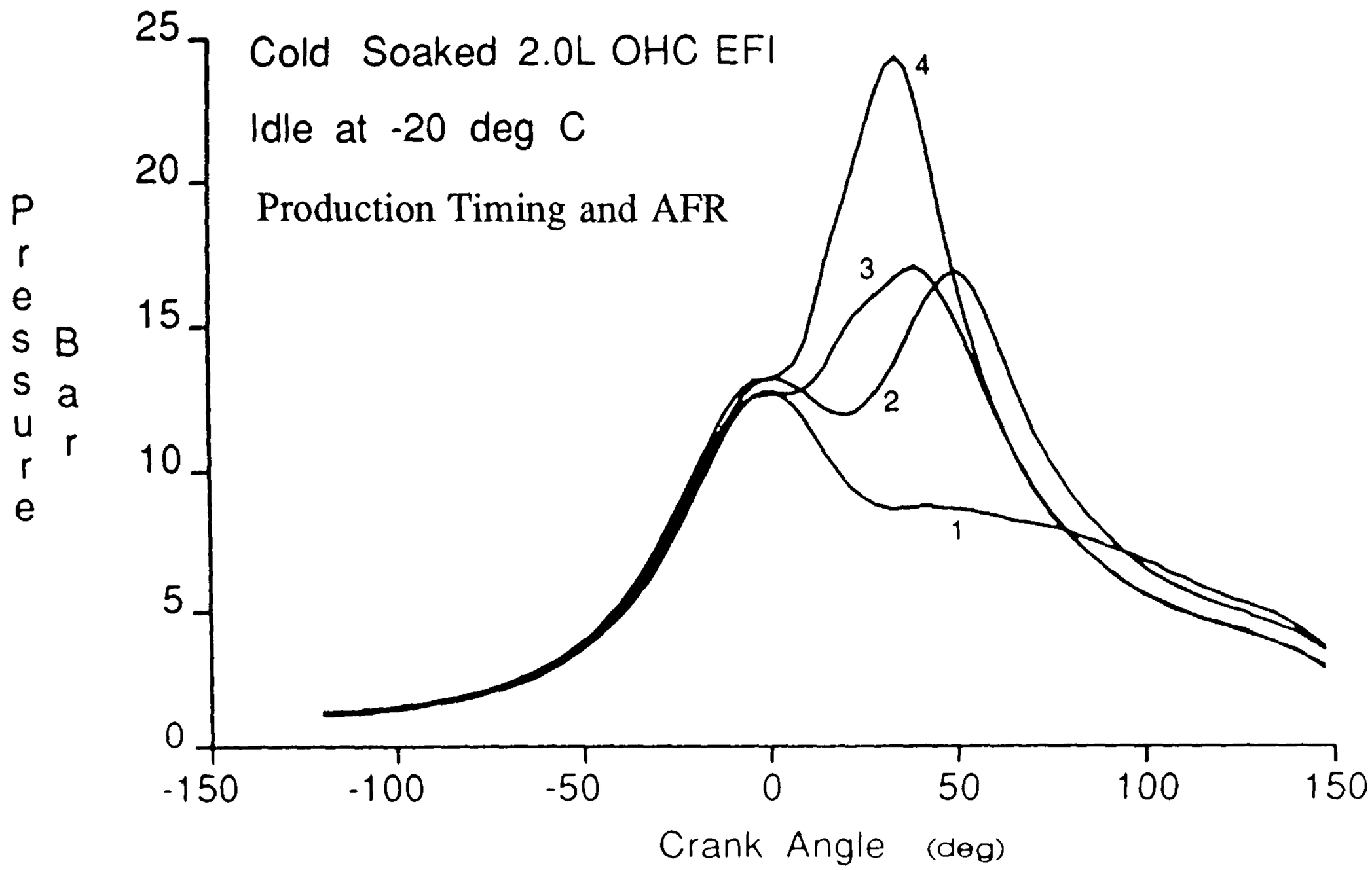

Fig 6.8 Anomalous Pressure Histories

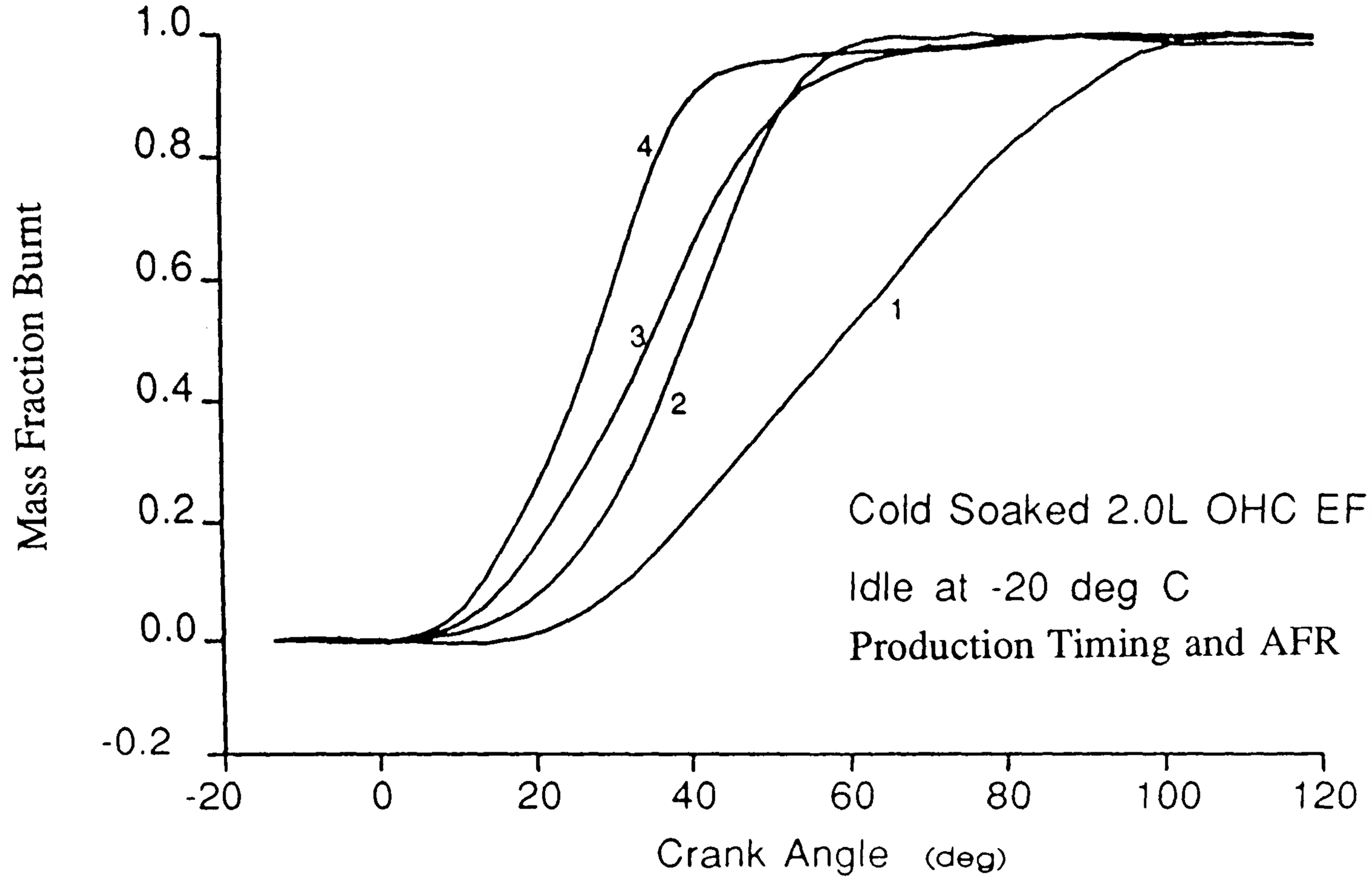

Fig 6.9 Mass Fraction Burnt Calculated from Anomalous Pressure Histories

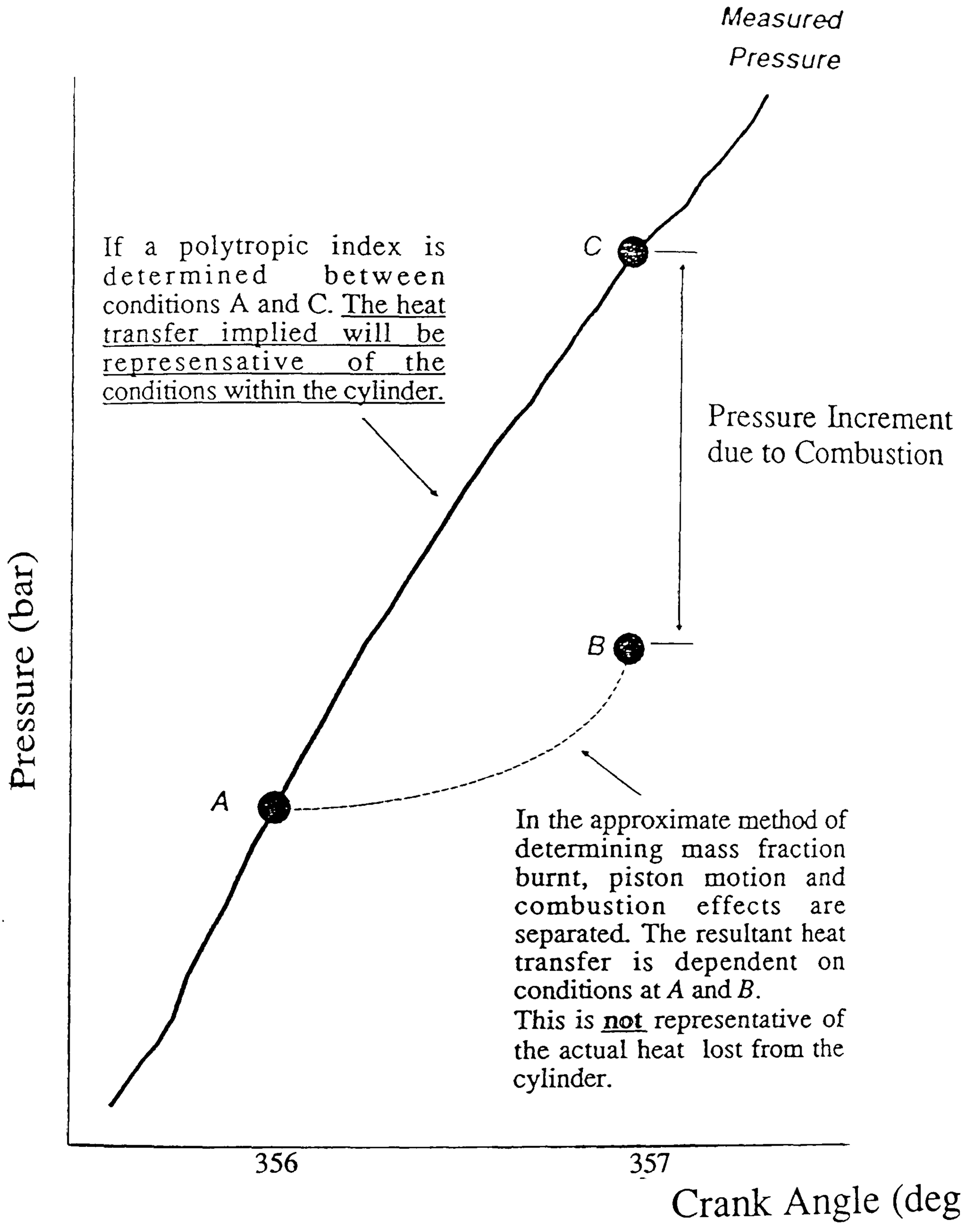

Fig 7.1 The Diffference Between Determining The Actual Heat Transfer Within The Cylinder Compared With The Heat Loss Implied In The Approximate Method Used To Determine Mass Fraction Burnt

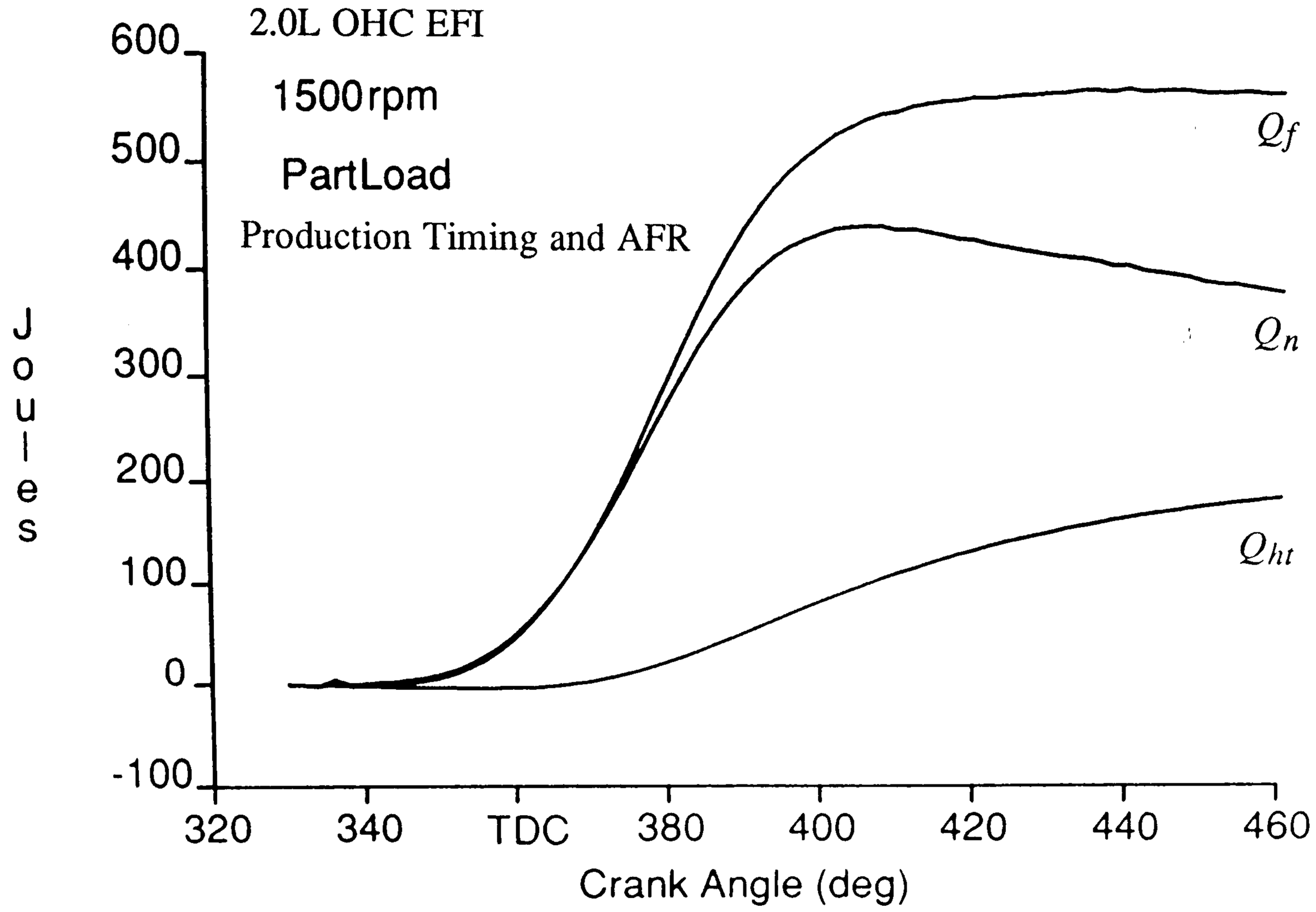

Fig 7.2 Example Output of the Heat Loss Method of Chapter 7

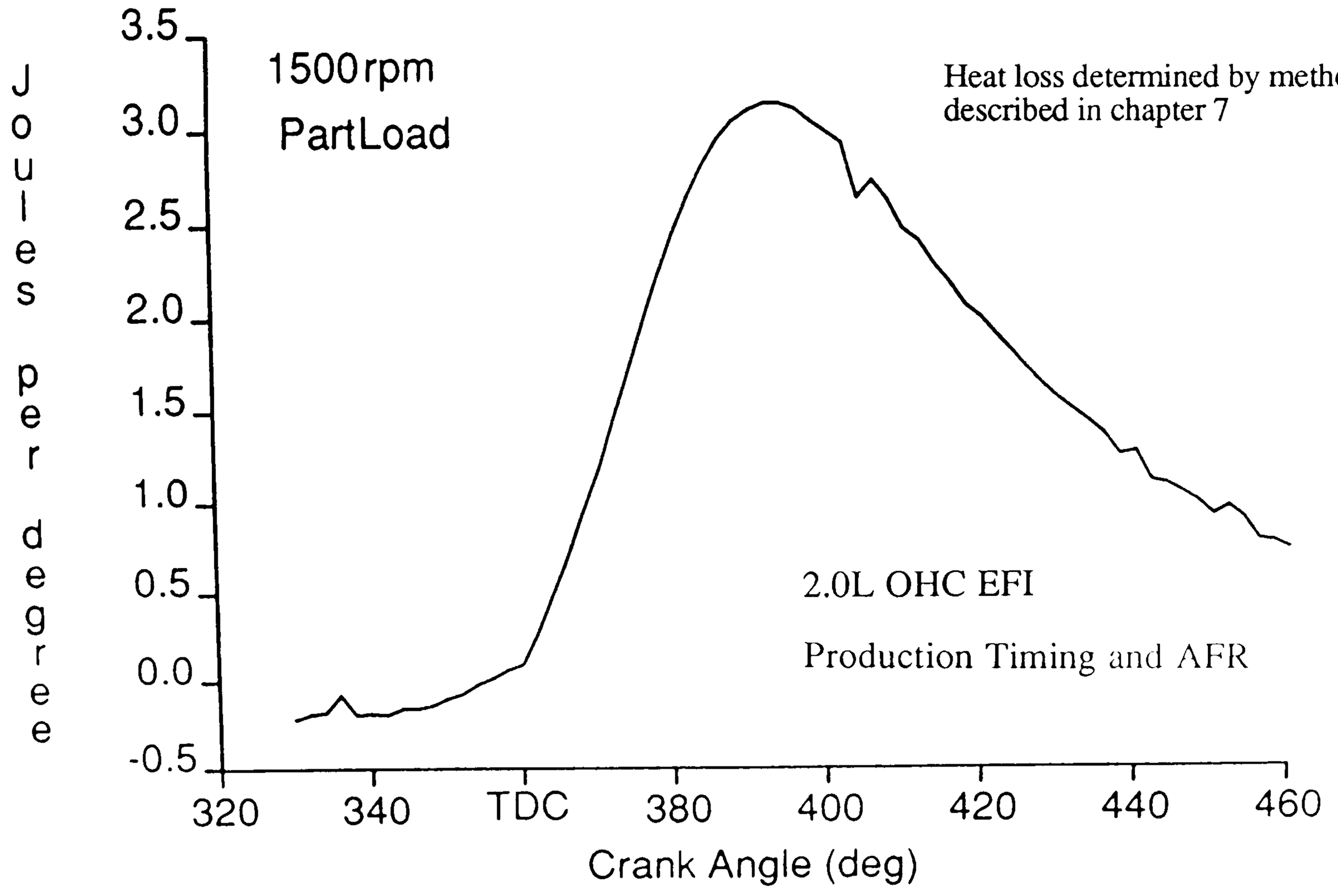

Fig 7.3 An Example of the Variation in Rate of Heat Loss

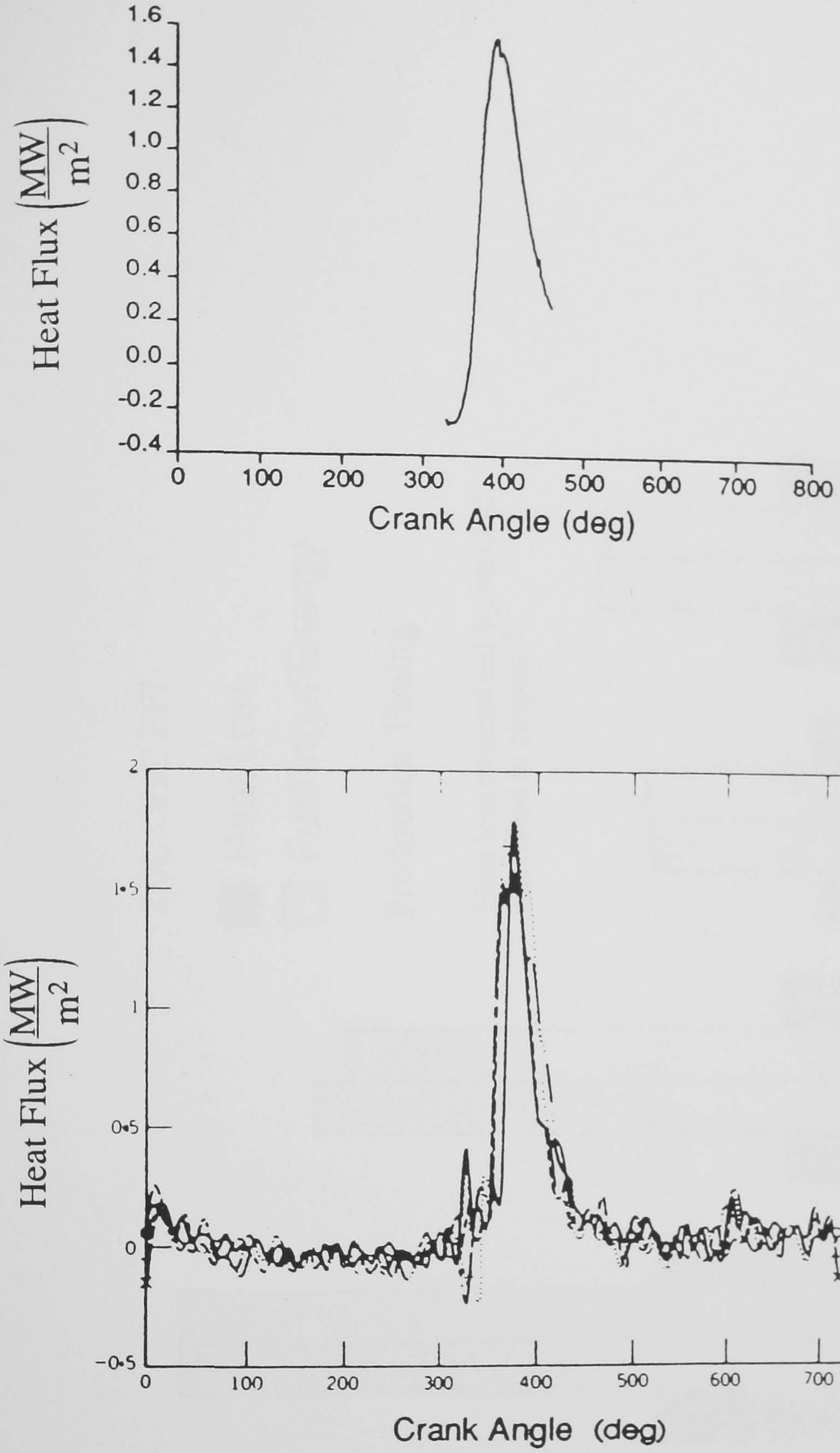

Fig 7.4 Comparison between the Instantaneous Heat Loss Calculated by the Approach suggested in Chapter 7 (TOP) at the WWMP, and Published Heat Flux (BOTTOM) Measured at Similar Conditions (1500 rpm, Delivery Ratio 0.4) from [7.3]

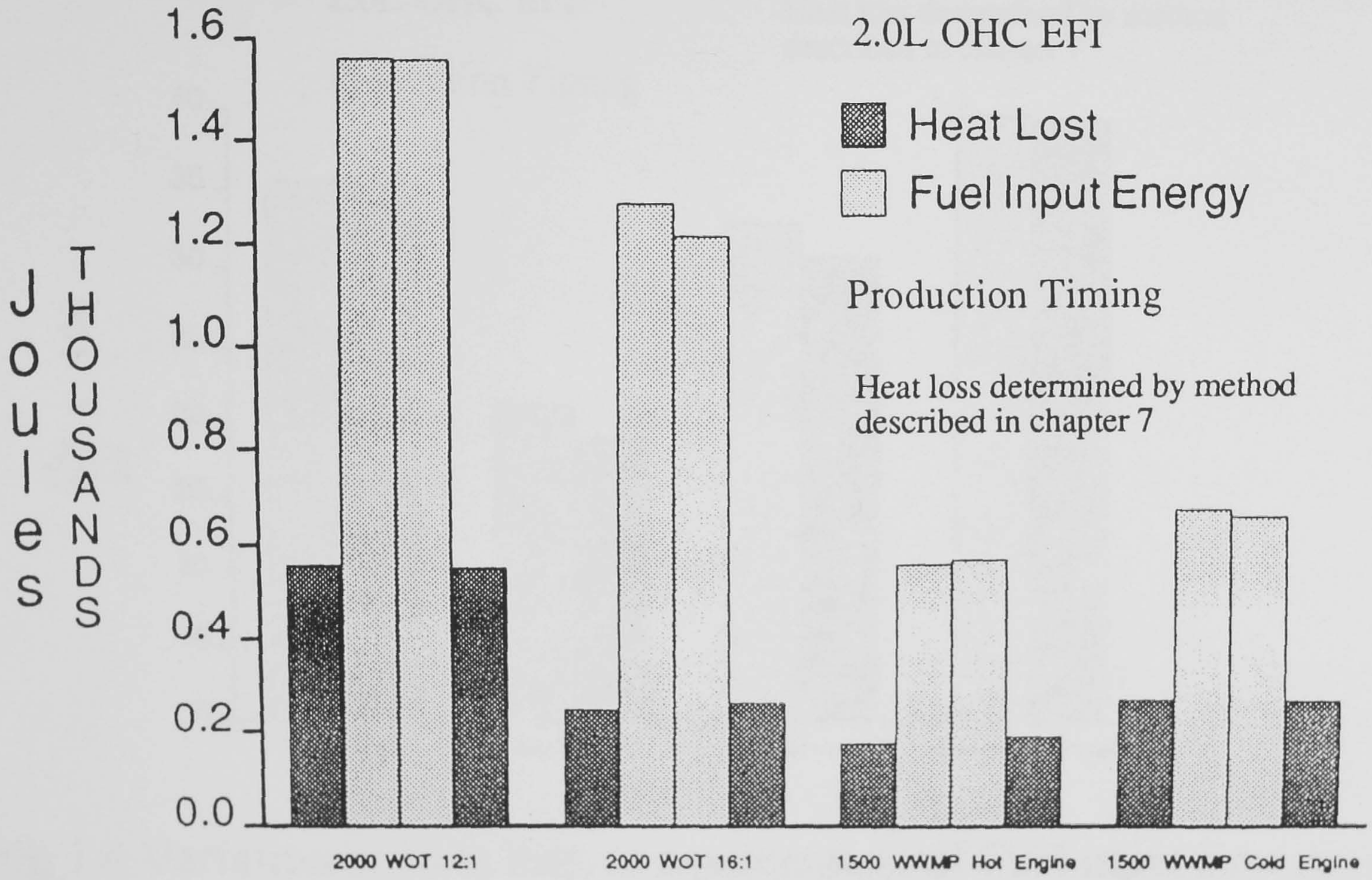

Fig 7.5 Changes in Heat Release and Loss as Operating conditions Altered.

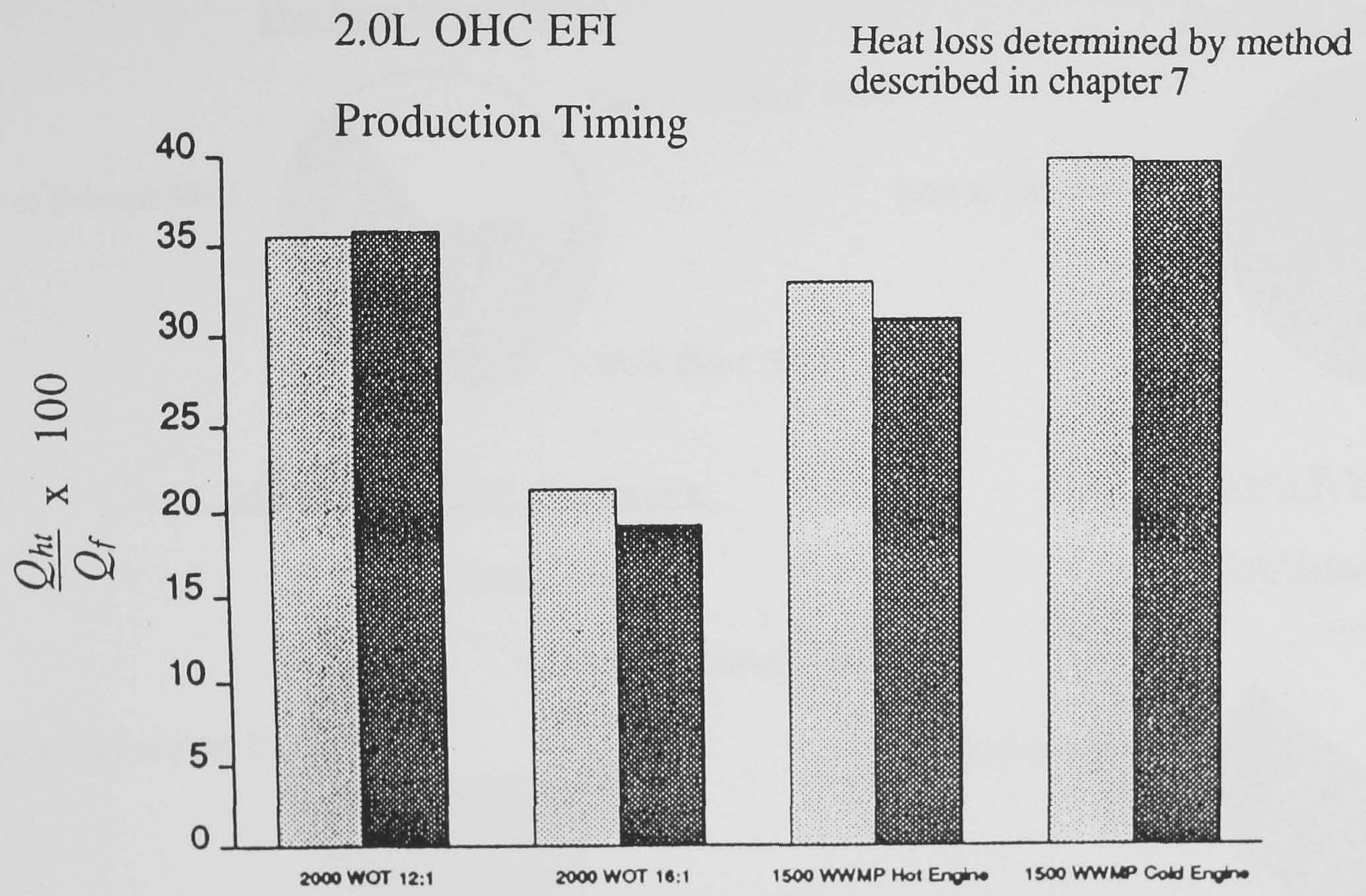

Fig 7.6 Variation of Heat loss, as a percentage of Fuel input Energy, as Engine Operating Conditions Altered

2.0L OHC EFI

2000rpm WOT, AFR 12:1

Fuel Input Energy 1560 J

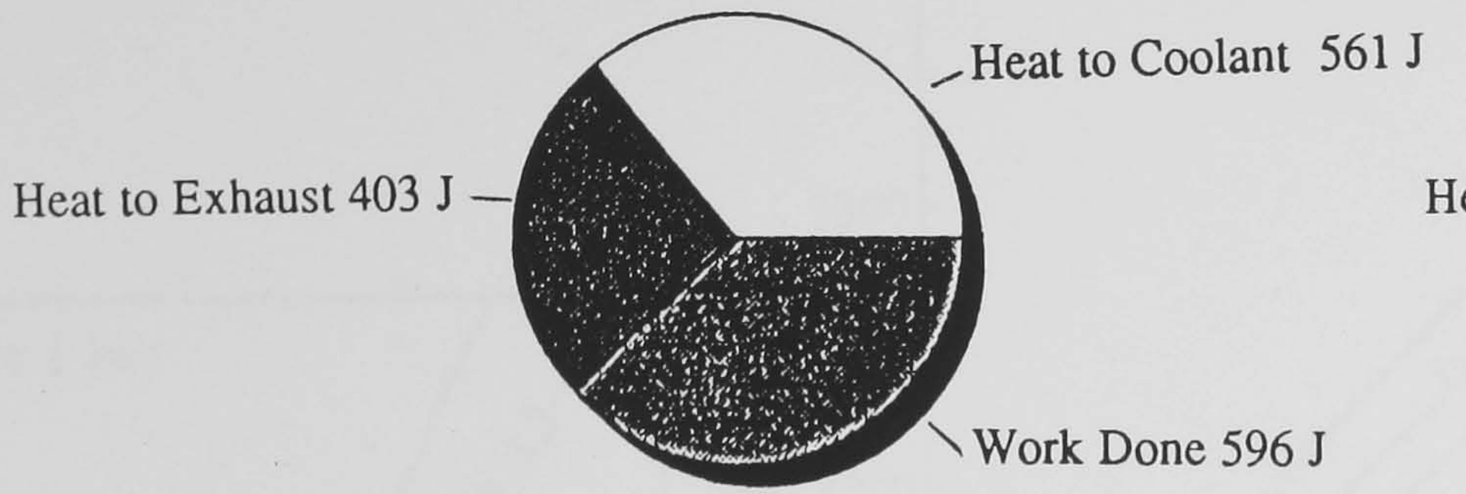

2000rpm WOT, AFR 16:1

Fuel Input Energy 1214 J

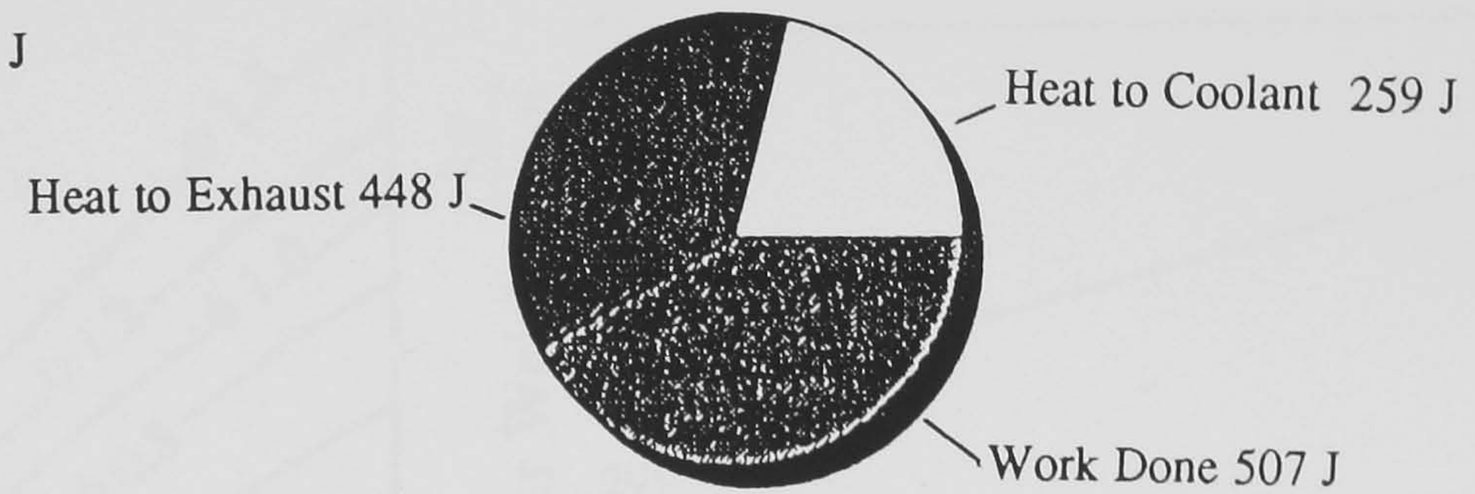

1500rpm WWMP, Hot Engine

Fuel Input Energy 569 J

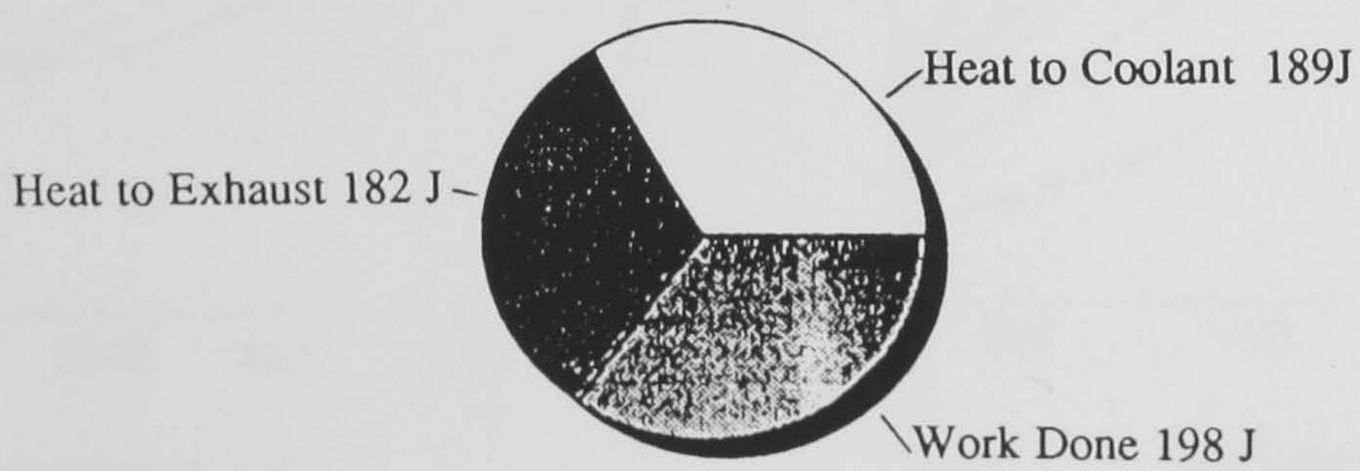

1500rpm WWMP, Cold Engine

Fuel Input Energy 673

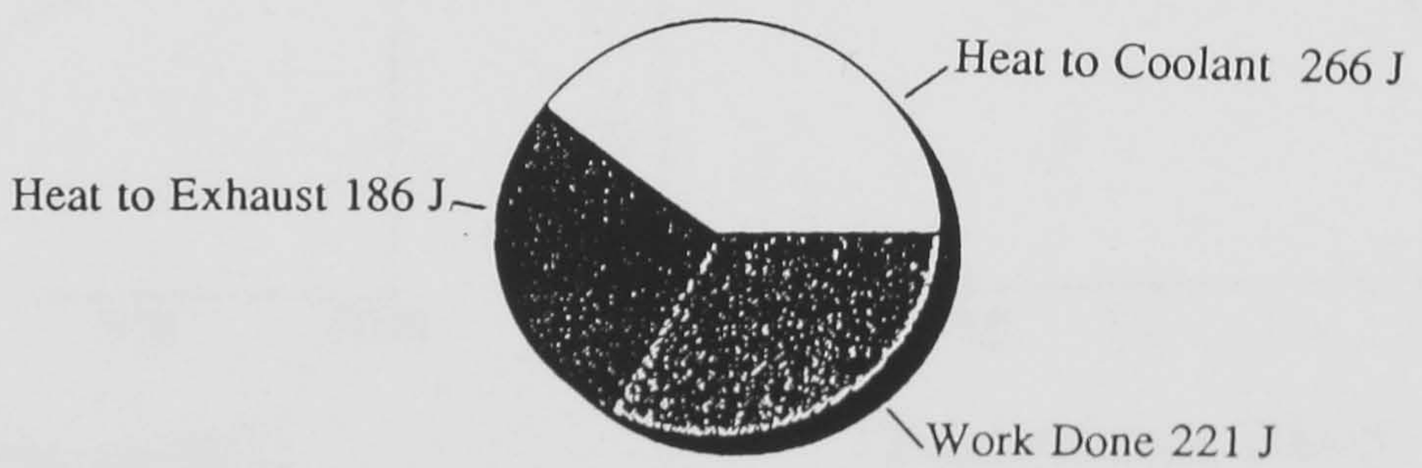

Fig 7.7 Pie Chart Representation of the Engine Heat Balance at Four Different Operating Conditions

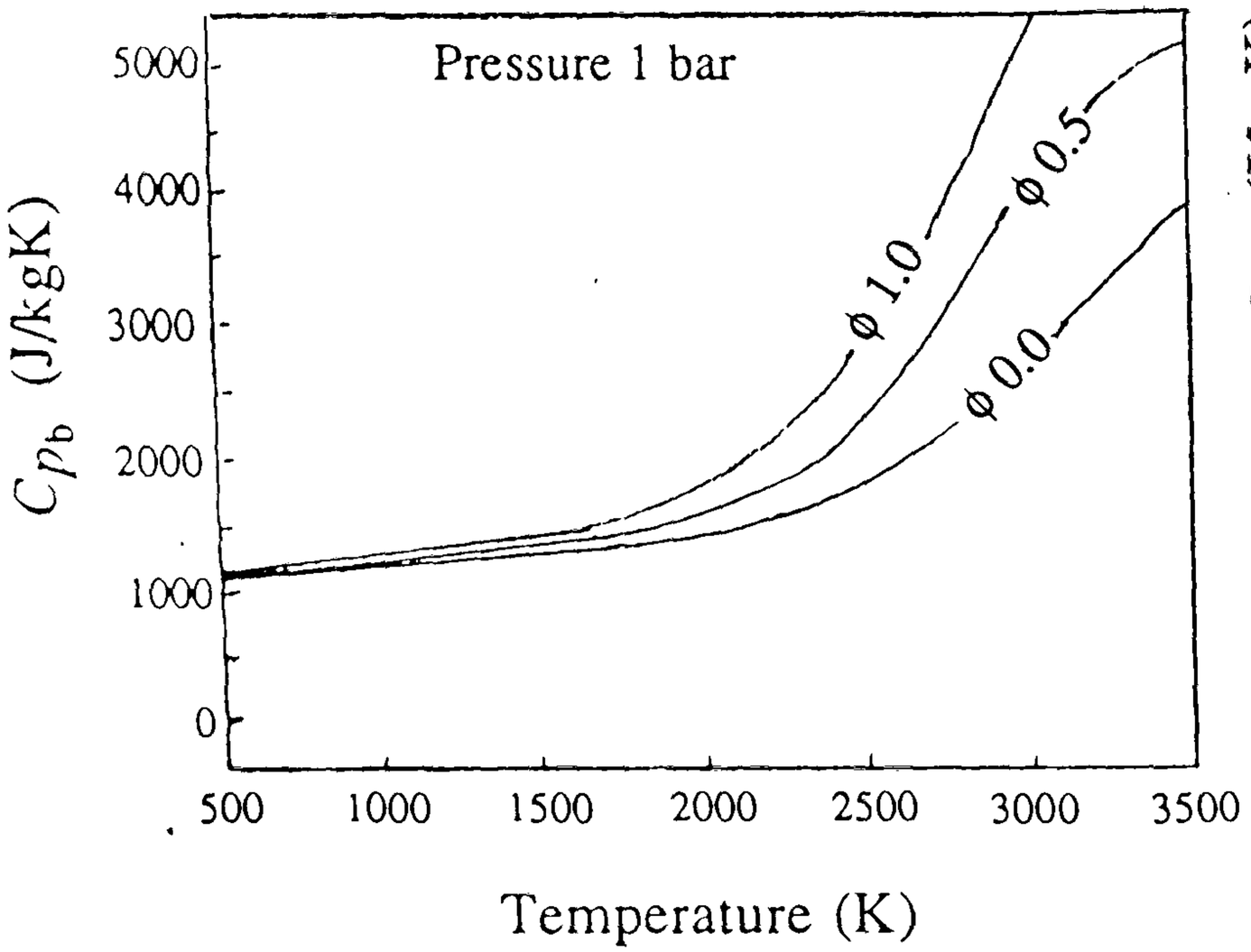

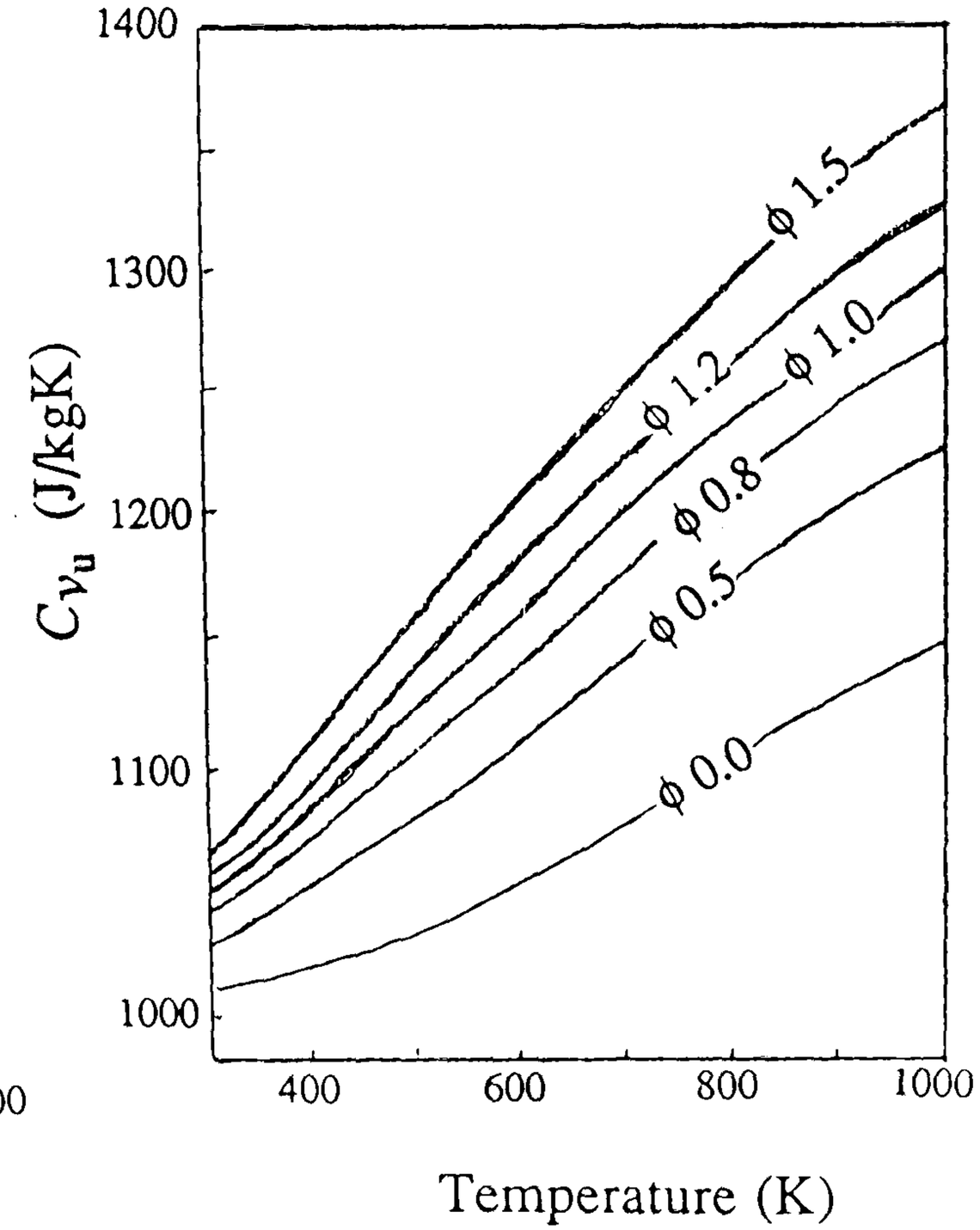

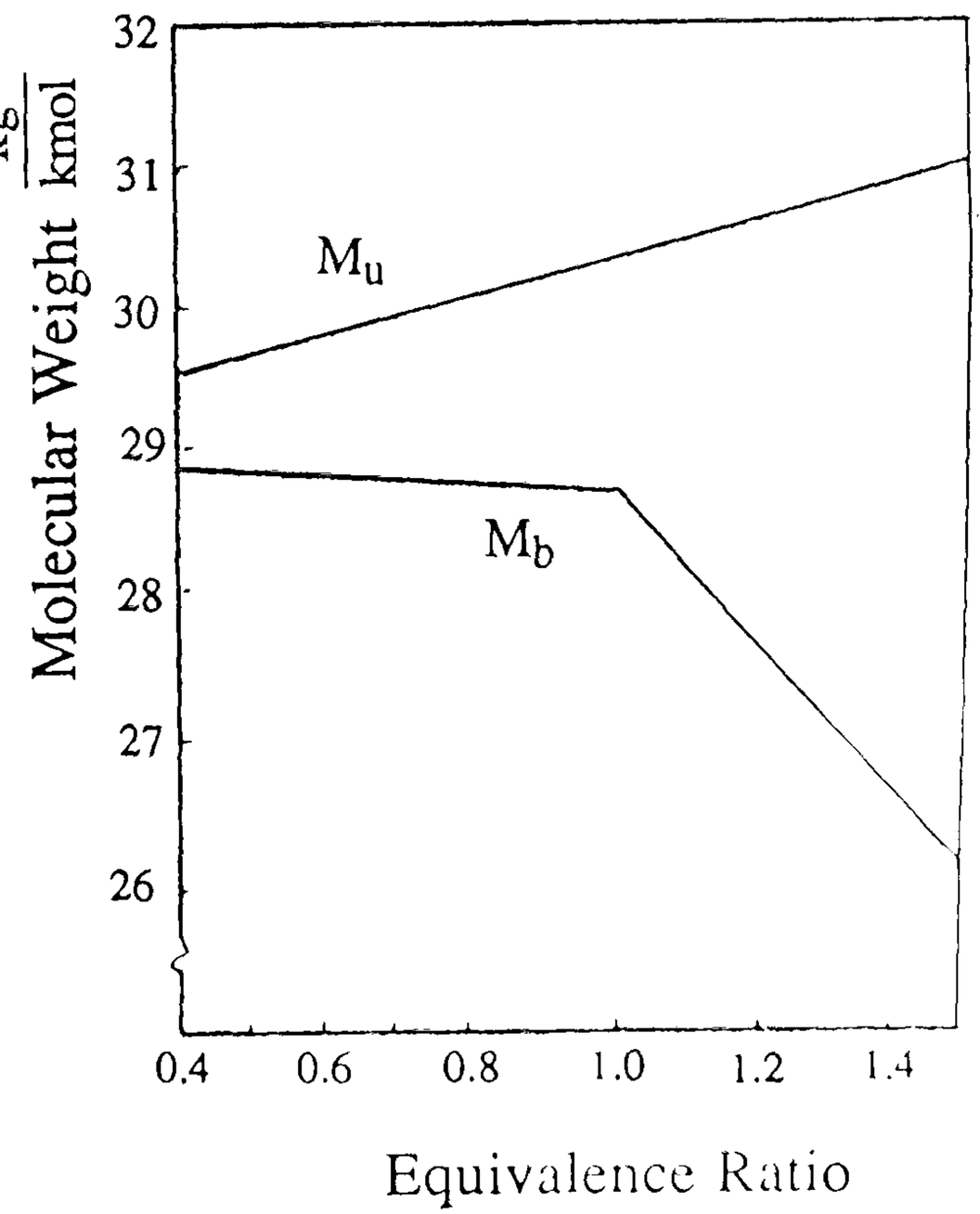

Fig 7.8 Thermodynamic Property Data, Adapted from Heywood[7.4]

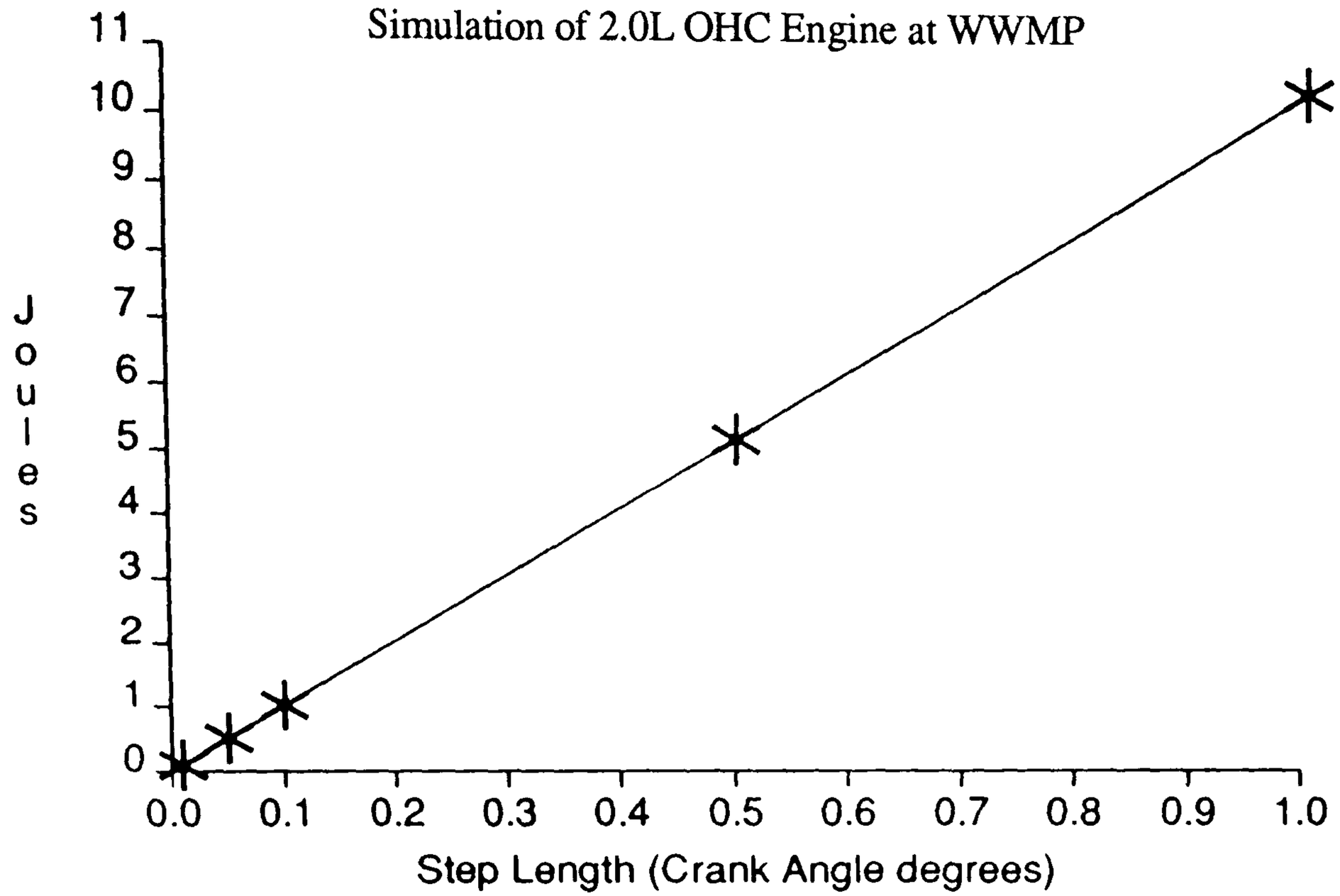

Fig 7.9 Predicted Heat Loss Variation as Simulation Step Size Decreased

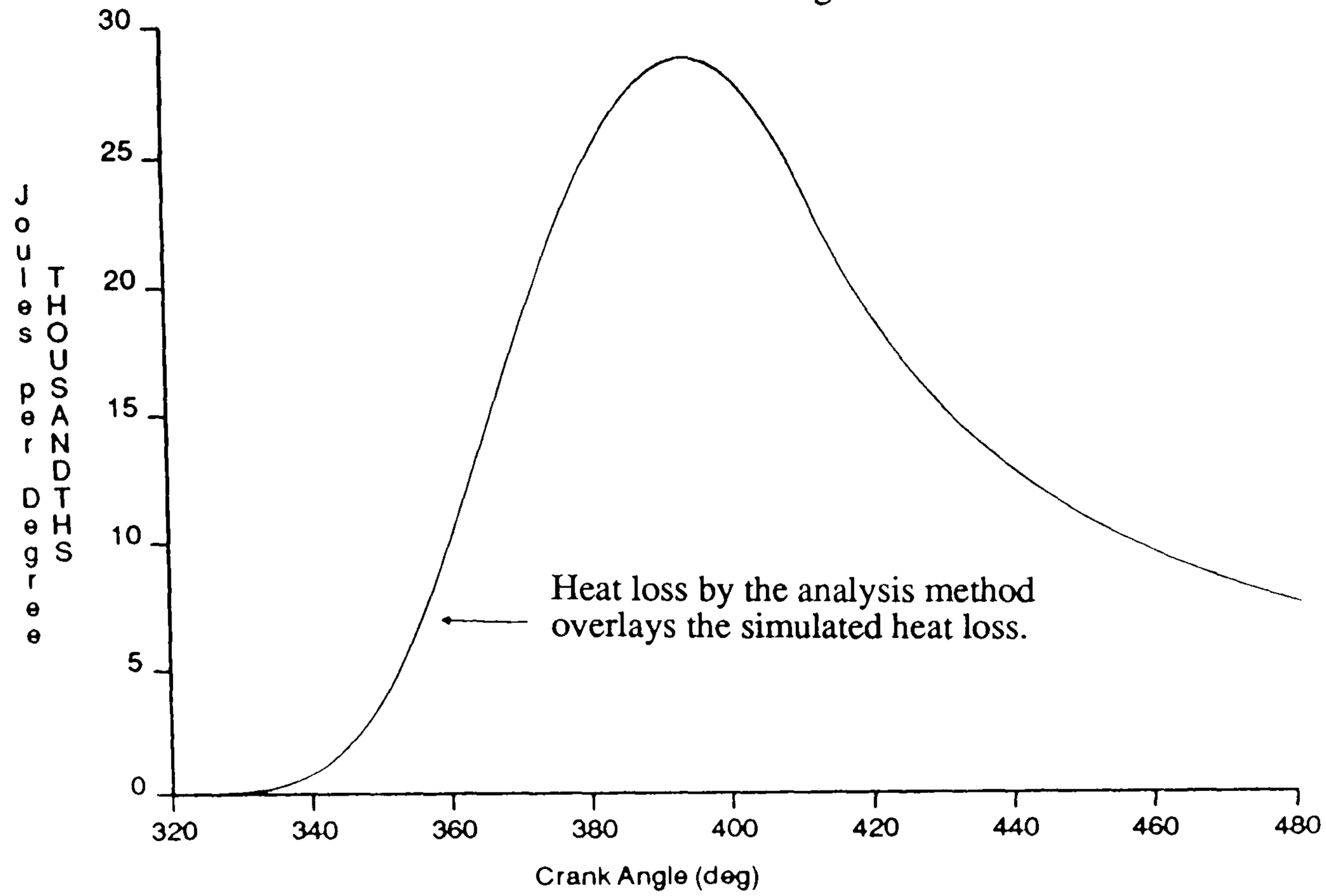

Fig 7.10 Comparison Between the Simulated Heat Loss (Eichelberg Correlation) and the Heat Loss Determined by the Method of Chapter 7

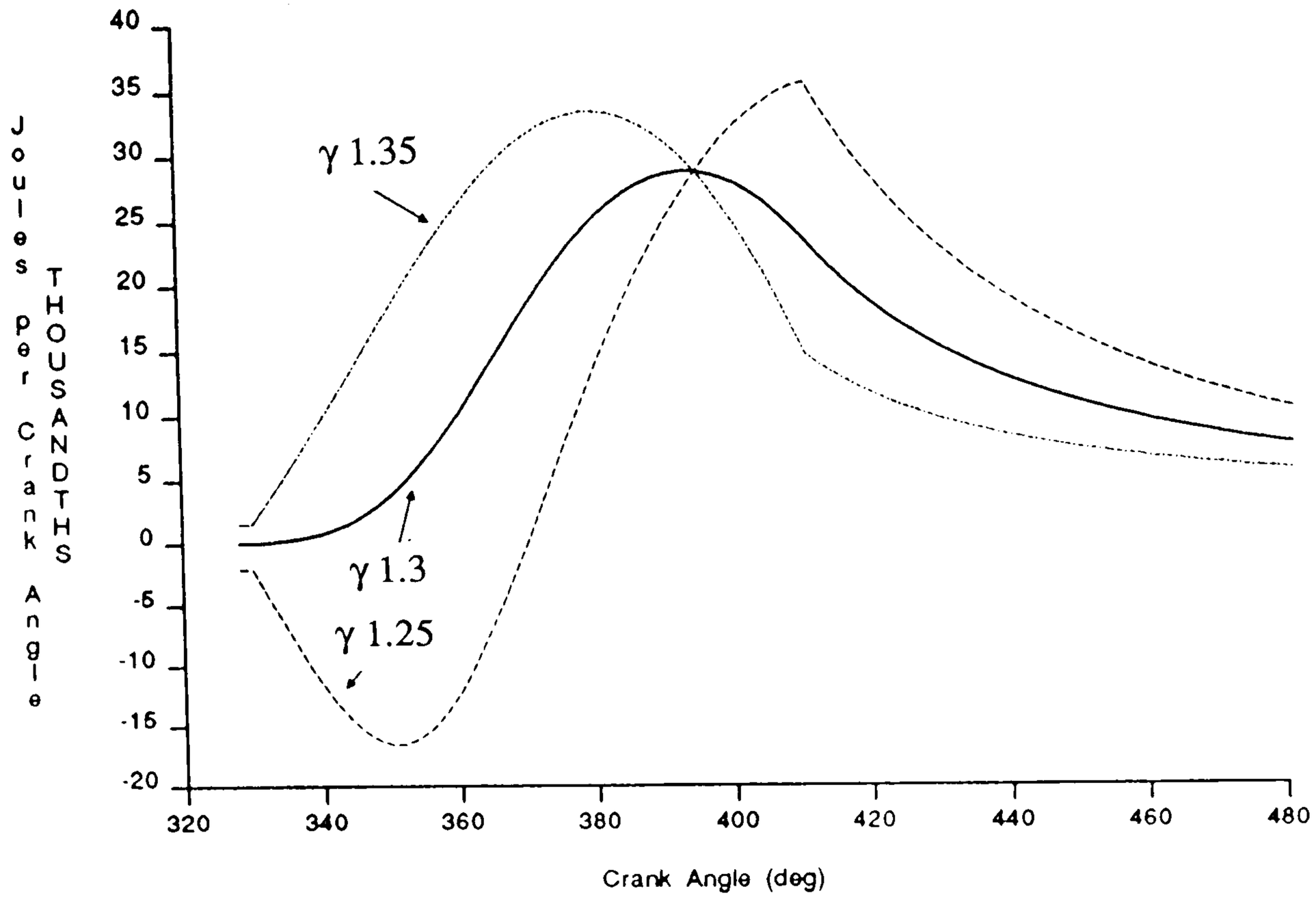

Fig 7.11 The Sensitivity of the Heat Loss Analysis to Specific Heat Ratio

Simulation of 2.0L OHC Engine, Operating at WWMP

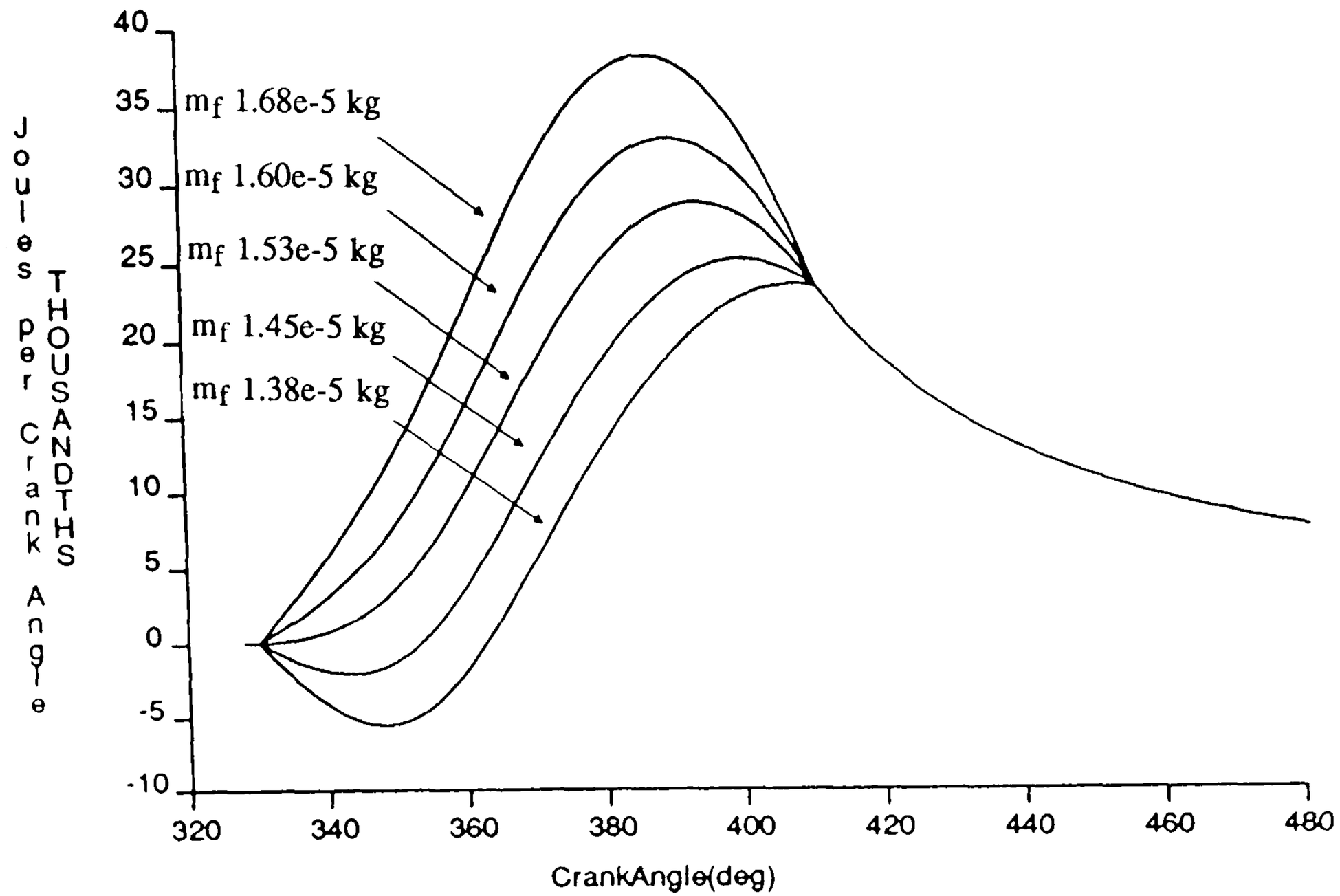

Fig 7.12 The Sensitivity of the Heat Loss Analysis to the Specified Fuel Mass

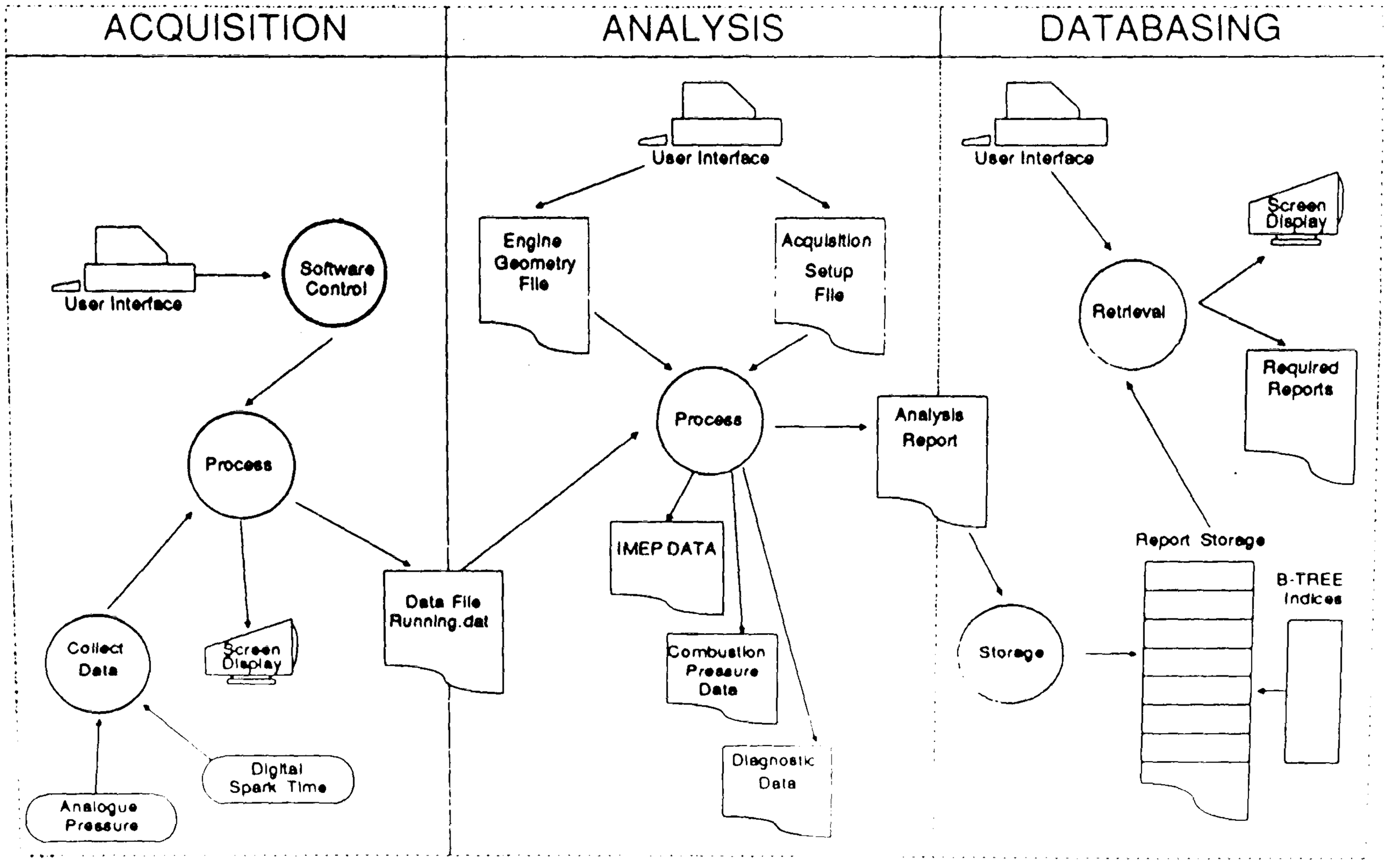

Fig 8.1 Data Flow Diagram for CPAS

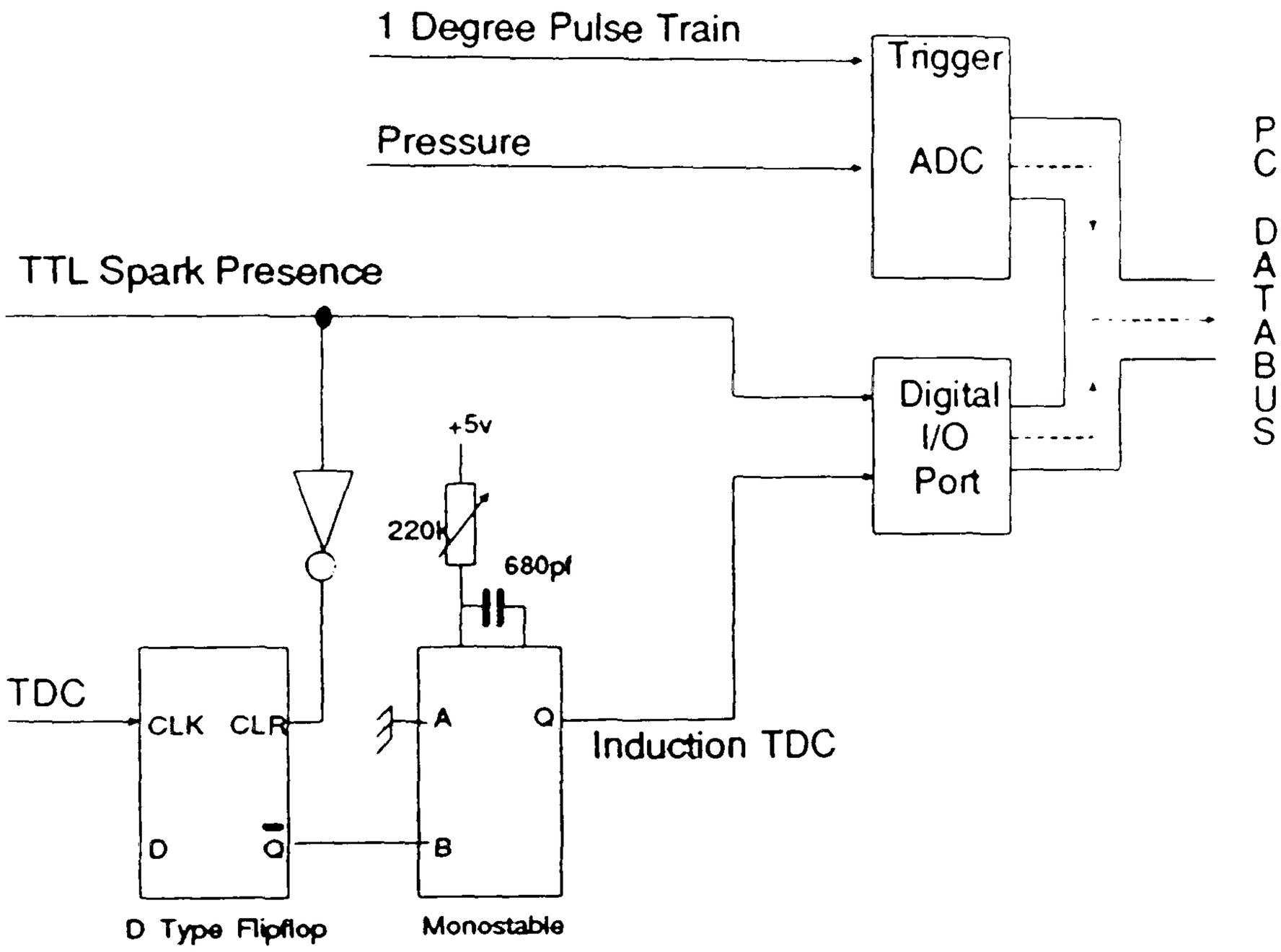

Fig 8.2 Acquisition Data Signals

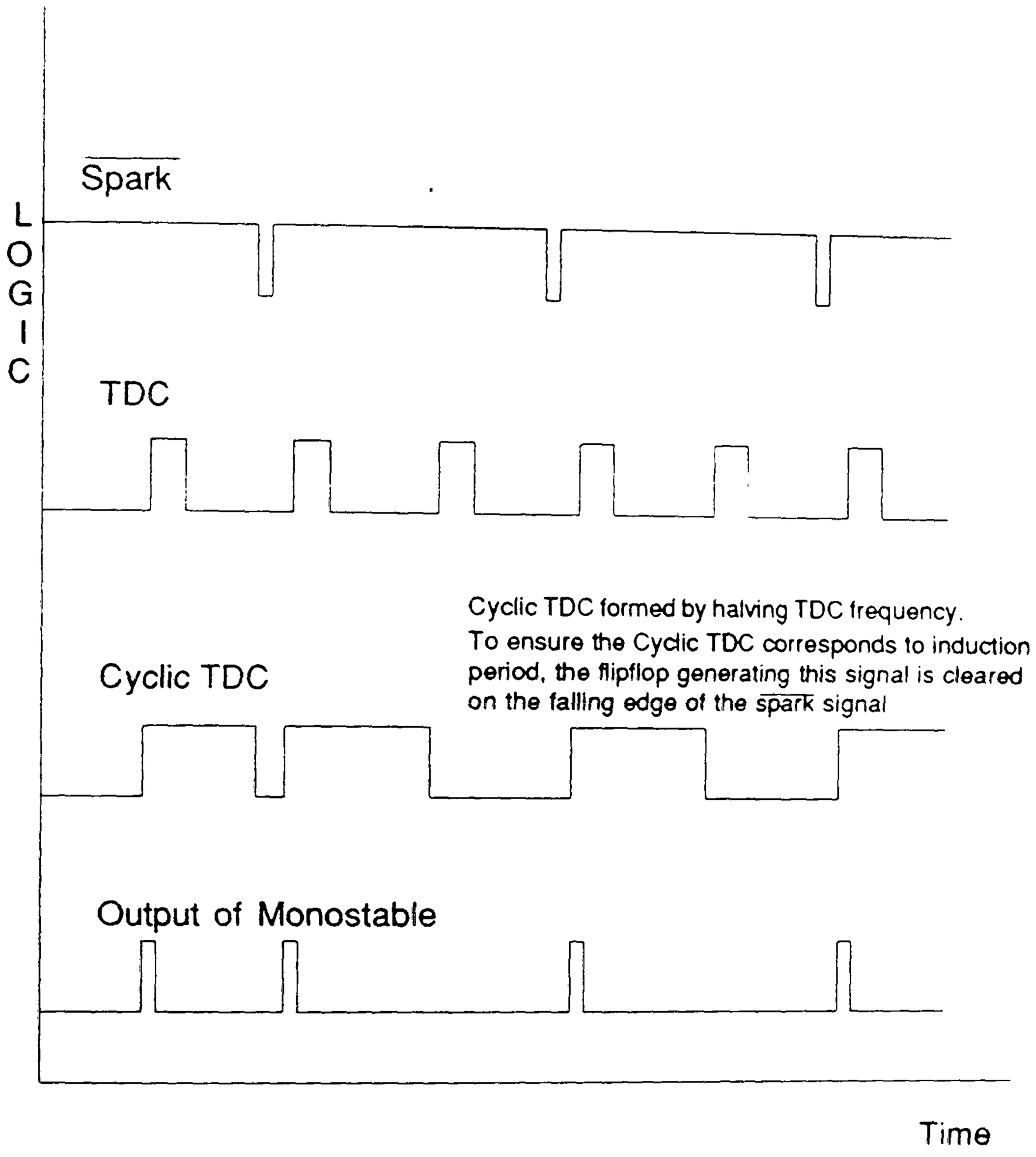

Fig 8.3 Logic Diagram showing Generation of Induction TDC Pulse

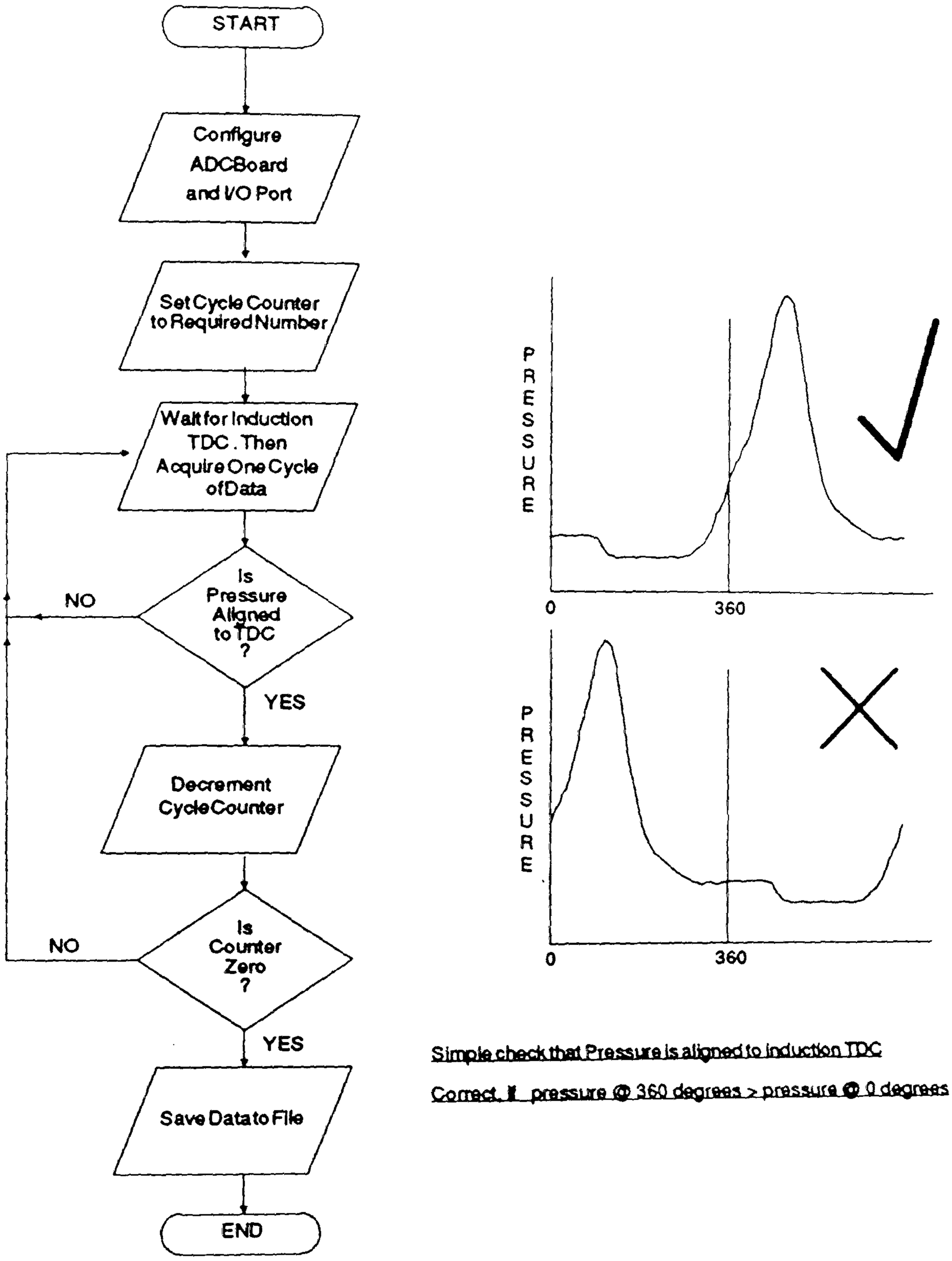

Fig 8.4 Simple Flow Chart for the Acquisition of Engine Data

PARAMETER		MEAN	COV
Max pressure (bar)		36.907	9.5259
Crank position (deg)		385.120	0.7111
Max pressure rise rate		1.879	30.1432
Crank position (deg)		382.99	1.4083
Max comb. press. rise rate		1.988	31.8467
Crank position (deg)		382.99	1.1174
IMEP	(bar)	9.355	1.8954
WMEP	(bar)	9.372	1.7310
PMEP	(bar)	-0.017	-155.4829
Spark advance		18.030	0.0167
Combustion length (deg)		72.43	1.8830
Total comb. pressure		47.43	3.9648
2% Burn duration (deg)		14.35	10.5928
10% Burn duration (deg)		23.04	7.4520
50% Burn duration (deg)		37.95	7.4377
90% Burn duration (deg)		52.70	8.6872
10-90% Burn duration (deg)		47.43	12.5350
Percentage Partial Burns		0.0000	
Percentage Misfires		0.0000	

Fig 8.5 Example Output Format of Analysis Report

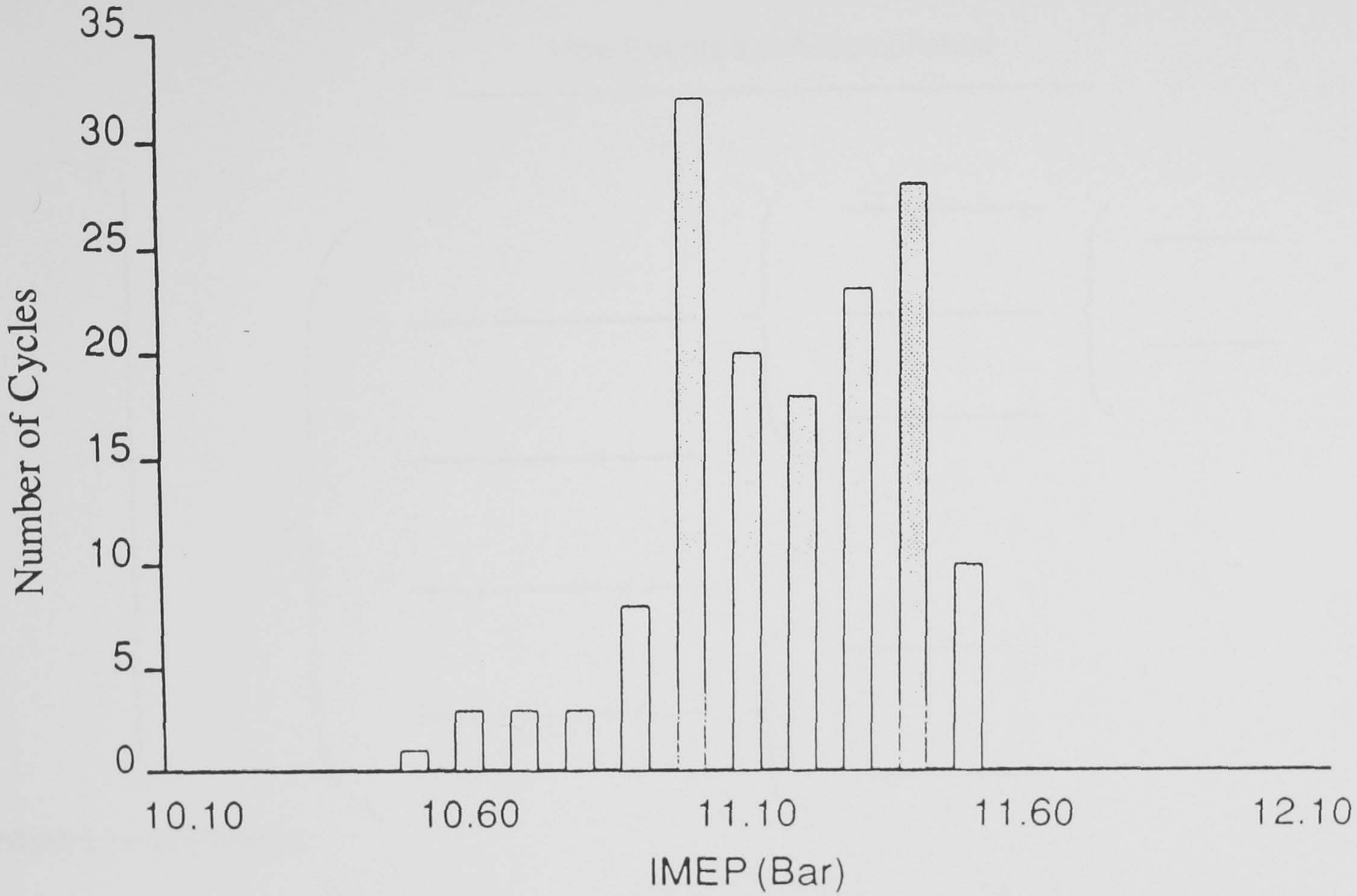

Fig 8.6 Sample Output of IMEP Frequency Data from CPAS

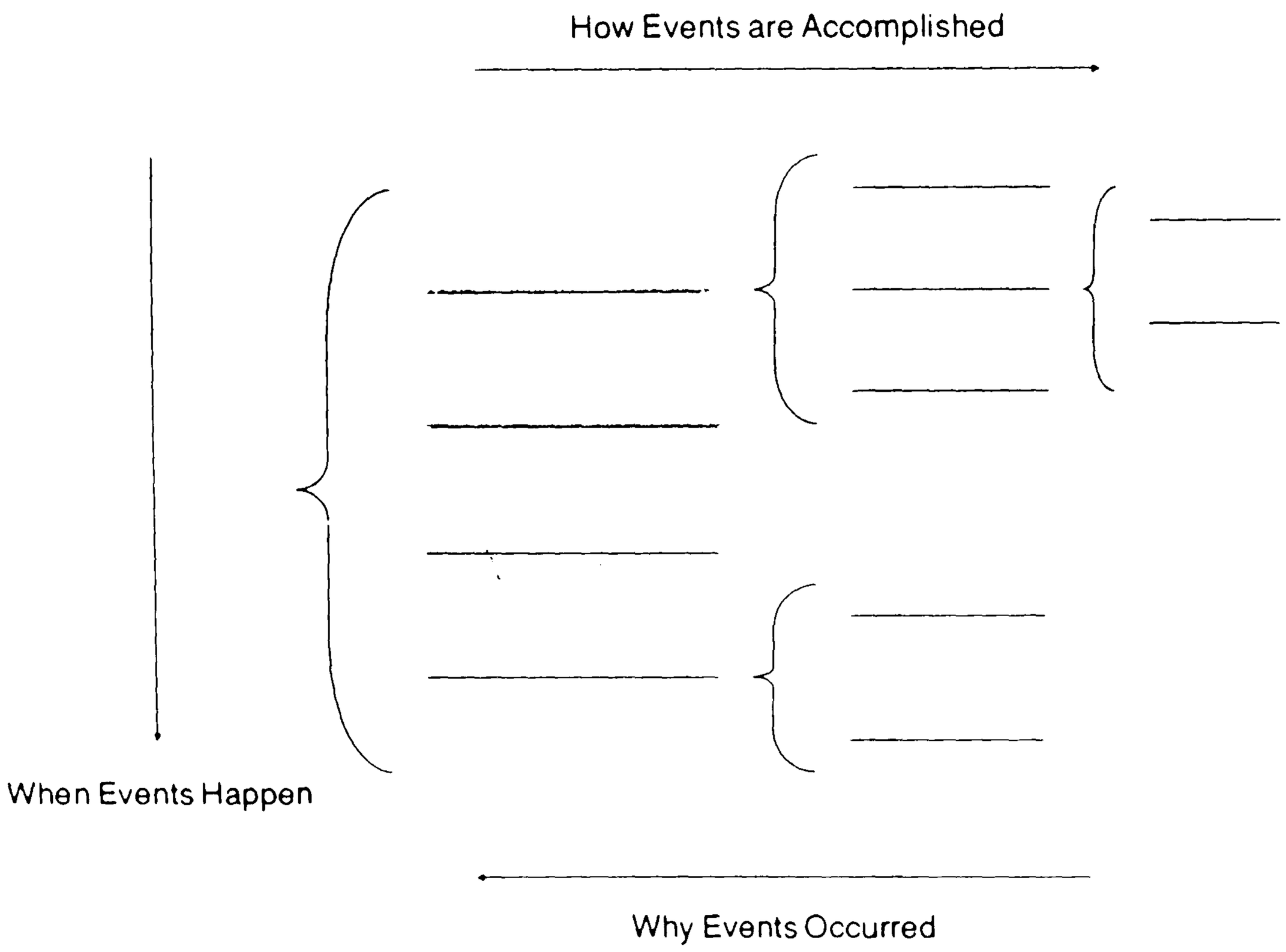

Fig 8.7 Information Flow in a Warnier-Orr Diagram

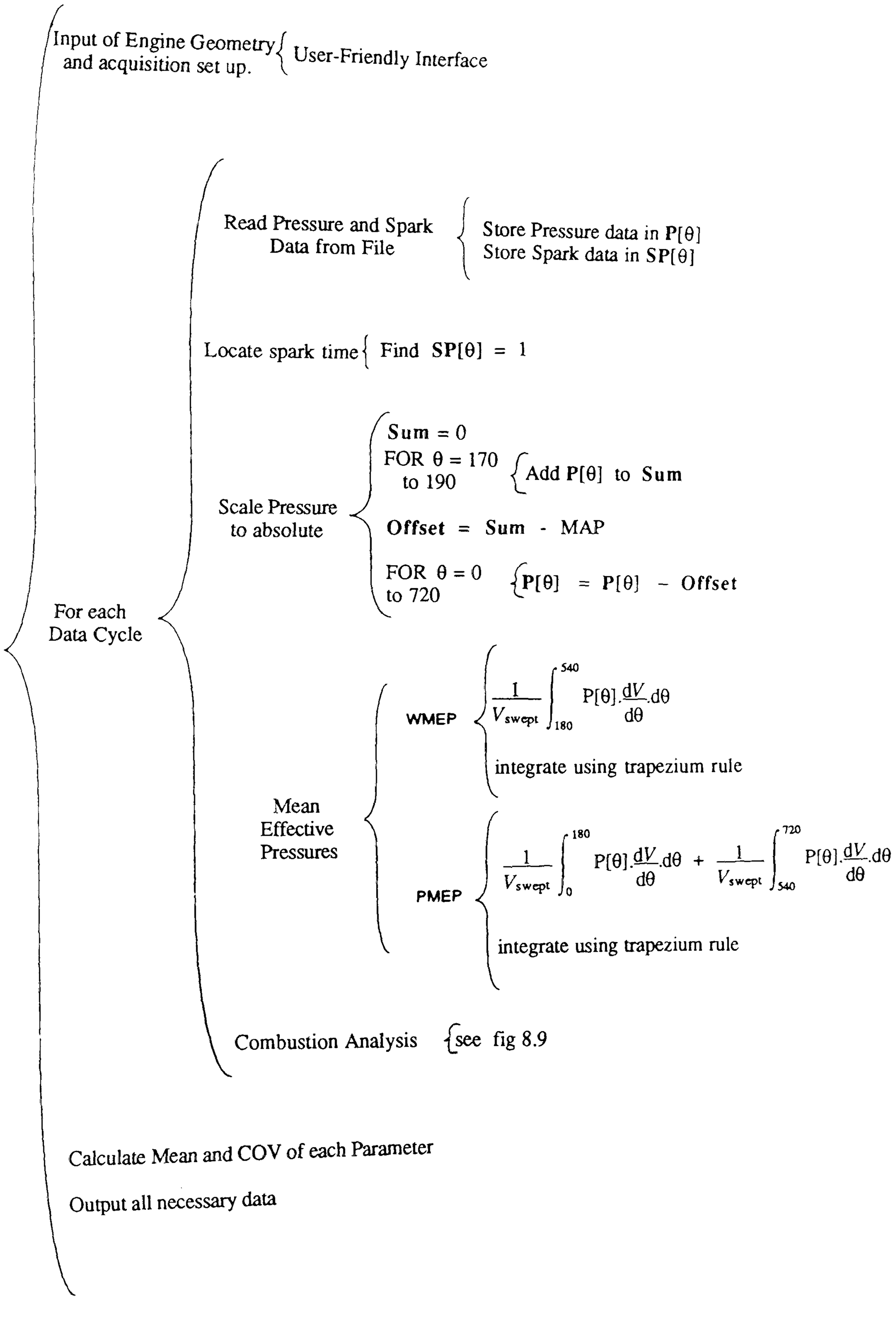

Fig 8.8 Warnier-Orr Diagram for Pressure Analysis Program

Index = 1.25 AND Index = 1.35 { For θ = 0 to 10 {

COMP1 = 0; COMP2 = 0; EXP1 = 0; EXP2 = 0

Calculate Increment of Combustion Pressure, ΔP_{ci} @ spark time - θ

IF(Index = 1.25) Add ΔP_{ci} to **COMP1**
ELSE Add ΔP_{ci} to **COMP2**

Calculate Increment of Combustion Pressure, ΔP_{ci} @ EVO - θ

IF(Index = 1.25) Add ΔP_{ci} to **EXP1**
ELSE Add ΔP_{ci} to EXP2

Compression Index = $1.25 - \frac{(1.35 - 1.25)\text{COMP1}}{\text{COMP2} - \text{COMP1}}$

Expansion Index = $1.25 - \frac{(1.35 - 1.25)\text{EXP1}}{\text{EXP2} - \text{EXP1}}$

Adjust Indices

Counter = 0

Sum = 0

FOR θ = Spark Time to EVO {

Pmax = -999; Prise = -999

IF(**P[θ] > Pmax**) **Pmax = P[θ]**

IF($\frac{dP}{d\theta}$ > **Prise**) **Prise** = $\frac{dP}{d\theta}$

Select Index Value { IF(Before significant combustion) Use compression index
ELSE Use expansion index

Calculate increments of combustion pressure and store in **PC[θ]**

Sum = Sum + PC[θ]

Add 1 to **Counter**

Crise = -999

For i = 0 to **Counter** {

IF($\frac{d(\Delta P_c)}{d\theta}$ > **Crise**) **Crise** = $\frac{d(\Delta P_c)}{d\theta}$

Mass Fraction Burnt, X @ i = **PC[i] / Sum**

Fig 8.9 Warnier-Orr Diagrams for Index Adjustment (top) and Combustion Analysis (bottom)

DATA RECORD CONFORMING TO SEARCH PARAMETERS

Record 1 of 1

Run number	1	
Rig name	1.6L CVH EFI	
Date	10 October 1986	
Condition	4	rpm
Speed	2200	Nm
Torque	60	
AFR	12	
Spark timing	30	BTDC
HC (FID)	300	ppm
HC (NDIR)	1200	ppm
NO_x	1200	ppm
CO	3	%vol
Injector location	near standard	
Injector timing	10	ATDC
Injector pulsewidth	30	ms
Injector frequency	cyclic	
Atmospheric pressure	1.01	bar
Relative humidity	11.0	%

Choose (U)pdate (N)ext page (L)ast page (H)ardcopy
Your choice>>

Fig 8.10 Sample Screen Display from Database search

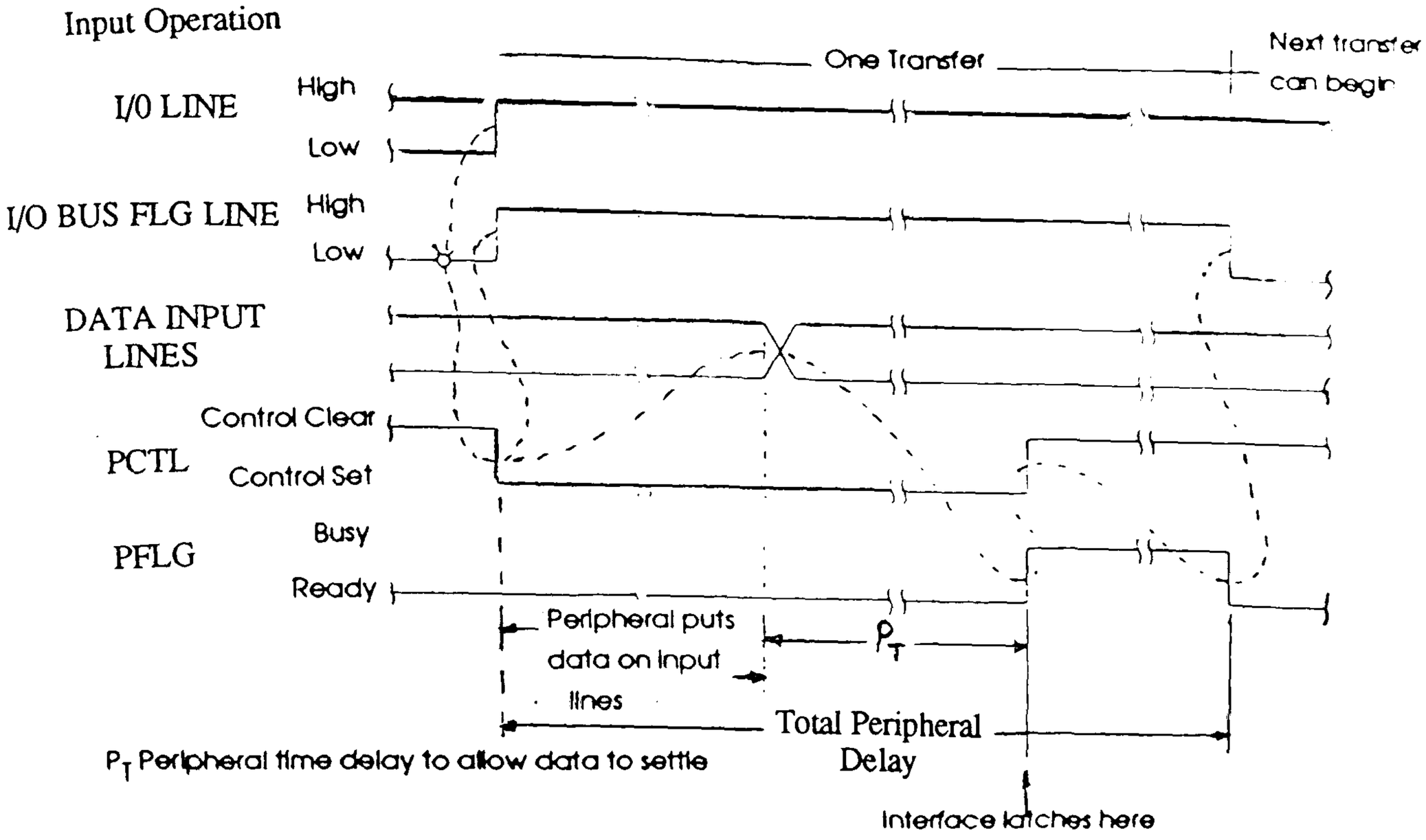

Fig 9.1A Full Mode Handshake Protocol for GPIO

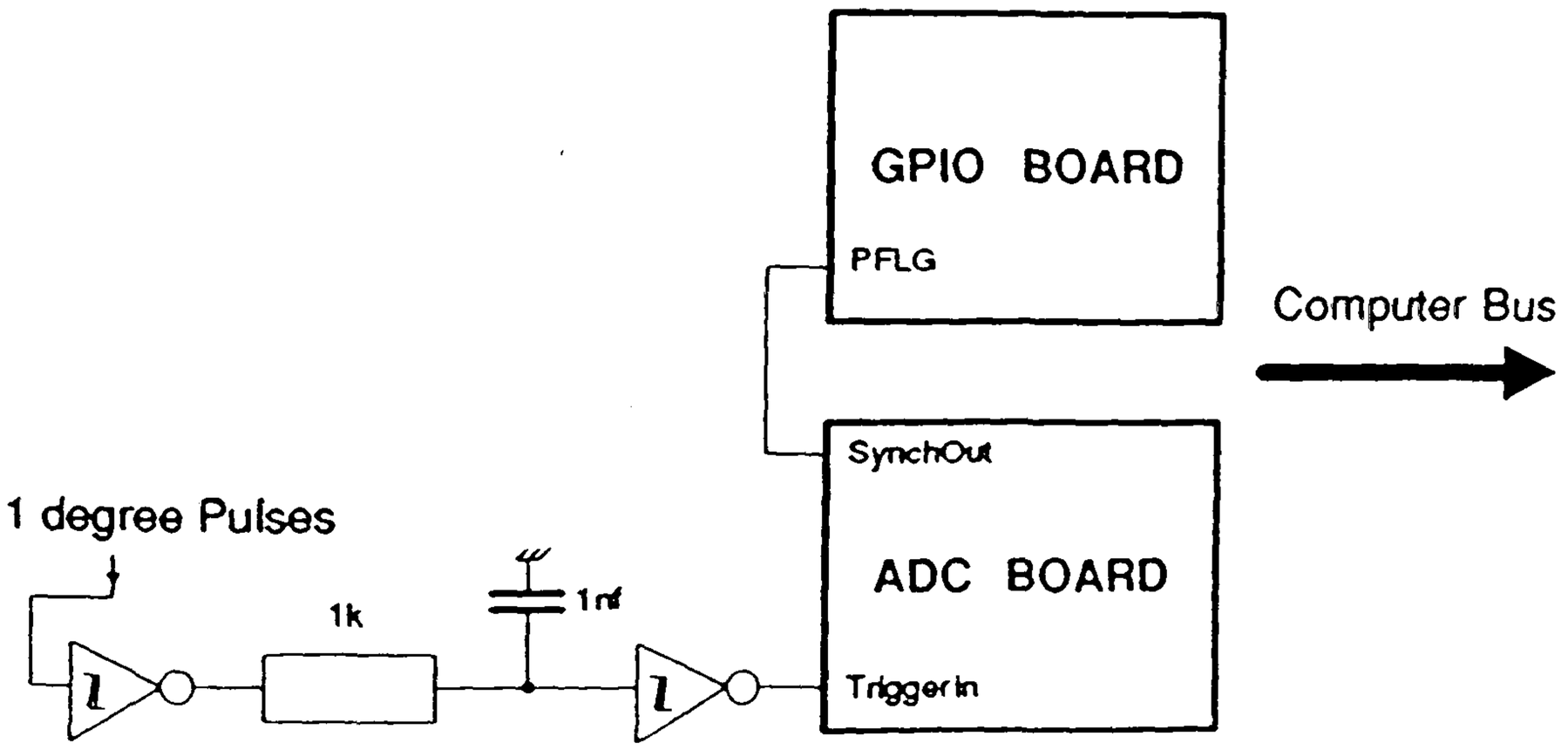

Fig 9.1B ADC and GPIO Interfacing Circuitry

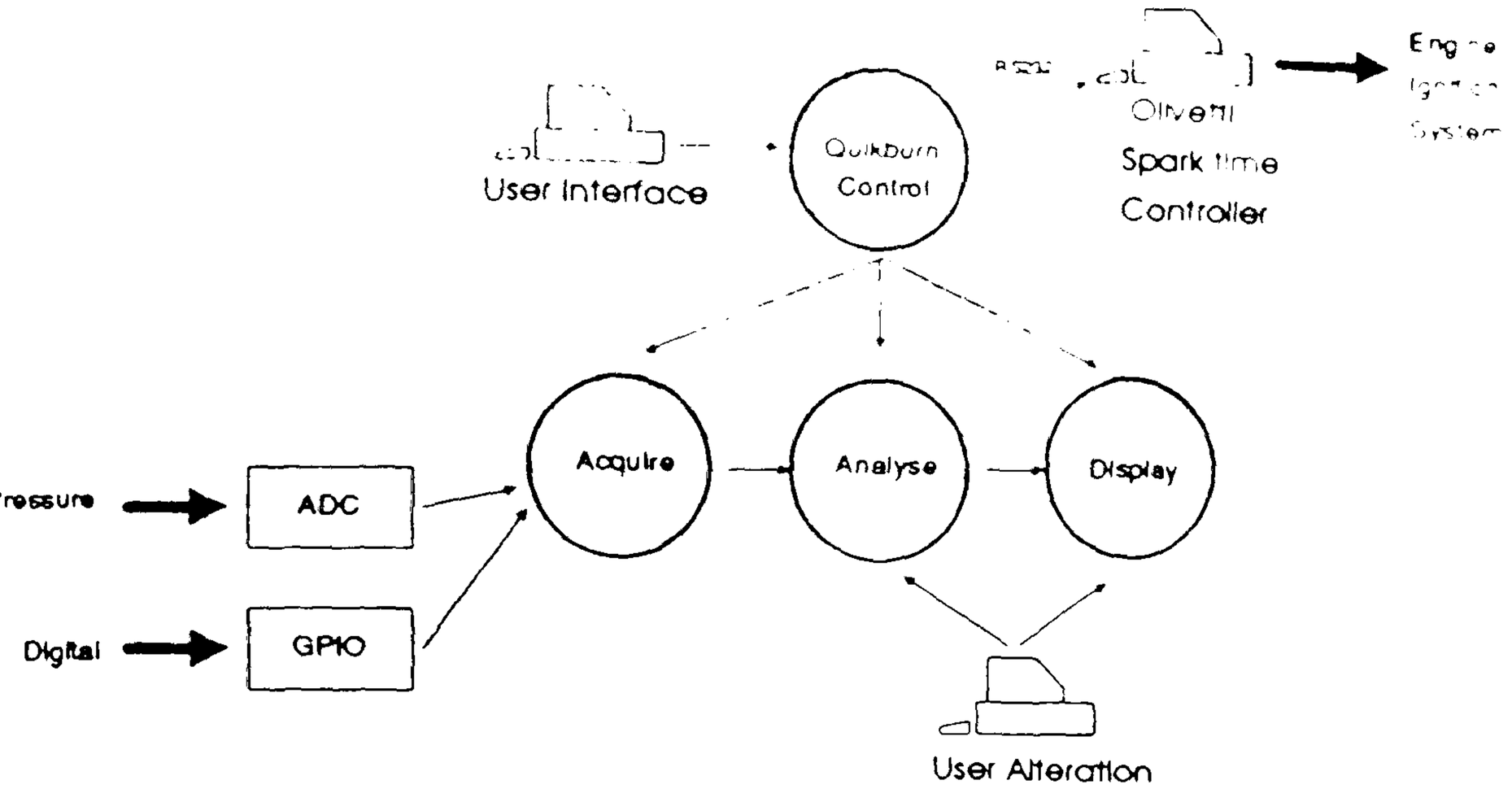

Fig 9.2A Quikburn Data Flow Diagram

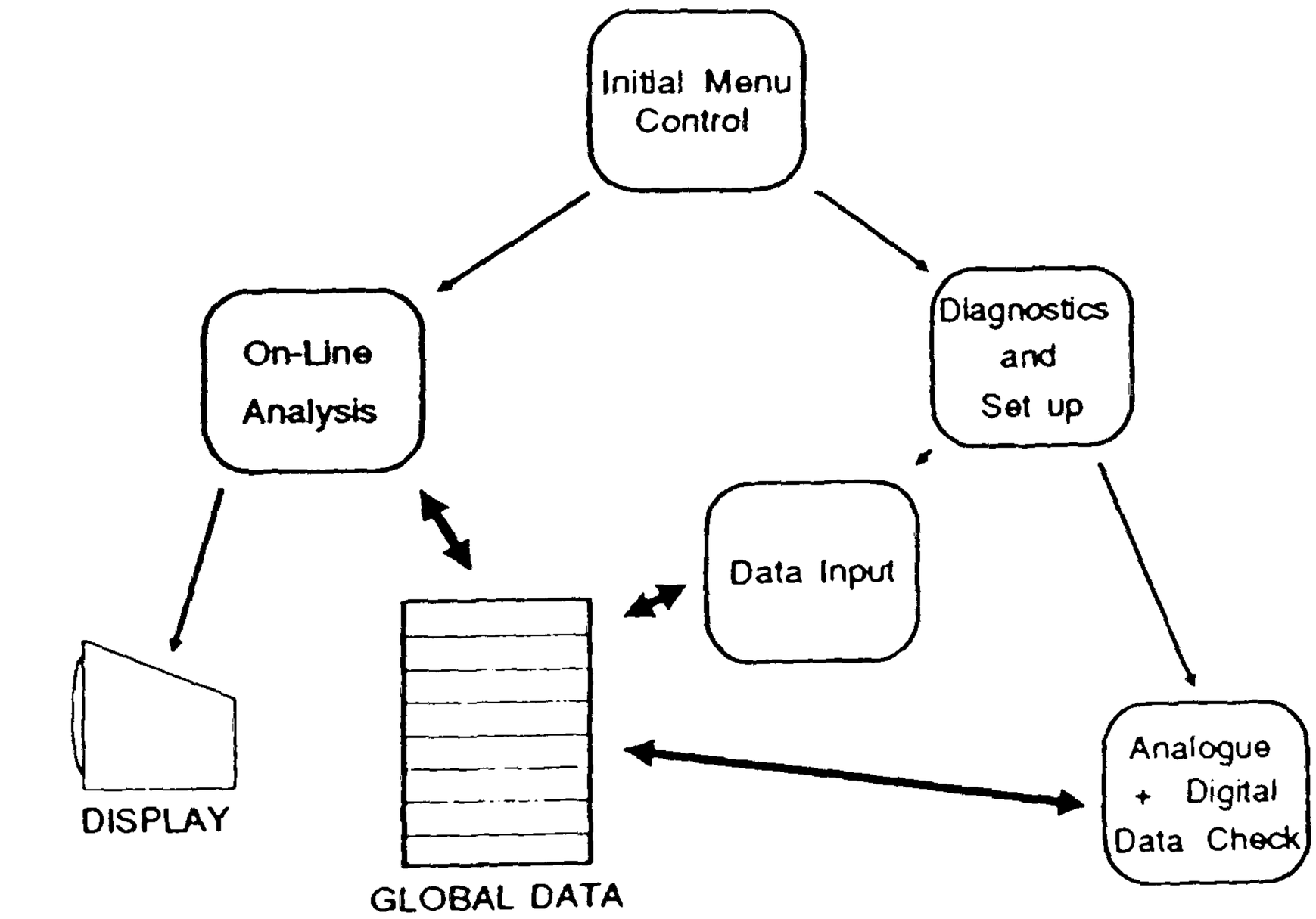

Fig 9.2B Quikburn Program Module Hierarchy

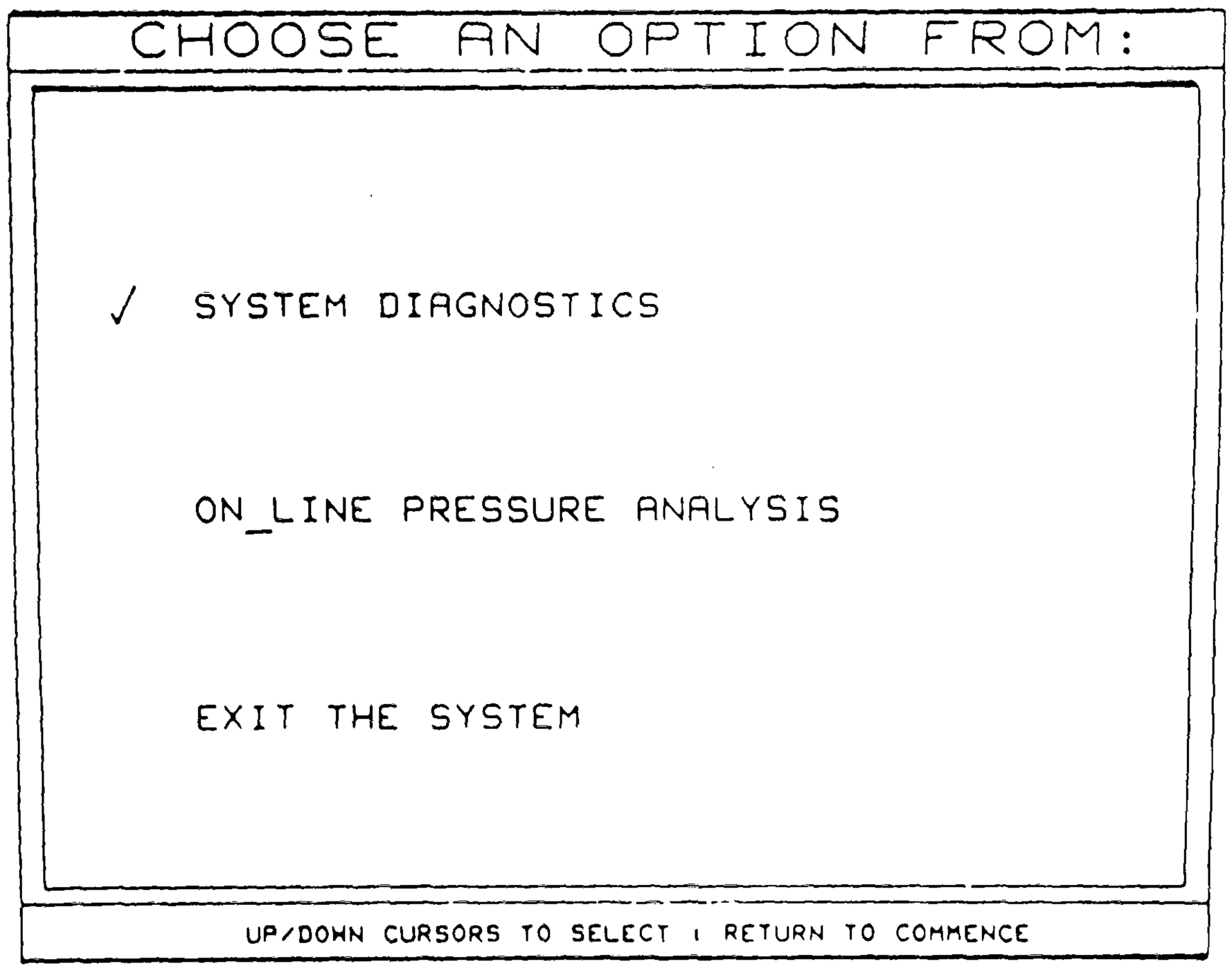

Fig 9.3 Main Quikburn Menu

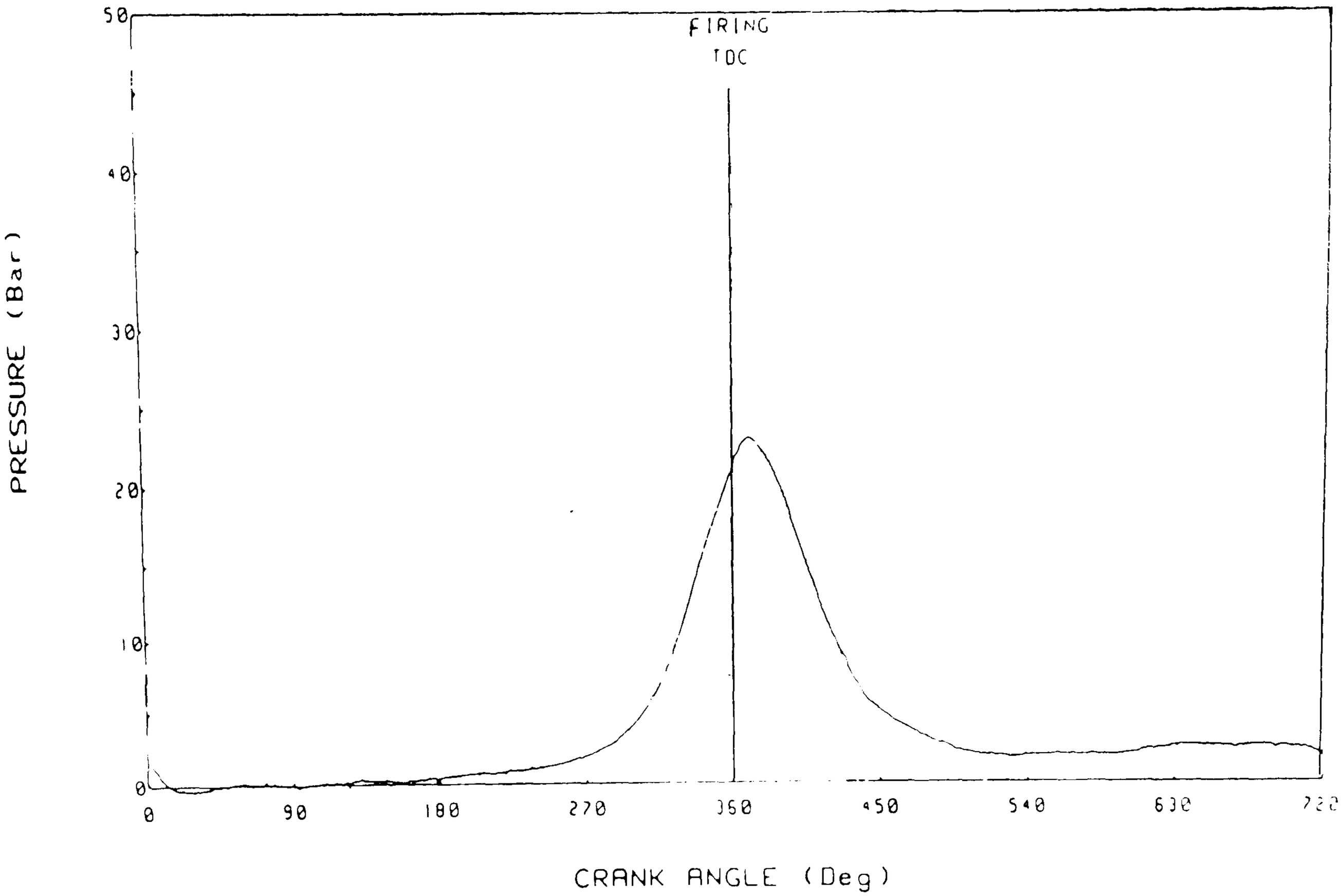

Fig 9.4 Quikburn Display of Average Cylinder Pressure

DIGITAL SIGNAL CHECK

SPEED (RPM)	REVOLUTIONS	CH1 COUNT	CH2 COUNT	CH3 COUNT	CH4 COUNT
1501.0	540	540	0	540	270

TDC PHASING CHECK

TDC CORRECT	TDC 1 DEG EARLY	TDC 1 DEG LATE	OTHER
540	0	0	0

Fig 9.5 Quikburn On Screen Acquired Digital Data Check

ENGINE GEOMETRY VALUES

PARAMETER	VALUE	RANGE
BORE (CM)	9.08	1 - 50
STROKE (CM)	7.694	1 - 50
CONROD LENGTH (CM)	12.695	1 - 50
CLEARANCE VOLUME (CC)	57	1 - 100
I.V.O (DEG BTDC)	100	0 - 180
E.V.O (DEG ATDC)	100	0 - 180

These Default values will be stored in file: ENG_DATA

Fig 9.6 Quikburn User-Friendly Data Input Screen

$$Pc[\theta] = \{P[\theta] - P[\theta - 1].\left[\frac{V[\theta - 1]}{V[\theta]}\right]^{n}\}.\frac{V[\theta]}{V_{TDC}}$$

Acquired Pressure $P[\theta]$

Polytropic Volume Ratio $Vr[\theta, n]$

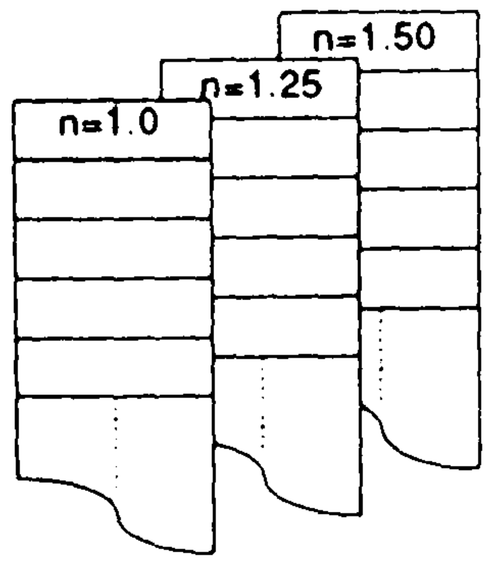

Reference Volume Ratio $Vref[\theta]$

$$\therefore\ Pc[\theta] = \{P[\theta] - P[\theta - 1].Vr[\theta, n]\}.Vref[\theta]$$

Fig 9.7 Fast Burnrate Determination using Lookup Tables

Array of Combustion Pressures
Summed upto each crank angle

Crank angle	Summed Pressure
1	3
2	5
3	14
4	18
5	20
6	27
7	23
8	30

Target is 50% burn point

Therefore, Target = 0.5x 30 = 15

Algorithm

Assign TOP to first element

Assign BOTTOM to last element

Repeat

MIDDLE = (TOP+BOTTOM)/2
If Target > value @ MIDDLE then move TOP to MIDDLE

else move BOTTOM to MIDDLE

Until TOP = MIDDLE

Algorithm in Action Locates Nearest Element
to 50% Burn target of 15 in 4 Attempts Equivalent to Log2 (8) +1

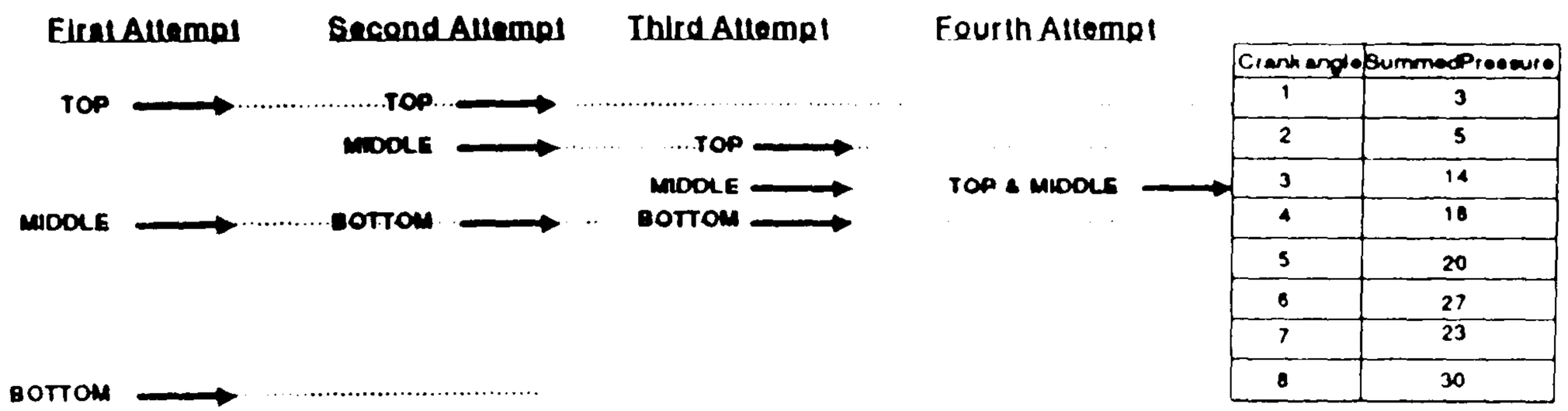

Fig 9.8 Binary Search Algorithm. Theory and Example.

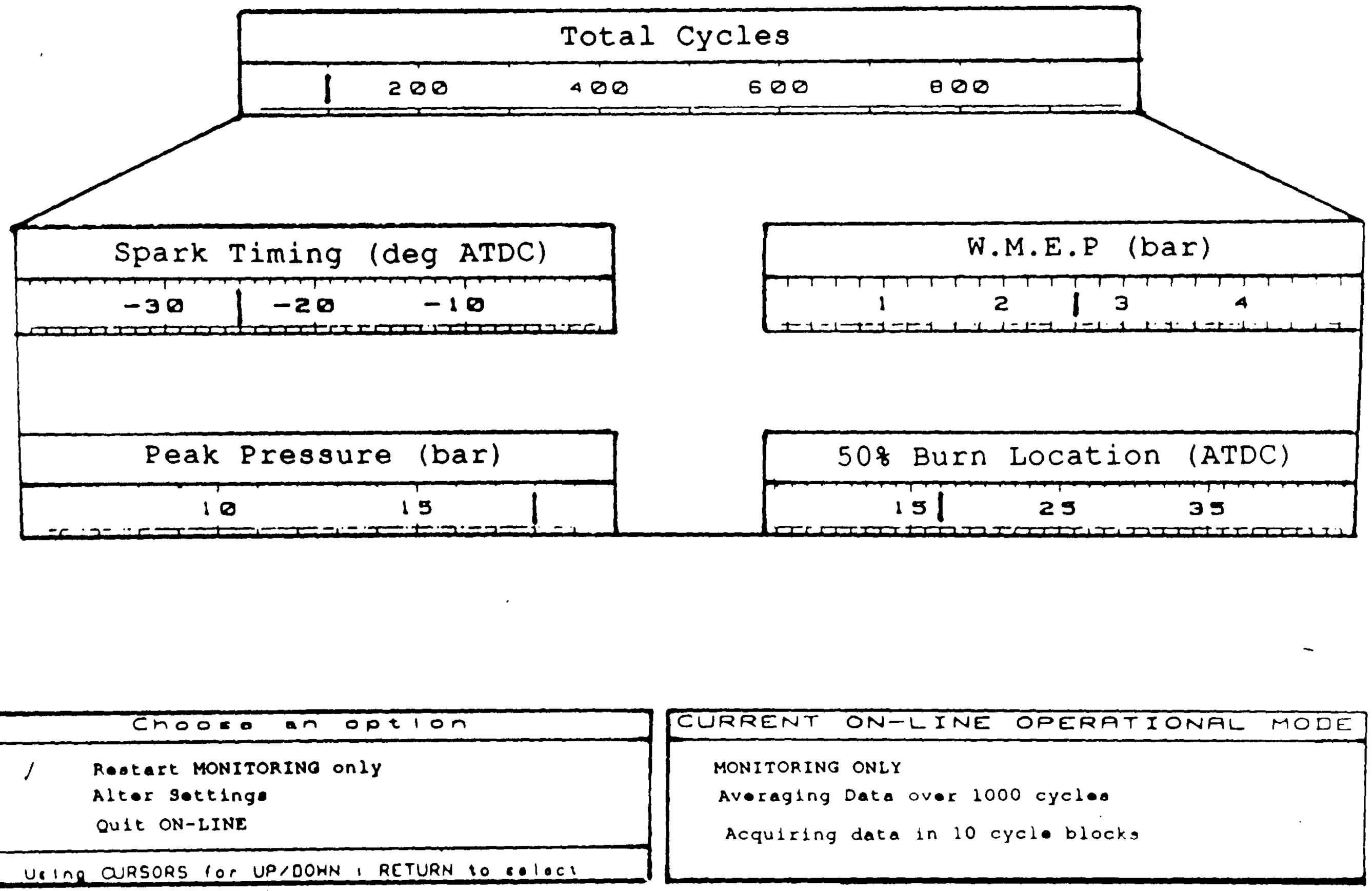

Fig 9.9 The Quikburn Online Combustion Analysis Display

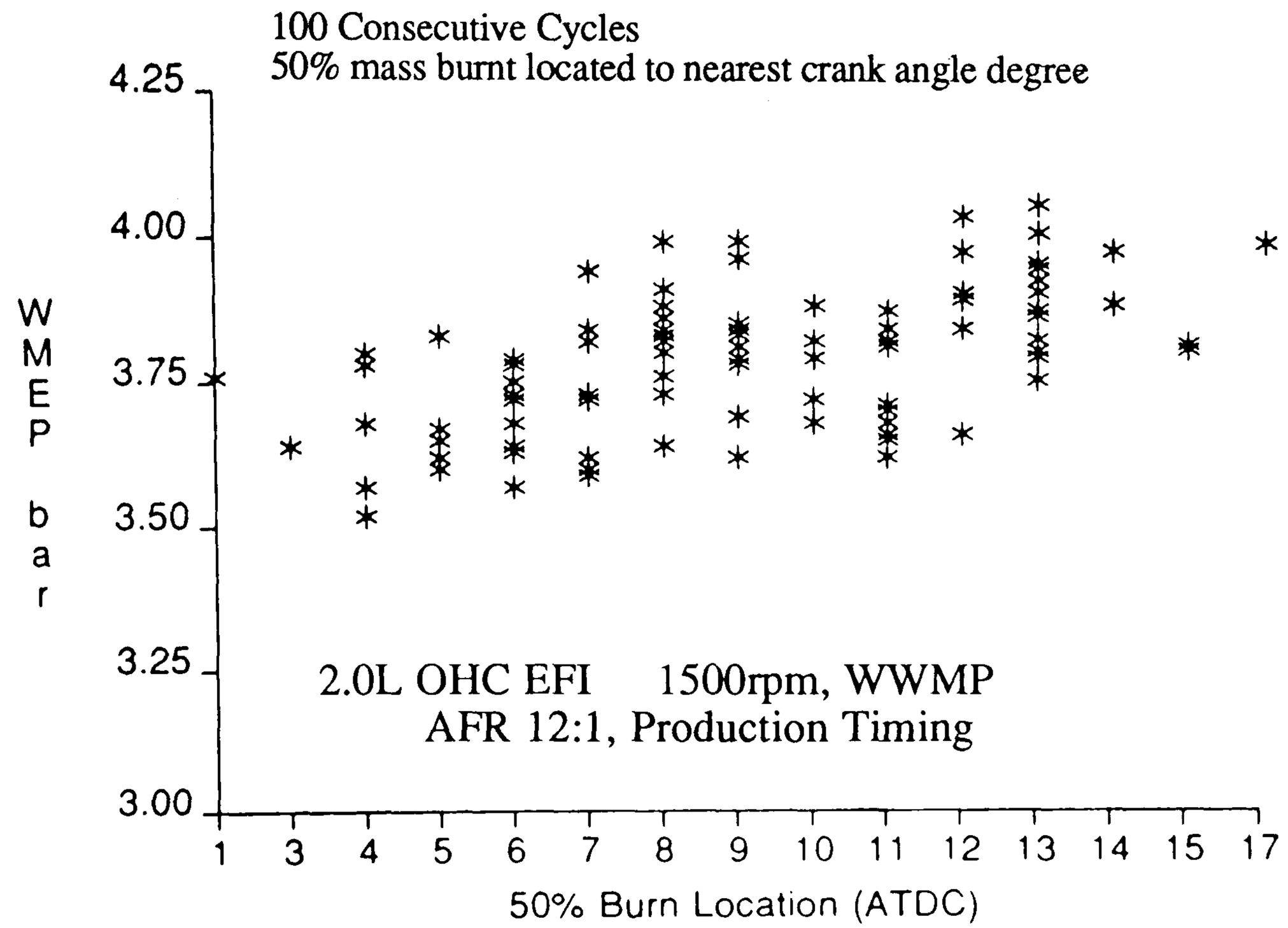

Fig10.1 Cyclic Variation of WMEP with its 50% Burn Location

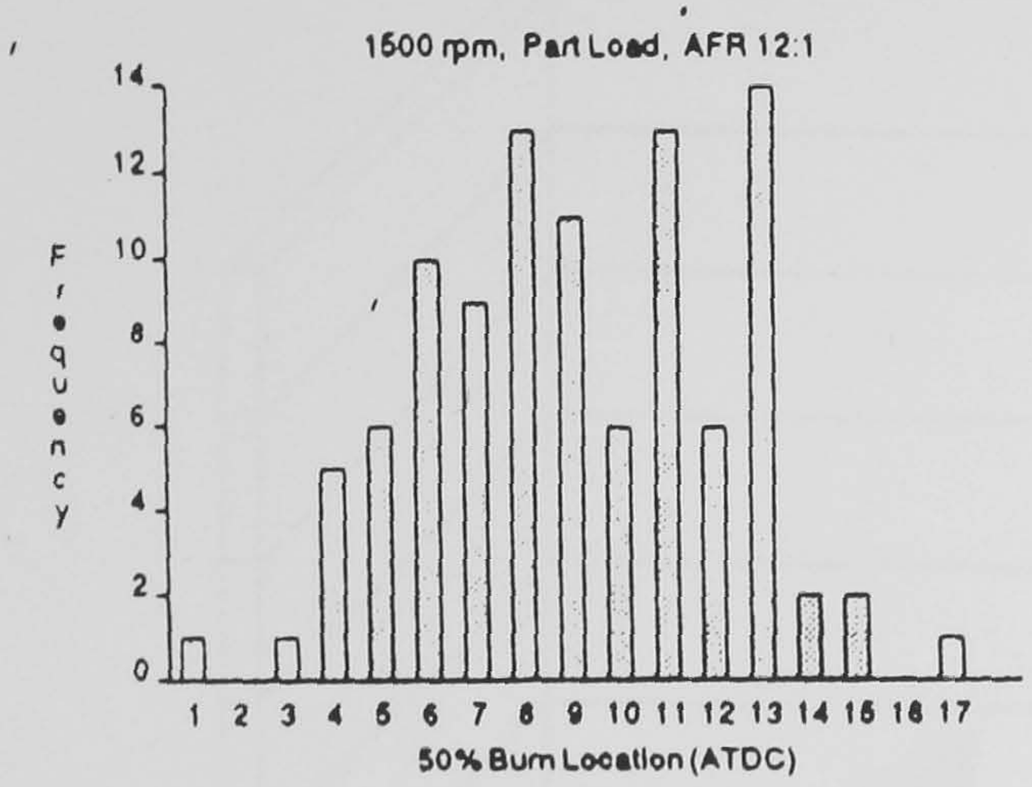

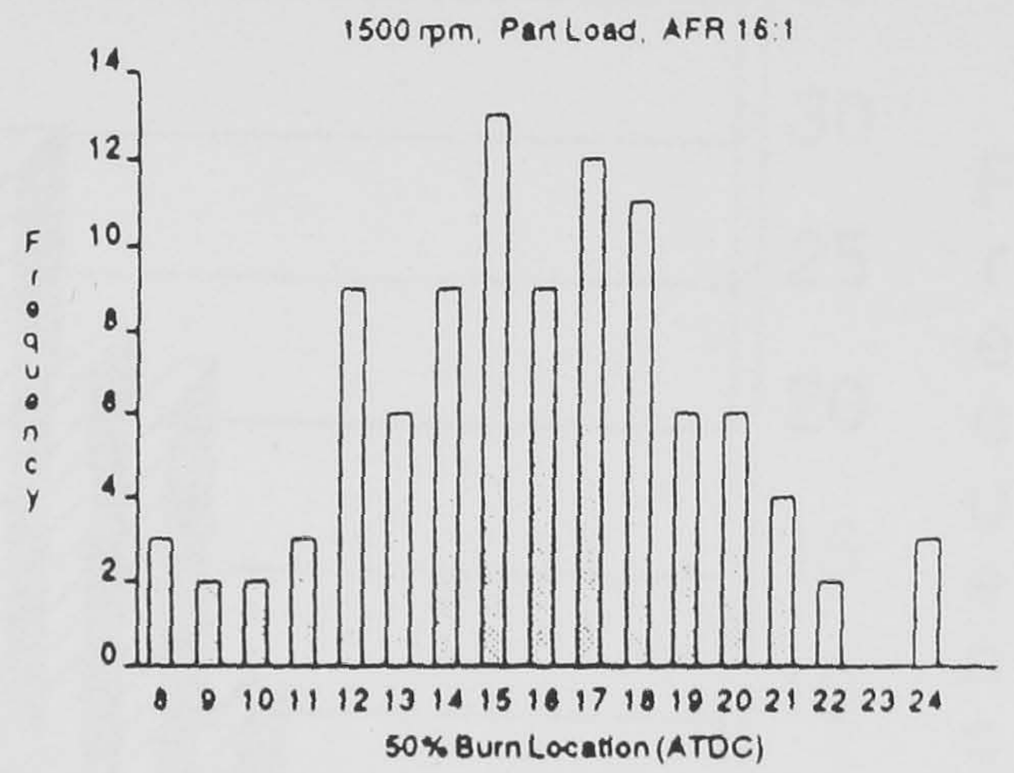

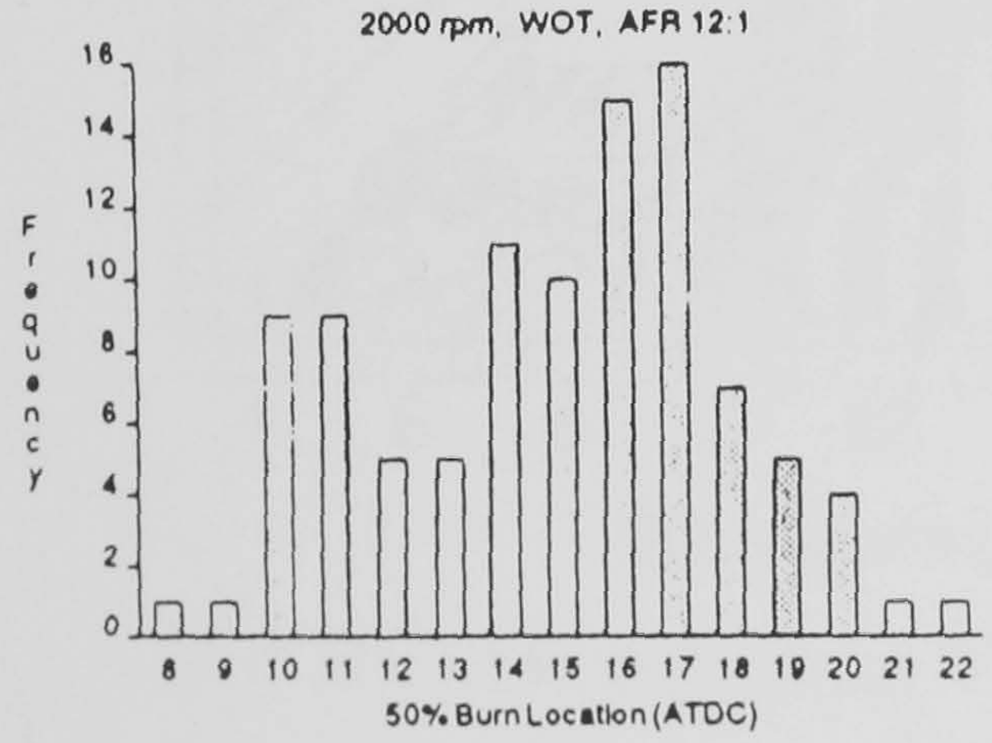

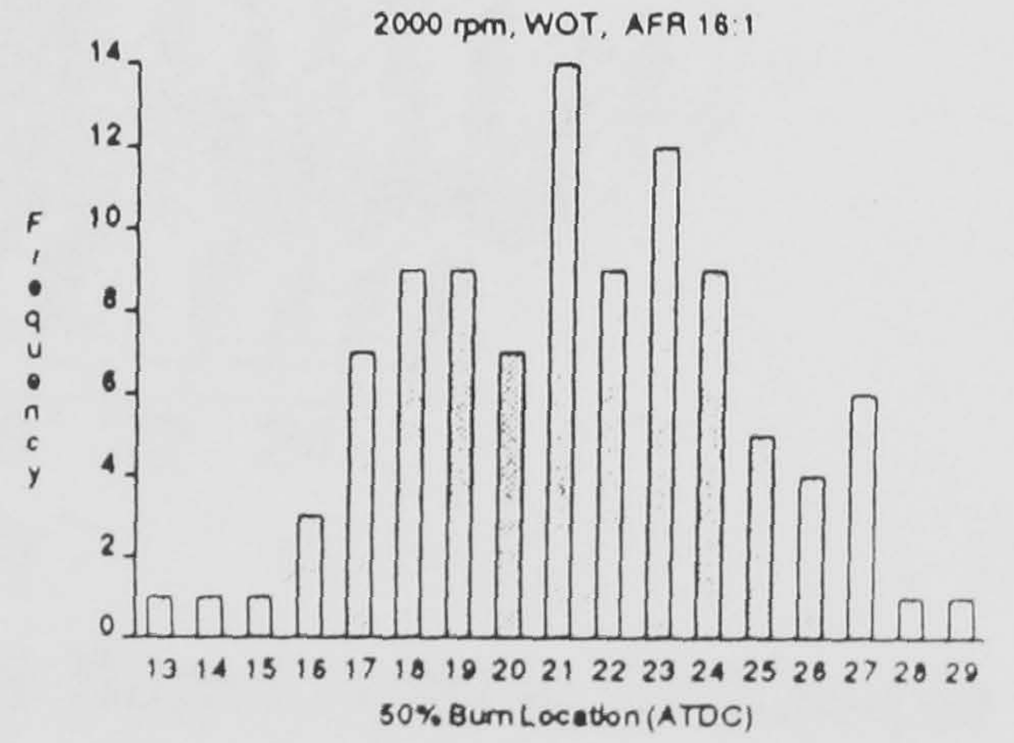

Fig 10.2 Distribution of 50% Mass Burnt Locations within a 100 Cycle Sample. Results from Four Different Operating Conditions on 2.0L OHC EFI with Production Ignition Timing

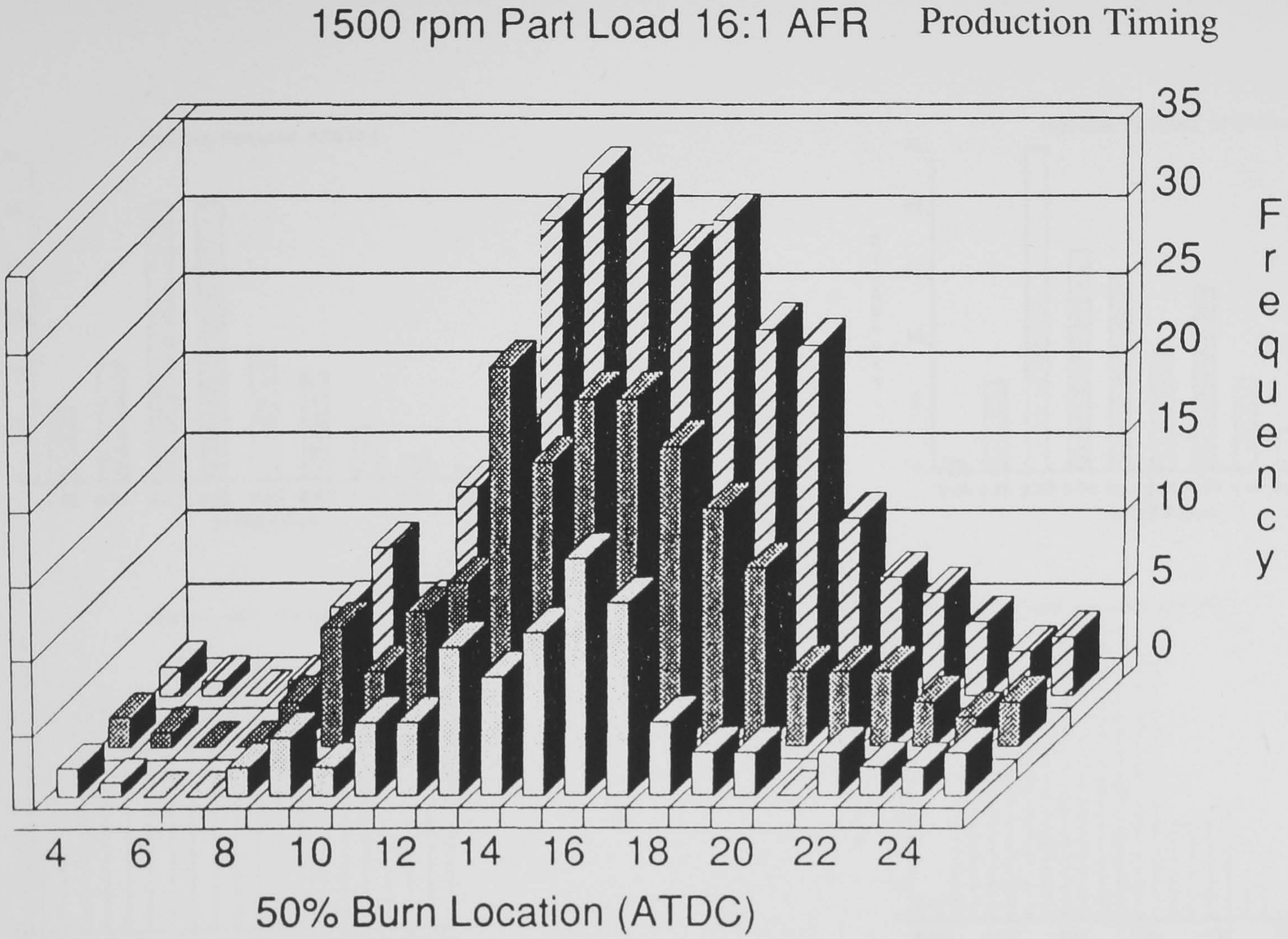

Fig 10.3 Distribution Variation of 50% Burn Location for Sample Sizes 100, 200, and 300 Cycles

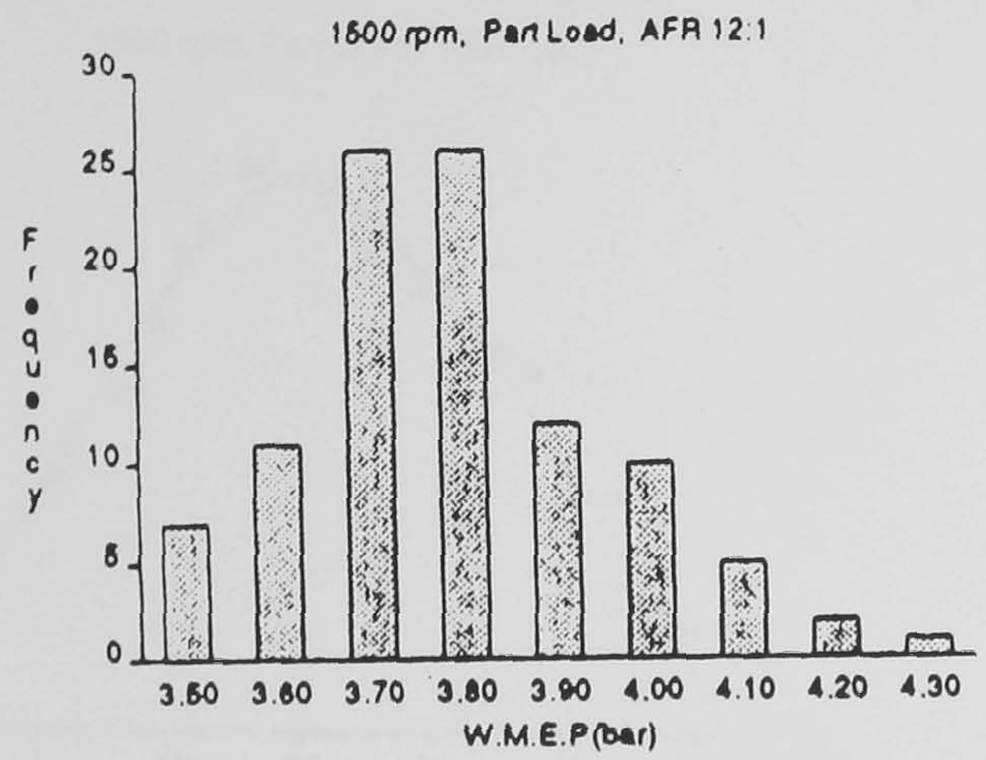

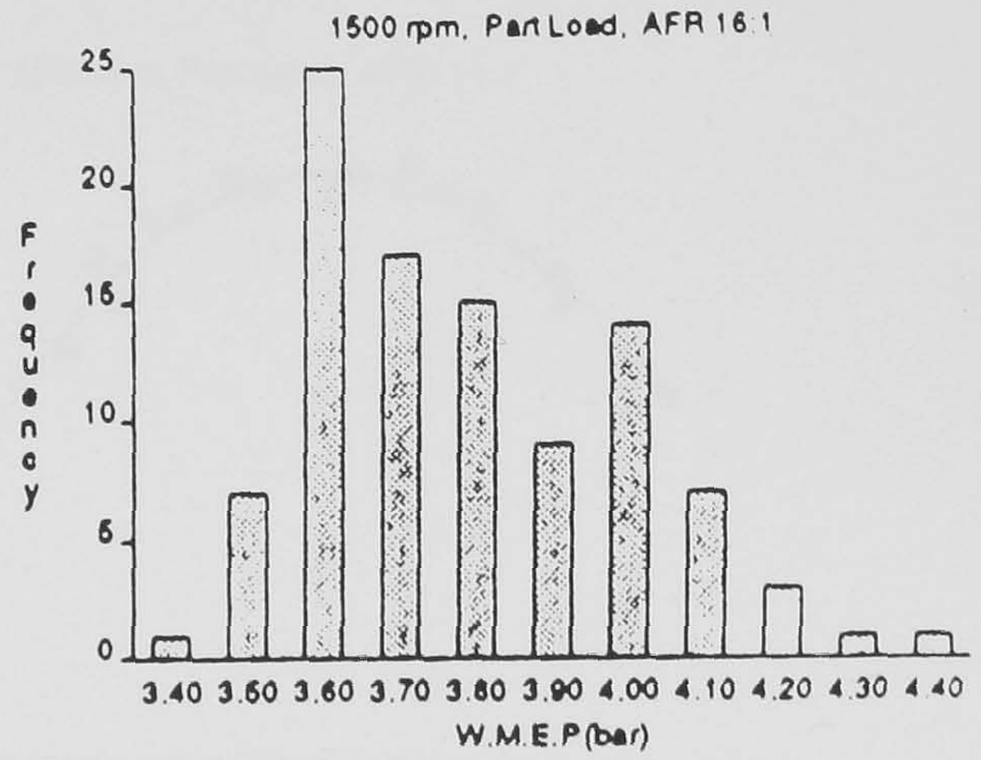

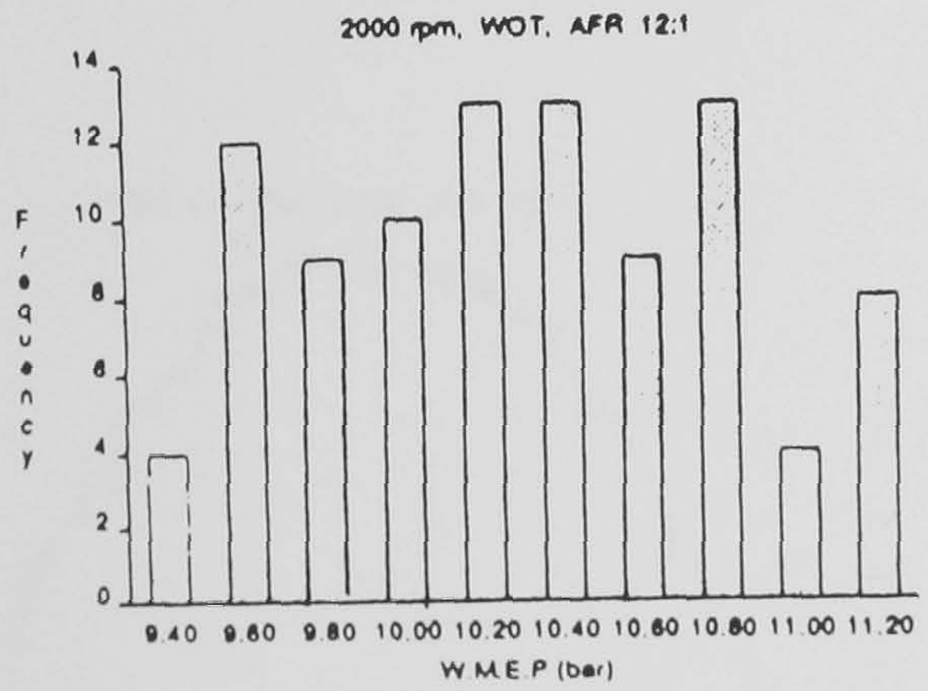

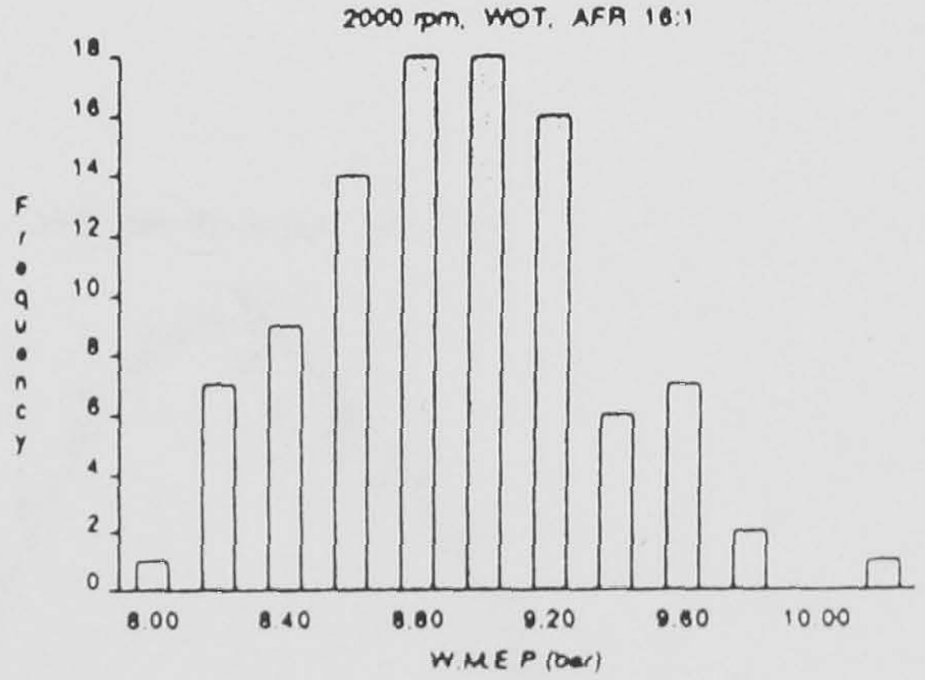

Fig 10.4 Distribution of WMEP within a 100 Cycle Sample. Results from Four Different Operating Conditions on 2.0L OHC EFI with Production Ignition Timing

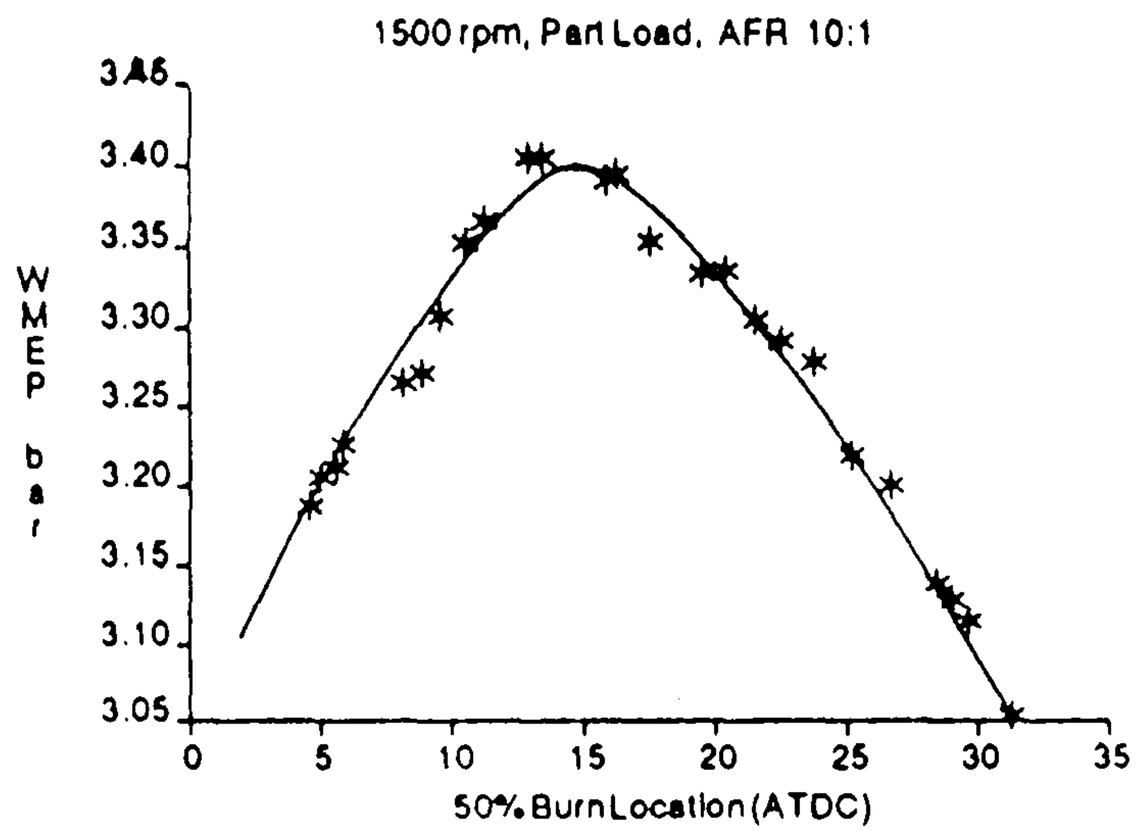

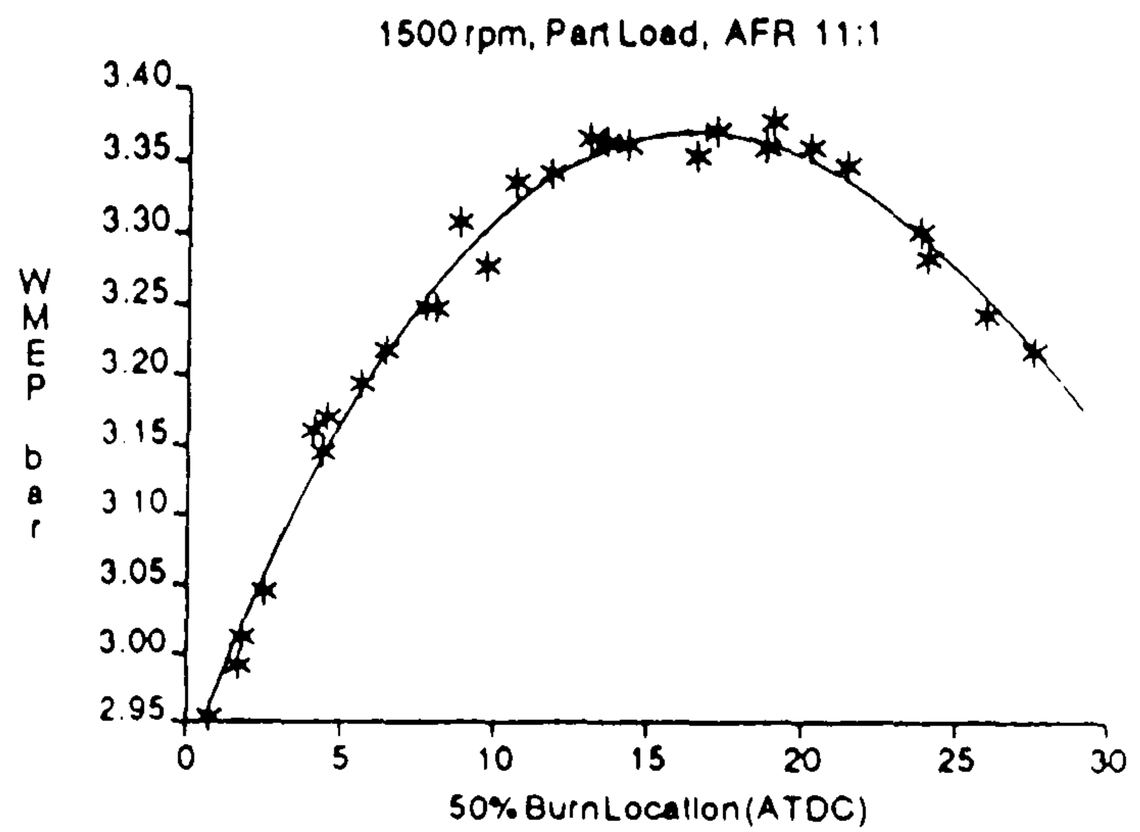

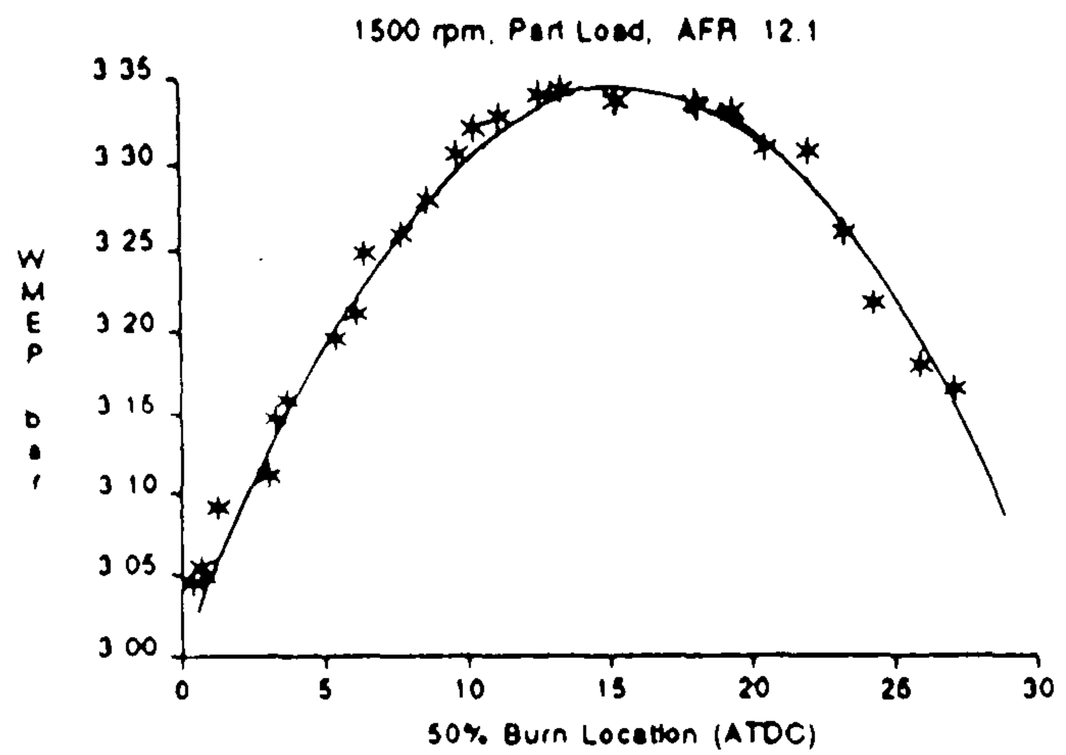

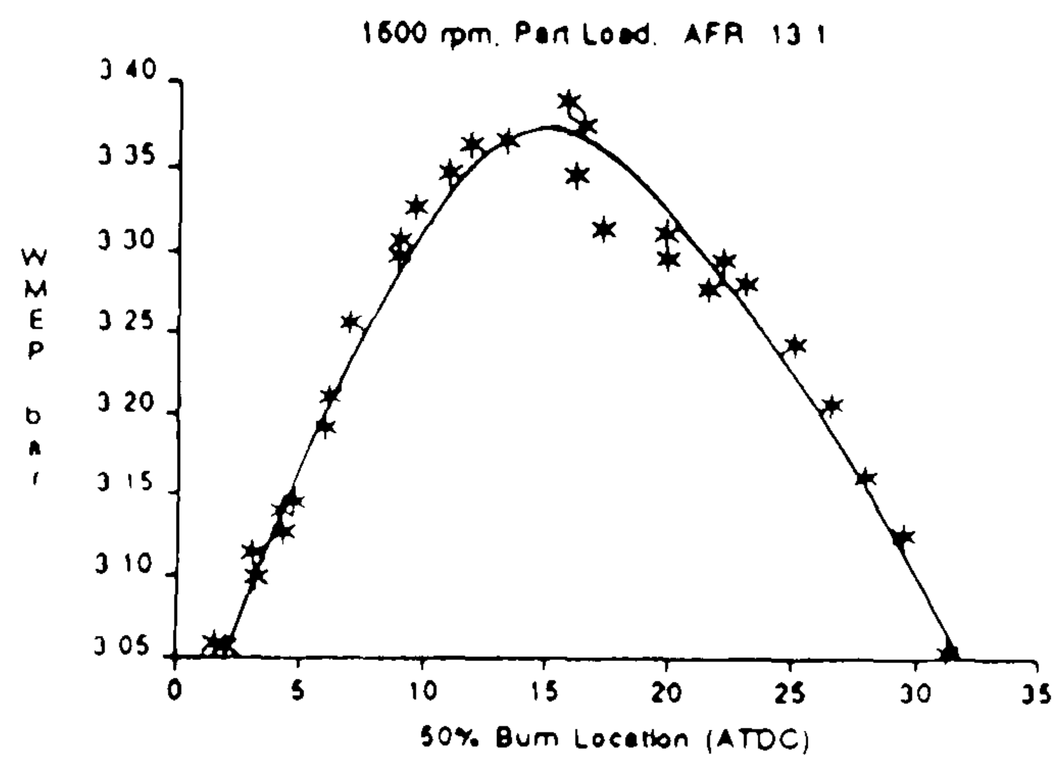

Fig 10.5 WMEP Variation with 50% Burn Location. Obtained by an Ignition Timing Sweep and Averaging 100 Cycles. 2.0L OHC EFI - Rich AFRs

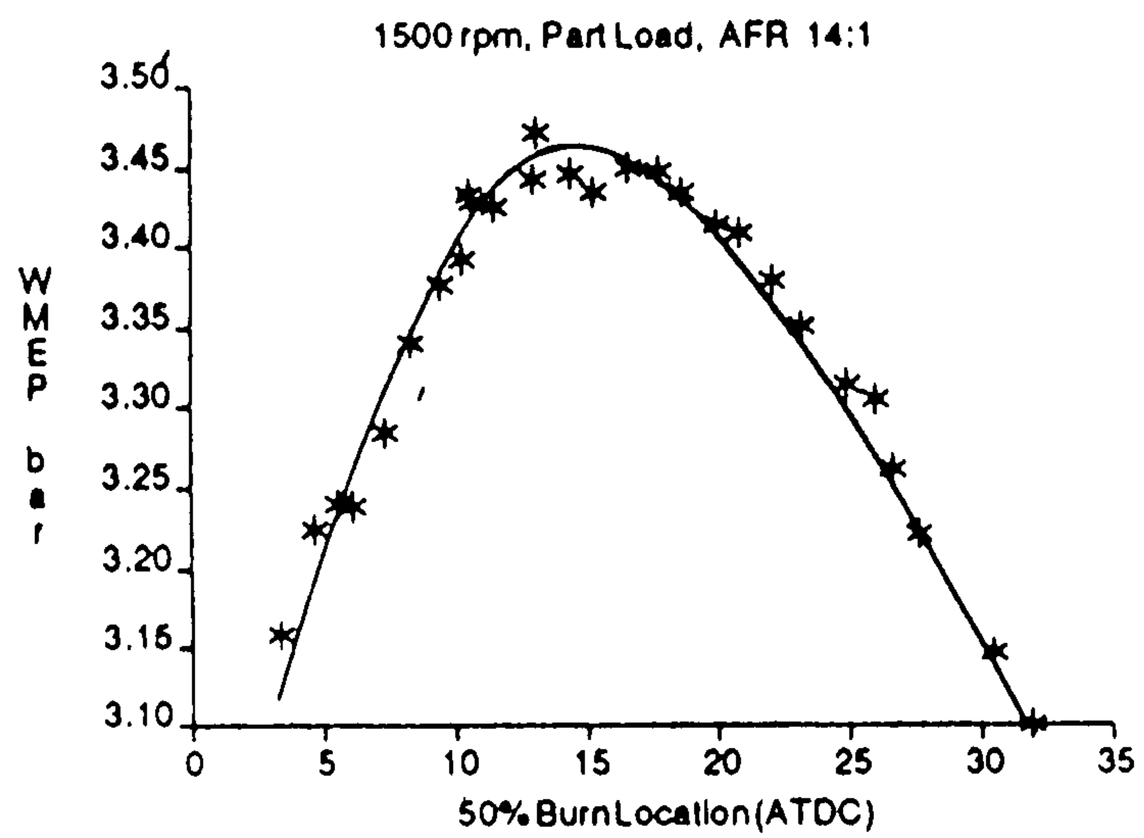

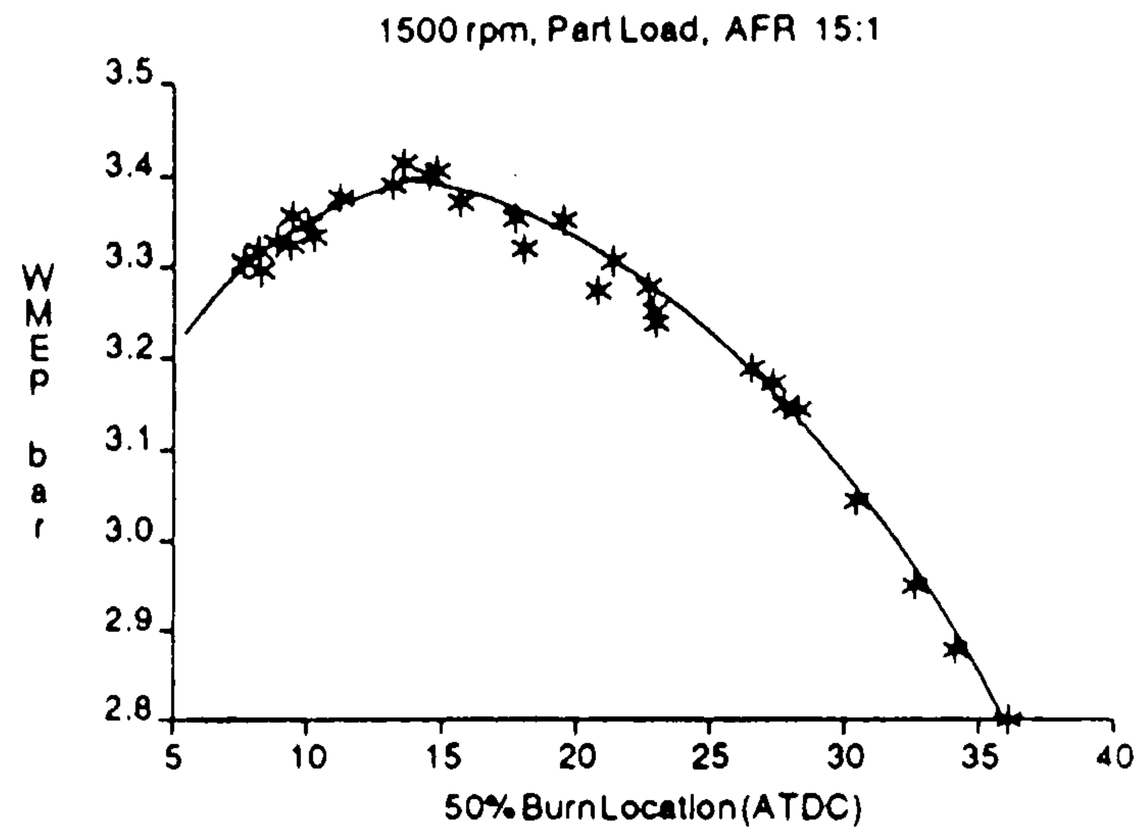

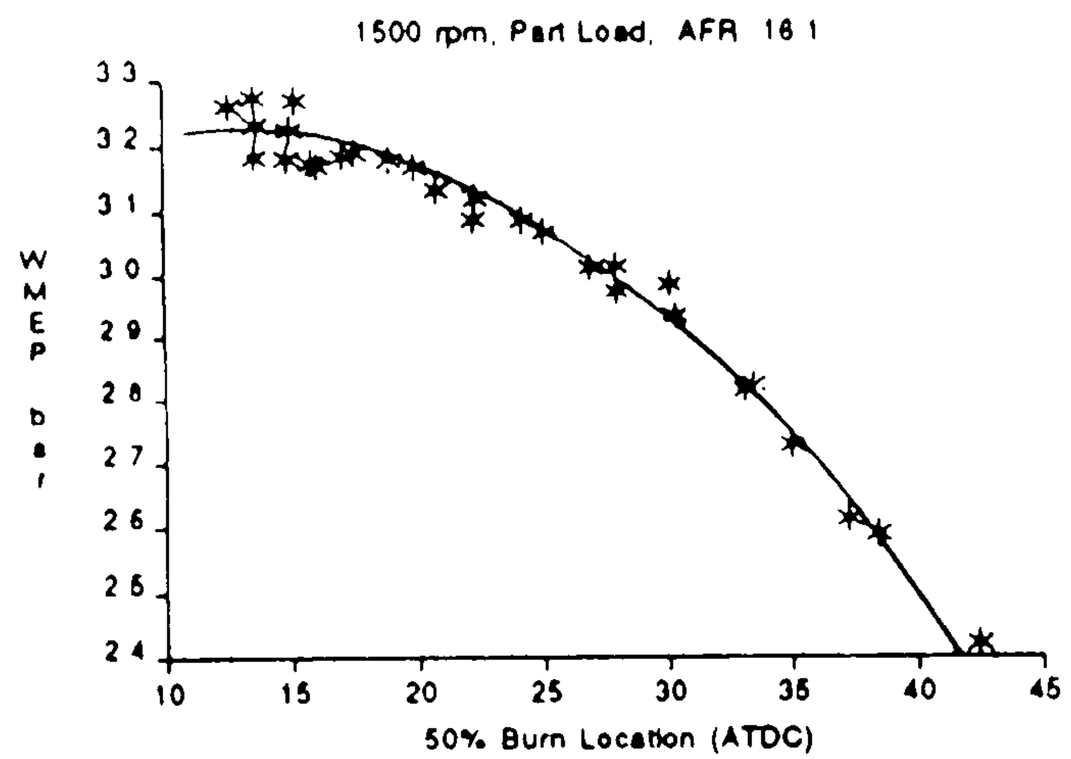

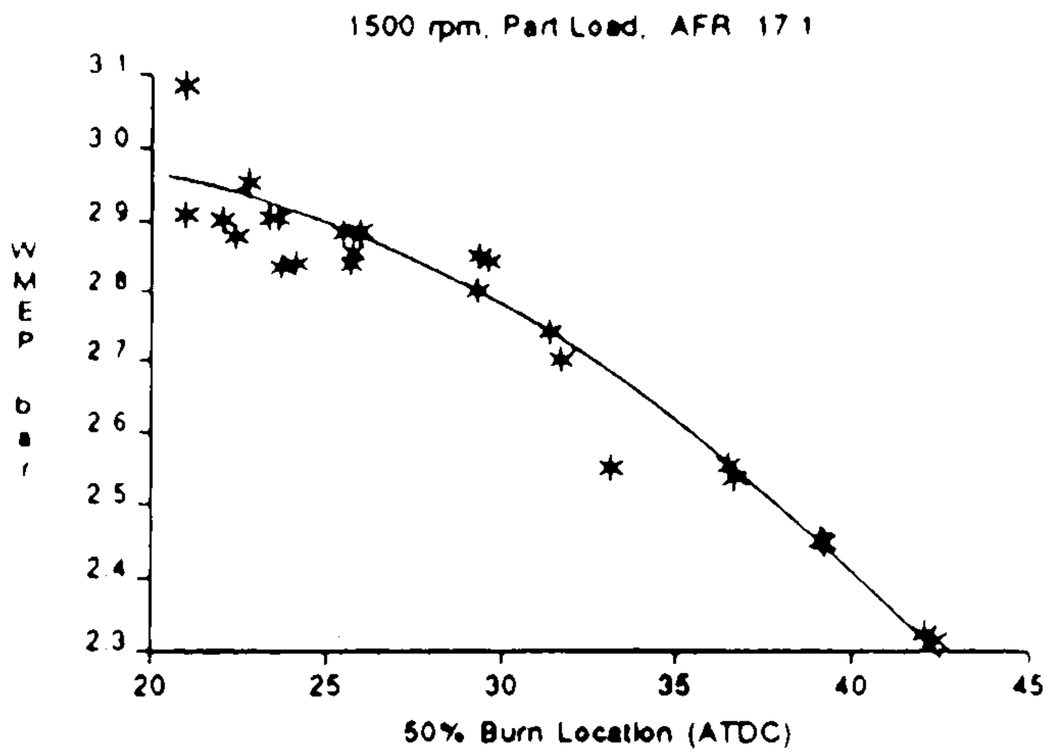

Fig 10.6 WMEP Variation with 50% Burn Location. Obtained by an Ignition Timing Sweep and Averaging 100 Cycles.
2.0L OHC EFI - Lean AFRs

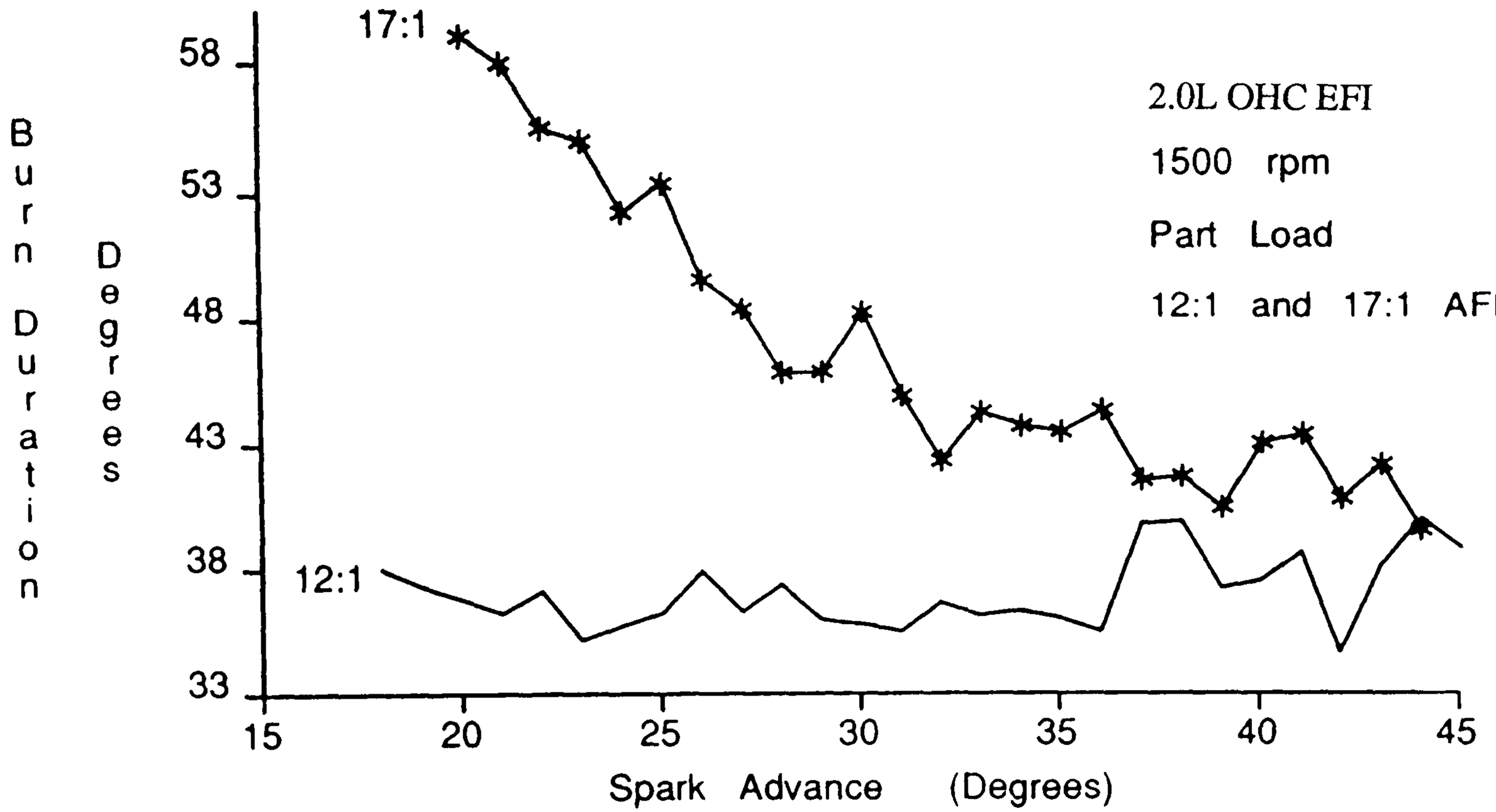

Fig 10.7 10-90% Burn Duration Variation with Spark Advance

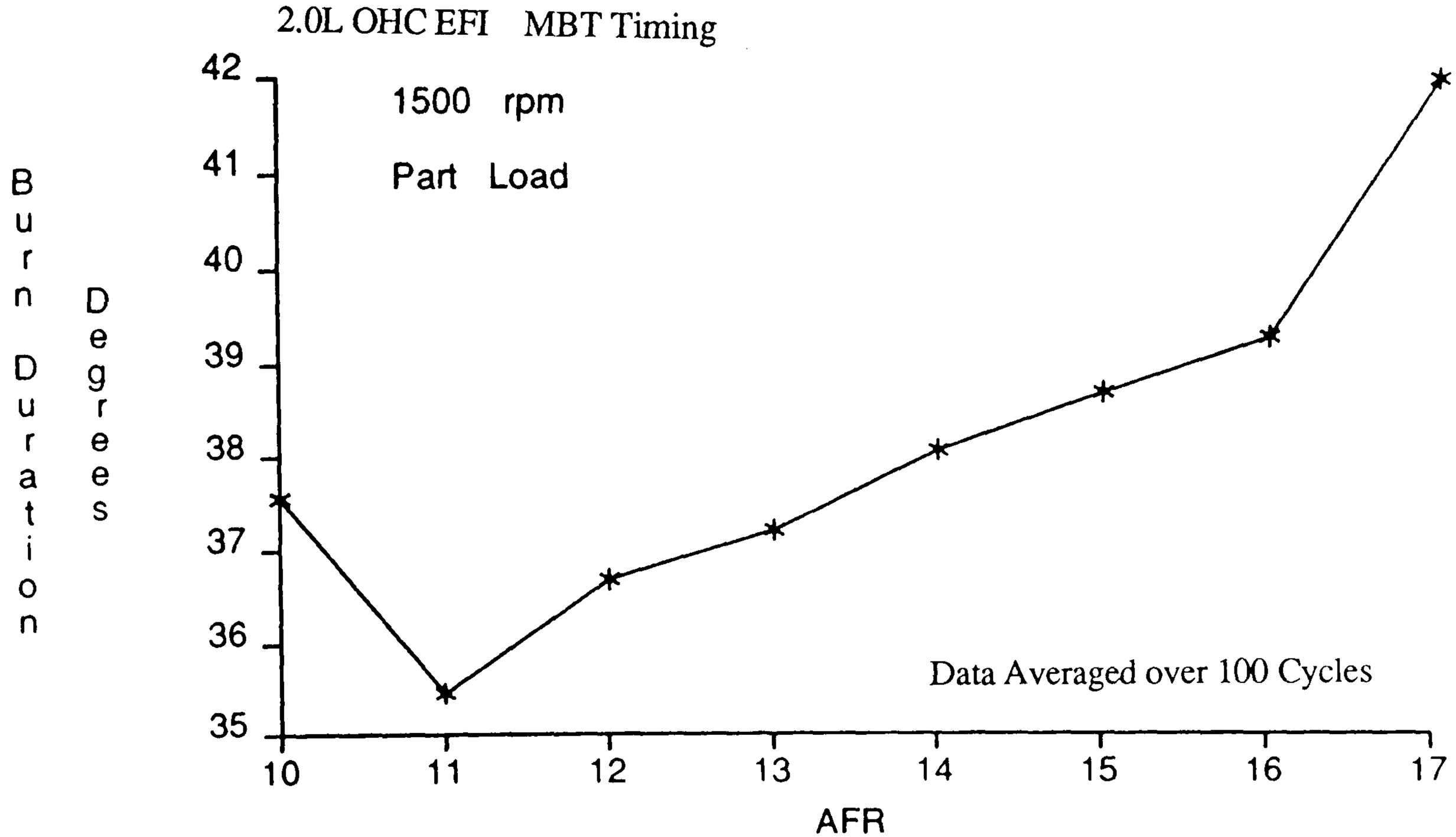

Fig 10.8 Relationship Between 10-90% Burn Duration and AFR

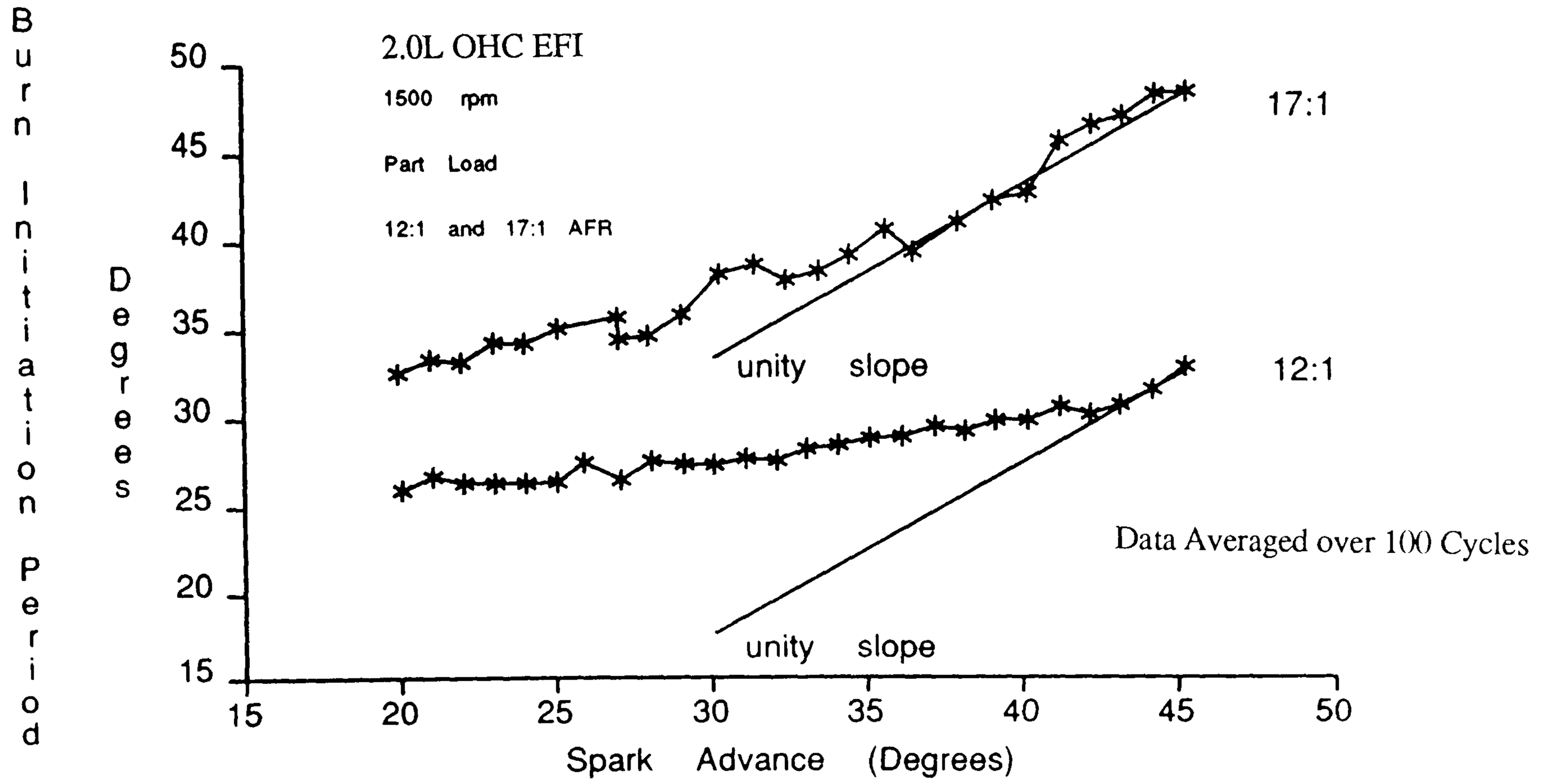

Fig 10.9 Relationship Between 0-10% Burn Duration and Spark Advance

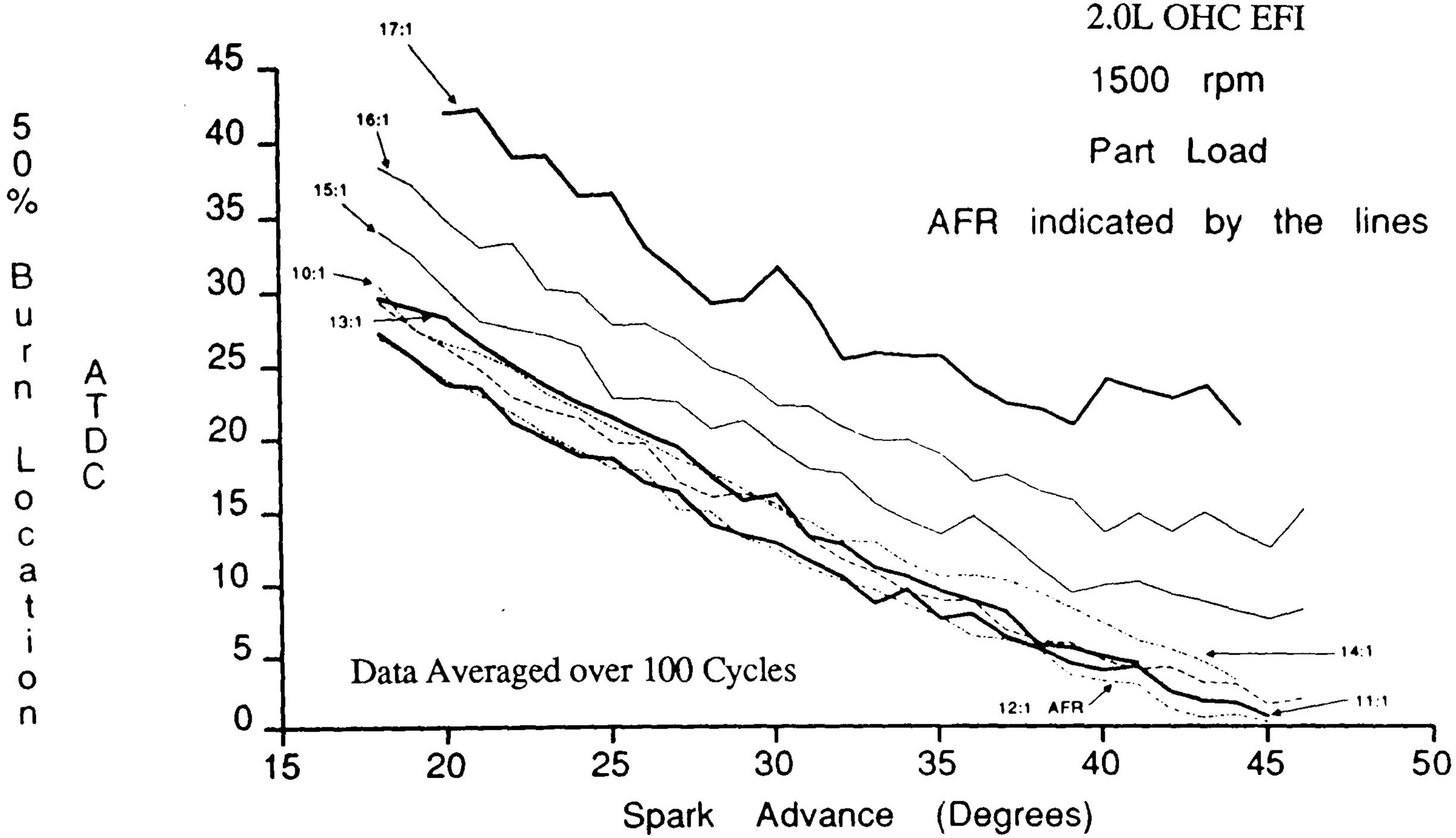

Fig 10.10 Variation of 50% Burn Location with Spark Advance

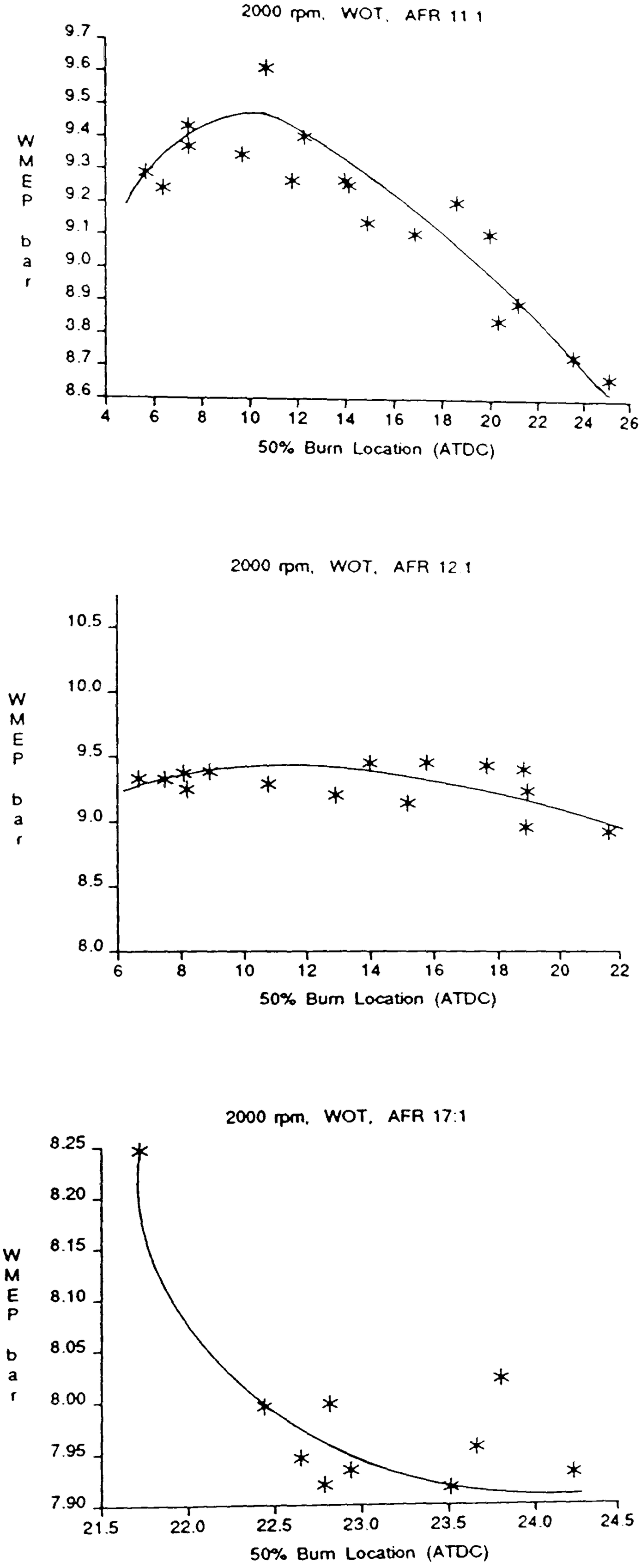

Fig 10.11 WMEP Variation with 50% Burn Location. Obtained by an Ignition Timing Sweep and Averaging 100 Cycles.
2.0L OHC EFI - Full Load

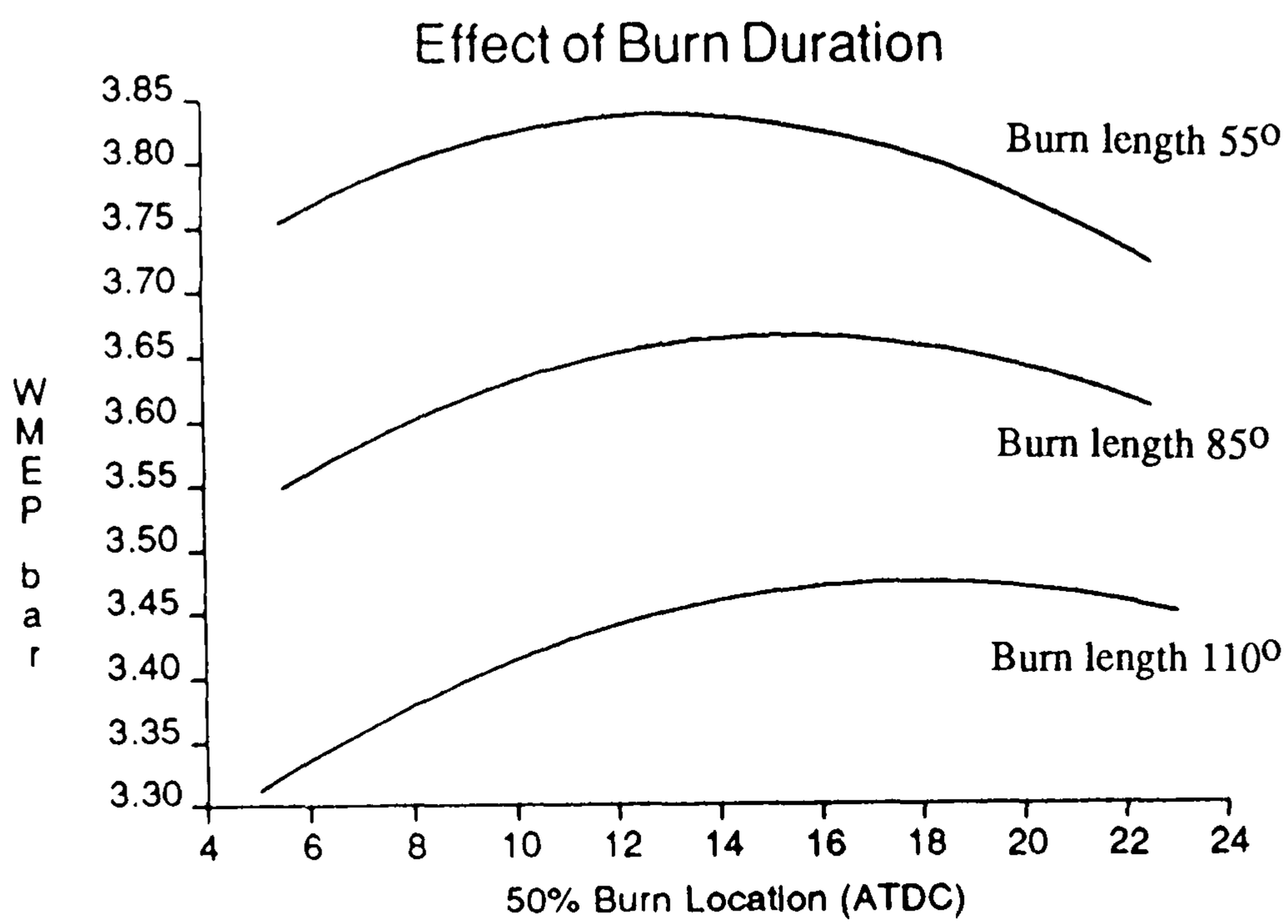

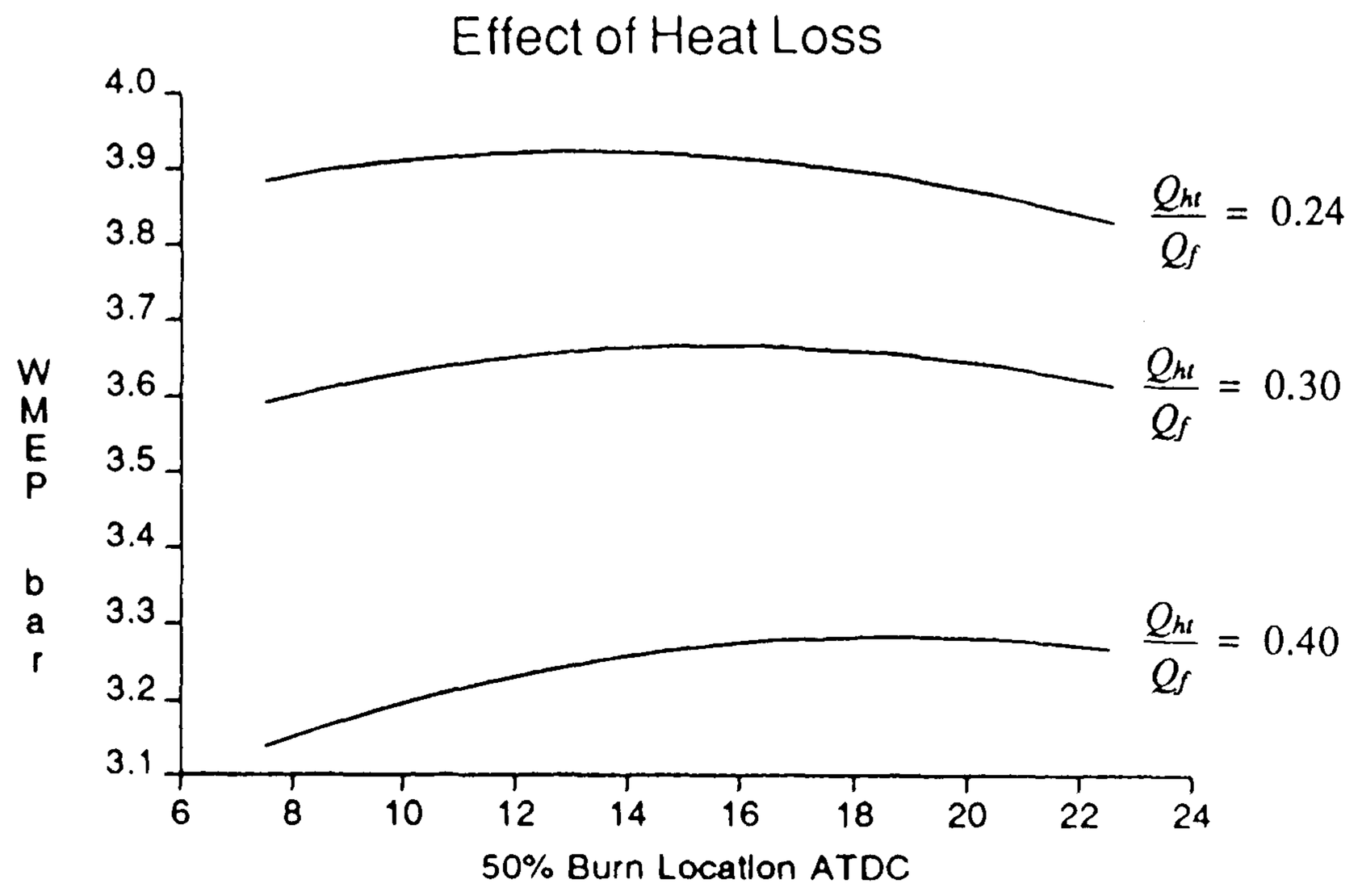

Fig 10.12 Influence of Burn Duration and Heat Loss on Optimum 50% Burn Location

Engine Simulation of 1500rpm WWMP

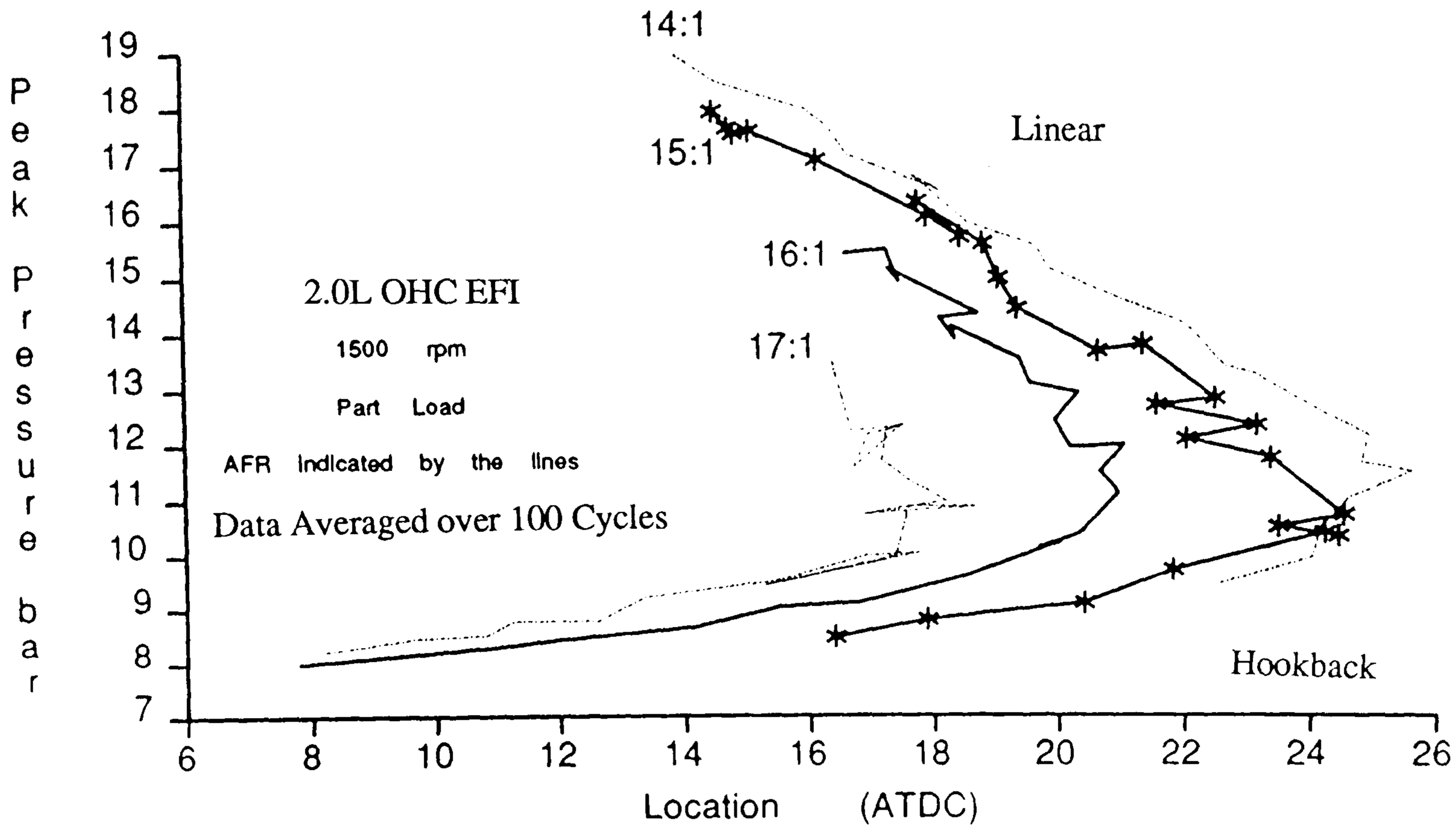

Fig 10.13 Variation of Peak Pressure and its Location

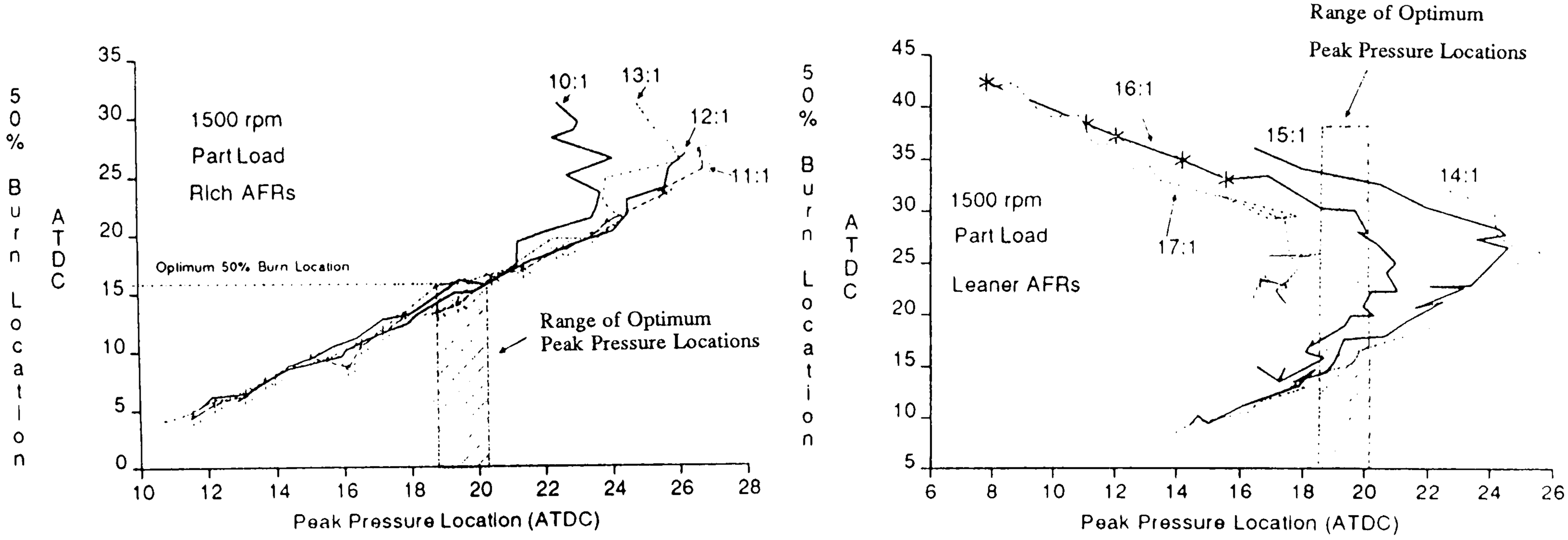

Fig 10.14 Relationship Between 50% Burn Location and Peak Pressure Location

2.0L OHC EFI. Data Averaged Over 100 Cycles